

Heterogeneous uptake of HO₂ radicals onto atmospheric aerosols

Pascale Sylvie Jeanne Matthews

Submitted in accordance with the requirements
for the degree of Doctor of Philosophy

The University of Leeds
School of Chemistry

August 2014



UNIVERSITY OF LEEDS

The candidate confirms that the work submitted is her own, except where work which has formed part of jointly authored publications has been included. The contribution of the candidate and the other authors to this work has been explicitly indicated below. The candidate confirms that appropriate credit has been given within the thesis where reference has been made to the work of others.

The results from the effloresced and deliquesced salts, the HO₂ uptake coefficient onto ammonium nitrate aerosols as a function of relative humidity and the time and HO₂ concentration dependence presented in Chapter 3 have appeared in the publication below. The FAGE signal as a function of time as well as the calibration of the SMPS measurement against the CPC measurement when using one or two neutralisers that were presented in Chapter 2 have also appeared in the publication below.

George, I. J., Matthews, P. S. J., Whalley, L. K., Brooks, B., Goddard, A., Baeza-Romero, M. T., and Heard, D. E.: Measurements of uptake coefficients for heterogeneous loss of HO₂ onto submicron inorganic salt aerosols, *Physical Chemistry Chemical Physics*, 15, 12829-12845, 2013.

Within this publication, I was responsible for the HO₂ uptake coefficient measurements onto ammonium nitrate aerosols over a range of humidities, the time dependent uptake coefficients for sodium chloride, ammonium nitrate and copper doped aerosols and all of the measurements showing a dependence of the uptake coefficient upon HO₂ concentrations. I was also responsible for the figure showing the FAGE signal as a function of time as well as the calibration plot of the SMPS measurement against the CPC measurement when using one or two neutralisers. The lead author Dr. Ingrid George was responsible for all of the other HO₂ uptake measurements reported in the paper as well as the ozone profiling figure shown in the paper.

The results from the Arizona Test Dust experiments presented in Chapter 7 as well as the dust size distribution and data analysis methodology for the dust experiments presented in Chapter 2 have appeared in the following publication:

Matthews, P. S. J., Baeza-Romero, M. T., Whalley, L. K., and Heard, D. E.: Uptake of HO₂ radicals onto Arizona test dust particles using an aerosol flow tube, *Atmos. Chem. Phys.*, 14, 7397-7408, 2014.

I was responsible for all of the measurements reported in this paper and I also ran the box model to see the impact of the uptake coefficient upon gaseous HO₂ concentrations.

This copy has been supplied on the understanding that it is copyright material and that no quotation from the thesis may be published without proper acknowledgement.

© 2014 The University of Leeds and Pascale Sylvie Jeanne Matthews

Acknowledgements

I would like to start by thanking my supervisors, Dwayne Heard and Maria Teresa Baeza-Romero (Maite), for all of the advice and guidance that they have given me over the last four years. I am extremely grateful to Dwayne for providing me with the opportunity to do such an interesting PhD project as well as for always having time to discuss my work. Maite is particularly thanked for her suggestions during our monthly meetings, during which she has always had many ideas of how to progress the project. I must also thank the National Environment Research Council for funding this work.

I would like to thank the members of the Heard and Seakins groups, both past and present, all of whom have helped me at some point during this project. Special thanks must go to Ingrid George for teaching me how to use the experimental setup during my first few months in Leeds. Lisa Whalley, Trevor Ingham, Mark Blitz and Fred Winiberg are particularly thanked for their help in troubleshooting and fixing FAGE and laser related problems. Lisa is also thanked for teaching me how to run the Cape Verde box model.

A huge amount of thanks go to Thomas Berkemeier, Manabu Shiraiwa and Uli Pöschl for their hard work in developing the KM-SUB model and adapting the code which allowed it to be used to interpret the HO₂ uptake coefficients measured in this work. I am grateful to them for giving me the opportunity of spending a week in Mainz in January 2013 and for the many hours since then that they have spent coding. I must also thank Markus Ammann for allowing me to spend two months at the Paul Scherrer Institute (PSI) making HO₂ uptake coefficient measurements onto secondary organic aerosol (SOA) formed in the PSI smog chamber, with the results of that work forming part of this thesis. I would also especially like to thank Manuel Krapf and Josef Dommen for running the PSI smog chamber and for constantly trying to make higher concentrations of SOA within the chamber.

Finally, I would like to thank my Mum, Dad and husband (Ryan) for their love and patience during the last four years.

Abstract

HO₂ uptake coefficients were measured onto a variety of sub-micron aerosols and over a range of experimental conditions using an aerosol flow tube coupled with a sensitive Fluorescence Assay by Gas Expansion (FAGE) cell. Experiments showed that the deliquesced salt aerosols had larger HO₂ uptake coefficients ($\gamma = 0.003 - 0.016$) than the effloresced salt aerosols ($\gamma < 0.004$). Similarly, solid organics had smaller uptake coefficients ($\gamma < 0.004$) than aqueous organics which were small ($\gamma < 0.004 - \gamma = 0.008$) unless metal ions were present. No observable dependence upon aerosol size or aerosol pH was measured for aqueous salt aerosols. The mass accommodation was measured as 0.5 ± 0.3 by doping the aerosols with copper. Measurements also showed that the HO₂ uptake coefficient was highly dependent upon the copper and iron concentrations and increased between copper concentrations of $10^{-4} - 10^{-2}$ M within the aerosol. However, the addition of organics such as EDTA and oxalic acid to copper doped aerosols decreased the HO₂ uptake coefficient by a factor of $\sim 50 - 100$. The HO₂ uptake coefficient onto copper doped sucrose aerosols increased with increasing relative humidity. Secondary organic aerosols were generated in situ in a smog chamber and small uptake coefficients were measured onto α -pinene derived aerosols ($\gamma < 0.001$) and 1,3,5 trimethylbenzene derived aerosols ($\gamma = 0.004 \pm 0.002$).

Measurements onto Arizona Test Dust (ATD) aerosols showed much higher HO₂ uptake coefficients ($\gamma = 0.018 \pm 0.006$) than salt and organic aerosols at an initial HO₂ concentration of 1×10^9 molecule cm⁻³ and increased with increasing humidity. Experiments were also performed over a temperature range of 263 -313 K onto effloresced sodium chloride and ammonium sulphate aerosols and onto deliquesced ammonium nitrate and copper doped ammonium nitrate. For the deliquesced ammonium nitrate aerosols the HO₂ uptake coefficient increased with decreasing temperature. Finally, a time and apparent HO₂ concentration dependence was observed for aqueous salt aerosols, copper doped aqueous aerosols and for ATD with larger HO₂ uptake coefficients at shorter times and at lower HO₂ concentrations. Modelling was performed using the kinetic multi-layer model of aerosol surface and bulk chemistry (KM-SUB) and showed that for undoped aqueous aerosols the time dependence could be explained by a decrease in the HO₂ concentrations along the flow tube. The apparent HO₂ concentration had the potential to be explained by a Fenton-like reaction whereby hydrogen peroxide exiting the injector was converted to HO₂ within the aerosols, due to the presence of trace amounts of transition metal ions, which then partitioned back to the gas phase.

Contents

Chapter 1: Introduction	1
1.1 The importance of understanding atmospheric chemistry	1
1.2 The importance of aerosols in the troposphere	3
1.3 The importance of HO _x in the troposphere	6
1.4 HO _x measurement techniques	10
1.4.1 Fluorescence Assay By Gas Expansion	10
1.4.2 Other HO _x measurement techniques	12
1.6 Heterogeneous chemistry	13
1.7 Comparison between measured and predicted HO ₂ concentrations during field campaigns	17
1.8 Modelling of uptake coefficients	18
1.8.1 The resistor model	18
1.8.1.1 Unreactive gas species	20
1.8.1.2 Reactive gas species	21
1.8.1.3 Reactive gas species including uptake at the aerosol interface	21
1.8.2 The KM-SUB model	22
1.9 The current understanding of aqueous HO ₂ chemistry	24
1.10 Solid aerosol chemistry	27
1.11 Techniques used to measure HO ₂ uptake coefficients in the laboratory	29
1.12 Laboratory measurements of the HO ₂ uptake coefficient	31
1.13 HO ₂ uptake coefficient parameterisations and models	33
1.13.1 Parameterisations of the HO ₂ uptake coefficient onto solid sodium chloride surfaces over a range of temperatures	33
1.13.2 Parameterisations of the HO ₂ uptake coefficient onto five different aerosol types	34
1.13.3 HO ₂ uptake coefficient model using known aqueous chemistry	35
1.14 Summary	38
Chapter 2: Experimental	40
2.1 Overview of the experimental setups	40
2.2 The flow regimes for the different experimental setups	43
2.3 HO ₂ generation	44

2.4 Aerosol generation	45
2.5 The reaction flow tube	47
2.5.1 A description of the reaction flow tube.....	47
2.5.2 The flow regime in the reaction flow tube.....	49
2.5.3 The temperature in the reaction flow tube	52
2.6 Particle detection and characterisation.....	54
2.6.1 The measurement of the total particle surface area.....	54
2.6.2 Characterising the phase of the aerosols	60
2.6.3 Characterising the metal ion content of the aerosols	63
2.7 Measurement of HO ₂ and FAGE calibration.....	64
2.8 The data analysis procedure for moving injector experiments	69
2.9 The data analysis procedure for fixed injector experiments	74
2.10 The data analysis procedure for mineral dust experiments.....	76
2.11 The error analysis procedure.....	79
2.12 Differences in the data analysis when the flow tube is not at room temperature or at atmospheric pressure.....	82
2.12.1 Correction of the aerosol surface area when the flow tube is not at room temperature	82
2.12.2 Correction of the diffusion coefficient when the flow tube is not at room temperature or atmospheric pressure	84
2.13 Hydrogen peroxide measurements.....	85
2.14 The Cape Verde box model	85
2.15 Summary	86
Chapter 3: Measurements of the HO₂ uptake coefficient onto inorganic salts at room temperature and atmospheric pressure	88
3.1 The importance of aerosols containing inorganic salts.....	88
3.2 Measurements of the HO ₂ uptake coefficient onto solid inorganic aerosols at room temperature	89
3.3 Measurements of the HO ₂ uptake coefficient onto aqueous inorganic aerosols at room temperature	93
3.4 Measurements of the HO ₂ mass accommodation onto copper-doped inorganic aerosols at room temperature	96
3.5 The HO ₂ uptake coefficient dependence upon copper and iron concentrations	99
3.6 The HO ₂ uptake coefficient dependence upon the pH of the aerosol.....	105
3.7 The HO ₂ uptake coefficient dependence upon relative humidity for aqueous aerosols	108

3.8 The dependence of uptake coefficients upon reaction time and initial radical concentration.....	111
3.9 Laboratory studies for the time dependence of the HO ₂ uptake coefficient onto aqueous aerosols	113
3.10 Laboratory studies for the HO ₂ uptake time dependence onto aqueous copper doped aerosols	116
3.11 Laboratory studies for the dependence of the HO ₂ uptake coefficient upon the initial HO ₂ concentration.....	118
3.12 Atmospheric Implications.....	121
3.13 Summary	124
Chapter 4: Measurements of the HO₂ uptake coefficient onto organic aerosols at room temperature and atmospheric pressure.....	126
4.1 The importance of organic aerosols in the troposphere	126
4.2 Measurements of the HO ₂ uptake coefficient onto single component organic aerosols	127
4.3 The uptake coefficient dependence upon humidity for humic acid aerosols.....	135
4.4 Measurements of the HO ₂ uptake coefficient onto copper doped sucrose aerosols	137
4.5 Measurements of the HO ₂ uptake coefficient onto copper doped ammonium sulphate aerosols containing EDTA	140
4.6 Measurements of the HO ₂ uptake coefficient onto copper doped ammonium sulphate aerosols also containing different atmospherically relevant organic compounds	143
4.7 Atmospheric implications	147
4.8 Summary	149
Chapter 5: Measurements of the HO₂ uptake coefficient onto secondary organic aerosols at room temperature	152
5.1 The importance of secondary organic aerosols.....	152
5.2 Comparison of instrument performance between the experimental setups at Leeds and PSI.....	154
5.3 Measurements of HO ₂ uptake coefficient measurements onto α -pinene and trimethylbenzene derived aerosols.....	155
5.4 Discussion of the HO ₂ uptake coefficient measurements onto α -pinene and trimethylbenzene derived aerosols.....	163
5.5 Atmospheric Implications.....	166
5.6 Summary	167
Chapter 6: Measurements of the HO₂ uptake coefficient onto inorganic salts at temperatures between 263 and 314 K and at atmospheric pressure.....	168
6.1 The importance of measuring the HO ₂ uptake coefficient over a range of temperatures	168

6.2 Measurements of HO ₂ uptake coefficients onto effloresced sodium chloride and ammonium sulphate aerosols over a range of temperatures	169
6.3 Measurements of HO ₂ uptake coefficients onto deliquesced ammonium nitrate aerosols over a range of temperatures	174
6.4 Measurements of HO ₂ uptake coefficients onto copper doped ammonium nitrate aerosols over a range of temperatures.....	182
6.5 Atmospheric Implications	188
6.6 Summary	189
Chapter 7: Measurements of the HO₂ uptake coefficient onto dust aerosols at room temperature	192
7.1 The importance of dust aerosols in the troposphere	192
7.2 Measurements of the HO ₂ uptake coefficient onto ATD aerosols.....	193
7.3 The HO ₂ uptake coefficient onto ATD aerosols as a function of relative humidity....	197
7.4 The HO ₂ uptake coefficient onto ATD aerosols as a function of the initial HO ₂ concentration.....	199
7.5 The HO ₂ uptake coefficient onto ATD aerosols as a function of time	206
7.6 The HO ₂ uptake coefficient onto cosmic dust	209
7.6 Atmospheric Implications	211
7.7 Summary	214
Chapter 8: Modelling of the HO₂ uptake coefficient using the KM-SUB model.....	217
8.1 The importance of modelling the HO ₂ uptake coefficient	217
8.2 A description of the KM-SUB model developed to calculate the HO ₂ uptake coefficient	218
8.3 Comparing the KM-SUB model to uptake coefficients measured during fixed injector and moving injector experiments.....	224
8.4 Intercomparison of the Thornton et al. expression with the KM-SUB model.....	227
8.5 Modelling of the HO ₂ uptake coefficient time dependence onto aqueous aerosols	233
8.6 Modelling the observed initial HO ₂ concentration dependence of the HO ₂ uptake coefficient onto aqueous aerosols	238
8.6.1 Investigating the effect of the changing aerosol pH due to dissociation of HO ₂ in the aerosol	239
8.6.2 Investigating the effect of a Fenton-like reaction	242
8.7 The dependence of the HO ₂ uptake coefficient upon the aerosol copper concentration	246
8.8 The dependence of the HO ₂ uptake coefficient upon time and initial HO ₂ concentration for copper doped aerosols	249
8.9 Modelling of the effect of changing the viscosity of the aerosols upon the HO ₂ uptake coefficient	253

8.10 Atmospheric Implications	255
8.11 Summary and future work	259
Chapter 9: Conclusions and future work	262

List of Tables

1.1 Methods that have been used and aerosols that have been studied to measure HO ₂ uptake coefficients in the literature.....	30
1.2 Macintyre and Evans' HO ₂ uptake coefficient parameterisations for different types of aerosols.....	34
2.1 Literature values for the deliquescence and efflorescence of some types of aerosol at 298K.....	60
3.1 Summary of HO ₂ uptake coefficients that have been measured for solid inorganic salt aerosols.....	92
3.2 Summary of HO ₂ uptake coefficients that have been measured for aqueous inorganic salt aerosols at a temperature of 293 ± 2 K.	95
3.3 Summary of HO ₂ uptake coefficients that have been measured for aqueous copper-doped aerosols at a temperature of 293 ± 2 K.	99
4.1 The HO ₂ uptake coefficient onto single component organic aerosols measured in this work and published in the literature at 293 ± 2.	131
4.2 Iron (II and III) concentrations that were measured in the atomiser solutions using ICP-MS for different organics dissolved in mQ water.	133
4.3 Copper (I and II) concentrations that were measured in the atomiser solutions using ICP-MS for different organics dissolved in mQ water.	133
4.4 The uptake coefficients that were measured for copper (II) sulphate doped ammonium aerosols containing either a 2 to 1 or 10 to 1 organic to copper molar ratio.	147
5.1 Summary of the reactants and conditions that were utilised for the HO ₂ uptake coefficient experiments that were carried out at the Paul Scherrer Institute.	162
6.1 The HO ₂ uptake coefficient onto effloresced sodium chloride and ammonium sulphate aerosols over a range of temperatures and at atmospheric pressure.	171
6.2 The HO ₂ uptake coefficient onto aqueous ammonium nitrate aerosols over a range of temperatures and at atmospheric pressure.	178
6.3 The HO ₂ mass accommodation onto aqueous copper-doped ammonium nitrate aerosols over a range of temperatures and at atmospheric pressure.	186
7.1 The HO ₂ uptake coefficients onto Arizona Test Dust aerosols measured in this work and published in the literature for ATD coated solid surfaces at different relative humidities, initial HO ₂ concentration and temperatures.	196
8.1 The initial parameters used in the KM-SUB HO ₂ uptake model.	223
8.2 The initial copper, HO ₂ and H ₂ O ₂ concentrations inputted into the KM-SUB model. ...	243
8.3 The three different sets of parameters used in the KM-SUB model.	243

List of Figures

1.1 The impact that different factors have on radiative forcing.	2
1.2 Typical number and volume distributions of atmospheric particles within the different aerosol modes.	4
1.3 The changing water content of sodium chloride aerosols as a function of relative humidity.	6
1.4 A schematic of the HO _x cycle.	7
1.5 A schematic of the different steps involved in the uptake of a gas-phase species in a liquid aerosol.	15
1.6 The median vertical profiles of different species during the ARCTAS campaign.	18
1.7 A schematic of the resistor model.	19
1.8 A schematic of the different layers within the KM-SUB model.	24
1.9 Measurements of the HO ₂ uptake coefficient published in the literature up to 2010.	32
1.10 The HO ₂ uptake coefficient calculated from the Thornton expression for aqueous aerosols under different conditions.	36
1.11 The HO ₂ uptake coefficient calculated as a function of copper molarity in the aerosol.	38
2.1 A schematic diagram of the experimental apparatus for the measurement of the kinetics of HO ₂ uptake.	42
2.2 The experimental setup for experiments performed in Leeds.	43
2.3 A schematic of the atomiser.	46
2.4 Cross-sectional view of the aerosol flow tube used in the uptake experiments.	48
2.5 Schematic of turbulent and laminar flow.	49
2.6 The O ₃ signal normalized to the signal at 30 cm obtained when moving the injector backwards and forwards along the flow tube.	51
2.7 The FAGE HO ₂ signal in the presence of ammonium sulphate aerosols at different injector positions along the flow tube.	52
2.8 The temperature gradients along the flow tube when the chiller was set to -10°C and 40°C.	53
2.9 A schematic of the DMA.	55
2.10 A graph showing the typical aerosol number concentrations and aerosol surface areas obtained per cubic centimetre.	56
2.11 The number distribution of the polystyrene latex beads as a function of diameter measured by the SMPS.	57
2.12 The normalised aerosol number distribution measured by the SMPS and APS for Arizona Test Dust aerosols.	58
2.13 A graph of the measured SMPS aerosol number with and without a second neutralizer in the aerosol flow.	59
2.14 A humidogram for copper-doped ammonium nitrate aerosols.	62

2.15 An example of the decrease in average radius and surface area seen when decreasing the relative humidity.	63
2.16 A schematic of the FAGE cell used to measure HO ₂	65
2.17 A diagram to illustrate the triggering for the PMT gating and photon-counting systems used during the experiments.	67
2.18 An example of the signal due to OH (with the NO off in the FAGE cell) and HO ₂ + OH (with the NO on in the FAGE cell) during a FAGE calibration.	68
2.19 Example of the relationship between the reaction time and the HO ₂ signal.	70
2.20 An example to show the difference between subtracting the wall loss from the observed rate constant and using the Brown correction to correct the observed rate constant.	72
2.21 The first order rate constant plotted against the aerosol surface area in a given volume.	73
2.22 k' plotted against the aerosol surface area when the injector was placed at different positions along the flow tube.	76
2.23 An example of the anticorrelation between the ATD aerosol number concentration and the FAGE signal.	77
2.24 An example of the linear correlation between the $\ln(\text{signal} - \text{background})$ and the Arizona Test Dust aerosol number concentration.	78
2.25 The gradient of the exponential fits such as those shown in Figure 2.24 ($0.25\gamma_{obs}A_{dt}$) plotted against time.	79
3.1 Examples of the pseudo-first order rate constant as a function of surface area for effloresced ammonium sulfate and sodium chloride aerosols at room temperature and atmospheric pressure.	90
3.2 Examples of the pseudo-first order rate constant as a function of surface area for aqueous sodium chloride, ammonium sulphate and ammonium nitrate aerosols at 293 ± 2 K and atmospheric pressure.	93
3.3 The pseudo first order rate constant as a function of surface area for ammonium sulphate aerosols and copper doped ammonium sulphate.	98
3.4 The HO ₂ signal with aerosols to that without aerosols as a function of copper (II) concentrations within the aerosols measured by Mozurkewich et al. (1987).	100
3.5 The HO ₂ uptake coefficient as a function of the estimated Cu(II) molality in the ammonium sulphate aerosols.	102
3.6 The inverse HO ₂ uptake coefficient as a function of the inverse of the estimated Cu(II) molality in the ammonium sulphate aerosols.	103
3.7 The HO ₂ uptake coefficient as a function of the estimated Fe molality in the ammonium sulphate aerosols.	105
3.8 The HO ₂ uptake coefficient for sodium chloride aerosols with hydrochloric acid or sodium hydroxide added into the atomiser solutions and ammonium sulphate aerosols containing a mixture of potassium hydrogen phthalate or potassium dihydrogen orthophosphate.	107
3.9 HO ₂ uptake coefficients for aqueous ammonium nitrate aerosols as a function of relative humidity.	110

3.10 The NO ₂ uptake coefficient onto soot surfaces measured by Ammann et al. (1998), Ammann et al. (1997) and by Gerecke et al. (1998).	112
3.11 The average uptake coefficient between time zero and the given time for ammonium nitrate and sodium chloride aerosols at different HO ₂ concentrations.	114
3.12 The average mass accommodation between time zero and the given time for copper-doped ammonium sulphate aerosols.	118
3.13 The pseudo-first order rate constant as a function of aerosol surface area for ammonium nitrate aerosols at an initial HO ₂ concentration of $1.1 \times 10^9 \text{ cm}^{-3}$ and $2.7 \times 10^9 \text{ cm}^{-3}$. ..	120
3.14 The effect of varying the HO ₂ uptake coefficient upon the HO ₂ gas phase concentrations under Cape Verde conditions.	122
4.1 The pseudo first order rate coefficient for HO ₂ loss as a function of aerosol surface area for different single component organic aerosols.	128
4.2 The HO ₂ uptake coefficient as a function of humidity for different single component organic aerosols measured in this work.	129
4.3 HO ₂ uptake coefficient as a function of relative humidity for aerosols containing a 20 to 1 sucrose to copper sulphate molar ratio.	139
4.4 The Cu : EDTA complex.	141
4.5 The HO ₂ uptake coefficient for aerosols containing a 20 to 1 ammonium sulphate to copper molar ratio as a function of the molar ratio of EDTA to copper in the aerosols.	141
4.6 The HO ₂ uptake coefficient as a function of copper molarity for aerosols containing a 20 to 1 ammonium sulphate to copper molar ratio and different concentrations of EDTA.	143
4.7 The pseudo first order rate coefficients as a function of aerosol surface area for copper doped ammonium sulfate aerosols and with malonic acid, citric acid, 1,2 diaminoethane, tartronic acid, EDTA and oxalic acid added.	146
5.1 The oxidation of α -pinene and 1,3,5 trimethylbenzene by OH.	153
5.2 The pseudo-first order rate constant as a function of aerosol surface area for ammonium sulphate aerosols and copper sulphate doped ammonium sulphate aerosols.	155
5.3 The PSI smog chamber housed in the wooden enclosure and the PSI PAM chamber. ..	158
5.4 The pseudo-first-order rate constants as a function of aerosol surface area for α -pinene derived aerosols and trimethylbenzene derived aerosols.	161
6.1 Examples of the pseudo-first order rate constant as a function of aerosol surface area for effloresced sodium chloride and effloresced ammonium sulphate at 263 K and 312 K.	170
6.2 The HO ₂ uptake coefficient measured onto effloresced sodium chloride aerosols in this work and onto surfaces coated with effloresced sodium chloride by Remorov et al. (2002) and Loukhovitskaya et al. (2009) over a range of temperatures.	172
6.3 The HO ₂ uptake coefficient onto effloresced sodium chloride aerosols and effloresced ammonium sulfate aerosols measured in this work as a function of temperature.	174

6.4	Examples of the pseudo first order rate constant as a function of aerosol surface area for aqueous ammonium nitrate aerosols at 263 K and 312 K.	177
6.5	The average HO ₂ uptake coefficients measured in this work onto aqueous ammonium nitrate aerosols as a function of temperature.	179
6.6	The free energy diagram first postulated by Nathanson et al. (1996) for the liquid vapour interface.	184
6.7	Examples of the pseudo-first order rate constant as a function of aerosol surface area for aqueous copper doped ammonium nitrate aerosols at 263 K and 292 K.	185
6.8	$\ln(\alpha / (1 - \alpha))$ as a function of $1000 / T$ for copper doped ammonium nitrate aerosols.....	186
7.1	Examples of $0.25\gamma\omega A_d t$ as a function of time at initial HO ₂ concentrations of $\sim 1 \times 10^9$ molecule cm ⁻³ and $\sim 3 \times 10^8$ molecule cm ⁻³ and at 10% RH and 70 % RH for Arizona Test Dust aerosols.	194
7.2	The measured HO ₂ uptake coefficient onto Arizona Test Dust aerosols at an initial HO ₂ concentration of 1×10^9 molecule cm ⁻³ and as a function of relative humidity.	197
7.3	The HO ₂ uptake coefficient as a function of relative humidity at an initial HO ₂ concentration of $\sim 1 \times 10^9$ molecule cm ⁻³ and $\sim 3 \times 10^8$ molecule cm ⁻³	200
7.4	The average uptake coefficient measured along the flow tube as a function of the HO ₂ concentration when the injector was placed at 30 cm along the flow tube.	202
7.5	Average HO ₂ uptake coefficient between time 0 and the given reaction time on the x-axis at a relative humidity of 10 % and at initial HO ₂ concentration of 1×10^9 molecule cm ⁻³ and 3×10^8 molecule cm ⁻³	207
7.6	Examples of $0.25\gamma\omega A_d t$ as a function of time for ATD and cosmic dust at a relative humidity of 10%, at 293 ± 2 K and at an initial HO ₂ concentration of 1×10^9 molecule cm ⁻³	210
7.7	The decrease in the solar noon maximum HO ₂ concentration using the Cape Verde model for different dust surface area concentrations and assuming a HO ₂ uptake coefficient of 0.031 ± 0.008	213
7.8	Schematic of the main reactions and processes that would need to be inputted into a model to understand HO ₂ uptake to dust aerosols.	215
8.1	A schematic of the KM-SUB model adapted for HO ₂ uptake.	219
8.2	An example of the actual HO ₂ uptake coefficient outputted by the model at each time point and the average HO ₂ uptake coefficient between time zero and each time point outputted by the KM-SUB model.	226
8.3	The simplified relationship between fixed injector experiments and the moving injector experiments.	227
8.4	The KM-SUB model output for the HO ₂ uptake coefficient as a function of time for 100 nm aqueous aerosols at a pH of 5 and with the gas phase HO ₂ concentration set to a constant concentration of 5×10^8 molecule cm ⁻³ and the temperature set to 293 K.	230
8.5	A comparison between the HO ₂ uptake coefficients predicted by the Thornton et al. model and from the KM-SUB model.	231

8.6 The HO ₂ concentration near the surface of the aerosol as a function of time and the flux of HO ₂ colliding with the surface of the aerosol as a function of time.	232
8.7 A comparison between the equilibrated HO ₂ uptake coefficients predicted by the Thornton et al. model and from the KM-SUB model as a function of aerosol copper molarity.	233
8.8 The HO ₂ uptake coefficient measured in this work for aqueous sodium chloride aerosols and outputted by the KM-SUB model assuming pH and HO ₂ concentration does not change over time.	235
8.9 The HO ₂ uptake coefficient measured in this work for aqueous sodium chloride aerosols and outputted by the KM-SUB model with changing HO ₂ concentrations.	236
8.10 The HO ₂ concentration decay over time obtained in this work for sodium chloride aerosols and predicted by the KM-SUB model.	237
8.11 The measured HO ₂ uptake coefficient onto aqueous sodium chloride aerosols with an initial HO ₂ concentration of 2.1×10^9 molecule cm ⁻³ and 7.1×10^8 molecule cm ⁻³ as a function of time and comparison with the KM-SUB model.	238
8.12 The change in the aerosol pH and the HO ₂ uptake coefficient as a function of time for sodium chloride aerosols with an initial HO ₂ concentration of 2.1×10^9 molecule cm ⁻³ and 7.1×10^8 molecule cm ⁻³ and for ammonium nitrate aerosols at an initial HO ₂ concentration of 1×10^9 molecule cm ⁻³ as a function of time.	240
8.13 The HO ₂ uptake coefficient for sodium chloride aerosols with hydrochloric acid or sodium hydroxide added into the atomiser solutions measured in this work and predicted by the KM-SUB model.	241
8.14 The HO ₂ uptake coefficient as a function of time for sodium chloride aerosols with an initial HO ₂ concentration of 2.1×10^9 molecule cm ⁻³ and 7.1×10^8 molecule cm ⁻³ and for ammonium nitrate aerosols at an initial HO ₂ concentration of 1×10^9 molecule cm ⁻³ as a function of time with a Fenton-like reaction added into the KM-SUB model.	245
8.15 The HO ₂ uptake coefficient as a function of time for sodium chloride aerosols with an initial HO ₂ concentration of 2.1×10^9 molecule cm ⁻³ and 7.1×10^8 molecule cm ⁻³ and for ammonium nitrate aerosols at an initial HO ₂ concentration of 1×10^9 molecule cm ⁻³ as a function of time with a Fenton-like reaction added into the KM-SUB model and with different reaction rate constants.	246
8.16 The HO ₂ uptake coefficient dependence upon the aerosol copper ion concentration measured in this work and predicted by the KM-SUB model.	249
8.17 The HO ₂ uptake coefficient outputted by the KM-SUB model for copper doped aerosols as a function of time.	251
8.18 The HO ₂ gas phase concentrations outputted by the KM-SUB model for copper doped aerosols as a function of time.	252
8.19 The HO ₂ uptake coefficients onto copper-doped sucrose aerosols measured in this work as a function of humidity and predicted by the KM-SUB model.	254
8.20 An example of the time evolution of the HO ₂ uptake coefficient for aqueous non-copper doped aerosols calculated by KM-SUB at different HO ₂ concentrations.	256

8.21 An example of the time evolution of the HO₂ uptake coefficient for aqueous non-copper doped aerosols calculated by KM-SUB at different aerosol sizes and concentrations. .257

8.22 An example of the time evolution of the HO₂ uptake coefficient for aqueous non-copper doped aerosols calculated by KM-SUB at different temperatures. 258

List of Abbreviations

AIDA	Aerosol Interaction and Dynamics in the Atmosphere
AIM	Aerosol Inorganic Model
AMS	Aerosol Mass Spectrometer
APS	Aerodynamic Particle Sizer
ARCTAS	Arctic Research of the Composition of the Troposphere from Aircraft and Satellites
ATD	Arizona Test Dust
BET	Brunauer-Emmett-Teller
CCN	Cloud Condensation Nuclei
CIMS	Chemical Ionization Mass Spectrometry
CPC	Condensation Particle Counter
DMA	Differential Mobility Analyzer
DMPS	Differential Mobility Particle Sizer
DOAS	Differential Optical Absorption
EDTA	Ethylenediaminetetraacetic acid
EPA	Environmental Protection Agency
EU	European Union
FAGE	Fluorescence Assay by Gas Expansion
GEOS-CHEM	Goddard Earth Observing System - Chemistry
HDPE	High-density polyethylene
HEPA	High Efficiency Particulate Air
ICP-MS	Inductively-Coupled Plasma Mass Spectrometry
IPCC	Intergovernmental Panel on Climate Change
K2-SURF	Kinetic double-layer model of aerosol surface chemistry and gas-particle interactions
KM-SUB	Kinetic multi-layer model of aerosol surface and bulk chemistry
MBL	Marine Boundary Layer
MCM	Master Chemical Mechanism
MEA	Mono ethanol amine sulphate
MFC	Mass Flow Controller
MIESR	Matrix Isolation Electron Spin Resonance
MMS	mono methyl amine sulphate
PAM	Potential Aerosol Mass
PM _{2.5}	Particulate matter smaller than 2.5 μm in diameter
PMT	Photomultiplier tube
PSC	Polar Stratospheric Clouds
PSI	Paul Scherrer Institute
PSL	Polystyrene latex
PTFE	Polytetrafluoroethylene

RH	Relative humidity
RHaMBLe	Reactive Halogens in the Marine Boundary Layer
SAMUM	Saharan Mineral Dust Experiment
SAPHIR	Simulation of Atmospheric PHotochemistry In a large Reaction Chamber
SMPS	Scanning Mobility Particle Sizer
SOA	Secondary Organic Aerosol
TMB	1,3,5 trimethylbenzene
TMI	Transition metal ion
UV	Ultraviolet

Chapter 1: Introduction

1.1 The importance of understanding atmospheric chemistry

Two of the major challenges facing society in the twenty first century are climate change and atmospheric pollution. A warmer troposphere (the lowest 10 – 15 km of the atmosphere) may lead to problems such as rising sea levels, changes in the patterns of precipitation and an increase in the frequency and severity of extreme weather events whereas atmospheric pollution is directly attributable to the deaths of many millions of people a year, as will be discussed below. In order to minimise both global warming and air pollution the overall physical structure and chemical composition of the atmosphere and the processes and reactions that control these need to be better understood, so that they can be included into mathematical models of the atmosphere. Using these mathematical models projections of future climate change and air quality can be made for different emission scenarios.

As discussed above, one of the main reasons for understanding atmospheric chemistry is to be able to predict future climate change, and thereby to reduce global warming. Since the beginning of the industrial revolution concentrations of greenhouse gases, such as CO₂, O₃, N₂O and CH₄, have increased (IPCC, 2013). These gases absorb infrared radiation and then re-emit it. The radiation is then converted to thermal energy via collisions that warm the troposphere. The global average temperature has been estimated to have increased by 0.85°C since 1880 (IPCC, 2013). Aerosols also play a part in climate change as they absorb and scatter radiation, and can change cloud properties. Radiative forcing (ΔF) is the change in net irradiance at the tropopause after a perturbation in the radiative energy budget of the Earth's climate system and may be due to changes in the concentrations of gas species or aerosols, changes in solar irradiance or changes in the reflectivity of the Earth's surface. A positive forcing tends to warm the troposphere, while a negative forcing tends to cool it. The radiative forcing is related to the surface temperature of the Earth (ΔT_S) and the climate sensitivity (λ) as shown by Equation 1.1:

$$\Delta T_S = \lambda \Delta F \quad (\text{E1.1})$$

The radiative forcing due to different greenhouse gases, aerosols and solar irradiance is presented in Figure 1.1. Figure 1.1 shows that there are still large uncertainties in the radiative forcing due to many atmospheric species.

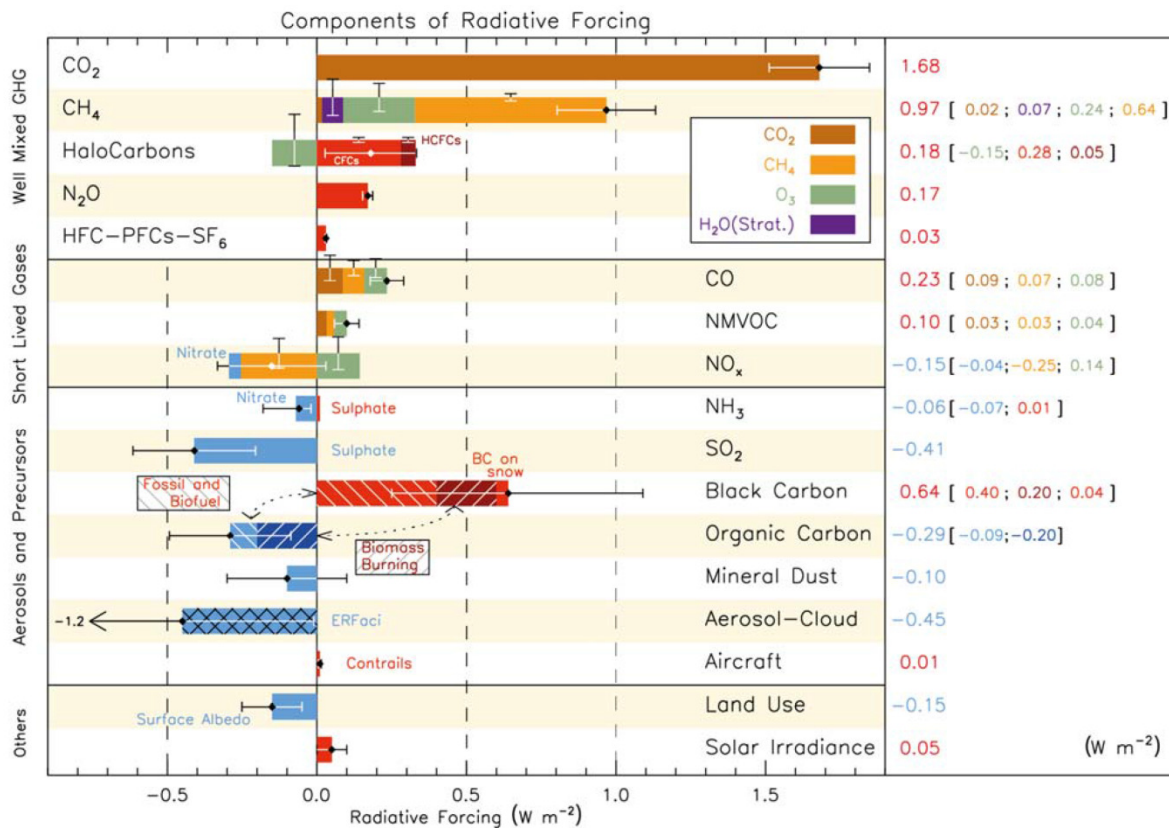


Figure 1.1: The impact that different factors have on radiative forcing. This figure is reproduced from the IPCC report (2013) on climate change.

The second major reason for having a thorough understanding of the chemistry of the atmosphere is in order to be able to predict and reduce concentrations of pollutants. One of the most serious pollutants in the atmosphere is ozone that can cause severe respiratory problems, and is formed in the presence of volatile organic compounds (VOCs), NO_x and sunlight. Scientists in the United States Environmental Protection Agency (EPA) have stated that ozone levels as low as 40 ppb can cause health effects in susceptible people (Weinhold, 2008). Aerosols can also cause severe health problems such as respiratory and cardiac problems. Particles which are smaller than 2.5 μm in diameter (PM_{2.5}) can be deposited in

the alveolar region of the lungs where gas exchange occurs (Seinfeld and Pandis, 2006). A recent modelling study estimated that 3.5 million cardiopulmonary and 220,000 lung cancer cases were attributable to the anthropogenic component of PM_{2.5} each year (Anenberg et al., 2010). EU legislation now states that the concentration of aerosols which are smaller than 10 μm in diameter (PM₁₀) should not exceed a yearly average of 40 $\mu\text{g m}^{-3}$ and a daily average of 50 $\mu\text{g m}^{-3}$ (<http://ec.europa.eu/environment/air/quality/standards.htm>).

1.2 The importance of aerosols in the troposphere

Aerosols have a diameter of ~ 1 nm to ~ 100 μm and are suspended in air. Smaller particles can be considered as clusters whereas larger particles will sediment out. The smallest aerosols with a diameter of less than 0.1 μm are known as the Aitken mode and provide the greatest number of aerosols in the troposphere. The accumulation mode consists of aerosols with a radius of $\sim 0.1 - 5$ μm , and the coarse mode consists of aerosols with a radius of 1 – 100 μm . Aerosols with a diameter of greater than 0.1 μm provide the greatest aerosol volume (or aerosol mass) in the troposphere. The coarse mode is dominated by aerosols that are formed by either wind or by erosion such as dust, sea salt and pollens, whereas the other modes tend to be formed by primary emissions, coagulation of smaller particles and secondary gas to particle conversion (Seinfeld and Pandis, 2006). The main components of the aerosol size distribution are shown in Figure 1.2.

As well as categorising aerosols by size, aerosols can also be classed as either primary or secondary. Primary aerosols are directly emitted into the atmosphere, and secondary aerosols are formed by gas-to-particle conversion. Primary aerosols include sea salt, mineral dust, biogenic aerosol (for example, pollen and spores) and carbonaceous aerosol (organic and black carbon). Examples of secondary aerosols include sulphate aerosol, secondary organic aerosol (formed by the oxidation of VOCs) and nitrate aerosol. Different aerosols tend to dominate in different locations around the world. Sulphate aerosols are found in the northern midlatitudes near industrial estates and are also generated by coal-burning power plants and oil refineries. Mineral dust has its highest concentrations in the equatorial Atlantic as this is just below the Sahara desert. Organic carbon is an important aerosol over regions of South America and Africa that burn biomass. Sea salt aerosols dominate in the high latitude oceans

(especially during winter), and are formed through wind and wave action on the surface layer of seawater. Finally, black carbon aerosols have high concentrations in particularly industrialised regions (NE US, Europe, SE Asia).

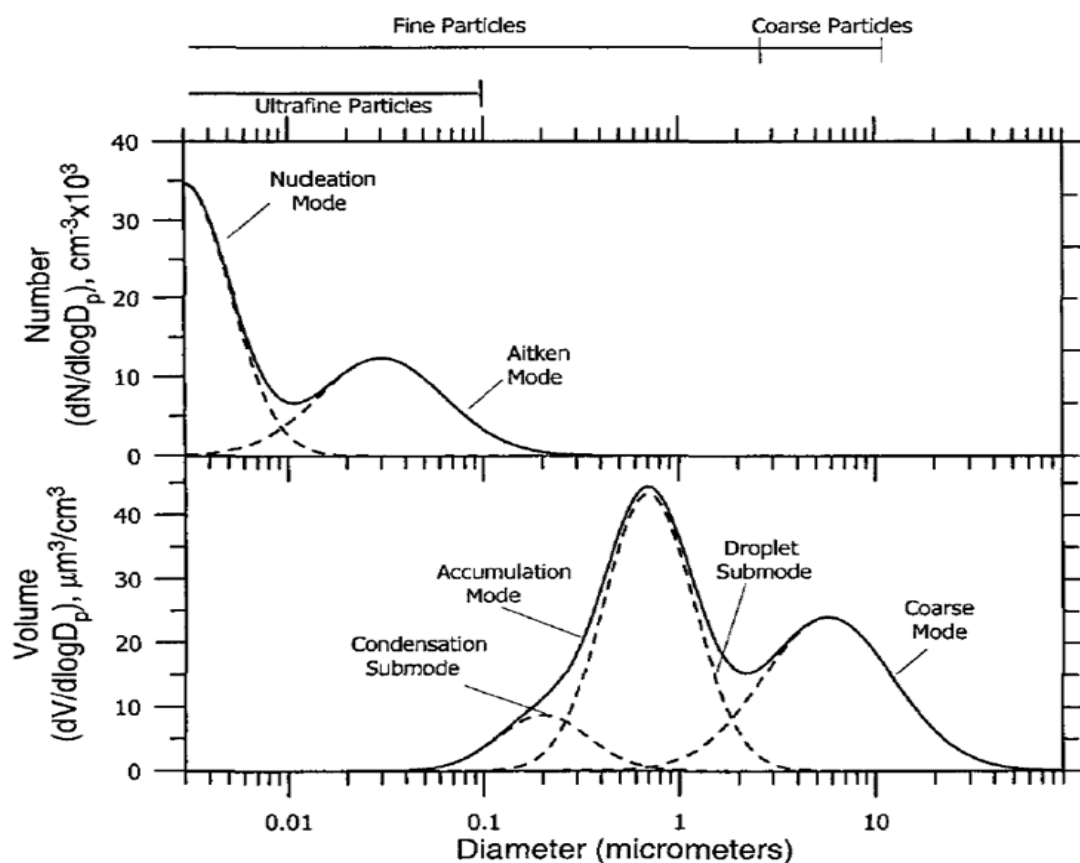


Figure 1.2: Typical number and volume distributions of atmospheric particles within the different aerosol modes. The figure is reproduced from Seinfeld and Pandis (2006).

Typical aerosol loadings in the troposphere vary from $\sim 1 \mu\text{g m}^{-3}$ to $100 \mu\text{g m}^{-3}$ although higher concentrations have been observed (Seinfeld and Pandis, 2006). For example, Schladitz et al. (2011) measured aerosol loadings of up to $542 \mu\text{g m}^{-3}$ in Cape Verde during January and February 2008 using a Differential Mobility Particle Sizer (DMPS) and an Aerodynamic Particle Sizer. PM_{2.5} levels in Beijing during January 2013 were recorded to have exceeded $800 \mu\text{g m}^{-3}$ (B.B.C. News, 2013). Other studies have collected aerosols on filters in order to estimate the average aerosol loadings over a given period and to estimate metal concentrations in the atmosphere, by extracting the metals from the filters and analysing the solutions using inductively coupled mass spectrometry (ICP-MS) (Laing et al.,

2014). The composition of tropospheric aerosols has also been measured in various locations using aerosol mass spectrometers (AMS). For example, Zhang et al. (2014) measured the composition of submicron aerosols using an AMS in Beijing in January 2013. Aerosols consisted of organics (50%), sulphate (22 %), nitrate (14 %), ammonium (10 %), and chloride (4 %), excluding water.

Aerosols are an extremely important constituent of the atmosphere as they can scatter and absorb radiation, and can act as cloud condensation nuclei. Aerosols can also have a large impact on health by causing and enhancing respiratory, cardiovascular, infectious and allergic diseases. Finally, aerosols can also affect the concentrations of trace gases and radicals in the atmosphere by heterogeneous chemical reactions, which is the subject of the work within this thesis. The composition of the aerosols may also be affected during these reactions. The oxidation products of some particle bound organics may also be more toxic than the original substance. For example, this is the case for polycyclic aromatic hydrocarbons (Atkinson and Arey, 1994).

The efficiency of heterogeneous chemistry can depend on both the composition and the phase of an aerosol. Some aerosols can exist as either a solid or a liquid depending on the relative humidity that can vary greatly within the troposphere. An example of an aerosol that can behave in this way is sodium chloride as shown in Figure 1.3. At low humidities the sodium chloride aerosols will be solid (point A in Figure 1.3). As the relative humidity increases the aerosol will remain solid (point B in Figure 1.3) until it reaches the deliquescence point which is the humidity at which the aerosol spontaneously absorbs water to become aqueous (point C in Figure 1.3). As the humidity keeps increasing the aerosol will grow as it absorbs more water (point D in Figure 1.3) in order to maintain thermodynamic equilibrium with the surroundings. However, as the humidity decreases the aerosol will decrease in size (point E in Figure 1.3) but will not crystallise until the efflorescence point (point F in Figure 1.3) where the aerosols reach a critical supersaturation. Deliquescence and efflorescence points of other aerosol types are given in Section 2.6.2. Figure 1.3 was obtained using the Aerosol Inorganic Model (AIM) which allows the aqueous phase concentrations of different salts and water to be calculated at different relative humidities and temperatures and is based upon experimental work published in the literature (Clegg et al., 1998; Wexler and Clegg, 2002).

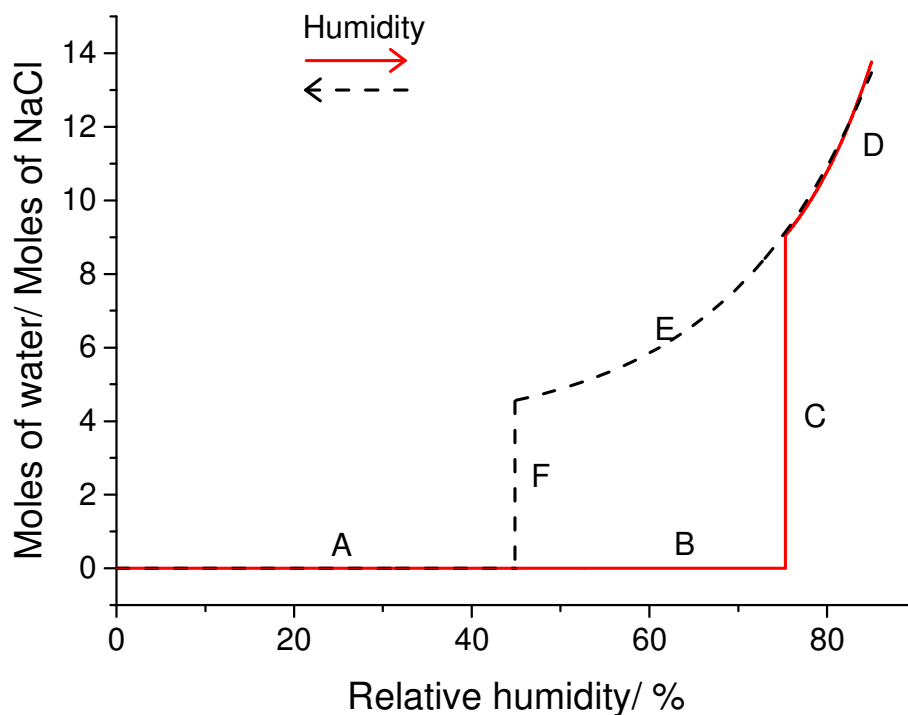


Figure 1.3: The changing water content of sodium chloride aerosols as a function of relative humidity. The water content is based upon the output of the Aerosol Inorganic Model (Clegg et al., 1998). The deliquescence point was set as 75.3 % RH and the efflorescence point was set as 45 % RH (Biskos et al., 2006; Finlayson-Pitts and Pitts, 2000). The red line represents increasing relative humidity, whilst the dashed black line represents decreasing relative humidity. See text for explanations of the letters A, B, etc.

1.3 The importance of HO_x in the troposphere

In order to be able to more accurately predict and reduce problems such as global warming and pollution, all of the important reactions occurring in the atmosphere must be understood. The two radicals OH and HO_2 play crucial roles in tropospheric chemistry as OH is responsible for the majority of the oxidation in the troposphere, whilst HO_2 cycles back to OH. Figure 1.4 shows the main reactions of OH and HO_2 in the atmosphere.

The ozonolysis of alkenes has also been shown to form OH via a complex set of reactions whereby ozone adds across the alkene double bond forming a Criegee radical which then decomposes to form carbonyl oxide and carbonyl products. The carbonyl oxides can then decompose to form aldehydes and OH (Criegee, 1975; Criegee and Wenner, 1949).

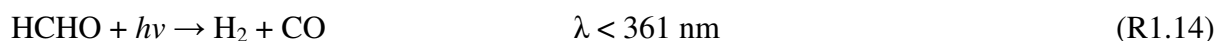
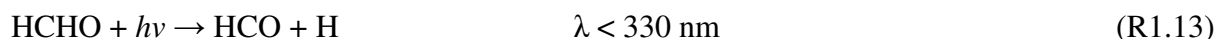
The initial and often rate-determining step for the removal of the majority of the trace gases in the troposphere is their reaction with the OH radical. The reaction of OH with either CO or O₃ will produce the HO₂ radical:



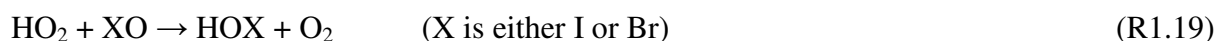
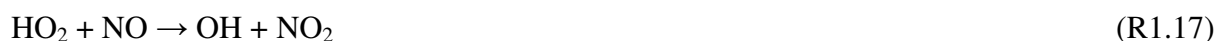
The OH radical can also be converted to HO₂ via a more complicated set of reactions with organic compounds, for example with methane and other alkanes:



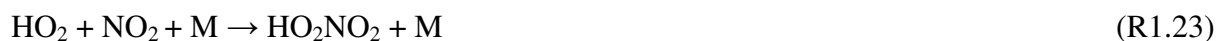
R' represents a molecule with one less CH₂ than R. It should also be noted that HCHO and R'CHO (produced in reaction 1.12) can be transformed into HO₂ via the following reactions:



The HO₂ radical can be cycled back to the OH radical by reaction with the NO radical, ozone or XO (in the presence of UV light) where X is either iodine or bromine. It should be noted that HOX may be removed in the presence of aerosols.



The OH and HO₂ radicals will continue to interconvert with each other until a chain termination step occurs. The loss of HO_x tends to occur through several routes; however, the main ones are the self-reaction of the HO₂ radical, the reaction of HO₂ with organic peroxy radicals (RO₂), the reaction of HO₂ with NO₂ and the formation of HNO₃ by reaction of OH with NO₂:



The products of these reactions (H₂O₂, ROOH and HNO₃) are highly soluble and can therefore be removed by wet deposition. They can also be photolysed releasing OH radicals. However, there are other possible termination reactions for HO_x species in the troposphere. The presence of aerosols has been observed to significantly reduce the HO₂ concentrations in the gas phase (e.g. Taketani et al. (2008)). However, there is some debate as to the exact HO₂ loss mechanism in the presence of aerosols as well as the products of reactions and therefore the loss of HO₂ to aerosols can be represented by Reaction 1.25. The possible mechanisms will be discussed further in Section 1.9 and 1.10.



1.4 HO_x measurement techniques

The OH and HO₂ radicals are difficult to measure in the field due to their short lifetimes of 0.01 – 1 second for OH and 5 – 100 seconds for HO₂, their low ambient concentrations ($\sim 10^6$ molecule cm⁻³ for OH and $\sim 10^8$ molecule cm⁻³ for HO₂) and their high loss rate to surfaces. Therefore, there were a few prerequisites for any instrument that was developed to measure OH and HO₂. First, the method had to be highly sensitive due to the low concentrations of the radicals. Secondly, OH concentrations vary greatly on short spatial scales and therefore the technique needed to sample at one point instead of averaging over a large spatial area. Thirdly, due to the extremely short lifetime of the radicals the measurement technique needed to have a very good temporal resolution. Lastly, it is also very important that more OH is not formed within the instrument whilst measuring. This could occur if lasers are utilised and form O(¹D) through the photolysis of ozone molecules. The O(¹D) molecule could then react via Reaction 1.2 to form two molecules of OH (Heard and Pilling, 2003; Stone et al., 2012).

Several techniques have now been developed to measure OH and HO₂. These techniques were first developed to measure HO_x in the field when OH was first postulated as being responsible for the majority of oxidation in the troposphere (Levy, 1971; Weinstock, 1969). The most widely used methods are laser induced fluorescence spectroscopy at low pressure, known as Fluorescence Assay by Gas Expansion (FAGE). However, Chemical Ionization Mass Spectrometry (CIMS), Differential Optical Absorption (DOAS) and Matrix Isolation Electron Spin Resonance (MIESR) have also been utilised to make HO_x measurements although MIESR is no longer used and DOAS is now only used in the Simulation of Atmospheric PHotochemistry In a large Reaction Chamber (SAPHIR) at Jülich. Each of these techniques is discussed in greater detail below.

1.4.1 Fluorescence Assay By Gas Expansion

FAGE is a low pressure laser induced fluorescence technique. By using a laser pulse it is possible to excite electrons, in the OH radical to an excited level, which may then drop down to the ground state producing fluorescence that can be measured and recorded. FAGE has

overcome the majority of the problems that previous laser induced fluorescence (LIF) instruments had when measuring OH. By operating at low pressure the number density of H₂O vapour is reduced significantly reducing quenching and its reaction with O(¹D) (Hard et al., 1979; Heard and Pilling, 2003). Moreover, a high proportion of the daylight background scattered light is excluded by the sampling nozzle. The low pressure also means that the OH fluorescence lifetime is extended beyond the length of the laser pulse, and that the Rayleigh and Mie scattering is reduced significantly which reduces the laser scattered background signal (Hard et al., 1979). Gating is used in the FAGE technique and can be described as making the first dynode negative compared to the photocathode in the photomultiplier tube for a period of time. This stops the flow of electrons along the photomultiplier tube and it is used in order to reduce the after pulse signal which is temporarily broad and overlaps with the OH fluorescence. A combination of a rotary pump and a roots blower can achieve a very fast linear flow and is used in the FAGE method to remove any OH that is produced by the O(¹D)/ H₂O reactions prior to the next laser pulse arriving. Although not much OH is produced and detected by the same laser pulse any O(¹D) that is formed would carry on reacting and would be detected by the next pulse. FAGE uses the 308 nm A-X (0,0) OH absorption band instead of the 282 nm (1,0) OH band used in the original FAGE system as the absorption cross section is approximately six times higher than at 282 nm and the O₃/H₂O interference is about 30 times less (Smith and Crosley, 1990; Zeng et al., 1998).

FAGE can measure HO₂ as well as OH. The main method of measuring HO₂ is by the chemical conversion of HO₂ into OH followed by the detection of OH by FAGE. This chemical conversion occurs by adding NO to the HO₂. Sufficient NO must be added so that there is a rapid conversion to OH. However, there is a competing reaction:



The competing reaction means that very high concentrations of NO should be avoided and consequently it is not possible to convert all of the HO₂ into OH. By altering the design of the NO injector, its position, the NO flow rate and the operating pressure it is possible to get high conversions of HO₂ into OH and conversions of up to 95% have been reported (Stevens et al., 1994). It is also possible to measure both OH and HO₂ by having two detectors. However, it should be noted that interferences from RO₂ have been reported (Fuchs et al., 2011; Whalley

et al., 2013). The FAGE cell utilised to make HO₂ measurements in this work will be described in greater detail in Chapter 2.

1.4.2 Other HO_x measurement techniques

Chemical ionisation mass spectrometry (CIMS) is a chemical method for measuring OH which was first developed by Eisele and Tanner (1991). OH is titrated with ³⁴SO₂ to form H₂SO₄ via the following reactions:



The isotope ³⁴SO₂ is utilised to avoid an interference from H₂³²SO₄ which is naturally present in the troposphere at much higher concentrations than H₂³⁴SO₄. The addition of NO₃⁻ (generated from HNO₃) then converts the H₂³⁴SO₄ to H³⁴SO₄⁻:



A background signal can be obtained by addition of propane or hexafluoropropene (Berresheim et al., 2000). The H³⁴SO₄⁻/NO₃⁻ ratio is then detected by mass spectrometry from which an initial OH concentration can be calculated. Similarly to FAGE, HO₂ can be converted to OH by reaction with NO. Although, CIMS is the most sensitive HO_x detection technique, other techniques such as FAGE do not require chemical conversion prior to detection.

Long path differential optical absorption spectroscopy (DOAS) uses the Beer-Lambert law shown in Equation 1.2 to measure the OH concentration, [OH]:

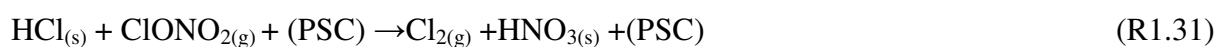
$$[\text{OH}] = \frac{\ln(I_0/I)}{\sigma_{\text{OH},\lambda}l} \quad (\text{E1.2})$$

where I and I_0 are the light intensities with and without OH respectively, $\sigma_{OH,\lambda}$ is the absorption cross section of OH at a wavelength of λ and l is the light path length. This is the only direct OH detection method, and only requires knowledge of the path length and OH absorption cross section. All other methods require calibration. However, DOAS has low sensitivity compared to FAGE and CIMS and also requires long path lengths.

Matrix isolation electron spin resonance (MIESR) is a technique for measuring HO₂ that was developed by Mihelcic et al. (1985). The HO₂ is trapped on an inert solid matrix at low temperatures of ~ 77 K. Electron spin resonance also known as electron paramagnetic resonance involves the movement of the unpaired electron between energy levels. When the electron moves to a lower energy level it emits a photon that can be detected by a spectrometer.

1.6 Heterogeneous chemistry

An example of aerosols taking part in a heterogeneous reaction is the formation of the Antarctic ozone hole. During the Antarctic winter a relatively isolated vortex forms and temperatures in the stratosphere plummet to about 180 to 190 K by mid-winter. Once temperatures fall below 195 K, Polar Stratospheric Clouds (PSCs) form. It is now known that the clouds are formed on liquid sulphate aerosols (Seinfeld and Pandis, 2006). PSCs provide surfaces that can catalyse certain reactions. The most important of these reactions is:



The chlorine gas molecules can then be photolysed, once sunlight returns at the end of the polar night, to produce Cl radicals that then react with ozone to form ClO and O₂. Removal of NO_x from the gas phase to the PSC slows the reformation of reservoir chlorine. A catalytic cycle involving the formation of the ClO dimer leads to major O₃ losses (it should be noted that [O] concentrations are low and therefore there is very little loss of ClO by reaction with O). In March 1995 some of the coldest temperatures ever recorded were experienced in the Arctic stratosphere and at the same time 50% ozone depletion was reported (Seinfeld and Pandis, 2006).

Another example of heterogeneous chemistry is the formation of acid rain. Sulphur dioxide and the OH radical can react in the gas phase to form HOSO₂ that then reacts with O₂ to form SO₃. If the SO₃ then enters an aqueous aerosol, it can react with water as shown by the reaction below to form sulphuric acid:



Acid rain may also be formed when HNO₃ (which is highly soluble) partitions to the aerosol phase. HNO₃ is the product of the reaction of NO₂ with OH.

A useful parameter when investigating the change in concentration of a gas due to aerosols being present is an uptake coefficient (γ). An uptake coefficient is defined as the probability that a molecule impacting a liquid or solid surface undergoes irreversible reaction (Schwartz, 1986b). The uptake coefficient may be different depending on a large variety of factors such as aerosol composition, temperature, aerosol pH and aerosol phase. The phase of both inorganic and organic aerosols may depend on the relative humidity of its surroundings, and whether the aerosols are above or below their deliquescence and efflorescence points as described in Section 1.2. Organic aerosols are believed to be liquids in the atmosphere although recent research has shown that this may not be the case, and that the aerosols may instead be glasses (Virtanen et al., 2010). Due to a large proportion of aerosols being in the liquid phase, one of the most important mechanisms to understand is the uptake of gases by aqueous and liquid aerosols. The mechanism consists of several processes that are illustrated by Figure 1.5.

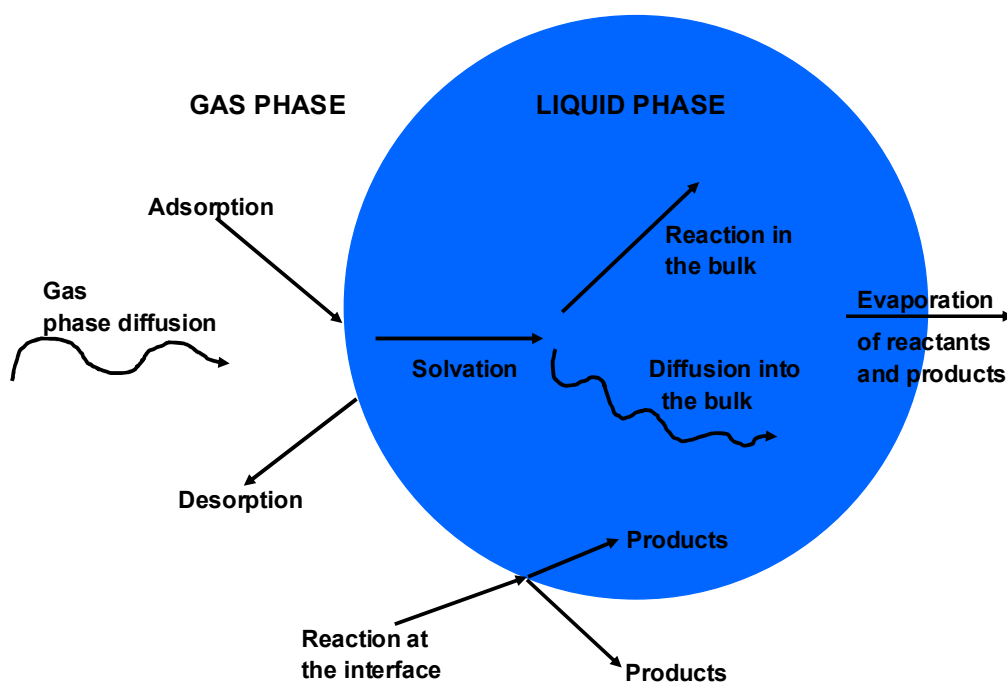


Figure 1.5: A schematic of the different steps involved in the uptake of a gas-phase species in a liquid aerosol. Adapted from Davidovits et al. (2006).

Figure 1.5 shows that many processes may affect the uptake coefficient. These processes are gas phase diffusion to the surface of the aerosol, adsorption and desorption to and from the surface, solvation into the bulk of the aerosol, diffusion into the bulk of the aerosol, reaction at both the interface and in the bulk and evaporation of both the reactants and the products. Depending on the species and the type of aerosol, some processes may become much more important than others. For example, if the aerosol is solid rather than liquid only gas phase diffusion and surface processes can occur. Another example is if the species reacts extremely quickly in the aerosol phase, it will have reacted at the surface before it has a chance to diffuse into the bulk.

The first step of the uptake mechanism illustrated in Figure 1.5 is a molecule in the gas phase diffusing to the surface of the liquid droplet. The molecule may then be adsorbed onto the surface of the aerosol. The probability of the molecule being adsorbed or absorbed is given by a mass accommodation coefficient (α) (also known as the sticking coefficient) which is defined as:

$$\alpha = \frac{\text{Number of gas molecules taken up by the surface}}{\text{Number of gas - surface collisions}} \quad (\text{E1.3})$$

If the molecule is taken up at the surface, then it can cross the interface and enter into the bulk. The rate at which diffusion into the bulk occurs is dependent upon the diffusion coefficient associated with the composition of the aerosol. This step is much slower than the diffusion in the gas phase and it can be the rate determining step for a reaction to occur if there are high reactant concentrations already in the aerosol and the rate of the chemical reaction is high. If there is an equal rate of adsorption and evaporation then a dynamic equilibrium is formed. This occurs if no reaction takes place in the liquid phase, or if there is a slow reaction compared to the uptake and diffusion of the reactant. The dynamic equilibrium is defined by Henry's law constant (H):

$$H = \frac{[X]}{P_X} \quad (\text{E1.4})$$

where $[X]$ is the equilibrium concentration of X (in mol L⁻¹) and P_X is the gas phase equilibrium pressure (in atm) which is related to both the volatility of the species and the temperature.

Once the reactant has been absorbed by the aerosol it may then react. This may occur close to the surface or throughout the whole bulk depending on the rate of the reaction compared to the rate of diffusion of the reactant in the bulk. It is important to note that if the reaction occurs close to the surface the reaction will depend on the aerosol surface area and will be proportional to the square of the radius of the aerosol (r^2), whereas if the reaction occurs throughout the whole bulk the reaction will be dependent upon the aerosol volume and will be proportional to r^3 . Therefore, the size of the aerosol is of great importance.

Liquid water has a typical diffusion coefficient of 10^{-5} cm² s⁻¹. However, the diffusion coefficient is expected to be much smaller in organic aerosols due to organic substances generally having greater viscosities than water (Abramson et al., 2013; Hosny et al., 2013; Power et al., 2013). Therefore, for organic aerosols reactions are much more likely to occur at the surface of the aerosol rather than in the bulk. Some types of gas molecules, such as some organic molecules containing both hydrophilic and hydrophobic functional groups, will not

cross an aqueous interface, but instead will act as surfactants and form unique chemical species at the interface. They can then react at the surface without ever entering the bulk of the aerosol.

1.7 Comparison between measured and predicted HO₂ concentrations during field campaigns

In many previous studies, models have overpredicted the concentration of HO₂ compared to observed concentrations during field campaigns (Brune et al., 1999; Cantrell et al., 1996; Carslaw et al., 2002; Carslaw et al., 1999; de Reus et al., 2005; Haggerstone et al., 2005; Jaegle et al., 2000; Kanaya et al., 2007; Kanaya et al., 2000; Mao et al., 2010; Olson et al., 2012; Smith et al., 2006; Sommariva et al., 2006; Sommariva et al., 2004; Stevens et al., 1994; Stone et al., 2012; Whalley et al., 2010). The overprediction has ranged from approximately 20 % to 95 % and has been attributed in most cases to HO₂ uptake by aerosols. For many studies such as during the ARCTAS campaign in the Arctic, and the Rishiri Island field campaign in Japan, as well as a few other field campaigns the uptake coefficient was estimated as 1, which is the maximum possible uptake (Kanaya et al., 2007; Mao et al., 2010). However, some historical differences in the marine boundary layer (MBL) are now able to be accounted for by reaction of HO₂ with halogen oxides (Reaction 1.19 and 1.20) (Bloss et al., 2005; Kanaya et al., 2002; Sommariva et al., 2006).

An example of the model overprediction of the gaseous HO₂ concentrations compared with observed concentrations is shown in Figure 1.6. Mao et al. (2010) measured the concentrations of HO₂ and other species over a range of altitudes in the Arctic during April 2008. Mao et al. (2010) showed that by including a HO₂ uptake coefficient that had been parameterised by Thornton et al. (2008) (which will be discussed in Section 1.13.3) a much better agreement between the modelled and the measured HO₂ concentrations could be achieved. Figure 1.6 also shows that the HO₂ loss to aerosols would have an impact on other species due to the chemistry that was discussed in Section 1.3. Finally, from Figure 1.6 it can also be noted that the product(s) of the HO₂ uptake would also have an impact upon the concentration of HO₂ and other species such as H₂O₂ may photolyse to reform OH. The

products of the HO_2 uptake by aerosols are currently unknown and possible products will be discussed in Section 1.9.

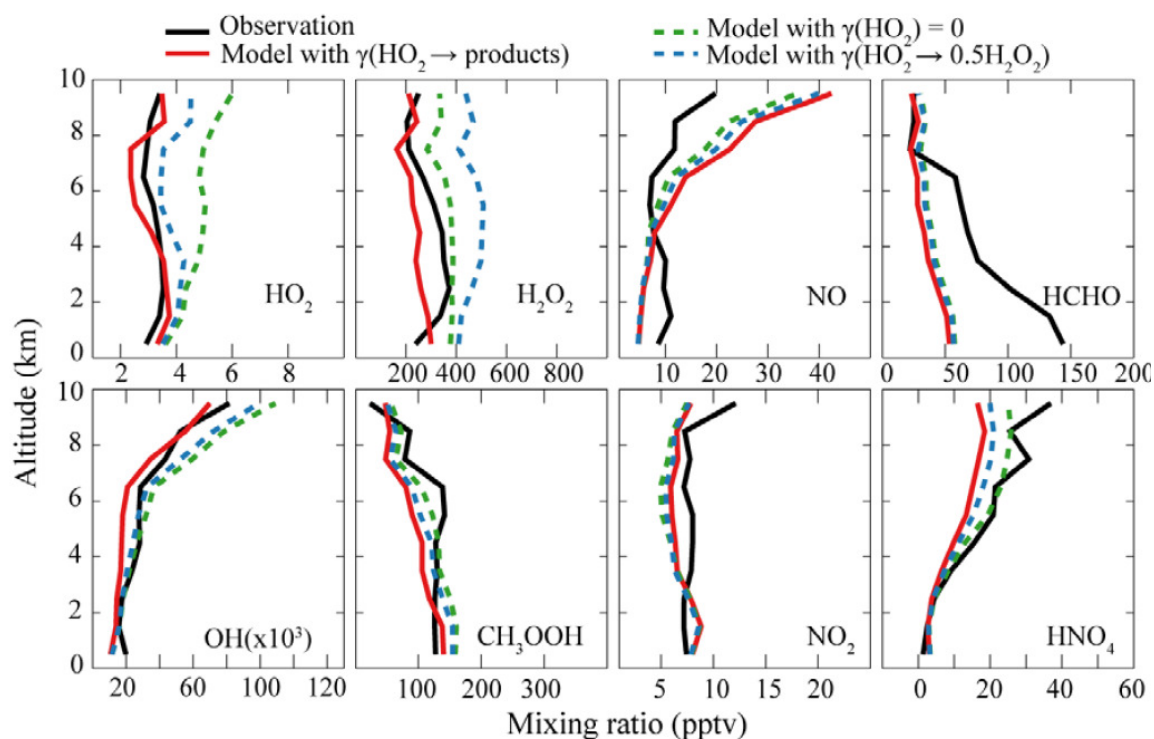


Figure 1.6: The median vertical profiles of different species during the ARCTAS campaign. The observed concentrations (black lines) are compared to the GEOS-CHEM model with no HO_2 uptake (green dashed line) and with a HO_2 uptake coefficient parameterised by Thornton et al. (2008) (as will be discussed in Section 1.13.3) leading to H_2O_2 formation (dashed blue line) or no H_2O_2 formation (red line). The figure is reproduced from Mao et al. (2010).

1.8 Modelling of uptake coefficients

1.8.1 The resistor model

A resistor model was developed by Schwartz (1986a) that described each uptake process as a resistance. Each resistance ($1/\Gamma$) can be combined in series or in parallel in an analogous way to an electrical circuit. The resistor model is shown in Figure 1.7:

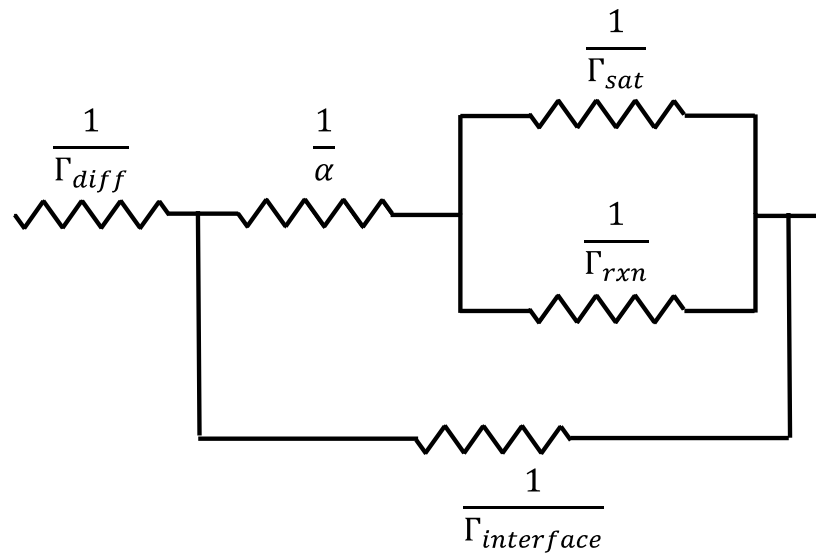


Figure 1.7: A schematic of the resistor model.

These resistances include α which is the mass accommodation and Γ_{diff} which is the gas transport coefficient and describes the gas phase diffusion limitation. It can be written as (Fuchs and Sutagin, 1970; Hanson et al., 1996; Widmann and Davis, 1997):

$$\frac{1}{\Gamma_{diff}} = \frac{0.75 + 0.238}{K_n(1 + K_n)} \quad (\text{E1.5})$$

where K_n is the Knudsen number which is equivalent to the gas phase mean free path divided by the radius of the aerosol.

Γ_{sat} is the solubility or liquid phase saturation limitation that can also be written as (Danckwerts, 1951; Hanson and Ravishankara, 1993):

$$\frac{1}{\Gamma_{sat}} = \frac{w}{4HRT} \sqrt{\frac{t\pi}{D}} \quad (\text{E1.6})$$

where w is the average molecular speed, H is the Henry's law constant, R is the gas constant, T is the temperature, t is the gas-aerosol interaction time and D is the liquid phase diffusion coefficient.

Γ_{rxn} is the limitation in the uptake coefficient due to liquid phase reactions and can be expressed as (Danckwerts, 1951, 1970):

$$\frac{1}{\Gamma_{rxn}} = \frac{w}{4HRT} \sqrt{\frac{1}{Dk_{rxn}}} \quad (E1.7)$$

where k_{rxn} is the rate of reaction in the aerosol bulk.

Finally, $\Gamma_{interface}$ is the limitation in the uptake coefficient due to surface reaction which can be written as (Hanson, 1997):

$$\frac{1}{\Gamma_{interface}} = \frac{w}{4k_{interface}b} \quad (E1.8)$$

where $k_{interface}$ is the rate of reaction at the aerosol surface, and b is the surface adsorption equilibrium constant. There are several possible scenarios for the uptake of a species into an aerosol depending on whether the species is reactive or unreactive, and whether there is reaction at the interface. Each scenario is described in the following sections.

1.8.1.1 Unreactive gas species

If the species that is being examined is not reactive with itself or with any of the other species in the aerosol, then the only processes that can occur are the diffusion of the species to the surface of the aerosol, adsorption and desorption into the aerosol and diffusion into the bulk of the aerosol. In this case the uptake coefficient can be written as:

$$\frac{1}{\gamma} = \frac{1}{\alpha} + \frac{1}{\Gamma_{diff}} + \frac{1}{\Gamma_{sat}} \quad (E1.9)$$

Equation 1.9 shows that the uptake into the aerosol will be controlled by the mass accommodation, the gas phase diffusion to the surface of the aerosol, and by the solubility of the species in the aerosol. With unreactive uptake, the uptake coefficient will tend to zero over time as the aerosols become saturated with the species.

1.8.1.2 Reactive gas species

If the species that is being examined is reactive in the bulk of the aerosol, then the resistor the uptake coefficient can be written as:

$$\frac{1}{\gamma} = \frac{1}{\alpha} + \frac{1}{\Gamma_{diff}} + \frac{1}{\Gamma_{sat} + \Gamma_{rxn}} \quad (\text{E1.10})$$

In this case the uptake coefficient could be limited by the mass accommodation, or by gas phase diffusion if the species is very soluble and very reactive. However, the uptake coefficient can also be limited by either the solubility of the rate of reaction in the bulk. If there is high solubility but a very low rate of reaction ($\Gamma_{sat} \gg \Gamma_{rxn}$) then, Equation 1.10 can be simplified to Equation 1.9. However, if the reaction is fast but the solubility is low then Equation 1.10 can be rewritten as Equation 1.11:

$$\frac{1}{\gamma} = \frac{1}{\alpha} + \frac{1}{\Gamma_{diff}} + \frac{1}{\Gamma_{rxn}} \quad (\text{E1.11})$$

1.8.1.3 Reactive gas species including uptake at the aerosol interface

When reactions occur at the surface of the aerosol as well as in the bulk, there are several processes competing with each other. In this case, the uptake will be limited by the mass accommodation if the reactions either at the interface or in the bulk are fast.

The uptake coefficient can then be written as:

$$\frac{1}{\gamma} = \frac{1}{\Gamma_{diff}} + \frac{1}{S} + \frac{1}{\frac{k_{sol}}{S k_{des}} + \frac{1}{\Gamma_{sat} + \Gamma_{rxn}} + \Gamma_{interface}} \quad (\text{E1.12})$$

In this case the mass accommodation (α) has been split into Equation 1.13 because the reaction at the aerosol interface occurs after thermal adsorption but before solvation into the bulk of the aerosol (Davidovits et al., 2006).

$$\frac{1}{\alpha} = \frac{1}{S} + \frac{k_{des}}{Sk_{sol}} \quad (\text{E1.13})$$

where S is the adsorption coefficient (the fraction of collisions that result in thermal accommodation to the surface of the aerosol), k_{des} is the rate of desorption from the surface and k_{sol} is the rate of solvation.

From Equation 1.12, it can be noted that either the diffusion of the gas molecules to the surface or the adsorption to the surface or the rate of reaction in the surface and bulk can be the rate determining steps for the uptake of gas molecules by aerosols. Whether the reaction occurs at the surface of the aerosol or in the bulk of the aerosol is dependent on the rate of transfer from the surface to the bulk, and the rate of desorption as well as the rates of reaction at the surface and in the bulk. Methods that have been used to measure uptake coefficients will be described in Section 1.11.

1.8.2 The KM-SUB model

Recently, a more complex model, the kinetic multilayer model for aerosol surface and bulk chemistry (KM-SUB) has been developed to describe uptake coefficients (Ammann and Pöschl, 2007; Pöschl et al., 2007). It is fully compatible with the resistor model as it accounts for gas phase diffusion, a Langmuir type adsorption (as will be discussed in Section 1.10) and desorption from the aerosol surface, surface and bulk reaction and diffusion into the bulk. However, unlike the resistor model, the KM-SUB model splits the aerosol and the gas phase into different layers. A volatile molecule or radical in the gas phase ($X_{(g)}$) could diffuse into the near-surface gas phase and then adsorb to the surface of the aerosol (forming a sorption layer). Once X has adsorbed to the surface, it could solvate into the near-surface bulk layer and then diffuse into the bulk layers (the model is capable of having hundreds of bulk layers). All of the processes described are reversible. For a non-volatile species (Y), the movements between layers are limited to a quasi-static surface layer, the near-surface bulk layer and the bulk layers as shown in Figure 1.8.

One of the main advantages of the KM-SUB model over the traditional resistor model is the ability to have a description of concentration and time dependences. By having different layers in the model, it is possible to predict the concentration of a specific species in a certain layer at a given time. It is therefore possible to predict concentration gradients of the species throughout the aerosol, and how this may affect the chemistry. Another advantage of the KM-SUB model is the ability of adding many different chemical species and physicochemical processes into the model. For example, it is possible to add several different volatile and non-volatile reactants into the KM-SUB model, and it is also possible to track the products of the reactions that are inputted into the model. The viscosity of the aerosol can also be easily varied in order to check the effect on the chemistry, and it is also possible to add an extra surfactant layer, which may have a different viscosity.

The KM-SUB model has previously been used to model NO_2 and ozone uptake onto soot, SO_2 uptake to acidic aerosols and ozone uptake to oleic acid particles, and how these uptake coefficients change over time and with different initial concentrations of gas phase species as will be discussed in Section 3.8 (Ammann and Pöschl, 2007; Shiraiwa et al., 2010). Other examples of its use include modelling NO_3 radicals reacting with organic aerosol components and the degradation of polycyclic aromatic hydrocarbons exposed to O_3 , NO_2 , H_2O , OH and NO_3 (Shiraiwa et al., 2009; Shiraiwa et al., 2012b). It should be noted that for solid aerosols the diffusion into the bulk of the aerosol is set to zero. Berkemeier et al. (2013) was also able to use the KM-SUB model to show that the uptake coefficient may be limited by a variety of factors such as mass accommodation, gas phase diffusion, the concentration of reactants in either the gas phase, on the surface of the aerosol, or in the bulk of the aerosol, the rates of reaction within the aerosol or, for viscous aerosols, the diffusion within the bulk of the aerosol. The KM-SUB model will be described in greater detail for HO_2 uptake in Chapter 8.

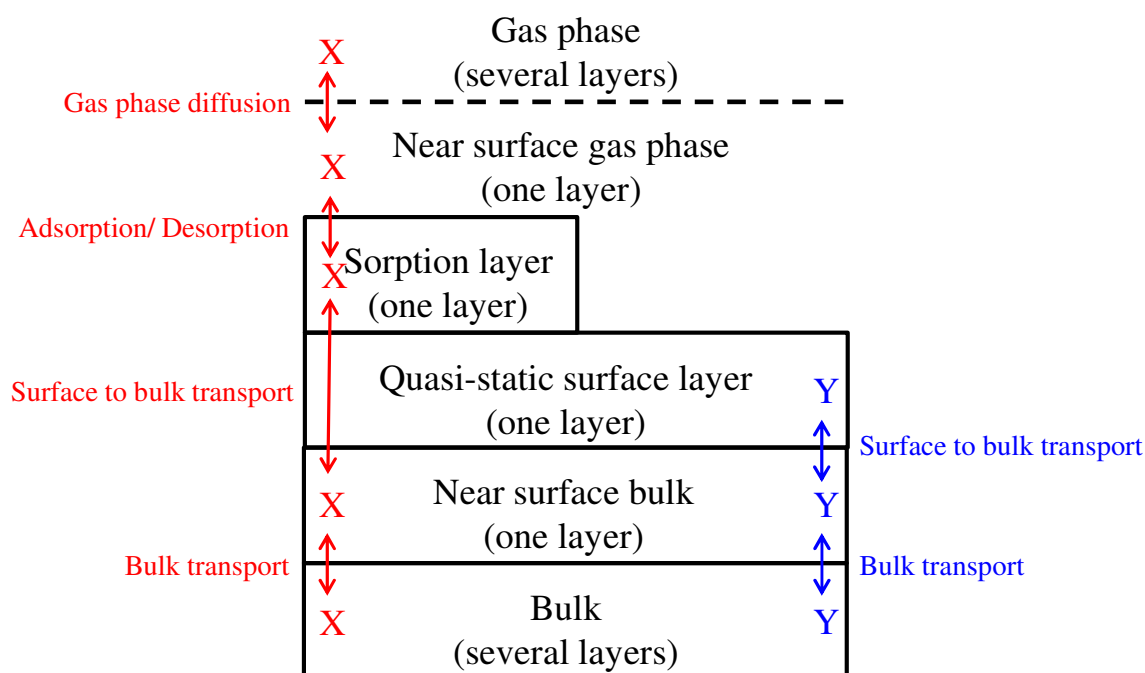
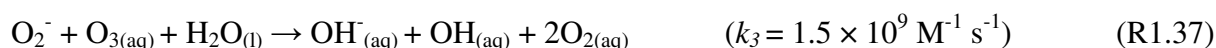


Figure 1.8: A schematic of the different layers within the KM-SUB model. X represents a volatile molecule whereas Y represents a non-volatile molecule. Adapted from Shiraiwa et al. (2010).

1.9 The current understanding of aqueous HO₂ chemistry

The reaction mechanism of HO₂ reacting with its conjugate base O₂⁻ and forming H₂O₂ in aqueous aerosols is believed to be (Jacob, 2000):

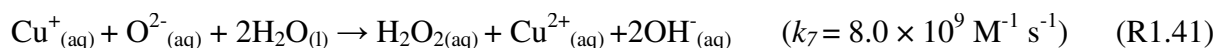
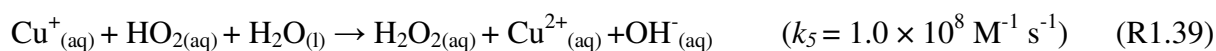
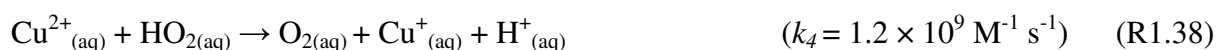


This is generally assumed to be the mechanism by which HO₂ is destroyed in the presence of aqueous aerosols. It should be noted that H₂O₂ has been observed in a laboratory experiment as a product of HO₂ uptake by sea salt aerosols (Loukhovitskaya et al., 2009). Reactions 1.33 – 1.37 show that the uptake coefficient should be dependent upon several factors. As the HO₂

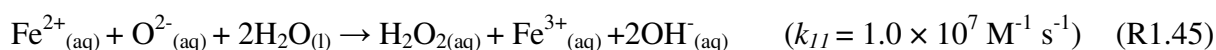
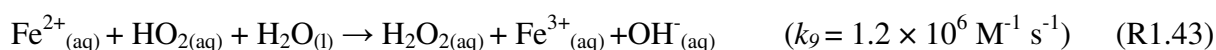
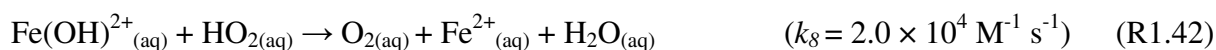
reaction is a second order reaction, the uptake should increase with increasing HO₂ concentration with the rate of the reaction being the rate-determining step. The uptake should also be pH dependent as HO₂ is a weak acid with a pKa of approximately 4.7. When the aerosol is more acidic, less HO₂ will enter the aqueous aerosol phase due to Le Chatelier's Principle. The uptake coefficient should also be temperature dependent due to the Henry's Law constant in Equation 1.14 being strongly temperature dependent, with higher uptake coefficients at lower temperatures expected. For example, Thornton et al. (2008) parameterised the Henry's law coefficient (in M atm⁻¹) as:

$$H_{HO_2}(T) = 9.4 \times 10^{-6} \exp\left(\frac{5.92 \times 10^{-3}}{T}\right) \quad (\text{E1.14})$$

However, when the aqueous aerosols are doped with copper the mechanism is believed to be (Jacob, 2000):



Copper acts as a catalyst to destroy HO₂ in this mechanism and forms hydrogen peroxide. Other transition metal ions are also thought to catalytically destroy HO₂ to form H₂O₂. For example the mechanism for HO₂ destruction for aerosols containing iron is postulated to be (Jacob, 2000):

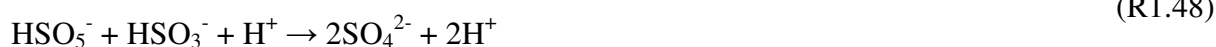


However, several studies have shown that if HO₂ uptake is included in models with the product being hydrogen peroxide, the hydrogen peroxide is overpredicted in the model compared to field observations (de Reus et al., 2005; Mao et al., 2010). Therefore, some other

HO₂ uptake mechanisms have been suggested which would not result in hydrogen peroxide as the final product being released back into the gas phase. For example, H₂O₂ could be protonated to HOOH₂⁺ which is a very strong oxidant and would therefore rapidly react to form water (Oiestad et al., 2001). However, this mechanism requires aerosols such as concentrated H₂SO₄ as a pH of less than zero is required for the mechanism to be effective (Bach and Su, 1994). Another mechanism involving sulphate aerosols was proposed by Cooper and Abbatt (1996). Cooper and Abbatt (1996) suggested that the following reaction could occur:

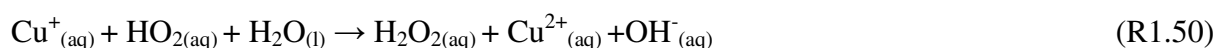


SO₅⁻ could then go on to react with O₂⁻, HCOO⁻ or HSO₃⁻. All of these reactions would form HSO₅⁻. It has been suggested that HSO₅⁻ could then react by either of the following reactions, both of which provide a terminal sink by conversion to water:

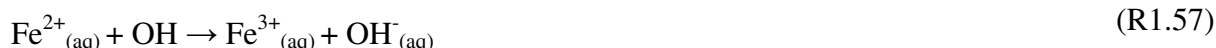
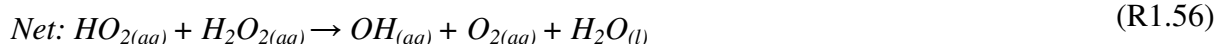
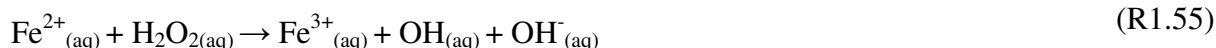
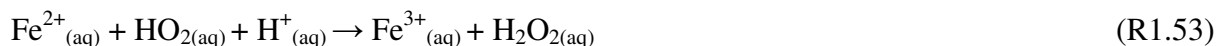


Another mechanism for uptake of HO₂ by sulphate aerosols would be the formation of a complex such as HO₂-H₂SO₄. It has been calculated that this complex would be stable both in the gas and the aerosol phase with a binding energy of 79.4 kJ mol⁻¹ (Miller and Francisco, 2001). It has also been calculated that the HO₂-H₂O complex would be stable with a binding energy of 35 kJ mol⁻¹ (Aloisio et al., 2000). However, the fate of these complexes if they actually exist is unknown.

Recently, another mechanism has been proposed by Mao et al. (2013) which suggests that if aerosols contain a mixture of copper and iron then the product of HO₂ uptake would be water rather than hydrogen peroxide due to the following reactions:



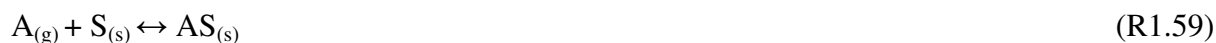
There are then three possible reactions that can occur:



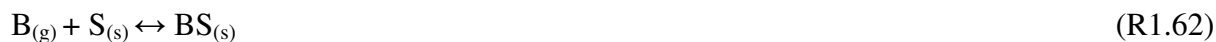
This mechanism will be discussed in further detail in Section 1.13.3.

1.10 Solid aerosol chemistry

The uptake of gases by solid aerosols is different than for aqueous aerosols as the reaction is limited to the surface of the aerosols, and no aqueous chemistry can occur. The Eley-Rideal and Langmuir-Hinshelwood mechanisms are believed to be two possibilities as to how radicals in the gas phase react on aerosol surfaces. For the Eley-Rideal mechanism, one of the radicals adsorbs onto the surface and the second radical reacts with it directly from the gas phase:



However, for the Langmuir-Hinshelwood mechanism both molecules are adsorbed onto the surface and undergo a bimolecular reaction:



It is not known whether the HO_2 self-reaction at aerosol surfaces occurs via the Eley-Rideal or the Langmuir-Hinshelwood mechanism as neither mechanism has been confirmed through

kinetic observations. It is difficult to test which of these mechanisms is occurring as they are usually differentiated by changing the concentration of either A or B. It would be expected that as the concentration of A increased so that ($[A] \gg [B]$) the rate of reaction would decrease for the Langmuir-Hinshelwood reaction whereas it would not affect the rate of reaction if the Eley-Rideal mechanism was occurring. However, in the case of HO_2 uptake both A and B in Reactions 1.59 to 1.63 are likely to be HO_2 as the product H_2O_2 has been observed as will be discussed below.

Radical uptake by inorganic aerosols can occur in one of two ways. Both self-reaction and oxidative processes (whereby the incoming species oxidises a component of the aerosol) have been observed. The product H_2O_2 has been observed from the self-reaction of HO_2 on salt surfaces and Br_2 has been formed from the self-reaction of BrO on ice (Abbatt, 1996; Loukhovitskaya et al., 2009). However, it is unknown what the heterogeneous oxidation mechanism actually is. For dust aerosols H_2O_2 was not observed during laboratory experiments (Bedjanian et al., 2013). There is also the possibility that HO_2 could react with a component of the solid aerosols, however, it is unknown what this would be or what the products might be.

It should be noted that for solid aerosols the surface coverage (θ) of the aerosol surface can be given by the Langmuir isotherm as follows:

$$\theta = \frac{\beta P}{1 + \beta P} \quad (\text{E1.15})$$

where β is a constant which increases with decreasing temperature and with an increasing binding energy of adsorption and P is either the gas phase pressure or concentration of the species. From Equation 1.15 it can be established that as the gas phase concentration of a species decreases the surface coverage would also decrease.

1.11 Techniques used to measure HO₂ uptake coefficients in the laboratory

There are several different methods that have been used to measure uptake coefficients (Kolb et al., 2010). Early measurements of uptake coefficients were mostly performed using Knudsen cells. A gas flows into the Knudsen cell where it is exposed to a surface that takes up the gas. The gas then exits the cell through an orifice that is connected to a low pressure system. The concentration of the gas entering the cell and exiting the cell can then be measured and the change in concentration is related to the uptake. Other methods to measure uptake coefficients rely on the same principle that is that the uptake coefficient is related to the change in the gas concentration (or a proportional quantity) after exposure to the aerosol. These other methods of measuring the uptake coefficients include flow tube studies, falling-drop apparatus experiments, bubble apparatus experiments, aerosol chamber experiments and liquid jet apparatus experiments.

From Table 1.1, it can be seen that all of HO₂ uptake coefficient measurements have been performed using a flow tube coupled with a HO₂ detection method (described in Section 1.4) with the exception of the work by Saathoff et al. (2001) where the HO₂ uptake coefficient was estimated using a model to describe the reactions happening a chamber in the presence of soot. The aerosol flow tube method works by varying the time that aerosols and HO₂ (released from an injector) flowing down a flow tube are in contact with each other. The HO₂ concentration and aerosol surface area are then measured. For the coated flow tube method, the HO₂ is released from an injector that is moved to different positions along the flow tube so that the HO₂ is in contact with the coating on the flow tube walls for different amounts of time. The coated moveable rod method works in a similar way, except that the HO₂ flows down the flow tube, and the contact time is varied by moving the coated rod to different positions along the flow tube, exposing the HO₂ to different amounts of the coated surface (Davis, 2008).

Technique	HO ₂ detection method	Initial HO ₂ concentration/ molecule cm ⁻³	Aerosols studied	Reference
Aerosol flow tube	Chemical amplifier-luminol detector	10 ⁸ - 10 ⁹	LiNO ₃ or NH ₄ HSO ₄ with and without Cu(II)	Mozurkewich et al. (1987)
Coated flow tube	Laser induced fluorescence	(0.5 – 3) × 10 ¹¹	H ₂ O and H ₂ SO ₄	Hanson et al. (1992)
Coated flow tube	Electron paramagnetic resonance	(0.03 – 3) × 10 ¹¹	Dry NaCl	Gershenson et al. (1995)
Coated flow tube	Resonance fluorescence detector	< 5 × 10 ¹⁰	H ₂ SO ₄ , water ice, NH ₄ HSO ₄ and (NH ₄) ₂ SO ₄	Cooper and Abbatt (1996)
AIDA chamber	Not measured directly (a model was used)	N/A	Soot	Saathoff et al. (2001)
Coated flow tube	Electron paramagnetic resonance	(0.4 – 5) × 10 ¹¹	Dry NaCl	Remorov et al. (2002)
Aerosol flow tube	Chemical ionisation mass spectrometer	~ 10 ¹²	H ₂ SO ₄ and (NH ₄) ₂ SO ₄ with and without Cu(II)	Thornton and Abbatt (2005)
Coated moveable rod in a flow tube	Modulated molecular beam mass spectrometer	(2 – 9) × 10 ¹¹	Dry synthetic sea salt, NaCl, NaBr and MgCl ₂ ·6H ₂ O	Loukhovitskaya et al. (2009)
Aerosol flow tube	FAGE	~ 10 ⁸	Various aqueous and solid salts and organics, (NH ₄) ₂ SO ₄ with Cu(II)	Taketani and Kanaya (2010); Taketani et al. (2009); Taketani et al. (2013); Taketani et al. (2008)
Coated moveable rod in a flow tube	Modulated molecular beam mass spectrometer	(0.35 - 3.30) × 10 ¹²	Arizona Test Dust	Bedjanian et al. (2013)
Aerosol flow tube	FAGE	(0.8 – 2.8) × 10 ⁹	Various aqueous and solid salts, (NH ₄) ₂ SO ₄ with Cu(II)	George et al. (2013) (This work)
Aerosol flow tube	FAGE	3 × 10 ⁸ and 1 × 10 ⁹	Arizona Test Dust	Matthews et al. (2014) (This work)

Table 1.1: Methods that have been used and aerosols that have been studied to measure HO₂ uptake coefficients in the literature. FAGE = Fluorescence Assay by Gas Expansion. AIDA= Aerosol Interaction and Dynamics in the Atmosphere.

Although coated surfaces are good for measuring small uptake coefficients ($\gamma < 10^{-3}$) due to their large surface area, there are many advantages of using aerosols over coated surfaces. Using aerosols rather than coating surfaces is a much better representation of the atmospheric aerosols found in the troposphere. Sub-micron sized particles in the troposphere are known to exist in thermodynamically metastable states, for example, as the humidity decreases below their deliquescence point, they will remain as liquids until they reach their efflorescence point. However, coatings will tend to solidify below the deliquescence point. Another issue with coatings is that their exact thickness needs to be known, otherwise the reacto-diffusive length (the depth to which the molecule diffuses before it reacts) cannot be calculated (Abbatt et al., 2012).

1.12 Laboratory measurements of the HO₂ uptake coefficient

The rates and mechanism of the HO₂ loss by aerosols are still uncertain. It is therefore essential to gain a better knowledge of the uptake of HO₂ by different aerosols under different conditions that are relevant to the atmosphere. If this is achieved then the uptake coefficients can be included within models, and this would provide better agreement with observations.

Jacob (2000) recommended using $\gamma(\text{HO}_2) = 0.2$ for all types of aerosols under all conditions. However, this suggestion was based only upon a few laboratory measurements and the results from a few box model studies (e.g. the measurements and modelling by Jaegle et al. (2000)). The recommendation was also made when reactive halogens were not being measured in field experiments, and therefore the removal of HO₂ by halogens was not taken into account. This meant that γ was overestimated compared to if the reactions with halogens had been accounted for. It has become clear from laboratory studies that a single value should not be used as the uptake coefficient of HO₂ does vary depending on the composition of the aerosol and the conditions. Therefore, more recent models have not used a single value for $\gamma(\text{HO}_2)$. For example, the Goddard Earth Observing System - Chemistry (GEOS-Chem) model contains five aerosol types (Macintyre and Evans, 2011). These are sulphate, sea salt, black carbon, organic carbon and dust. A temperature dependence as well as a relative humidity dependence can also be included within models. New parameterizations can be made based on measurements made in laboratory experiments. There have already been several

laboratory measurements of the uptake of HO_2 by aerosols. These are summarised in Figure 1.9.

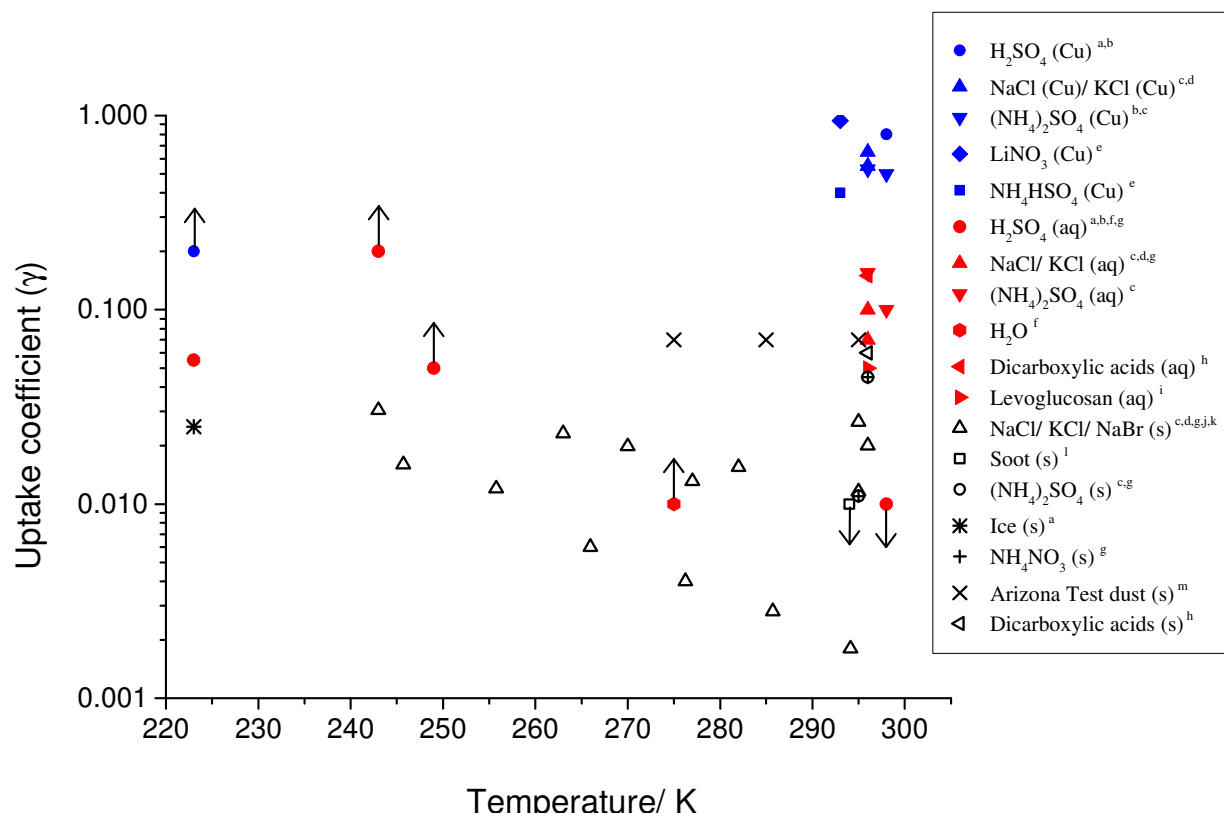


Figure 1.9: Measurements of the HO_2 uptake coefficient published in the literature up to 2010. The blue points represent aqueous copper-doped aerosols or surfaces, the red point represent aqueous aerosols or surfaces and the black points represent solid aerosols or surfaces. The arrows mean ‘less than’ or ‘greater than’. The literature references in the legend are: (a) Cooper and Abbatt (1996) (b) Thornton and Abbatt (2005) (c) Taketani et al. (2008) (d) Taketani et al. (2009) (e) Mozurkewich et al. (1987) (f) Hanson et al. (1992) (g) Gershenson et al. (1995) (h) Taketani et al. (2013) (i) Taketani (2010) (j) Loukhovitskaya et al. (2009) (k) Remorov et al. (2002) (l) Saathoff et al. (2001) (m) Bedjanian et al. (2013). Adapted from Mao et al. (2010).

A few trends can be seen in Figure 1.9. There are larger uptake coefficients in the presence of copper ions ($\gamma = 0.4 - 0.9$). The uptake also increases when there is an aqueous surface instead of a solid surface, and it also tends to increase with decreasing temperature. However, there is also a large variability in the measured uptake coefficients. For example, for dry ammonium sulphate the measured uptake coefficients vary by a factor of five. There is also a disagreement over the HO_2 uptake mechanism. Taketani et al. (2008) observed first order

kinetics, whereas, Thornton and Abbatt (2005) observed second order kinetics for a constant aerosol concentration. It is therefore crucial to investigate the factors affecting the HO₂ uptake coefficients in order to better understand the HO₂ aerosol uptake mechanism, and consequently to improve models. The factors that may affect the uptake coefficient are the presence of transition metal ions, the temperature, the relative humidity, the phase of the aerosol, the pH, the size of the aerosol, and the extent to which the surface of the aerosol is becoming saturated.

1.13 HO₂ uptake coefficient parameterisations and models

A parameterisation is an equation describing how a value changes as one or more variables are changed and is based upon measurements. Uptake coefficients can be parameterised to describe the impact of variables such as temperature or the initial gas concentration. Such parameterisations can be inputted into atmospheric models, so that the trends observed in the laboratory can be reproduced when making predictions about gas radical concentrations. Remorov et al. (2002) and Loukhovitskaya et al. (2009) both parameterised the HO₂ uptake coefficient onto solid sodium chloride surfaces based on their laboratory measurements. Macintyre and Evans (2011) parameterised the HO₂ uptake coefficient by five different types of aerosol (sulphate, organic carbon, black carbon, sodium chloride and dust) based on very limited laboratory measurements. Finally, Thornton et al. (2008), modelled the HO₂ uptake coefficient using the known aqueous chemistry discussed in Section 1.9 and described by Reactions 1.34 – 1.41 and Mao et al. (2013) included the redox chemistry shown by Reactions 1.52 – 1.58.

1.13.1 Parameterisations of the HO₂ uptake coefficient onto solid sodium chloride surfaces over a range of temperatures.

Remorov et al. (2002) and Loukhovitskaya et al. (2009) performed experiments using a flow tubes coated with dry sodium chloride and a moveable injector containing HO₂ over a range of temperatures. Remorov et al. (2002) stated that between 243 - 300 K the measured uptake coefficients were independent of the initial HO₂ concentration, and could be given by the following Arrhenius equation:

$$\gamma = (5.66 \pm 3.62) \times 10^{-5} \exp[(1560 \pm 140)/T] \quad (\text{E1.16})$$

Between 243 – 345 K the experiments showed that the uptake coefficient decreased significantly. Loukhovitskaya et al. (2009) stated that the HO₂ uptake coefficient could be given by the following Arrhenius equation:

$$\gamma = (2.2 \pm 0.7) \times 10^{-8} \exp[(3340 \pm 90)/T] \quad (\text{E1.17})$$

These parameterisations will be discussed in greater detail in Chapter 6 where the effect of temperature upon the HO₂ uptake coefficient is investigated.

1.13.2 Parameterisations of the HO₂ uptake coefficient onto five different aerosol types

Macintyre and Evans parameterised the HO₂ uptake coefficient using data from laboratory studies. The parameterisations are summarised in Table 1.2. The parameterisation shows that generally, the uptake coefficient will increase with decreasing temperature and they are generally in the form of Arrhenius equations. The HO₂ uptake coefficient increases with decreasing temperature as the Henry's law constant is temperature dependent meaning that at low temperatures more HO₂ partitions to the aqueous phase.

Aerosol	Uptake coefficient	Reference
Sulphate	$\alpha \times \beta$ where $\alpha = 5.14545 \times 10^{-4} \exp(1560/T)$ $\beta = (-26.1818 \exp(-0.078 \times RH) + 1.74545)$	Remorov et al. (2002) Taketani et al. (2008)
Organic carbon	0.025	Ivanov et al. (1999)
Black carbon	0.01	Saathoff et al. (2001)
Sodium chloride	$5.66 \times 10^{-5} \exp(1560/T)$ (RH < 62 %) 0.05 (RH ≥ 62 %)	Remorov et al. (2002) Taketani et al. (2008)
Dust	0.1 (RH ≥ 50 %); 0.05 (RH < 50 %)	Hanel (1976) reported in Dentener et al. (1996)

Table 1.2: Macintyre and Evans' HO₂ uptake coefficient parameterisations for different types of aerosols.

1.13.3 HO₂ uptake coefficient model using known aqueous chemistry

The expression that was derived by Thornton et al. (2008) was based on detailed calculations that assumed HO₂ self-reaction (shown by Reactions 1.34 – 1.38 in Section 1.9) and assessed the effects of aerosol pH, temperature, particle size and aqueous phase diffusion limitations on the rate of HO₂ loss by aerosol uptake. The equation was derived by assuming that in the absence of aqueous-phase mass transport limitations, the difference between the rate of HO₂ entering the aerosol and the rate of the products evaporating must be equal to the rate of Reactions 1.36 and 1.37 throughout the whole of the aerosol. The equation was based on the resistor model (discussed in Section 1.8.1) and is shown below:

$$\frac{1}{\gamma^{HO_2}} = \frac{1}{\alpha^{HO_2}} + \frac{3wN_A}{8000(H_{eff}RT)^2 k_{eff}[HO_{2(g)}]r_p} \quad (E1.18)$$

where γ^{HO_2} is the uptake coefficient of HO₂, α_{HO_2} is the mass accommodation coefficient, w is the molecular thermal speed of HO₂, N_A is Avogadro's number, H_{eff} is the effective Henry's law defined in Equation 1.19, R is the universal gas constant, T is the temperature, k_{eff} is the effective second order rate constant defined in equation 1.20, $[HO_{2(g)}]$ is the concentration of HO₂ and r_p is the particle radii:

$$H_{eff} = H_{HO_2} \left(1 + \frac{K_{eq}}{[H^+]}\right) \quad (E1.19)$$

where H_{HO_2} is the physical Henry's law constant estimated to be approximately 3900 M atm⁻¹.

$$k_{eff} = \frac{k_1 \left(\frac{K_{eq}}{[H^+]_{aq}}\right) k_2}{\left(1 + \frac{K_{eq}}{[H^+]_{aq}}\right)^2} \quad (E1.20)$$

The parameterisation resulted in HO₂ concentration, temperature and pH dependencies of the HO₂ uptake coefficient that are shown in Figure 1.10:

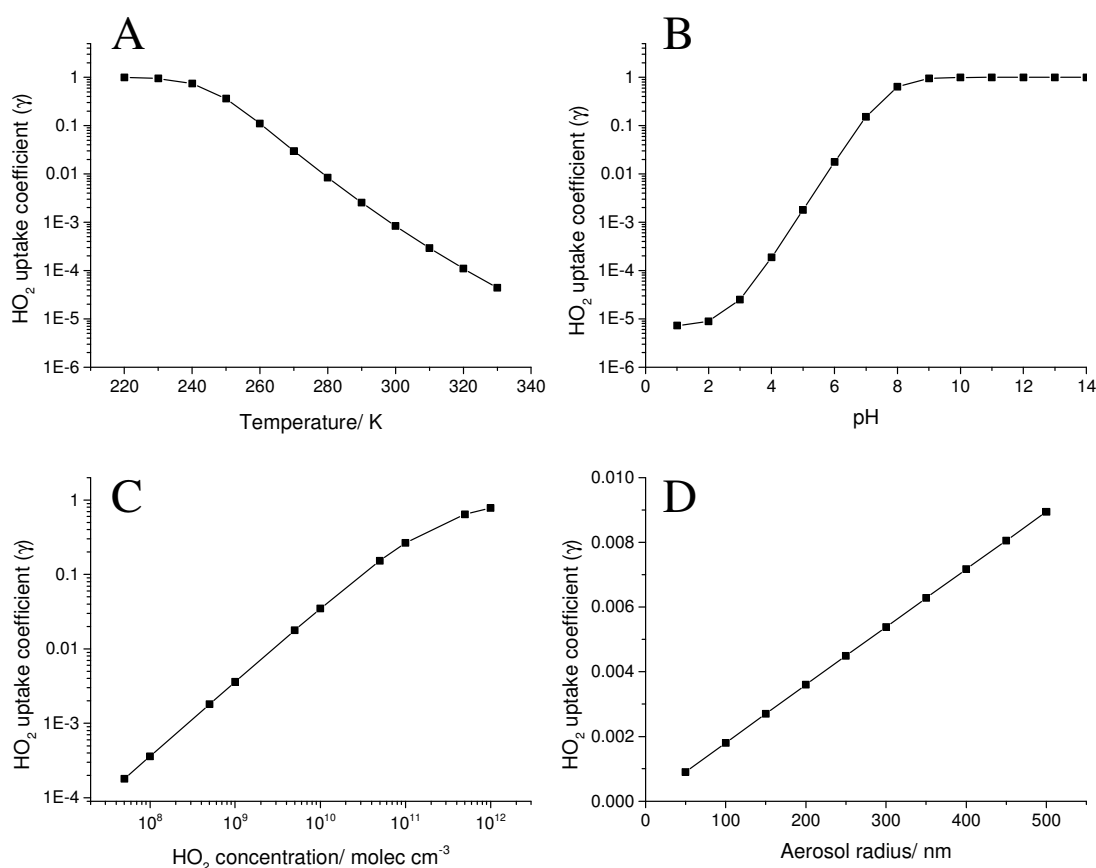


Figure 1.10: The HO₂ uptake coefficient calculated from Equation 1.18 for aqueous aerosols. (A) γ as a function of temperature for an aerosol radius of 100 nm, a pH of 5 and a HO₂ concentration of 5×10^8 molecule cm⁻³. (B) γ as a function of aerosol pH for an aerosol radius of 100 nm, a temperature of 293 K and a HO₂ concentration of 5×10^8 molecule cm⁻³. (C) γ as a function of HO₂ concentration for an aerosol radius of 100 nm, a temperature of 293K and a pH of 5. (D) γ as a function of aerosol radius at a temperature of 293 K, a pH of 5 and a HO₂ concentration of 5×10^8 molecule cm⁻³.

Thornton et al. (2008) also stated that for copper-doped aerosols the uptake coefficient could be written by the following equation:

$$\frac{1}{\gamma^{HO_2}} = \frac{1}{\alpha^{HO_2}} + \frac{w}{H_{eff}RT\sqrt{k^I D_{aq}Q}} \quad (E1.21)$$

where k^I is the pseudo first order rate constant equivalent to $k^{II}[TMI]$ and k^{II} is the second order rate constant for the reaction between HO₂ + Cu²⁺ and O₂⁻ + Cu²⁺ obtained using the

rate constants for Reaction 1.39 and 1.41 and equation 1.18. Q is given by the following equation (Hanson and Lovejoy, 1995):

$$Q = \left(\coth(q) - \frac{1}{q} \right) \quad (\text{E1.22})$$

where q is given by the following equation:

$$q = r \sqrt{\frac{k^l}{D_{aq}}} \quad (\text{E1.23})$$

where r is the radius of the aerosols and D_{aq} is the HO_2 diffusion in the aerosol. Equation 1.21 allowed for the HO_2 uptake coefficient to be calculated as a function of copper ion concentration. Figure 1.11 shows that the uptake coefficient is limited by aqueous chemistry at low copper molarities. However, as the copper concentration increases the uptake coefficient increases until the uptake coefficient is only limited by the mass accommodation at $\sim 10^{-4}$ M.

It should be noted that Mao et al. (2013) also modelled the HO_2 uptake coefficient using the redox chemistry shown by Reactions 1.53 – 1.58. Mao et al. (2013) observed several trends. Firstly, as the Cu/Fe ratio decreased the uptake coefficient increased and the hydrogen peroxide yield increased as Reactions 1.43 and 1.44 became less dominant. Secondly, as the pH increased there were higher uptake coefficients (similarly to in the Thornton et al. (2008) model). However, at higher pH hydrogen peroxide could be destroyed by $\text{Fe}(\text{OH})^+$ which is five orders of magnitude faster than reaction with Fe^{2+} . Finally, Mao et al. (2013) showed that when keeping the Cu/Fe ratio constant at 0.05 but reducing the copper concentration, a rapid decrease is observed when the copper concentration is reduced to below 5×10^{-4} M. Above this concentration the uptake coefficient appears to be essentially limited by the mass accommodation and solubility of the HO_2 . This is in agreement with the model results shown in Figure 1.9. However, the Mao et al. (2013) model has not yet been tested experimentally. In this thesis one of the aims is to confirm the relationships shown in Figure 1.10 and Figure 1.11.

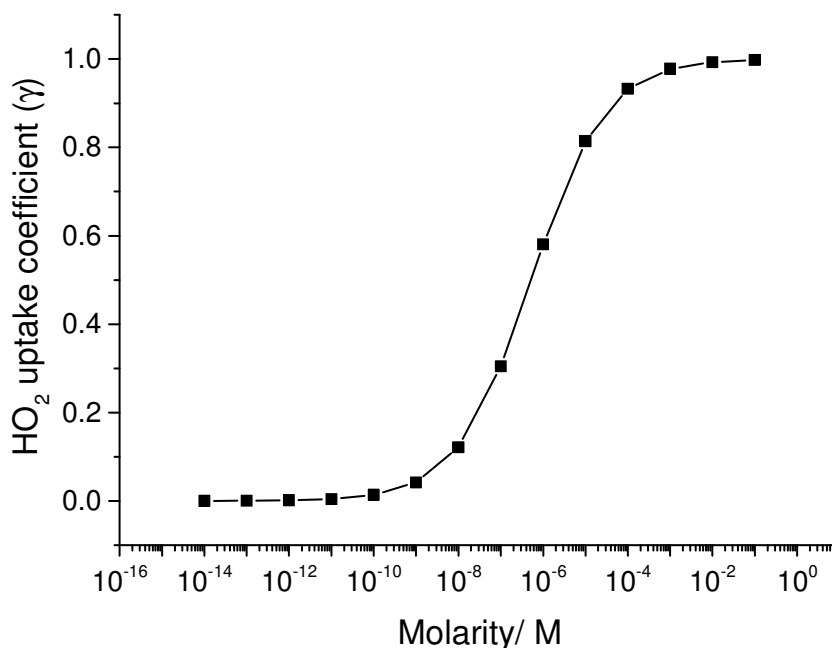


Figure 1.11: The HO₂ uptake coefficient calculated from Equation 1.21 as a function of copper molarity in the aerosol. The pH was set to 5 and the aerosol radius was 100 nm. The mass accommodation was set to 1.

1.14 Summary

The HO₂ radical is extremely important in the troposphere as it is closely coupled with OH that controls the concentrations of many trace species associated with climate change and air quality. However, during many field campaigns the concentration of HO₂ has been significantly lower than the concentration predicted by box models. This discrepancy has often been attributed to HO₂ uptake by aerosols. However, there have been relatively few laboratory studies of HO₂ uptake onto different types of aerosols and a large range of values have been obtained. A few trends have been observed from the laboratory experiments such as larger uptake coefficients for aqueous copper doped aerosols ($\gamma > 0.2$ to $\gamma = 0.94$) than for aqueous aerosols containing no metals ($\gamma = 0.01 - 0.2$) and larger uptake coefficients for aqueous aerosols than for solid aerosols ($\gamma = 0.004 - 0.07$).

The HO₂ uptake coefficients in the literature have been obtained using a variety of methods and under various conditions. The majority of these measurements have used either an

aerosol flow tube or a coated injector flow tube or injector coupled with a method of HO₂ detection. The methods of detection have included CIMS, FAGE and electron paramagnetic resonance. However, only a few of the laboratory measurements of the HO₂ uptake measurements made by different groups and published in the literature have been in agreement with each other.

Although a few parameterisations have been utilised in models, more HO₂ uptake coefficient measurements are required in order to fully understand the HO₂ uptake mechanism. The recent development of the KM-SUB model and the Thornton et al. (2008) model should also enable laboratory measurements to be related to the known HO₂ aqueous chemistry. If a thorough knowledge of the behaviour of HO₂ uptake coefficient under different conditions could be achieved, the parameterisations that are used in global models could be made more accurate and precise enabling a better understanding of current concentrations of trace gases in the atmosphere as well as better predictions of future concentrations.

In this thesis, the aims were to measure the HO₂ uptake coefficients onto a range of aerosols including salts (both effloresced and deliquesced), organics, copper and iron doped salts, dust and aerosols with different pH. Another goal was to measure the HO₂ uptake coefficient over different conditions including a range of temperatures, relative humidities, reaction times and HO₂ concentrations. By making these measurements the relationships predicted by the Thornton et al. (2008) model could be tested and developed using the KM-SUB model. The combination of experiments and modelling could enable a better understanding of the discrepancies in the laboratory measurements of the HO₂ uptake coefficients published in the literature.

Chapter 2: Experimental

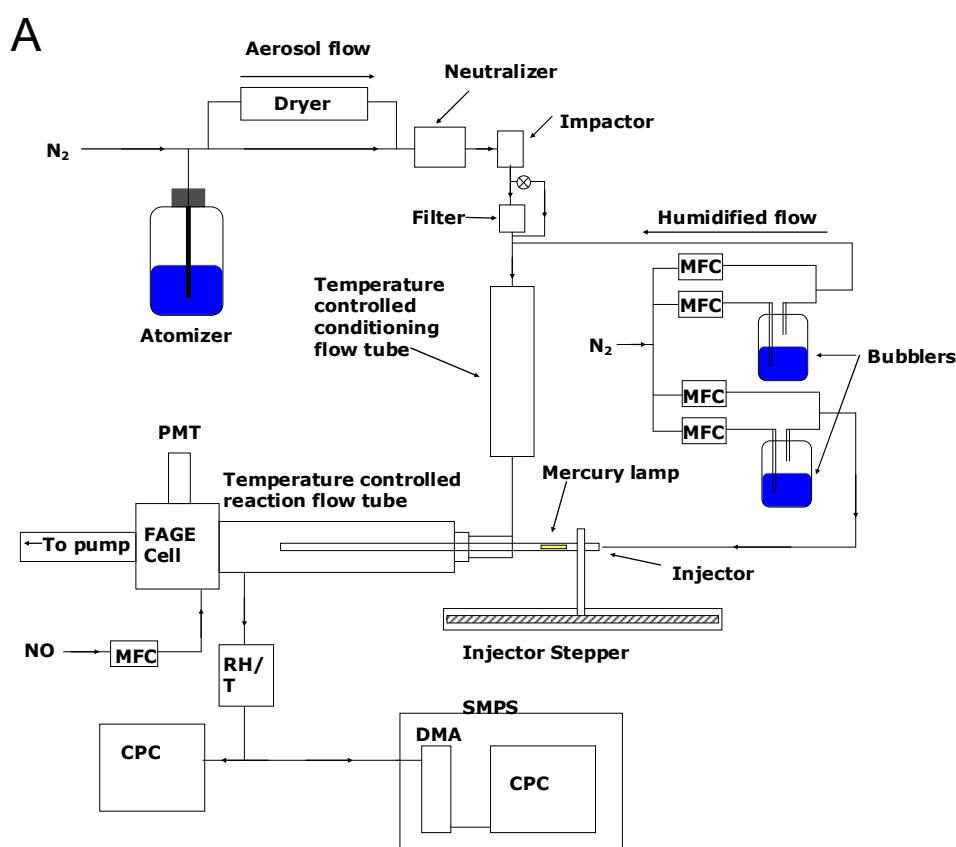
2.1 Overview of the experimental setups

Figure 2.1 shows schematic diagrams of the three experimental setups that were used to measure the uptake coefficients of HO₂ onto different types of aerosol. The first experimental setup (Figure 2.1A) was employed for the majority of experiments, the second experimental setup (Figure 2.1B) was only used for mineral dust experiments and the third experimental setup (Figure 2.1C) was employed for secondary organic aerosol experiments at the Paul Scherrer Institute (PSI) in Switzerland. A photograph of the setup used for the experiments in Leeds is shown in Figure 2.2. The main differences between the three experimental setups were the aerosol generation method, the position of the CPC (Condensation Particle Counter), the carrier gas for the aerosol flow, the use of denuders for the chamber experiments and whether the flows were pushed through or pumped from the flow tube and other equipment. The atomiser was not used when producing mineral dust aerosols, as placing the mineral dust in water could have changed the composition of the dust due to certain soluble chemicals such as sodium oxide and calcium oxide dissolving into the water. The aerosol generation method for mineral dust did not produce a constant aerosol output, and therefore the CPC was used to record the changing concentration in real-time (this is discussed further in Section 2.6.1). During the secondary organic aerosol (SOA) experiments (Figure 2.1C) the aerosols were produced in a large smog chamber at PSI and the aerosol carrier gas was air rather than nitrogen. Cobalt oxide and charcoal denuders were used in order to remove trace gases that were formed in the chamber. The flows also had to be pumped through the equipment rather than pushed as both the smog chamber and the flow tube were at atmospheric pressure. All of these experimental differences will be discussed in greater detail in the following sections.

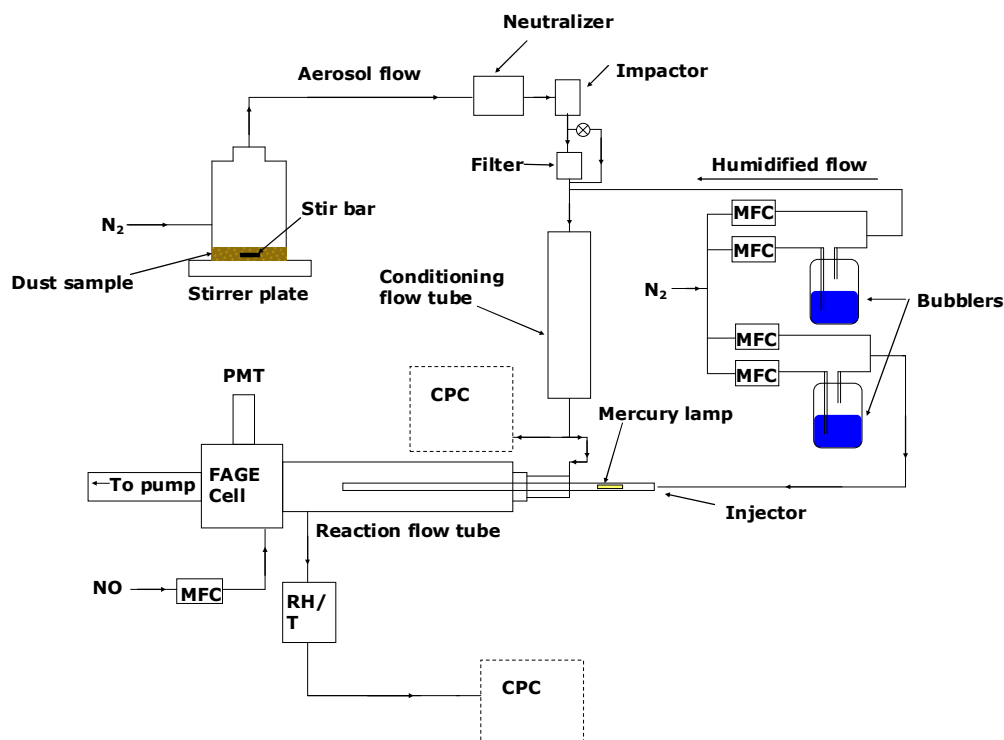
The kinetics of the HO₂ heterogeneous loss were measured by two different methods. For ‘moving injector’ experiments, the injector (which introduced the HO₂ into the flow tube) was moved backwards and forwards along the flow tube. By moving the injector to different positions along the flow tube the time for which the HO₂ and the aerosols were in contact

changed. This allowed pseudo-first-order decays of HO₂ along the flow tube to be measured both in the absence of aerosols and in the presence of different concentrations of aerosols. For ‘fixed injector’ experiments the injector was placed in one position along the flow tube whilst the aerosol concentration was varied. This process was then repeated at different positions along the flow tube. These two methods are discussed in greater detail in Sections 2.8 and 2.9.

The HO₂ concentration was measured in a Fluorescence Assay by Gas Expansion (FAGE) cell at the end of the flow tube, whilst the aerosol surface area was measured by a Scanning Mobility Particle Sizer (SMPS). All of the experiments performed in Leeds were at atmospheric pressure (~ 970 - 1040 mbar) whereas the pressure in the flow tube for the secondary organic aerosol experiments at the PSI were between 904 and 987 mbar. Further details of the experimental setup are given in the following sections.



B



C

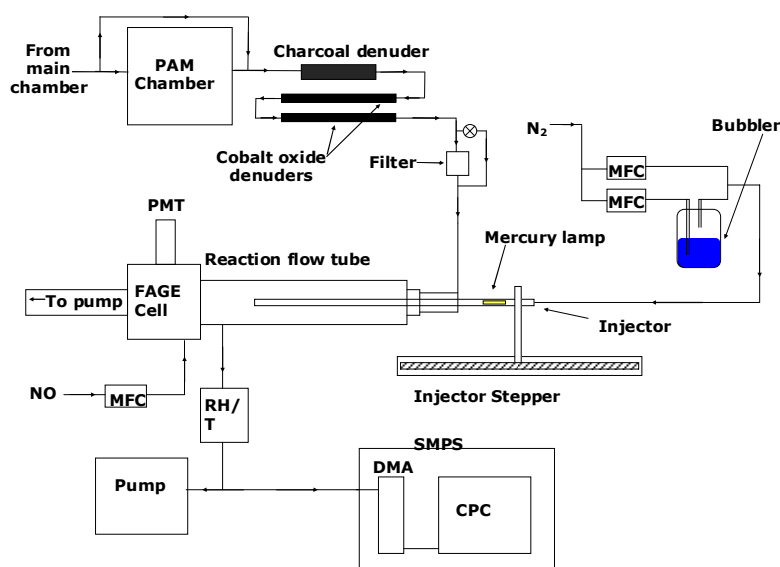


Figure 2.1: A schematic diagram of the experimental apparatus for the measurement of the kinetics of HO_2 uptake in the presence of (A) aerosols which could be produced using an atomiser, (B) mineral dust aerosols and (C) secondary organic aerosols. MFC = mass flow controller; DMA = Differential Mobility Analyzer; SMPS = Scanning Mobility Particle Sizer; CPC = condensation particle counter, PMT = photomultiplier tube and FAGE =for Fluorescence Assay by Gas Expansion PAM= Potential Aerosol Mass. Main chamber refers to the PSI Smog Chamber.

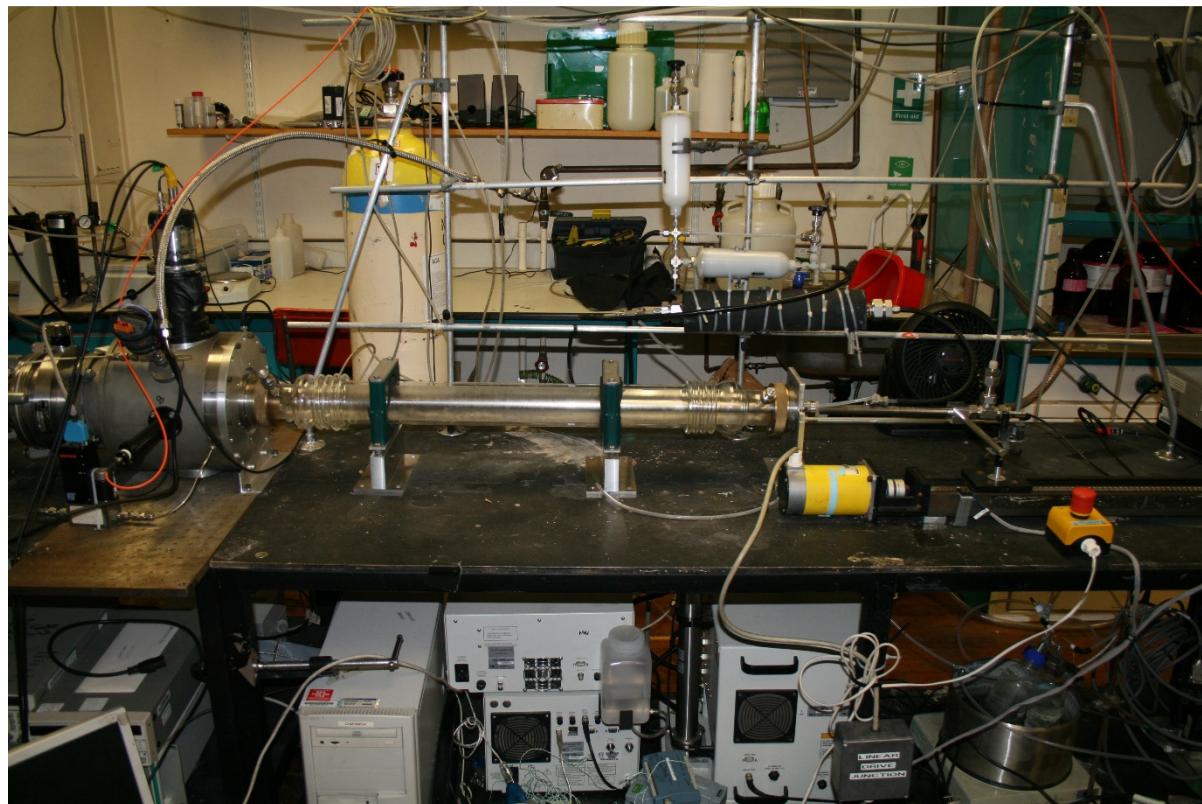


Figure 2.2: The experimental setup for experiments performed in Leeds. On the left of the photograph is the FAGE cell, which is connected to the aerosol flow tube. The injector is entering the flow tube and is attached to the injector stepper, shown on the right of the photograph. Below the table the back of the SMPS and APS and the bubblers are shown. The HEPA filter and conditioning flow tubes are also pictured in the centre of the photograph.

2.2 The flow regimes for the different experimental setups

The carrier gas used for all of the experiments performed in Leeds was nitrogen which was generated from outside air (University of Leeds departmental nitrogen) and was then passed through a purifier (TSI, model 3074B). The HO₂ flow, the humidified flow and the NO flow were controlled using five mass flow controllers (Brooks, model 5850S and MKS, model 1179A). The required humidity was obtained by mixing together and altering the ratio of a dry flow and a flow which had been passed through a water bubbler. The total flow rate passing through the reaction flow tube was always kept between 5.1 and 5.5 L min⁻¹.

The carrier gas for the experiments performed at the PSI was nitrogen, which was also generated from outside air (PSI departmental nitrogen) for the HO₂ flow, and air (PSI departmental air) for the aerosol flow. Denuders were used to remove trace gases, charcoal was used to remove ozone and cobalt oxide was used to remove NO_x species (Ammann, 2001; Lee and Davidson, 1999). For these experiments, there was no humidified flow, and the only way of changing the humidity was by humidifying the chamber which was done before the experiment was started. The total flow rate passing through the flow tube was $5.2 \pm 0.2 \text{ L min}^{-1}$.

2.3 HO₂ generation

HO₂ radicals were formed by the photolysis of water vapour using a mercury lamp (L.O.T. Oriel, model 6035) followed by reaction with oxygen, found in trace amounts (normally specified as 20 – 30 ppm) in the nitrogen supply, via the following reactions:



Assuming a 30 ppm mixing ratio of O₂ in the nitrogen, the lifetime of the H atom due to Reaction 2.2 at atmospheric pressure would be $\sim 17 \mu\text{s}$ and would therefore lead to rapid conversion to HO₂. The mercury lamp was placed at the end of the injector (110 cm, 1.9 cm outer diameter (O.D.), 1.6 cm inner diameter (I.D.)) furthest from the exit. The injector contained Teflon inserts (1.5 cm O.D, 0.8 cm I.D.) which reduced the loss of HO₂ to the walls of the injector. By placing the mercury lamp at the end of the injector there was the longest possible time for the nitrogen to cool down before entering the flow tube, although it did present disadvantages including: (1) larger HO₂ wall losses within the injector; (2) longer reactions times for HO₂ + HO₂ reaction to happen within the injector and larger production of H₂O₂. There was also an externally mounted fan (Micromark) pointed directly at the end of the injector in order to cool down the region that the mercury lamp was heating. The thermocouples placed inside the flow tube (see Figure 2.4 in Section 2.5.1) showed that the HO₂ flow was within 1 K of room temperature when it entered the reaction flow tube. The flow rate of the HO₂ flow was $1.31 \pm 0.03 \text{ L min}^{-1}$. The OH formed in Reaction 2.1 was lost

within the injector, which was confirmed by checking that if the lamp was turned on and off, with the NO flow turned off (so that no HO₂ would be detected), the signal did not change.

For the majority of experiments the HO₂ radical was formed at a concentration of $\sim 1 \times 10^9$ molecule cm⁻³ exiting the injector and assuming full mixing with the other flows. However, it was possible to change the initial HO₂ concentration by changing the current of the lamp from 2 mA to 20 mA which produced initial HO₂ concentrations of between 3×10^8 molecule cm⁻³ and 3×10^9 molecule cm⁻³. The initial concentration of HO₂ was determined from an OH calibration of the FAGE cell (see Section 2.7), and by propagating the wall loss back to 4.3 cm along the flow tube (the position at which the FAGE cell sampled).

2.4 Aerosol generation

For the majority of experiments, polydisperse aerosols were produced using an atomiser (model 3076, TSI). The atomiser works by drawing up a liquid from a bottle which is then atomised using a fast nitrogen jet that has passed through a pin hole. The small aerosols will follow the nitrogen flow out of the top of the atomiser whereas larger droplets are drained back into the bottle. Most experiments were performed using a 1% w/v solution of a salt or organic in MilliQ (mQ) water which was placed in the atomiser. All chemicals used were from and were from Fisher Scientific, Sigma-Aldrich or Acros Organics unless it has been specifically stated otherwise in another chapter. If a different concentration was used this will also have been stated explicitly in the relevant chapter. All chemicals used had a purity of at least 99% apart from humic acid (Acros Organics) that had a purity of between 50 - 60 %. Effloresced aerosols were produced by passing the aerosols produced by the atomiser through a diffusion dryer (a long tube (53.5 cm) filled with a silica gel desiccant) to generate a relative humidity lower than the efflorescence humidity. The relative humidity within the experimental setup was then controlled to make sure that it did not exceed the deliquescence point of the aerosols. When aqueous aerosols were required the diffusion dryer was bypassed. The relative humidity throughout the experimental setup was then kept above the efflorescence point of the aerosols. Relative humidities of 5 % to 80 % were able to be achieved within the aerosol flow tube. Efflorescence and deliquescence were discussed in

greater detail in Section 1.2. For insoluble organics (stearic acid, oleic and squalene) the aerosols were generated by homogeneous nucleation. Homogeneous nucleation involved placing the organic into a steel tube and passing a 0.5 slpm flow over the organic whilst heating the tube to 379 – 384 K for stearic acid, 410 – 416 K for oleic acid and 412 - 413 K for squalene.

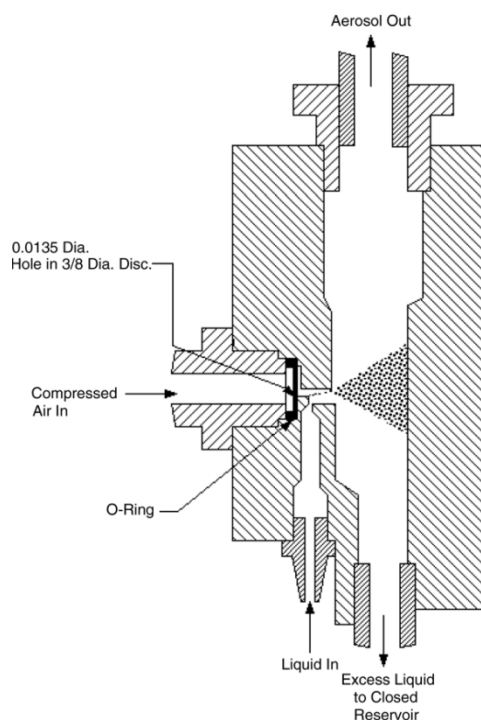


Figure 2.3: A schematic of the atomiser (model 3076, TSI) reproduced from (TSI, 2005).

For mineral dust experiments, a dust disperser was designed. This consisted of a 500 ml high-density polyethylene (HDPE) bottle (Thermo Scientific Nalgene) that had two holes drilled into it (one through the lid and one 5 cm from the base of the bottle). Two 1/4" O.D. tubes were placed through the holes and affixed to the bottle using Araldite. Nitrogen entered the dust disperser through the tube on the side of the bottle and left through the tube at the top of the bottle. A stir bar (polytetrafluoroethylene (PTFE) covered, 45 mm) was placed in the bottle and the bottle was placed on top of a magnetic stirrer (Gallenkamp, 8640677) which was set to the maximum stirring speed. The combination of the stirring and the nitrogen flow produced a 'dust cloud' in the bottle. Unlike the atomiser, the dust disperser generated a non-stable aerosol concentration.

For the SOA experiments the aerosols were produced by the oxidation of either α -pinene or trimethylbenzene (TMB). The volatile organic compounds (VOCs) were oxidised using either ozone from an ozone generator in the smog chamber, by adding NO_2 to the smog chamber in the presence of UV light or by the photolysis of water vapour in the PAM chamber. These three different types of experiments and the formation of SOA from the oxidation of VOCs will be described in much greater detail in Section 5.3. Photographs and detailed descriptions of both chambers are also included in Section 5.3.

Once the aerosols had been produced (with the exception of SOA), they were passed through an impactor with a 0.071 cm pinhole (TSI 1035900) which limited the maximum diameter of the aerosols produced by the atomiser, that passed through the flow tube, to ~ 700 nm (which was tested experimentally by comparing size distributions with and without the impactor present). The impactor works by causing the flow passing through the pinhole to be accelerated. Larger particles contained within the flow impact onto a plate opposite the pinhole whereas smaller particles follow the flow and exit the impactor. However, when mineral dust (Arizona Test Dust, 0-3 Micron) was used larger aerosols (> 700 nm) were observed passing through the impactor, although the reason for this remains unclear. The concentration of aerosols entering the flow tube was controlled using a high efficiency particulate air (HEPA) filter (composed of a mat of randomly arranged fibreglass fibres) and a bypass. The proportion of the flow passing through the bypass compared to the filter was controlled using a needle valve. In order to determine the wall loss in the absence of aerosols all of the flow passed through the filter. The aerosol flow from the atomiser was always kept constant at $1.0 \pm 0.1 \text{ L min}^{-1}$ and was monitored on the SMPS screen.

2.5 The reaction flow tube

2.5.1 A description of the reaction flow tube

The flow tube used during the experiments, which is shown in Figure 2.4, had an inner diameter of 5.9 cm and a length of 107 cm. One end of the flow tube was attached to a FAGE cell and this end also had an outlet for the flow to enter the SMPS. The other end of the flow

tube had two inlets through which the humidified aerosol flow entered. The injector tip had small holes drilled into the side of it, which meant that the HO₂ flow was released perpendicularly to the aerosol flow. By releasing the HO₂ flow perpendicularly to the aerosol flow good mixing of the flows was expected (see Section 2.5.2). The inside of the flow tube was coated with halocarbon wax (Halocarbon Wax Corporation- wax 600) which meant that the HO₂ radicals were only exposed to unreactive carbon-halogen bonds which reduced the loss of HO₂ to the walls of the flow tube (De Haan et al., 1999). The temperature of the flow tube was able to be controlled by cooling a mixture of water and ethylene glycol to the desired temperature and then pumping it through the jacket of both the conditioning flow tube and the reaction flow tube. The flow tube was wrapped in neoprene which is a very insulating material. Calibrated thermocouples were placed at the ends of the flow tube in order to measure the temperature of the flow. The relative humidity inside the flow tube was monitored using relative humidity probes (Rotronic HC2-S, accuracy $\pm 1\%$) placed near the end of the flow tube and / or placed just after the flow tube. The concentration of aerosols exiting the flow tube was measured to be within 1% of the concentration of aerosols entering the flow tube.

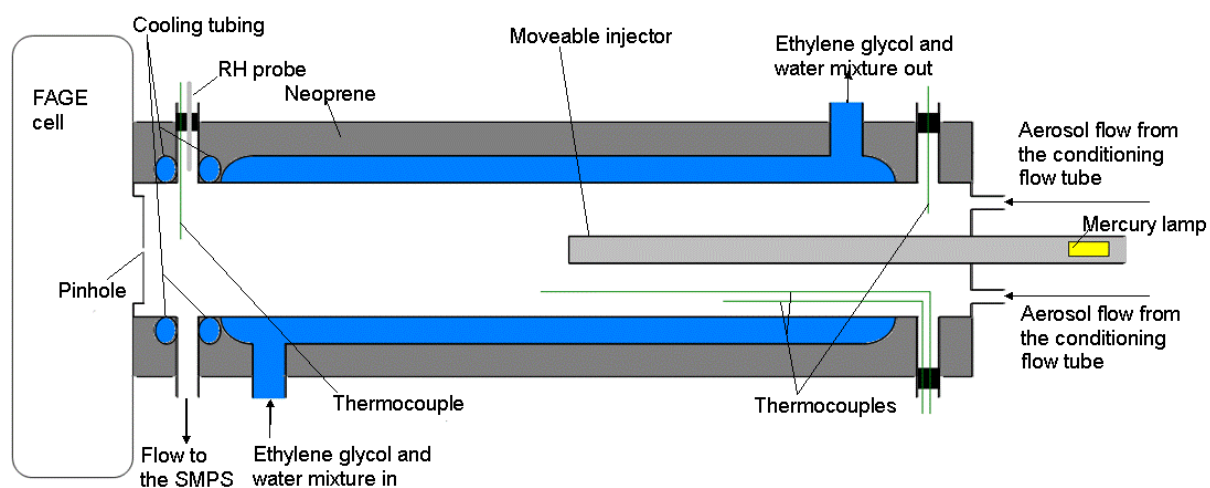


Figure 2.4: Cross-sectional view of the aerosol flow tube used in the uptake experiments. The diagram is not to scale.

2.5.2 The flow regime in the reaction flow tube

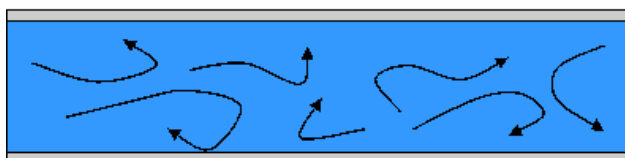
The flow velocity (v) in the aerosol flow tube varied between approximately 3.0 and 3.4 cm s⁻¹, giving a Reynolds number (Re) in the region of 110 to 130 using the following equation:

$$Re = \frac{vD\rho}{\mu} \quad (\text{E2.1})$$

where D is the diameter of the flow tube, ρ is the density of the nitrogen and μ is the viscosity of the nitrogen.

A Reynolds number is a dimensionless number which is a measure of the ratio of inertial forces to viscous forces and can be used to identify the flow regime. A Reynolds number of greater than ~ 4000 means that turbulent flow is occurring whereas a Reynolds number of less than ~ 2300 is characteristic of laminar flow (Holman, 2002). Therefore, the flow in the flow tube should definitely have been laminar. The turbulent and laminar flow regimes are illustrated in Figure 2.5.

TURBULENT FLOW



LAMINAR FLOW

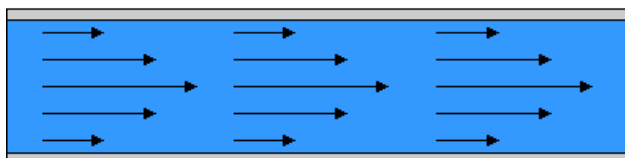
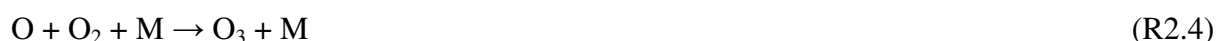


Figure 2.5: Schematic of turbulent and laminar flow. The length of the arrows represents the velocity.

The mixing time of the aerosol flow with the HO₂ flow is given by $r^2/5D_g$, where r is the radius of the flow tube and D_g is the gas-phase diffusion coefficient of HO₂ which has been estimated to be 0.25 cm²s⁻¹ in nitrogen at 298 K and 760 Torr (Mozurkewich et al., 1987).

The mixing time was therefore approximately 7 seconds which is equivalent to complete mixing occurring during the first 24 cm from the injector. However, in order to demonstrate that mixing was indeed only occurring for the first 24 cm along the flow tube and that there was a laminar flow, an ozone profiling method was used. Ozone was produced by the photolysis of oxygen in zero air (BOC, 18- 21% oxygen) using the mercury lamp in the injector and is shown in the following reactions:



An ozone analyser (ThermoElectron 49 C, detection limit 1 ppb) sampled ozone in the centre of the flow tube through a ¼ inch O.D. tube at 8 cm from the FAGE pinhole. Ozone loss to the halocarbon wax coated walls of the flow tube is slow ($\gamma \leq 10^{-6}$) and therefore, when moving the injector to different positions along the flow tube the signal due to ozone was expected to remain within 2 % along the flow tube for a well-mixed flow (Slade and Knopf, 2013). The result of this experiment is shown below in Figure 2.6.

From Figure 2.6, it can be seen that from approximately 20 cm (~ 7 seconds) ozone concentrations remain within 5 % of the values measured at 30 cm (~ 10 seconds) and that all concentrations are within 10 % of the concentration at 30 cm. Therefore, it was decided that all of the data would be collected between 20 and 70 cm (~ 7 – 20 seconds). A second method was also utilised in order to check the mixing and is described below.

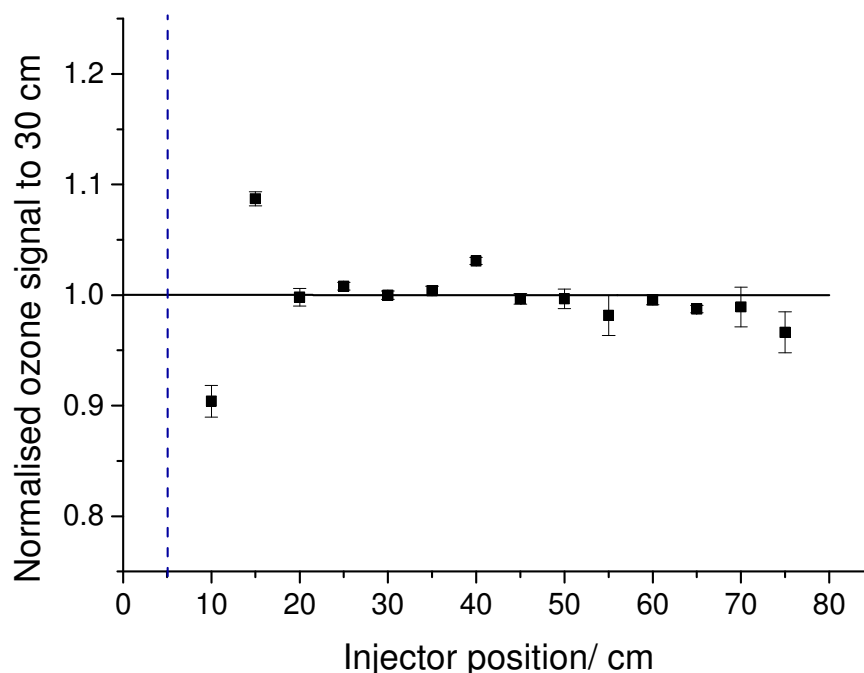


Figure 2.6: The O_3 signal normalized to the signal at 30 cm obtained when moving the injector backwards and forwards along the flow tube with distances representing the injector position along the flow tube. The O_3 was being measured inside the flow tube at 5 cm (blue dashed line) from the FAGE cell (see Figure 2.4) and in the radial centre. The total flow rate through the flow tube was 5.3 slpm. The error bars represent the standard deviation in the data.

The second method to check the mixing involved moving the injector towards and away from the FAGE cell and recording the signal (HO_2 detection by FAGE will be discussed in Section 2.7). As the HO_2 is injected into the flow tube perpendicularly to the rest of the flow, it was expected that it would take a certain amount of time for the HO_2 to mix and diffuse into the centre of the flow tube. As the FAGE cell samples from the centre of the flow tube (see Section 2.7 on FAGE detection of HO_2), an increase in signal was initially expected with increasing time (due to the HO_2 mixing and diffusing into the centre), followed by a decrease in signal due to wall loss. This method suggested that when the injector was ~15 cm along the flow tube the HO_2 flow was well mixed into the rest of the flow (Figure 2.7) and therefore no HO_2 signals were recorded at distances ≤ 15 cm.

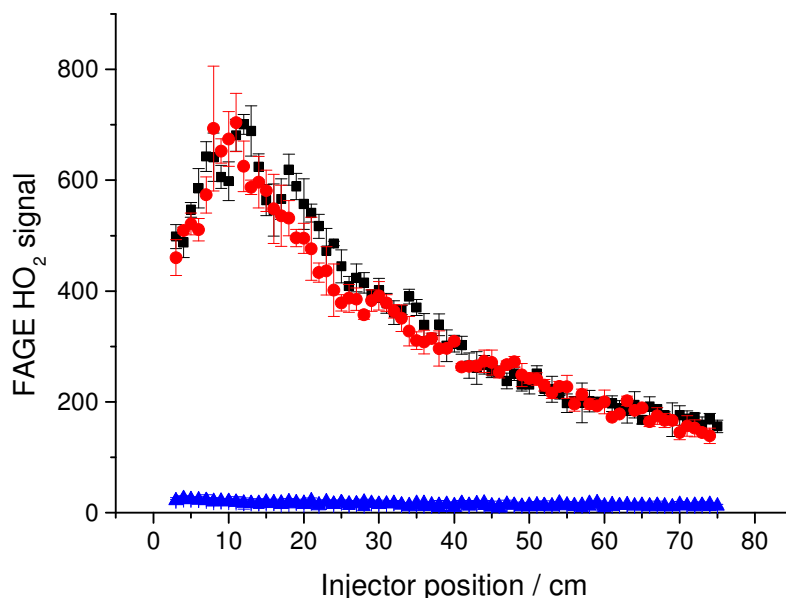


Figure 2.7: The FAGE HO₂ signal in the presence of ammonium sulphate aerosols at a concentration of $1.4 \times 10^6 \text{ cm}^{-3}$ at different injector positions along the flow tube. With the NO on, the injector was moved away from the FAGE cell (black points) and towards the FAGE cell (red points). With the NO off the measured signal represented the OH + background signal (blue points).

Aerosol profiles were also run to check the mixing of the aerosols into the flow. The humidified aerosol flow and the injector flow were set to match experimental conditions. The aerosols were measured along the flow tube and in different radial positions by placing a tube that was connected to the CPC in these positions. When the tube was very close to the injector ($\sim 1 \text{ cm}$) the aerosol number concentration was approximately 25 % higher in the centre of the flow tube than when measuring next to the sides of the flow tube. However, at 10 cm from the injector the aerosol concentration was constant across the flow tube (within 5 % error) and did not decrease at longer distances along the flow tube.

2.5.3 The temperature in the reaction flow tube

The majority of experiments performed in this work were done at room temperature. However, there was a set of experiments where the temperature was varied between -10°C and 40°C . The temperature during these experiments was varied by pumping a 50:50 mixture

of water and ethylene glycol, that had been cooled or heated through the jackets of both the conditioning flow tube and the main flow tube as well as through a cooling tube (see Figure 2.4). The temperature of the water and ethylene glycol mixture was adjusted and the mixture was pumped through the equipment using a refrigerated circulator (Thermo Scientific HAAKE, DC50-K35). The temperature gradients between -10°C and 40°C were measured along the top (next to the jacket) and middle (or centre) of the flow tube by moving thermocouples to different positions along the flow tube.

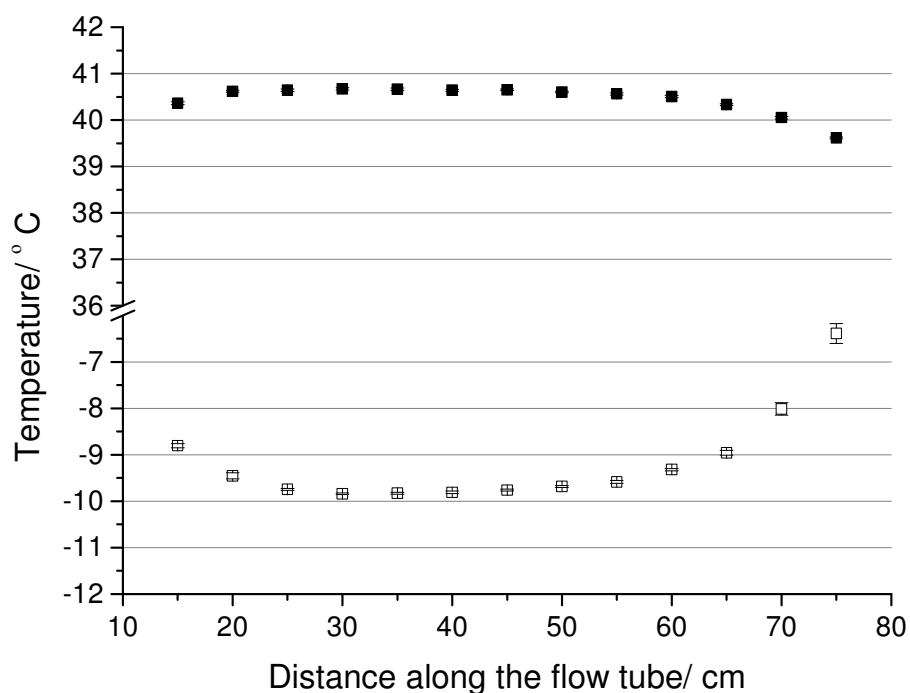


Figure 2.8: The temperature gradients along the flow tube when the chiller was set to -10°C and 40°C (the two extreme temperatures). The injector tip was radially centred and placed at 75 cm from the end of the flow tube which was open to the atmosphere at 0 cm. The flows were the same as the flows used during experiments.

Having axial or radial temperature gradients within the flow tube when cooling or warming the flow tube would mean that the reactions were taking place at a range of temperatures rather than at one single temperature. Another problem with having temperature gradients could be that the flow would be disrupted due to convection within the flow tube and there would probably also be humidity gradients which could also potentially affect the uptake.

The results of the temperature gradient experiments showed that after 5 cm from the injector the temperature stayed within two degrees and after 10 cm from the injector the temperature stayed within one degree (Figure 2.8). The temperature at the top of the flow tube was always measured as being within one degree of the temperature in the centre of the flow tube. Therefore, there should not be large amounts of convection or large humidity gradients in the flow tube. Close to the injector, the flow temperature was slightly affected by the temperature of the flow leaving the injector. At the end of the flow tube (at short distances) there was some mixing with the air outside the flow tube which also affected the measured temperature. However, during actual experiments, the flow tube was not exposed to the air at one end and therefore, this air could not mix in to the flow tube. Instead, the FAGE cell was attached to the flow tube. During experiments, the temperature at this end of the flow tube was monitored using a thermocouple at approximately 10 cm (as shown in Figure 2.4). It was found that the temperature remained within one degree of the expected temperature, as set by the chiller) when the FAGE cell was attached to the flow tube.

2.6 Particle detection and characterisation

2.6.1 The measurement of the total particle surface area in a given volume

The total particle surface area was measured using a SMPS (TSI, model 3080 for experiments performed in Leeds, a custom built instrument was used for experiments performed in Switzerland). The SMPS in Leeds consisted of a neutraliser (TSI, model 3077), a DMA (TSI, model 3081) and a CPC (TSI, model 3775) whereas in Switzerland the SMPS consisted of a neutraliser (Kr-85), a DMA (length 93.5 cm, inner radius 0.937 cm and outer radius 1.961 cm) and a CPC (TSI, model 3775). Inside the neutraliser the aerosols collide with bipolar ions (a mixture of positive and negative ions) which give the aerosols a known charge distribution. The DMA consists of two concentric metal cylinders, and a schematic cross section of it is shown in Figure 2.9. The inner cylinder has a negative voltage applied to it whilst the outer cylinder is grounded. The aerosol flow and a sheath flow enter the top of the DMA. Particles with a certain diameter will exit through a slit at the bottom of the DMA. The aerosols that exit through that slit depends on the sheath flow rate, the charge on the aerosol

(whether it is positive or negative and the magnitude), the dimensions of the DMA and the negative voltage that has been applied to the central cylinder. Therefore, the DMA allows aerosols to be size selected by changing the voltage on the central cylinder. The aerosols in each size bin can then be counted using the CPC. In the CPC the aerosols enter a cooled condenser where butanol vapour condenses onto them so that they grow into larger droplets (several micrometres in diameter) that can be detected by an optical detector. At low aerosol concentrations ($< 5 \times 10^4 \text{ cm}^{-3}$) each aerosol is detected as an individual pulse whereas at higher concentrations ($> 5 \times 10^4 \text{ cm}^{-3}$) light scattering due to the aerosols can be used to determine an aerosol concentration from an internal calibration. All measurements in this work were made in the low aerosol mode with each aerosol size bin containing fewer than $5 \times 10^4 \text{ cm}^{-3}$ particles.

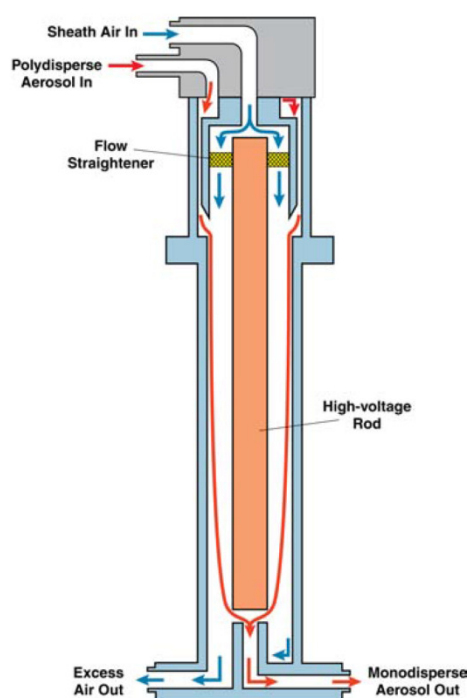


Figure 2.9: A schematic of the DMA (model 3081). The figure is reproduced from (TSI, 2009).

Particles with a diameter in the range of 14 nm to 700 nm were measured. There were no aerosols which were greater in size than 700 nm as these had been removed by the impactor (except when mineral dust was being used as discussed in Section 2.4). Particles smaller than 14.6 nm in diameter were also not measured but would have contributed less than 1% of the

total surface area. Each scan took three minutes and the aerosol size distribution was measured at least twice during each decay for a moving injector experiment and once for each concentration for a fixed injector experiment. A typical distribution obtained during an experiment is shown in Figure 2.10.

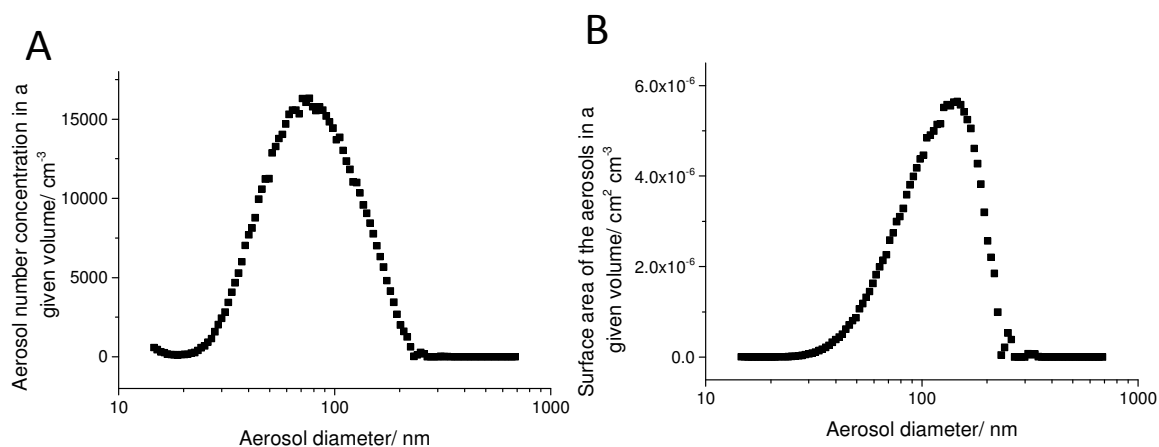


Figure 2.10: A graph showing the typical (A) aerosol number concentrations and (B) aerosol surface areas obtained per cubic centimetre for the distribution of aerosol diameters that are found. This was a plot obtained for ammonium nitrate aerosols at a relative humidity of 77 %, 293K and atmospheric pressure.

The accuracy of the SMPS size measurements was tested using Polystyrene latex (PSL) beads (Sigma-Aldrich) of known sizes (81 ± 3 nm, 152 ± 5 nm, 199 ± 6 nm, 299 ± 6 nm, 350 ± 7 nm and 491 ± 4 nm) that were suspended in mQ water. The SMPS measured the size distribution of the beads. The SMPS data were then fitted with log normal peaks (Figure 2.11A). The aerosol diameter at the peak maximum was then plotted against the actual diameter of the beads which produced a graph with a slope of 0.983 and an R^2 value of 0.9997 (Figure 2.11B).

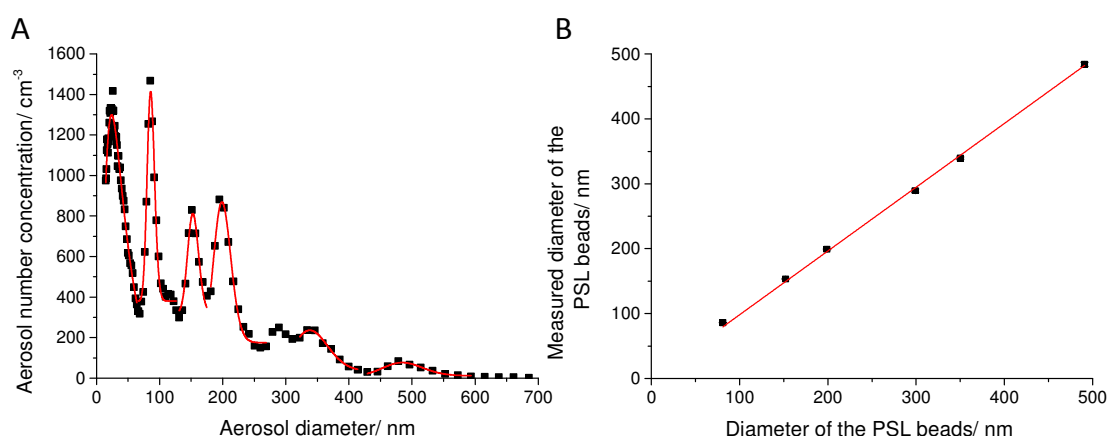


Figure 2.11: (A) The number distribution of the polystyrene latex (PSL) beads as a function of diameter measured by the SMPS. The red lines are the log normal fittings to the data. (B) The peaks of the log normal fittings against the actual size of the PSL beads. The slope of the line was 0.983.

For mineral dust experiments, the aerosol concentration was not stable over a period of three minutes. Therefore the aerosol number concentration was recorded using a second CPC which took a reading every one second. By using a combination of the average SMPS scans, which measured up to 700 nm and by also measuring the size distribution using an Aerodynamic Particle Sizer (APS, TSI, 3321) the entire distribution could be measured (Figure 2.12). As the APS measures the time of flight of the aerosols between two points the Aerodynamic diameter (D_a) needed to be converted into a Stoke's diameter (D_s), measured by the SMPS, using the following equation:

$$D_s = \frac{D_a}{\sqrt{\rho\beta}} \quad (\text{E2.2})$$

where ρ is the density of the aerosols (assumed to be 2.7 g cm⁻³ for Arizona Test Dust) and β is a shape factor correction that accounts for the non-sphericity of the aerosols. For Arizona Test Dust a β value of 1.8 gave the best agreement between the APS and the SMPS size distributions, which is similar to the value of 1.6 used by Tang et al. (2012) for Saharan dust aerosols. The number concentration distribution could then be used to find the average radius of the aerosols and, by assuming spherical particles.

$$A_{total} = 4\pi r_{av}^2 N_{total} \quad (\text{E2.3})$$

where A_{total} is the total surface area of the distribution, N_{total} is the total number of aerosols in the distribution and r_{av} is the average radius of one aerosol in the size distribution. The average radius was determined to be 273 nm and 271 nm for Arizona Test Dust and for a proxy of cosmic dust respectively (see Section 7.6 for more information about cosmic dust). The average surface area of one aerosol (A_d) can then be calculated by assuming spherical particles using the following equation:

$$A_d = 4\pi r_{av}^2 \quad (E2.4)$$

By knowing the average surface area of one aerosol, the number concentrations in a given volume measured by the CPC can be converted to surface areas in a given volume that is used to measure the uptake coefficient as described in Section 2.10.

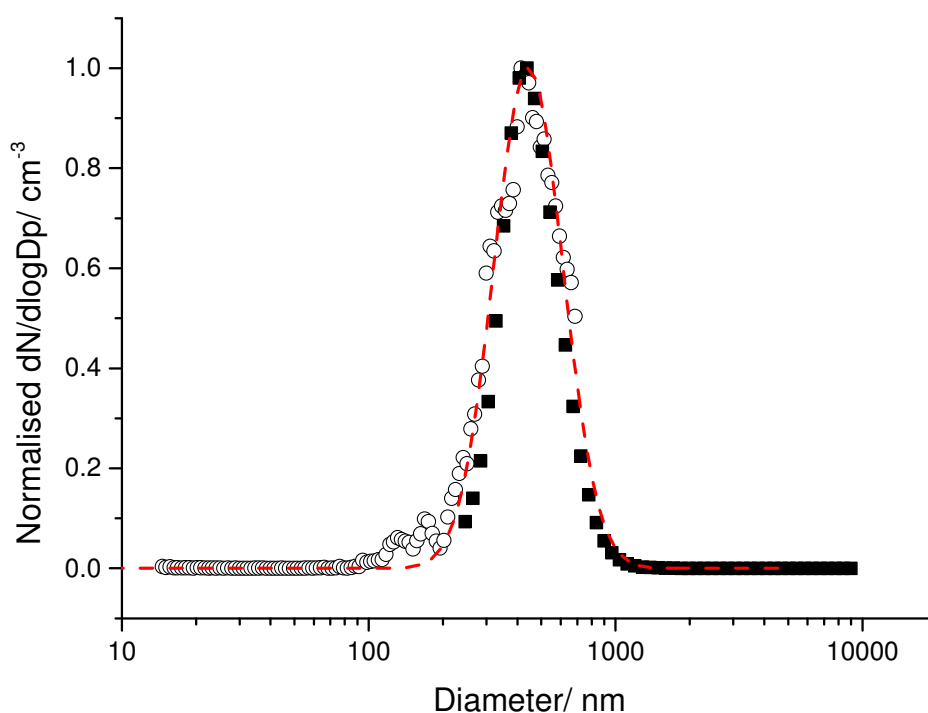


Figure 2.12: The normalised aerosol number distribution measured by the SMPS (white points) and APS (black points) for Arizona Test Dust aerosols. The red line represents a log normal fitting to both of the distributions.

In order for the concentration to be correctly measured by the SMPS, the aerosols had to be neutralised to a given charge distribution. A test was performed to check whether the neutraliser in the SMPS would ensure the necessary charge distribution or whether a second neutraliser (Grimm 5522) was needed. The test consisted of changing the aerosol number concentration and then measuring it using both the SMPS (which relied on a given charge distribution) and a CPC (which did not rely on a given charge distribution). The total number concentration for the SMPS was obtained by integrating over all of the aerosol sizes. The result of this test is shown in Figure 2.13 which shows that with only the SMPS neutraliser the aerosol concentration started to be overpredicted at $\sim 6 \times 10^5 \text{ cm}^{-3}$ due to the aerosols not being fully neutralised. However, with the Grimm neutraliser placed just after the atomiser, the measured SMPS concentration agreed with the CPC within 5 % error. Therefore, the Grimm neutraliser and the SMPS neutraliser were used for all experiments. Using a neutraliser before the flow tube also had the added advantage that the aerosols were less likely to coalesce or to be lost to the walls of the flow tube due to static charges.

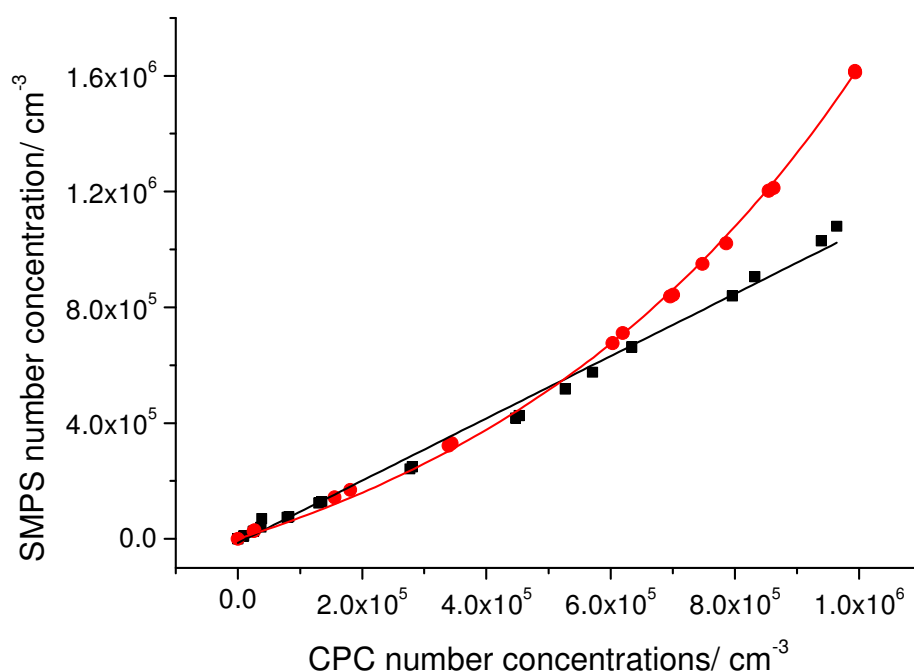


Figure 2.13: A graph of the measured SMPS aerosol number concentrations against the CPC number concentrations for aqueous NaCl particles with (black squares) and without (red circles) a second neutralizer in the aerosol flow. The black points were fitted with equation $y = 1.05x$ and the red points were fitted with the equation $y = -4.4 \times 10^5 + 4.4 \times 10^5 \exp(1.6 \times 10^{-6}x)$.

2.6.2 Characterising the phase of the aerosols

It was important to know whether aerosols were aqueous or solid during the experiments. Literature values of the deliquescence and efflorescence relative humidities for different aerosols, used in this thesis, at 298K and atmospheric pressure are summarised in Table 2.1.

Aerosol type	Deliquescence relative humidity/ %	Efflorescence relative humidity/ %
Ammonium sulfate	79.9 ^a	36 – 43 ^e
Ammonium nitrate	61.8 ^a	No crystallization observed at 0% RH ^f
Sodium chloride	75.3 ^a	45 ^g
Malonic acid	69 ^b	6 ± 3 ^b
Oxalic acid	~ 100 ^b	< 5 ^b
Glutaric acid	~ 88 ^c	22.5 – 36 ^c
Humic acid	60 – 75 ^d	< 5 ^d

Table 2.1: Literature values for the deliquescence and efflorescence of some types of aerosol at 298K. (a) Finlayson-Pitts and Pitts (2000) (b) Braban et al. (2003) (c) Pant et al. (2004) (d) Gysel et al. (2004) (e) Ciobanu et al. (2010) (f) Lightstone et al. (2000) (g) Biskos et al. (2006)

A diagram of how the volume of ammonium sulphate aerosols changes with increasing and decreasing relative humidities was shown in the humidogram in Figure 1.3 in Section 1.2, which showed that as the relative humidity decreases the aerosol volume decreases until the efflorescence point is reached. Below the efflorescence point, the aerosols are dry and therefore a decrease in relative humidity does not affect the volume of the aerosols. If the humidity is then increased, the aerosols remain at the same size until the deliquescence point is reached. This change in the size of the aerosols was used to investigate aerosols where the deliquescence and efflorescence points were not in the literature.

In order to know whether an aerosol was aqueous or solid for a given relative humidity (if the information could not be ascertained from the literature) either a humidogram, shown in Figure 2.14, was created or a much quicker phase test, shown in Figure 2.15, was performed.

If the aerosols were deliquesced, a decrease in the relative humidity would cause a reduction in the average radius of the aerosol as well as a decrease in the total surface area of the aerosols. On the other hand, if the aerosols were effloresced or solid a reduction in the relative humidity would not affect the average radius of the aerosols or the total surface area (Figure 1.3 in Section 1.2). The reduction in relative humidity did not affect solid aerosols as there was no liquid present to evaporate and hence reduce the volume and radius. For copper-doped ammonium nitrate experiments, which were performed at different temperatures and are discussed in Section 6.4, a humidogram was created by comparing the average surface area per aerosol in each experiment. Each point represents a different experiment and by comparing experiments the phase of the aerosols could be determined. As can be seen from Figure 2.14, for a given relative humidity deliquesced aerosols were at least a factor of two larger than effloresced aerosols, and also increased in size with increasing humidity, whereas effloresced aerosols remained the same size over a range of humidities. There is also good agreement between the change in the size of the copper-doped ammonium nitrate aerosols over a range of relative humidities, and the size predicted for ammonium nitrate aerosols predicted by the AIM model (Clegg et al., 1998; Wexler and Clegg, 2002), which allowed a temperature correction in the aerosol size, as described in Section 2.12.1, to be made between the DMA and the flow tube. It should be noted that the humidity in the DMA was only measured during the determination of wall losses during these experiments. If the relative humidity probe had been attached to the DMA during uptake experiments with aerosols, it could have affected the aerosol concentration or distribution. However, the humidity appeared constant in the DMA between the beginning and the end of an experiment.

However, there were some aerosol types where the efflorescence and deliquescence points were unknown but where experiments were only done at one relative humidity. For these aerosols a quick check (instead of a more time consuming humidogram) was carried out to determine the phase of the aerosol. The humidity was decreased slightly and the aerosol surface area distribution was measured using the SMPS. The total aerosol number concentration was kept constant for both humidities. If a decrease in the peak radius and a decrease in the surface area was observed, it could be concluded that at the higher humidity the aerosols were aqueous, whereas if no change in the peak radius and surface area were measured the aerosols were dry at the higher humidity.

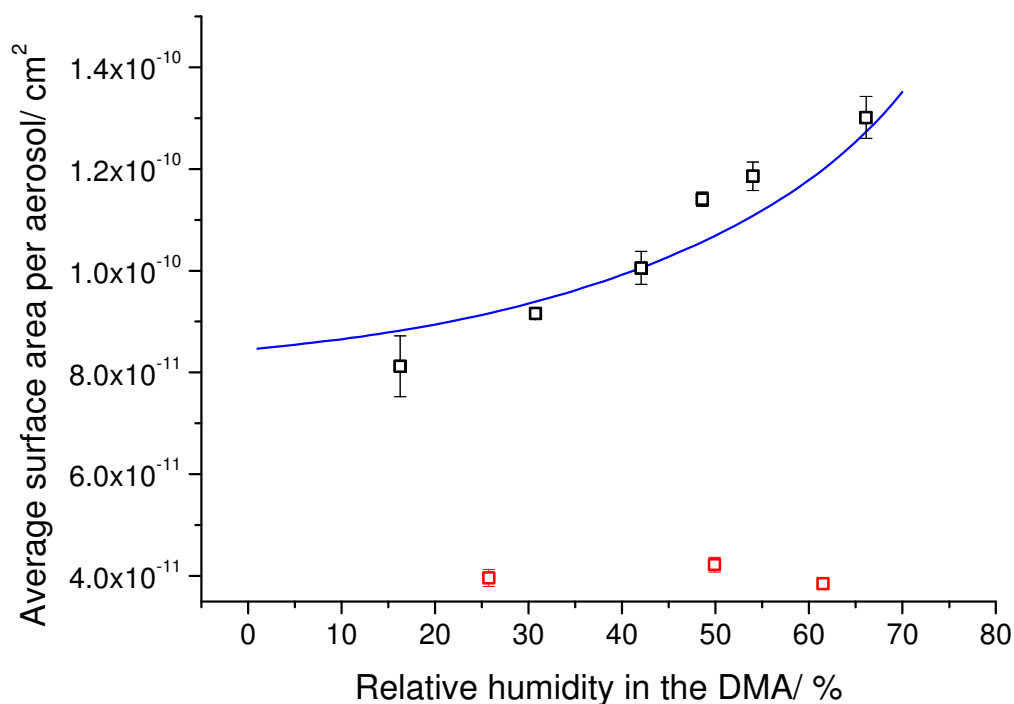


Figure 2.14: A humidogram for copper-doped ammonium nitrate aerosols. The black points represent deliquesced copper-doped ammonium nitrate whereas the red points represent effloresced copper-doped ammonium nitrate. The copper-doped ammonium nitrate aerosols were produced from a solution which consisted of 0.8 g ammonium nitrate and 0.125 g copper sulphate dissolved in 500 ml mQ water. The blue line is for comparison purposes and represents the expected behaviour of ammonium nitrate aerosols according to the aerosol inorganic model (AIM) model. These points have been normalised to agree with the black point at 42 % RH.

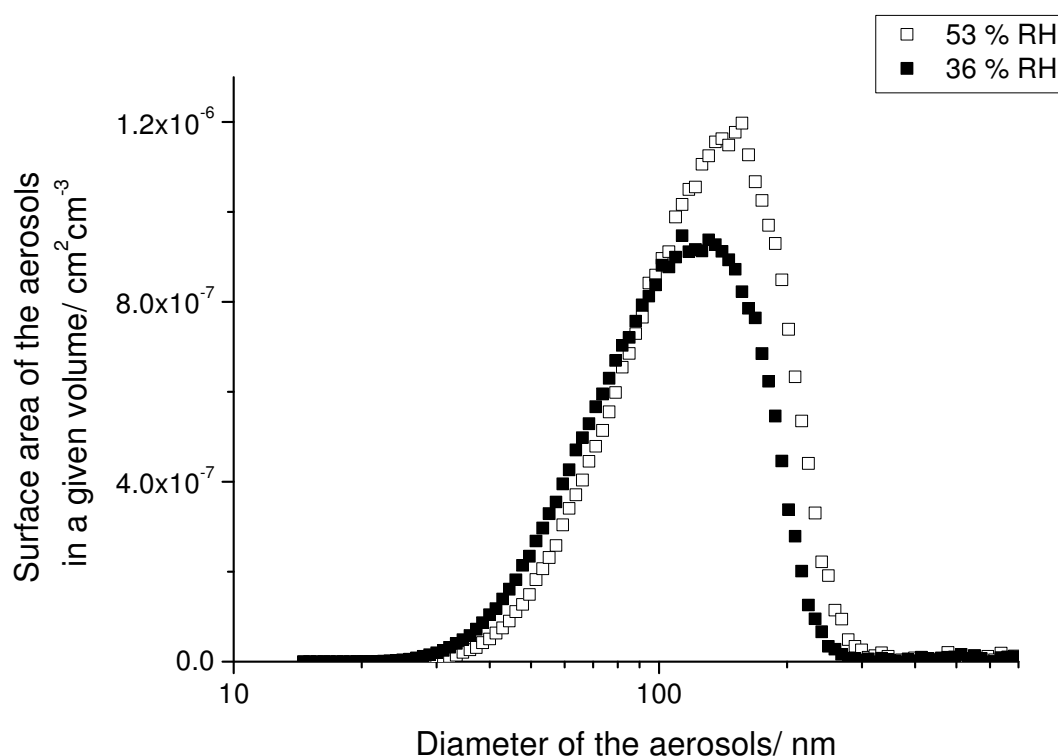


Figure 2.15: An example of the decrease in average radius and surface area seen when decreasing the relative humidity from 53 % to 36 % for ammonium sulphate aerosols that had been buffered to a pH of 7.2 using potassium dihydrogen orthophosphate and sodium hydroxide. At both relative humidities the same concentration of aerosols were present. The moles of ammonium sulphate were ten times the mole of the buffer. The decrease in radius and surface area shows that the aerosols must have been wet at a relative humidity of 53 %.

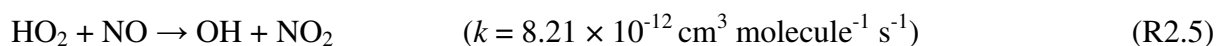
2.6.3 Characterising the metal ion content of the aerosols

As the metal ion content of an aerosol can affect the magnitude of the HO_2 uptake coefficient, all of the atomiser solutions were analysed for their copper and iron ion content. The analysis was performed in the Department of Engineering at the University of Leeds using Inductively-coupled Plasma Mass Spectrometry (ICP-MS, Perkin Elmer Elan DRCe, sensitivity 1 ppt). ICP-MS works by converting the samples into aerosols that are then introduced into an argon plasma that consists of argon ions that are caught in oscillating electric and magnetic fields and collide with other argon atoms at a temperature of 6000 - 10000 °C. Once the aerosols enter the plasma the aerosols are desolvated and the elements in the aerosol are turned into gaseous atoms that are then ionised. These ions can then be detected by the mass spectrometer.

The technique relied on a calibration and therefore copper and iron standards were made up in mQ water. A blank sample consisting of mQ water was also run in the ICP-MS so that the metal concentrations in mQ water could be subtracted from the sample concentrations. The standards that were made consisted of 6 different copper (II) and iron (II) concentrations (10 ppt, 100 ppt, 1 ppb, 10 ppb, 100 ppb and 1 ppm).

2.7 Measurement of HO₂ and FAGE calibration

The HO₂ radicals were measured by the Fluorescence Assay by Gas Expansion (FAGE) technique (Heard, 2006; Heard and Pilling, 2003; Zeng et al., 1998). The FAGE cell used in the experiments is illustrated in Figure 2.16 and approximately 3.6 litres per minute (65 - 72% of the total flow) were drawn from the flow tube through a 0.7 mm pinhole. The HO₂ that entered the FAGE cell was converted into OH via the following reaction:



The NO (BOC, 99.5%, EC No. 233-271-0) was added approximately 5 cm downstream from the pinhole into the FAGE cell at a rate of 50 ml min⁻¹ in order to ensure that there was rapid conversion of HO₂ into OH. The photodiode (New Focus, 2032) was directly opposite to the laser beam entering the FAGE cell in order to be able to measure the laser power so that the signal could then be normalised to take into account fluctuations in laser power. The OH fluorescence was focused onto the photocathode of a channel photomultiplier tube (Perkin Elmer, C-943P), kept at -2900 V, using fast optics and was passed through a bandpass filter (Barr Associates, 308 nm, FWHM = 8 nm). A photon counting card (Becker and Hickl GmbH, PMS-400) was used to measure individual photons due to OH fluorescence.

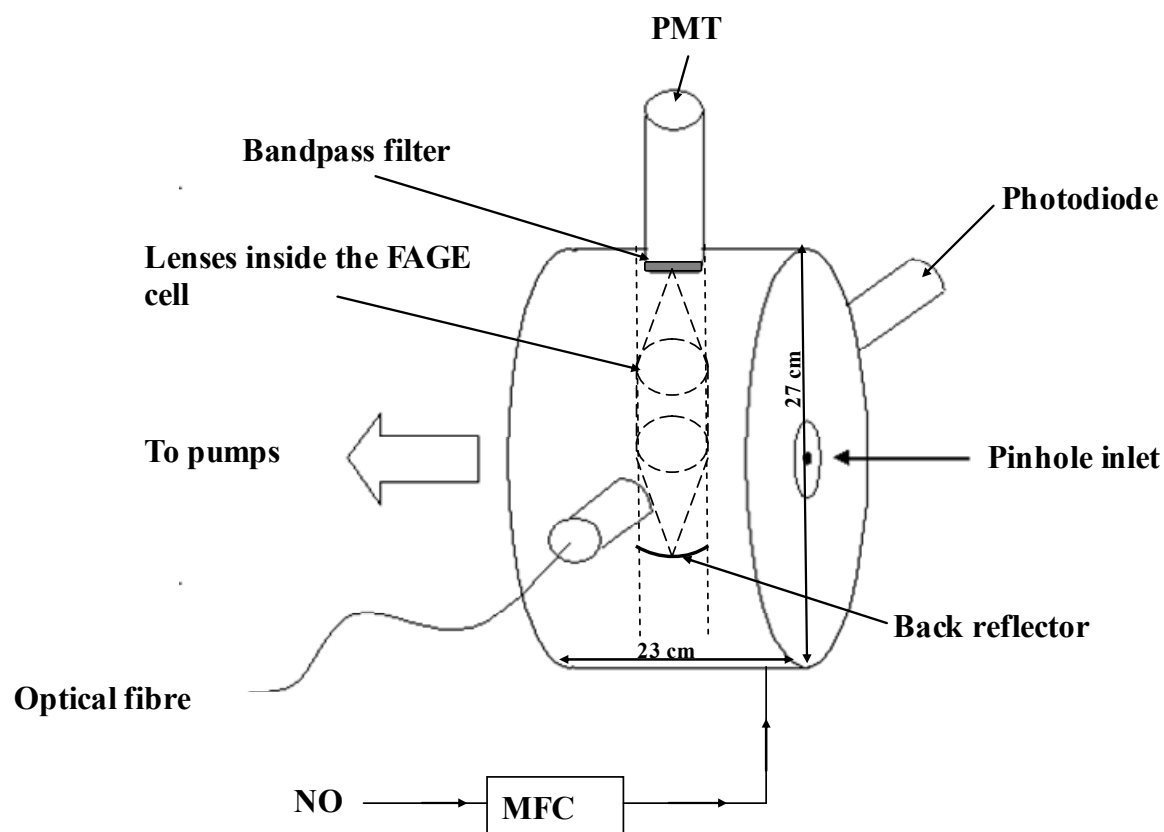


Figure 2.16: A schematic of the FAGE cell used to measure HO_2 . The diagram is not to scale.

A frequency-doubled dye laser (Sirah Laser und Plasmatechnik, GmbH) that was pumped by an Nd:YAG laser (JDSU Q201-HD Q-series) producing 532 nm radiation was utilised in these experiments. The wavelength of 308 nm produced by the dye laser was tunable which enabled a scan to be carried out to find an on line position. Approximately, 10% of the UV light produced by the laser went to a reference cell whereas the remainder went into an optical fibre (5 m, Oz optics) via a fibre launcher (Oz optics). The optical fibre was connected to a sidearm of the FAGE cell containing baffles to reduce scattered light. Approximately, 10 - 25 mW entered the FAGE cell. The reference cell produced OH by the thermal decomposition of water vapour which passed over a Nichrome wire (Stevens et al., 1994). The OH fluorescence was focused onto the photocathode of a channel photomultiplier tube (Perkin Elmer, C-943P) and individual photons due to OH fluorescence were measured using a photon-counting card (Becker and Hickl GmbH, PMS-400). The reference cell was ungated whereas the gating triggering for the FAGE cell signal is described below.

The $Q_1(2)$ transition line of OH ($A^2\Sigma^+ - X^2\Pi_1$; $v' = 0 - v'' = 0$) was utilised to measure the OH signal in both the FAGE cell and the reference cell. The Nd:YAG pumped dye laser operated at a pulse repetition rate of 5 kHz with a pulse energy of $\approx 2.4 \mu\text{J}$ at 308 nm. The FAGE cell was continuously evacuated using a combination of a rotary pump (Edwards, model E1M80) and a roots blower (EH1200). The FAGE cell was kept at 0.6 - 0.9 Torr and was monitored using a capacitance monitor (Tylan General, CDC 11). The gas throughput velocity in the cell was sufficient to remove any OH that was produced by any ozone photolysis followed by the $O(^1D) / H_2O$ reaction before the next laser pulse arrived. If the fluorescence imaging area was not flushed in between laser pulses and $O(^1D)$ was produced, the subsequent laser pulse would be able to detect OH that would have been formed by $O(^1D)$ that had continued to react (Zeng et al., 1998). A gated photomultiplier tube (PMT) was employed to measure the OH fluorescence. The gating triggering is illustrated in Figure 2.17. Gating is necessary in order to reduce the laser scatter that specifically overlaps with the OH fluorescence. Therefore, the flow of electrons along the PMT is stopped for a certain amount of time until the laser scatter is deemed small enough compared to the fluorescence. The photon counter then measures the fluorescence combined with the background signal. The photon counter also measures the background signal during a second gate B (see Figure 2.17), which can be subtracted from the first measurement in Gate A. Finally, it should be noted that experiments demonstrated Mie scattering due to the presence of aerosols did not significantly increase the background signal.

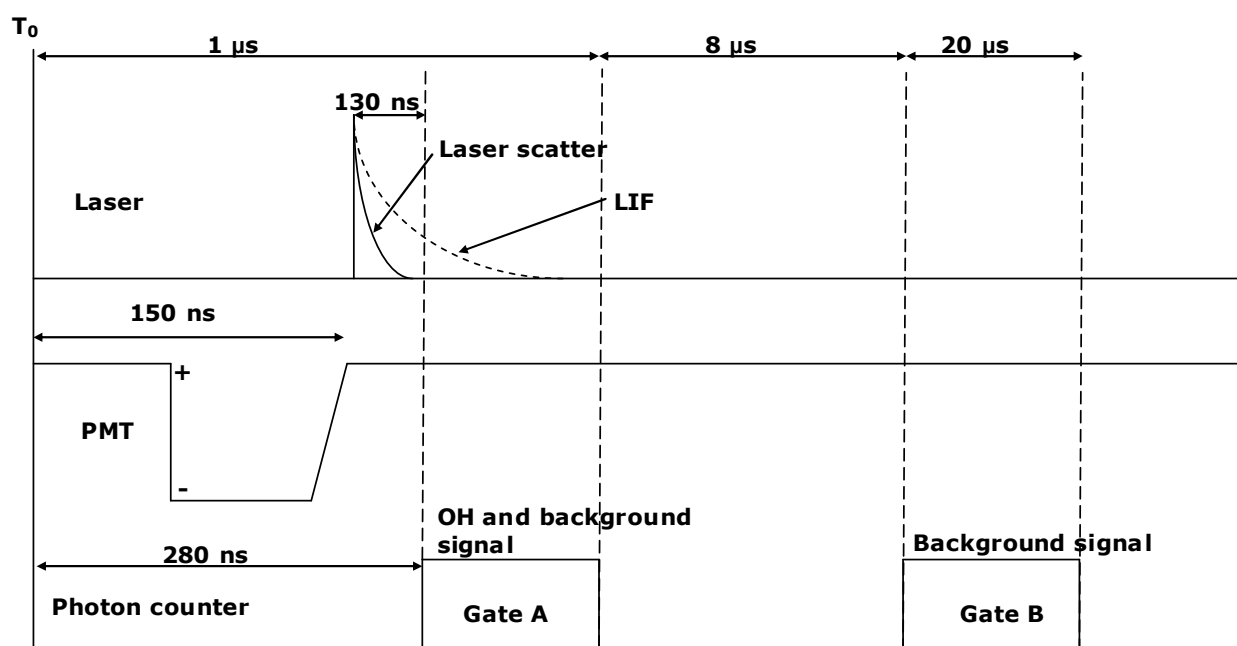


Figure 2.17: A diagram to illustrate the triggering for the PMT gating and photon-counting systems used during the experiments. The diagram is not to scale.

During the FAGE cell calibration, humidified air was photolysed in an aluminium flow tube referred to as a wand, containing a mercury lamp and formed a 1:1 ratio of OH and HO₂ (Reactions 2.1 and 2.2). The lamp current was varied to change the OH and HO₂ concentrations. The concentration of HO₂ was then calculated by using the following equation:

$$[OH] = [HO_2] = [H_2O] \sigma_{H_2O,185nm} \varphi_{OH} F_{185nm} t \quad (E2.5)$$

where $[H_2O]$ is the concentration of water vapour in the humidified air, $\sigma_{H_2O,185nm}$ is the absorption cross-section of water at 185 nm, φ_{OH} is the quantum yield of OH radicals from H₂O vapour photolysis, F_{185nm} is the flux of 185 nm light from the mercury lamp and t is the irradiation time. A graph of the FAGE signal against the calculated OH and HO₂ concentrations was then plotted to calculate the FAGE sensitivity as shown in Figure 2.18. $F_{185nm}t$ was determined by N₂O actinometry that involved passing N₂O mixed with zero air through the calibration wand. The following reactions could then occur:





The NO produced by Reaction 2.8 was measured using a commercial NO_x analyser (TEI 42C) and $F_{185nm}t$ at different lamp currents could be determined using the following equation (Faloona et al., 2004):

$$F_{185t} = \frac{[\text{NO}](k_4[\text{O}_2] + k_5[\text{N}_2] + (k_6 + k_8)[\text{N}_2\text{O}])}{2k_8\sigma_{\text{N}_2\text{O}}[\text{N}_2\text{O}]^2} \quad (\text{E2.6})$$

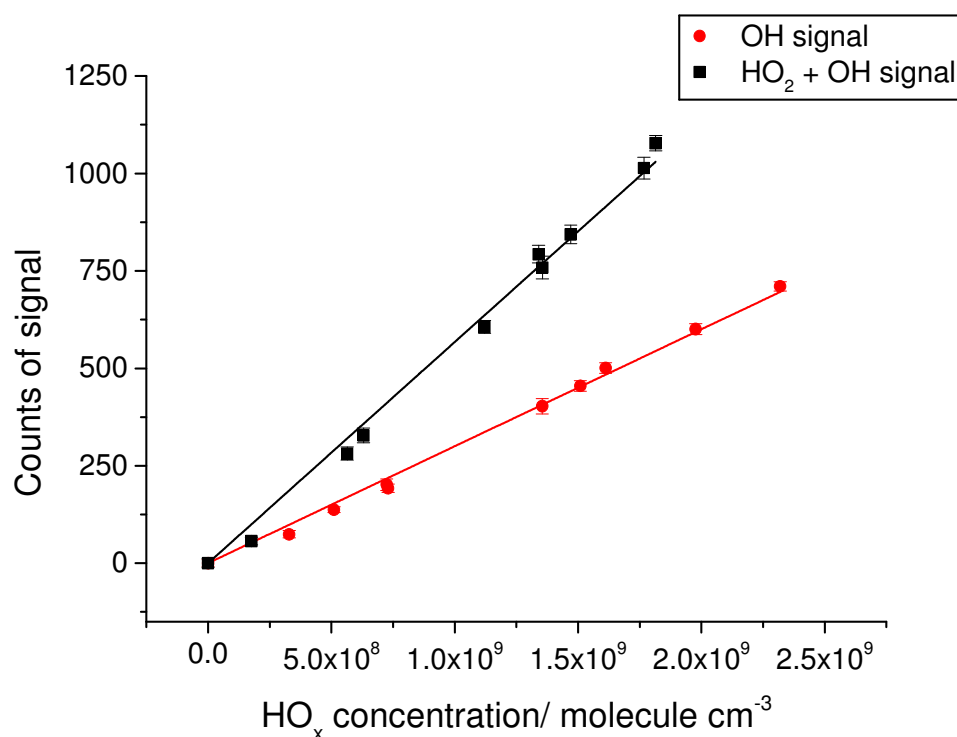


Figure 2.18: An example of the signal due to OH (with the NO off in the FAGE cell) and HO₂ + OH (with the NO on in the FAGE cell) during a FAGE calibration at a laser power of 5 mW. The HO₂ sensitivity was calculated as $5.4 \times 10^{-8} \text{ mW}^{-1} \text{ molecule}^{-1} \text{ cm}^3$.

2.8 The data analysis procedure for moving injector experiments

The FAGE signal was normalized by dividing the signal by the fractional change in laser power over a run. For example if the laser power decreased by 1 % the HO₂ signal would be divided by 0.99. The background signal was subsequently subtracted from the FAGE signal in order to give the HO₂ signal intensity. Figure 2.19 shows the natural log of HO₂ signal intensity plotted against time was plotted with direct weighting given to the uncertainties in the points and was plotted for both experiments in the absence of aerosols (to obtain the wall loss) and with different concentrations of aerosols present in the flow tube. These graphs were plotted because the HO₂ decays appeared to follow first order kinetics (as described below) when the total surface area of the aerosols was constant.

If the uptake of HO₂ follows first order kinetics when the surface area of the aerosols is constant then the rate is given by:

$$\frac{d[HO_2]}{dt} = -k[HO_2] \quad (E2.7)$$

where k is the rate constant. Integrating this equation on both sides gives:

$$\ln[HO_2] = -kt + c \quad (E2.8)$$

At time $t=0$ the concentration of HO₂ is the initial concentration of HO₂, $[HO_2]_0$ which results in Equation 2.9:

$$\ln[HO_2]_t = \ln [HO_2]_0 - k_{obs}t \quad (E2.9)$$

where $[HO_2]_0$ is the initial concentration of HO₂, k_{obs} is the first order rate constant for the heterogeneous reaction of HO₂ with the aerosol particles and t is the reaction time. The reaction time was found as it is related to the injector position by the following equation:

$$t = \frac{Ad}{F} \quad (E2.10)$$

where t is the reaction time, A is the cross sectional area of the flow tube, d is the injector position and F is the flow rate of gases through the flow tube. The HO₂ + HO₂ gas phase

reaction could also be contributing towards the observed wall loss. However, assuming a rate coefficient of $2 \times 10^{-12} \text{ cm}^3 \text{ molecule}^{-1} \text{ s}^{-1}$ and a HO_2 concentration of $1 \times 10^9 \text{ molecule cm}^{-3}$, the product $k[\text{HO}_2]$ is only $2 \times 10^{-3} \text{ s}^{-1}$ which is small compared to the observed decay (e.g. 0.019 s^{-1} in Figure 2.19).

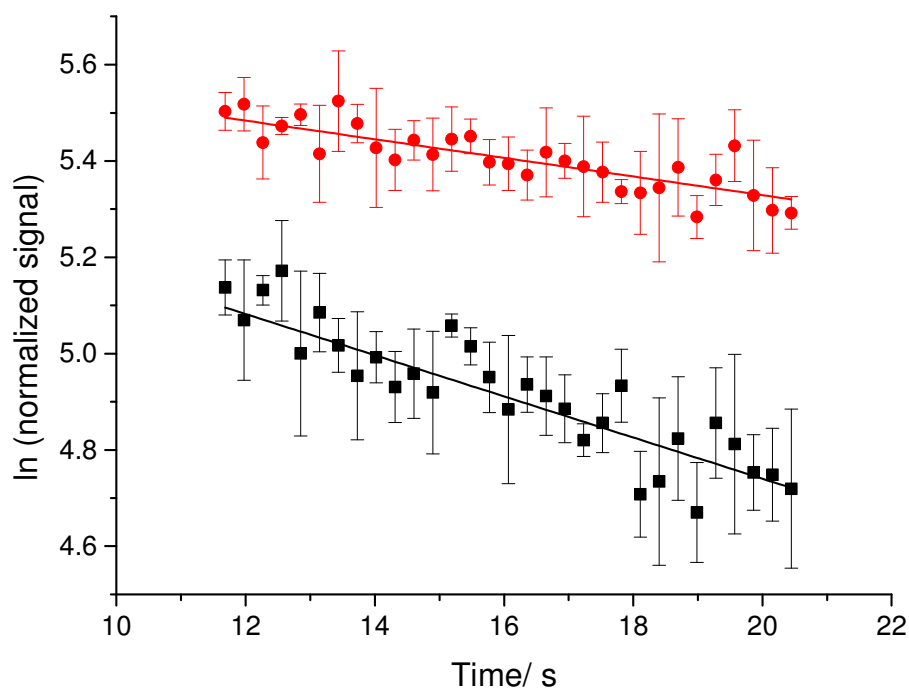


Figure 2.19: Example of the relationship between the reaction time (i.e the time for which HO_2 has been in the presence of aerosols) and the HO_2 signal. The red circles represent a typical HO_2 wall loss for a relative humidity of 70 %, whereas the black squares represent the HO_2 decay seen with a surface area of $4.6 \times 10^{-4} \text{ cm}^2 \text{ cm}^{-3}$ ammonium nitrate aerosols present in the flow tube. The error bars represent one standard deviation. The gradient of the wall loss ($-k_{\text{wall}}$) was -0.019 s^{-1} and the gradient when aerosols were present (k_{obs}) was -0.043 s^{-1} .

In order to account for the loss of HO_2 to the wall of the aerosol flow tube the experiments were performed under the same conditions but without any aerosols present. The Brown correction (Brown, 1978) was then used to correct for the wall loss and diffusion under non-plug flow conditions. The corrected k' values tend to be 10 - 40% higher than the values obtained by just subtracting the wall loss values from the HO_2 decay ($k_{\text{obs}} - k_{\text{wall}}$). An example of the difference can be seen in Figure 2.20.

The Brown correction (Brown, 1978) was required due to the laminar flow in the flow tube (see Section 1.5.2). If there was no radial difference in the flow rate (i.e. plug flow) then the distance along the flow tube would be equal to the reaction time multiplied by the flow velocity. In this case, the concentration of HO₂ would be given by the following equation:

$$[HO_2] = [HO_2]_0 e^{-k_{obs}z/\langle u \rangle} \quad (E2.11)$$

where k is the first order rate constant, $\langle u \rangle$ is the average carrier flow velocity and $[HO_2]_0$ is equal to $[HO_2]$ when the distance, z , is zero.

However, the laminar flow that exists in these experiments (as described in Section 2.5.2) means that there is a parabolic flow profile and a radial gradient in the concentration of HO₂. The degree of the radial gradient is dependent on the flow velocity, the reaction rate at the walls and the molecular diffusion rates. This means that Equation 2.11 can be modified:

$$[HO_2](r) = [HO_2]_0(r) e^{-k'z/\langle u \rangle} \quad (E2.12)$$

where k' is a function of $\langle u \rangle$, the diffusion coefficient of HO₂, the true first order rate constant k_{obs} and a rate constant k_w for a first order wall reaction and r is a distance from the flow tube centre.

The actual solution to the problem of finding k' from k_{obs} is very complex. However, R. L. Brown (Brown, 1978) published a solution to the problem in a paper called 'Tubular Flow Reactors with First-Order Kinetics'. The Brown correction in this work was solved using a Fortran code as described in the Brown (1978) paper.

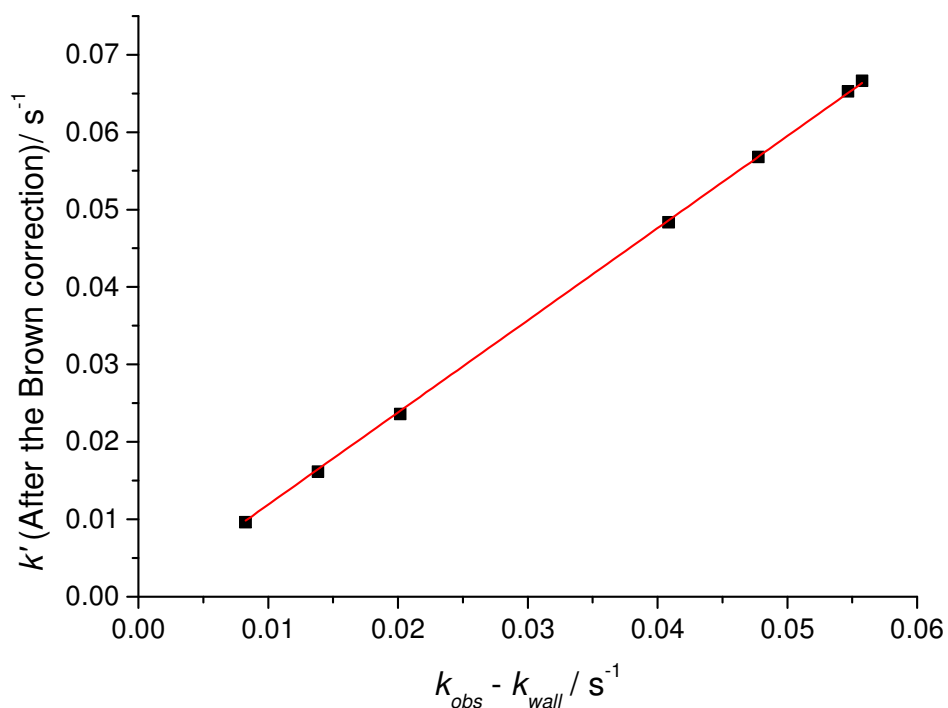


Figure 2.20: An example to show the difference between subtracting the wall loss from the observed rate constant and using the Brown correction to correct the observed rate constant. This graph had a gradient of 1.19, giving a 19 % increase in the rate constant.

The first order rate constant that had been corrected for the Brown correction (k') is related to the uptake coefficient (γ_{obs}) by the following equation:

$$k' = \frac{\gamma_{obs}\omega_{HO_2}}{4} S \quad (\text{E2.13})$$

where ω_{HO_2} is the molecular thermal speed of HO_2 (cm s^{-1}) and S is the total surface area of aerosols in a given volume ($\text{cm}^2\text{cm}^{-3}$). Therefore, the first order rate constant was plotted against the aerosol surface area in a given volume should produce a straight line going through the origin, as shown in Figure 2.21.

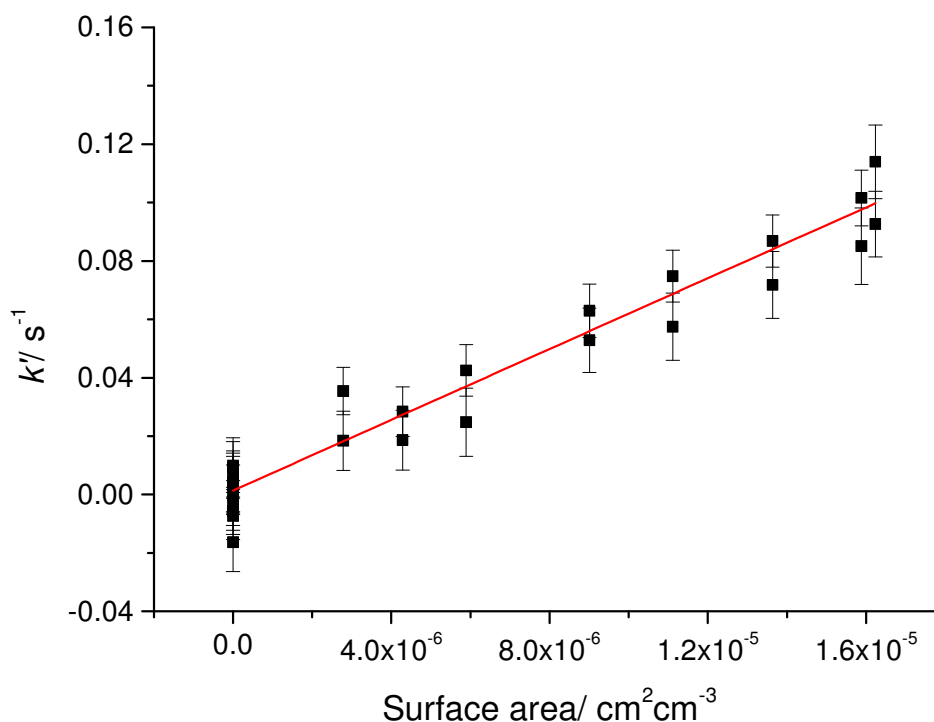


Figure 2.21: The first order rate constant (k') plotted against the aerosol surface area in a given volume for aerosols produced from a solution that contained 0.125 g of copper sulphate and 0.8 g of ammonium nitrate dissolved in 500 ml mQ water. The relative humidity was 60 % and the temperature was 293 K. Each point was weighted according to its error. The second point at each surface area represents a repeat. The error bars represent one standard deviation. The R^2 value of the graph was 0.94 and after further analysis, an uptake coefficient of 0.58 ± 0.04 was obtained.

However, the uptake coefficient had to be corrected in order to take into account gas phase diffusion. When either the uptake coefficient or the aerosol radius is large the concentration of a species near the surface of the aerosol can become depleted leading to a lower flux of molecules colliding with the surface of the aerosols and to an under prediction of the HO_2 uptake coefficient. A correction for this gas phase diffusion effect was done using the following equations but the correction changed the uptake coefficient by less than 1 % unless the uptake coefficient was close to 1 (Fried et al., 1994; Fuchs and Sutagin, 1970):

$$\gamma_{corr} = \frac{\gamma_{obs}}{(1 - \gamma_{obs}\lambda(r_s))} \quad (\text{E2.14})$$

The values of $\lambda(r_s)$ are given by the following equation:

$$\lambda(r_s) = \frac{0.75 + 0.283K_n}{K_n(1 + K_n)} \quad (\text{E2.15})$$

where K_n is the Knudsen number and is defined by the equation:

$$K_n = \frac{3D_g}{\omega_{HO_2}r_s} \quad (\text{E2.16})$$

where D_g is the gas phase diffusion coefficient of HO_2 which has been estimated to be approximately $0.25 \text{ cm}^2 \text{ s}^{-1}$ (Mozurkewich et al., 1987), ω_{HO_2} is the molecular thermal speed of HO_2 (cm s^{-1}) and r_s is the mean-surface-area-weighted radius of the aerosol distribution which is defined as:

$$r_s = r_{peak} \exp [2.5(\ln\sigma)^2] \quad (\text{E2.17})$$

where r_{peak} is the radius for the peak of the distribution and σ is the geometric standard deviation. For experiments where the HO_2 uptake coefficient was small, and indistinguishable from the wall losses, an upper limit (or limit of detection) for the HO_2 uptake coefficient was given. The upper limit was determined from 2 standard deviations of the average wall loss in the experiment which was inputted into equation 2.13 with the highest aerosol surface area used in the experiment.

2.9 The data analysis procedure for fixed injector experiments

Fixed injector experiments consisted of placing the injector in one position along the flow tube rather than the injector being pulled backwards and forwards along the flow tube. Once the injector was in a certain position, both the aerosol surface concentration and the HO_2 signals were recorded. The aerosol concentration was then changed several times and each time the HO_2 signal was measured. This method allowed the average uptake coefficient to be measured for the time that it took the flow to travel between the injector and the FAGE cell.

This method meant that k_{obs} values could not be obtained from the gradient of a k_{obs} against time graph, as was the case of the moving injector experiments. Instead, k_{obs} values were obtained using the following methodology.

The signal when there are aerosols present can be described as:

$$\frac{\ln[HO_2]_{t,aerosol} - \ln[HO_2]_0}{t} = -k_{aerosol} - k_{wall} \quad (E2.18)$$

where $[HO_2]_0$ is still the HO_2 concentration at time zero.

The signal without aerosols present can be described as:

$$\frac{\ln[HO_2]_{t,aerosol=0} - \ln[HO_2]_0}{t} = -k_{wall} \quad (E2.19)$$

Subtracting Equation 2.19 from Equation 2.18 gives:

$$\frac{\ln[HO_2]_{t,aerosol} - \ln[HO_2]_{t,aerosol=0}}{t} = -k_{aerosol} \quad (E2.20)$$

Hence, $k_{aerosol}$ is obtained for each given aerosol concentration, and graphs of the k' values (the Brown corrected rate constants) against the surface areas were plotted for each injector position as shown in Figure 2.22. An average uptake coefficient for the time taken for the flow to travel between the injector and the FAGE cell was then calculated using Equation 2.13 and was corrected for gas phase diffusion limitations using Equations 2.14 to 2.16 given in Section 2.8.

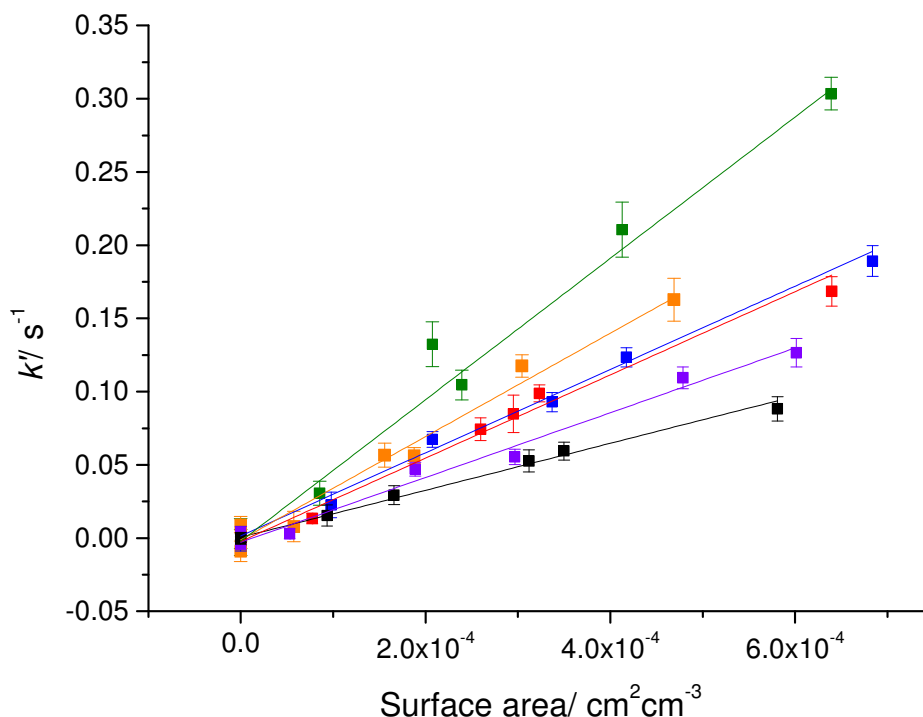


Figure 2.22: k' plotted against the aerosol surface area when the injector was placed at 20 cm (green), 30 cm (orange), 40 cm (blue), 50 cm (red), 60 cm (violet) and 70 cm (black) along the flow tube. Aqueous sodium chloride aerosols at 60 % RH were used in this experiment at the temperature was 293 ± 2 K. The error bars represent 1 standard deviation.

2.10 The data analysis procedure for mineral dust experiments

The experimental methodology used for mineral dust aerosol generation meant that a stable dust concentration was not able to be achieved over a time period of three minutes (the time needed for an SMPS scan). Therefore, the aerosol number concentration was monitored using a CPC placed either just before the flow tube or just after the flow tube. The actual aerosol concentration in the flow tube was calculated using the dilution equation:

$$N_{flow\ tube} = \frac{N_{CPC}(F_{total} - F_{HO_2})}{F_{total}} \quad (E2.21)$$

where $N_{flow\ tube}$ is the aerosol number concentration in the flow tube, N_{CPC} is the number concentration measured by the CPC, F_{total} is the total flow entering the flow tube and F_{HO_2} is the total flow from the injector.

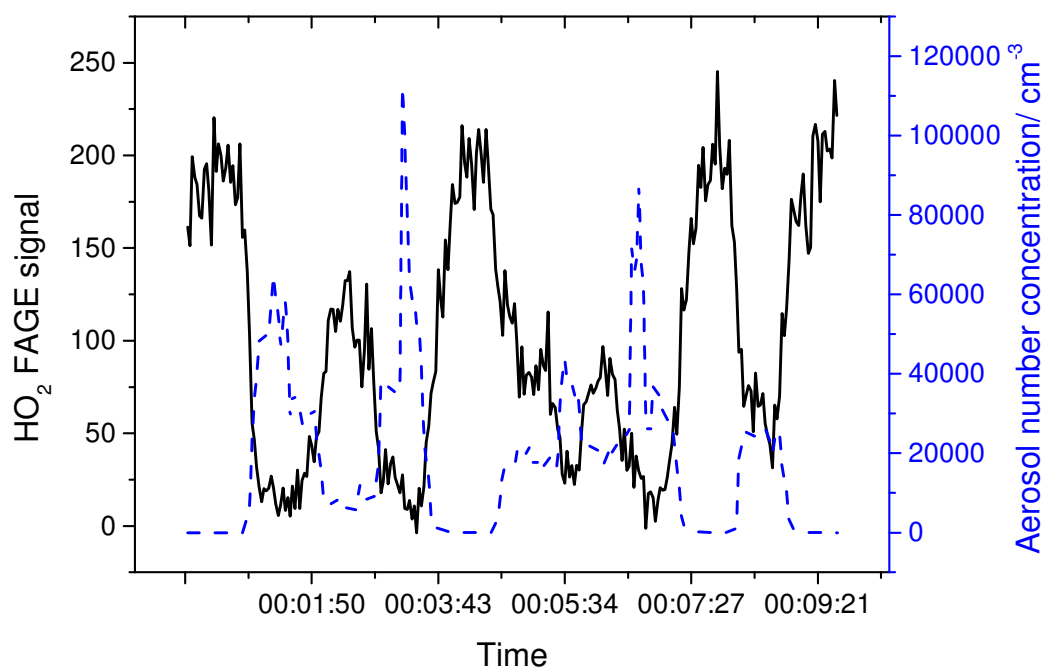


Figure 2.23: An example of the anticorrelation between the ATD aerosol number concentration (blue dotted line, right hand axis) and the FAGE signal (black solid line, left hand axis) at 293 ± 2 K and atmospheric pressure.

In order to analyse the data for the mineral dust experiments the time between when the CPC was measuring and the time when the HO_2 signal was being measured had to be matched up to each other. If the CPC was measuring before the flow tube, the time difference was due to the time it took for the flow to pass through the flow tube, whereas, if the CPC was measuring after the flow tube, the time difference was due to the time that it took the flow to pass through the tubing connecting the flow tube to the CPC. Once the time difference had been accounted for, an anticorrelation was observed between the HO_2 signal and the aerosol number concentration, as shown in Figure 2.23. The natural log of the background subtracted HO_2 signal plotted against the aerosol number concentration is shown in Figure 2.24. The gradient of this graph is equal to $0.25\gamma_{obs}wA_d t$, where A_d is the average surface area of one aerosol which can be calculated from Equations 2.3 and 2.4 in Section 2.6.1.

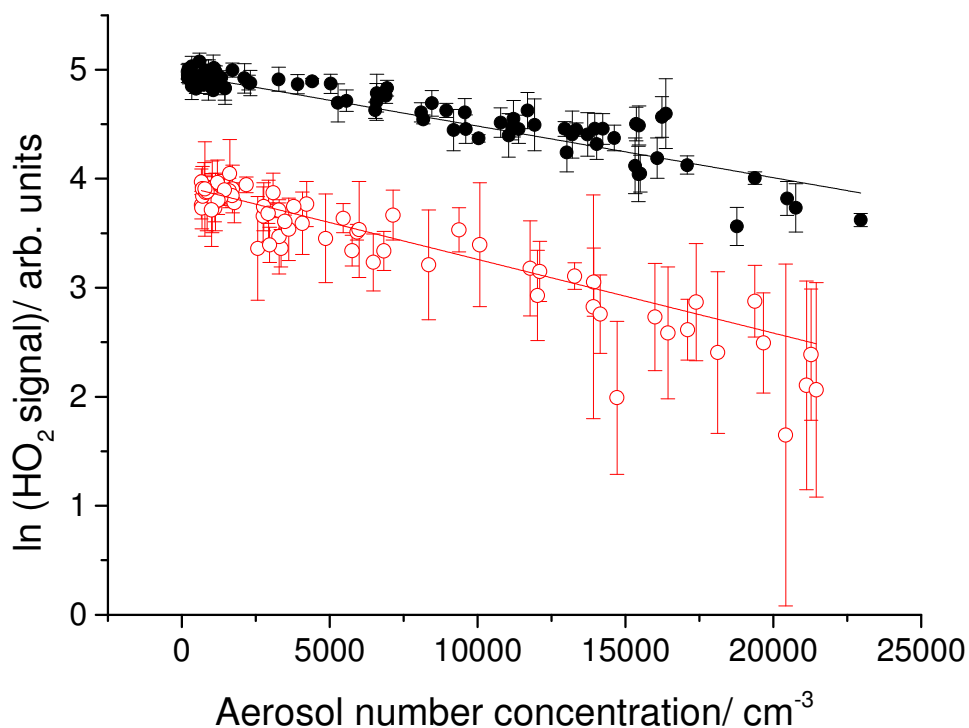


Figure 2.24: An example of the linear correlation between the $\ln(\text{signal} - \text{background})$ and the Arizona Test Dust aerosol number concentration at a relative humidity of 76 %, 293 ± 2 K and atmospheric pressure and at injector positions of 30 cm (black points) and 80 cm (red points). The error bars represent 1 standard deviation.

Therefore, γ_{obs} was obtained by plotting $0.25\gamma_{obs}wA_d t$ against time, t , and obtaining a gradient of $0.25\gamma_{obs}wA_d$ as shown in Figure 2.25. γ_{obs} was corrected using the Brown correction and was then converted to γ_{corr} to correct for gas phase diffusion using Equations 2.14 to 2.16 as has been done for the previous methods.

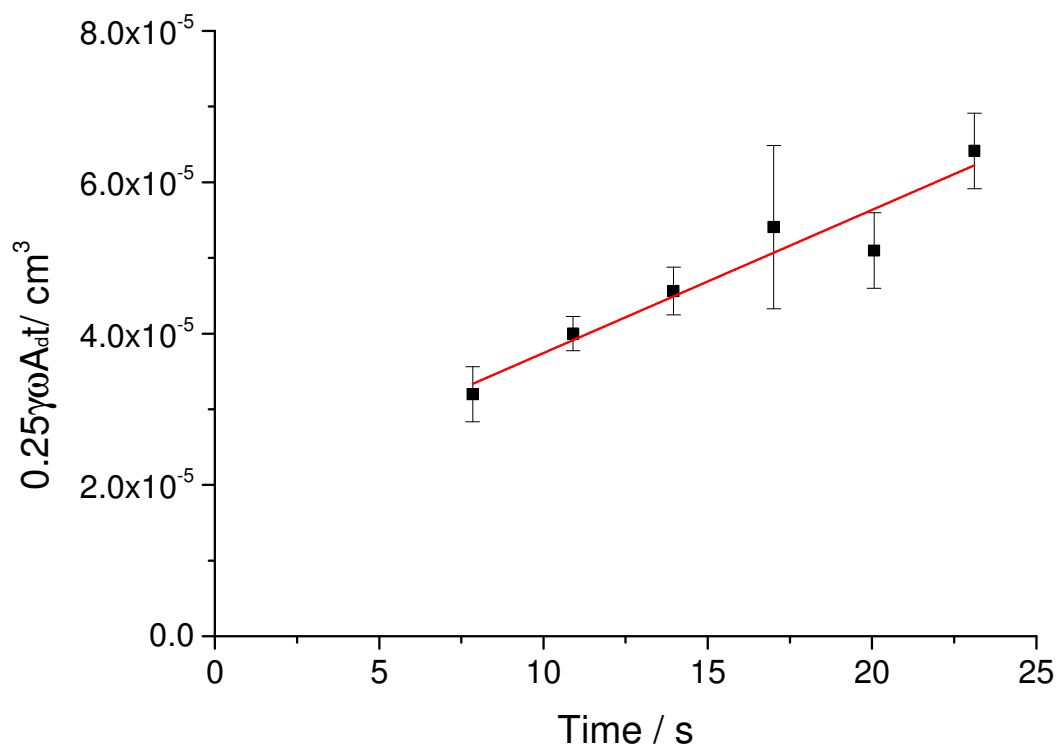


Figure 2.25: The gradient of the exponential fits such as those shown in Figure 2.24 ($0.25\gamma_{obs}wA_d t$) plotted against time, for which the gradient is $0.25\gamma_{obs}wA_d$ allowing γ_{HO_2} to be obtained. The error bars represent 2 standard deviations in the exponential fits.

2.11 The error analysis procedure

The error analysis procedure for moving injector experiments is described below with small differences in the error analysis for fixed injector and dust experiments being described at the end of this section. The FAGE software recorded a signal every second. For each injector position the signal was averaged over 3 seconds and the error in the signal (E_{signal}) was the standard deviation of the three measurements. In order to calculate the error in the background ($E_{background}$) the standard deviation in the measurements of the background made over ~ 4 - 5 minutes was calculated.

The background signal was subtracted from each signal with the error ($E_{signal-background}$) being given by the following equation:

$$E_{\text{signal-background}} = \sqrt{E_{\text{signal}}^2 + E_{\text{background}}^2} \quad (\text{E2.22})$$

The error in the natural log of the background subtracted signal ($E_{\ln(\text{signal-background})}$) was calculated using the equation below:

$$E_{\ln(\text{signal-background})} = \frac{E_{\text{signal-background}}}{\text{Signal} - \text{background}} \quad (\text{E2.23})$$

The natural log of the background subtracted background was plotted against time in Origin 8.1 software for all decays along the flow tube in the absence and presence of different aerosol concentrations. The software outputted errors in the gradients of the graphs ($E_{k_{\text{obs}}}$). The average k_{wall} was calculated with the error ($E_{k_{\text{wall,av}}}$) being the standard deviation of the averaged k_{wall} measurements. The average k_{wall} was subtracted from all of the pseudo first order rate constants in both the absence and presence of different aerosol surface area concentrations (k_{obs}) and the error ($E_{k_{\text{obs-kwall,av}}}$) was calculated using the following equation:

$$E_{k_{\text{obs-kwall,av}}} = \sqrt{E_{k_{\text{obs}}}^2 + E_{k_{\text{wall,av}}}^2} \quad (\text{E2.24})$$

The Brown correction increased $k_{\text{obs-kwall,av}}$ to k' by a given factor (B) for each experiment with the factor depending on the wall loss, the flow rate and the dimensions of the flow tube. Therefore, the error in k' ($E_{k'}$) is:

$$E_{k'} = B E_{k_{\text{obs-kwall,av}}} \quad (\text{E2.25})$$

The Origin 8.1 software outputted an error in the gradient of the graphs of k' against aerosol surface area. The error in the gradient of the graphs was equivalent to an error in $(\gamma_{\text{obs}} \times \omega_{\text{HO2}}) / 4$. Therefore, the error in the gradient was multiplied by a factor of 4 and divided by ω_{HO2} in order to obtain an error in γ_{obs} . Finally, the error was corrected for gas phase diffusion by multiplying the error in γ_{obs} by $\gamma_{\text{corr}} / \gamma_{\text{obs}}$.

For fixed injector and dust experiments the majority of the error analysis procedure described above is applicable, however, due to slight differences in the data analysis there were also differences in the calculation of errors. For fixed injector experiments instead of plotting the natural log of the background subtracted signal against time Equation 2.20 was utilised to obtain values of k_{obs} . Therefore, the error in k_{obs} was:

$$E_{k_{obs}} = \frac{\sqrt{E_{\ln[HO_2]t,aerosol}^2 + E_{\ln[HO_2]t,aerosol=0}^2}}{t} \quad (E2.26)$$

where $E_{\ln[HO_2]t,aerosol}$ is the error in the HO₂ signal in the presence of aerosols and $E_{\ln[HO_2]t,aerosol=0}$ is the error in the HO₂ signal in the absence of aerosols. It should be noted that for fixed injector experiments the error in the FAGE signal was the standard deviation of all measurements made at a certain aerosol surface area. For dust experiments errors in $0.25\gamma_{obs}\omega A_d t$ and $0.25\gamma_{obs}\omega A_d$ were obtained from the error in the gradients of graphs shown in Figure 2.24 and 2.25, respectively, outputted by the Origin 8.1 software.

Errors in the aerosol surface areas were not included as they were small compared to the errors in the signal. If there were large variations in the surface area the decays would not be expected to be linear and any data would have been discarded. For the majority of moving injector experiments a CPC was also attached to the experimental setup which showed that the aerosol number concentration did not vary by more than 5 % over the 10 minutes that it took to record a decay. Systematic errors included errors in the dimensions of the flow tube and flow rates, however, these were not included as they were negligible compared to other random errors.

2.12 Differences in the data analysis when the flow tube is not at room temperature or at atmospheric pressure

2.12.1 Correction of the aerosol surface area when the flow tube is not at room temperature

Initially attempts were made to place the DMA in a freezer which would have been kept at the same temperature and relative humidity as the flow tube. However, temperature gradients developed in the freezer leading to convection within the DMA and to no aerosols being measured. Therefore, the DMA was always kept at room temperature whilst the temperature in the conditioning and reaction flow tubes was varied. When the flow tube was not at room temperature the relative humidity within it was different to the relative humidity in the DMA which was always kept at room temperature. Therefore, when experiments were performed with aqueous aerosols, a correction in the total aerosol surface area had to be made. When the flow tube was at a temperature which was lower than room temperature, the relative humidity in the flow tube would be greater than in the DMA, and therefore the total aerosol surface area would be larger in the flow tube than the surface area measured by the SMPS. Alternatively, when the flow tube was at a temperature which was higher than room temperature, the humidity in the flow tube was lower than in the DMA, which meant that the total aerosol surface area in the flow tube was smaller than the surface area measured by the SMPS.

The Aerosol Inorganic Model (AIM) (Clegg et al., 1992; Wexler and Clegg, 2002), discussed in Section 2.6.2, enables the total volume (for one mole of a salt) per cubic centimetre of aerosol to be calculated at different temperatures and humidities. Therefore, by entering the aerosol type, the humidity and the temperature inside the flow tube into the model a volume for one mole of salt per cubic centimetre was calculated. Likewise, by entering the temperature and the humidity inside the DMA into the model a volume for one mole of salt per cubic centimetre was calculated. The following methodology was then used in order to correct the measured surface area.

Aqueous aerosols were assumed to be spherical and therefore their surface area (S) was given by:

$$S = 4\pi r^2 \quad (\text{E2.27})$$

Likewise, the volume of the aerosols (V) would be given by:

$$V = \frac{4}{3}\pi r^3 \quad (\text{E2.28})$$

The Atmospheric Inorganic Model can give the volume for one mole of salt per cubic centimetre at different humidities. The fractional change in volume would be given by:

$$\frac{V_1}{V_2} = \frac{r_1^3}{r_2^3} \quad (\text{E2.29})$$

where V_1 is the volume for one mole of salt per cubic centimetre at the flow tube temperature and humidity, V_2 is the volume for one mole of salt per cubic centimetre at the DMA temperature and humidity.

The fractional change in surface area can similarly be given by:

$$\frac{S_1}{S_2} = \frac{r_1^2}{r_2^2} \quad (\text{E2.30})$$

where S_1 is the aerosol surface area in the flow tube, S_2 is the aerosol surface area measured in the DMA.

Therefore, by combining equations 2.29 and 2.30, Equation 2.31 was obtained:

$$S_1 = S_2 \sqrt[3]{\left(\frac{V_1}{V_2}\right)^2} \quad (\text{E2.31})$$

Equation 2.31 can then be used to correct the total surface area of the aerosols when it is measured at a different humidity to the humidity in the flow tube. For example, for a specific experiment performed with the flow tube at 0 °C and the DMA at 20 °C the relative humidity in the DMA was 18 % compared to a relative humidity of 48 % in the flow tube. This led to a

15 % increase in the aerosol surface area measured by the SMPS. The flow rate and volume of the gas within the flow tube was also corrected to take into account the temperature.

It should be noted that the correction in the aerosol surface area limited the aqueous aerosols that could be investigated to ammonium nitrate, as it does not effloresce over a range of temperatures. Copper-doped ammonium nitrate was also used as a check could be done to find whether the aerosols were effloresced or deliquesced, and the deliquesced aerosols appeared to grow in a similar way to pure ammonium nitrate aerosols, as shown in Figure 2.10. However, this correction could not correct between effloresced and aqueous aerosols, and it was calculated for sodium chloride and ammonium nitrate that even at 10 °C, if the DMA was kept above the efflorescence points, the flow tube would exceed 100 % RH. If the relative humidity in the flow tube exceeded 100 % RH there would be condensation on the flow tube walls leading to high wall losses and the aerosols would grow in size to form droplets which would be likely to be deposited and would be too large to be measured by the SMPS.

For effloresced salts no surface area correction was required. Below the deliquescence point the aerosol surface area does not change with relative humidity for effloresced salts, the surface area remains constant as there is no aqueous phase which can increase or decrease in volume as the humidity changes. However, when effloresced salt experiments were performed at different temperatures it had to be ascertained that the effloresced aerosols were never exposed to humidities above their deliquescence point.

2.12.2 Correction of the diffusion coefficient when the flow tube is not at room temperature or atmospheric pressure

The gas phase diffusion coefficient of HO₂ has been estimated to be 0.25 cm²s⁻¹ at room temperature (≈ 293 K). However, no data for the HO₂ gas phase diffusion coefficient at other temperatures could be found in the literature, and it is known that the gas phase diffusion increases as the temperature increases with increasing temperature. The following calculation derived by Fuller et al. (1966) was used in order to correct for the different temperatures:

$$D_{HO_2}(T) = D_{HO_2}(293K) \frac{T^{1.75}}{293^{1.75}} \quad (E2.32)$$

For the SOA experiments that were performed at PSI in Switzerland the flow tube was not at atmospheric pressure. The pressure in the flow tube varied from 904 to 987 mbar due to the flows being pumped through the flow tube and due to a restriction in the flow before the flow tube (possibly, because the flow had to pass through the charcoal denuder). It is known that as the pressure decreases the diffusion coefficient increases. The following calculation derived by Reid et al. (1987) was used to correct the diffusion coefficient for the different pressures:

$$D_{HO_2}(P) = \frac{1013 D_{HO_2}(1013 \text{ mbar})}{P} \quad (E2.33)$$

2.13 Hydrogen peroxide measurements

The hydrogen peroxide exiting the injector was measured using a hydrogen peroxide monitor (AL-2021) at PSI. The hydrogen peroxide reacted with *p*-hydroxyphenylacetic acid which was catalysed by peroxidase. This reaction produced a fluorescent dimer that fluoresced when exposed to a UV lamp at 325 nm and was detected at 400 and 420 nm. The fluorescence could then be detected. The method relied on a calibration that was performed using liquid standards containing known hydrogen peroxide concentrations. These concentrations were then converted into gas phase mixing ratios. Measurements were made at two different lamp currents (20 mA and 5 mA) and at two different injector positions (30 cm and 70 cm) at room temperature and for the usual experimental conditions. The limit of detection of the instrument was ~ 10 ppt.

2.14 The Cape Verde box model

Once HO₂ uptake coefficients had been measured they could be inputted into a box model in order to check the impact that the uptake would have upon HO₂ concentrations. The model had been developed in order to calculate expected concentrations of OH and HO₂ and for

comparison with measured concentrations during the Reactive Halogens in the Marine Boundary Layer (RHAMBLe) field campaign (Whalley et al., 2010). The RHAMBLe field campaign took place during May and June 2007 at the Cape Verde Atmospheric Observatory (Carpenter et al., 2010). The model contained rate constants from the Master Chemical Mechanism (MCM) version 3.1 (Saunders et al., 2003) and was constrained using concentrations of species that were measured during the RHAMBLe field campaign. These species included hourly measurements of VOCs, NO_x, CO, CH₄ and *j*(O¹D) (Whalley et al., 2010). Reactions of IO and BrO with HO₂ were also included within the model and the halogen reaction scheme was constrained using measurements of the diurnal cycle of [IO] and [BrO] averaged for May 2007.

The first order rate constant for loss of HO₂ by aerosol uptake was then calculated in the model using Equation 2.13 that was introduced in Section 2.8:

$$k_{obs} = \frac{\gamma_{obs}\omega_{HO_2}}{4} S \quad (\text{E2.13})$$

The measured uptake coefficient and aerosol surface area had to be inputted into the model and it was then run using the FACSIMILE integrator (Sweetenham and Curtis, 1987). Further details about the model outputs will be given in the atmospheric implication sections of Chapters 3 to 7.

2.15 Summary

In this chapter, three different experimental setups have been described. The first experimental setup was used for aqueous and solid aerosols that could be produced using an atomiser. The second experimental setup was for dust experiments and involved stirring dust in a bottle which was then entrained into a nitrogen flow. Finally, for the third experimental setup, SOA was formed in a chamber and the aerosols were then pumped through the equipment. All of the experiments formed HO₂ from the photolysis of water vapour in the presence of O₂ in a moveable injector, and the HO₂ was measured using a sensitive FAGE cell. By moving the injector to different positions along the flow tube (either continuously or

by placing it in several fixed positions) which altered the HO₂-aerosol exposure time, HO₂ uptake coefficients could be measured.

Checks were performed to verify the flow regime and the development of a mixed profile using both ozone profiles and aerosol profiles in the flow tube. Temperature gradients inside the flow tube were also measured. The results at -10 °C showed that after 5 cm from the injector the temperature stayed within two degrees and after 10 cm from the injector the temperature stayed within one degree. The aerosols were characterised for metal ions by ICP-MS and the phase of the aerosols were checked by running humidograms. The accuracy of the SMPS measurements was verified by measuring PSL beads of known sizes. It was also determined that two neutralisers were required to accurately measure the size distribution of the aerosols when the number concentration was higher than $6 \times 10^5 \text{ cm}^{-3}$. The methodology for measuring hydrogen peroxide out of the end of the injector was also described in this chapter. Finally, the Cape Verde box model was briefly described, allowing the impact of aerosols on HO₂ concentrations to be estimated by inputting the uptake coefficients that are measured in this work. Further details of some of the procedures are contained in subsequent chapters and a description of the KM-SUB model developed in Mainz is given in Chapter 8.

Chapter 3: Measurements of the HO₂ uptake coefficient onto inorganic salts at room temperature and atmospheric pressure

3.1 The importance of aerosols containing inorganic salts

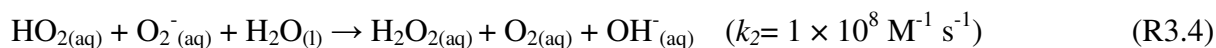
Sulphate, chloride, ammonium and nitrate ions are major components of tropospheric aerosol. For example, during a recent field campaign in Paris, Crippa et al. (2013) made measurements using an aerosol mass spectrometer, and found that more than a third of the average aerosol mass fraction could be attributed to these ions. The average mass fraction (excluding water) contained 25.2 % sulphate, 6.5 % ammonium, 5.1 % nitrate and 0.4 % chloride ions. The majority of chloride that is found in the troposphere originates from sea salt aerosols. Sulphate ions in aerosols are formed by the oxidation of SO₂ which is produced by anthropogenic activities such as fossil fuel burning, and by the eruption of volcanoes. Sulphate can also be formed by marine phytoplankton that produce dimethyl sulphide which oxidises to SO₂. Ammonium ions are emitted directly into the atmosphere from sewage, fertilisers, the soil and animals. Particle nucleation (i.e. the formation of new particles) can also occur in the presence of H₂SO₄ and a base such as NH₃ (e.g. (Benson et al., 2009)). Nitrate ions are formed from NO₂ which is produced by fossil fuel combustion, soil and lightning. The NO₂ radical can be converted to HNO₃ which can then react with either NH₃ or NaCl in the aerosol phase to form ammonium nitrate.

Due to the high concentrations of sulphate, ammonium, nitrate and chloride ions in tropospheric aerosols, experiments were performed in this work with sodium chloride, ammonium sulphate and ammonium nitrate aerosols. In this chapter, HO₂ uptake coefficient measurements onto deliquesced and effloresced salt aerosols will be discussed, as well as measurements onto copper and iron doped ammonium sulphate. The impact of aerosol pH, relative humidity (RH), reaction time and initial HO₂ concentration will also be investigated in this chapter.

3.2 Measurements of the HO₂ uptake coefficient onto solid inorganic aerosols at room temperature

At low relative humidities a large proportion of aerosols in the atmosphere will be solid rather than aqueous. For example, as stated in Table 2.1 in Section 2.6.2, the efflorescence humidities of ammonium sulphate and sodium chloride are 36 - 43 and 45% respectively, meaning that below these relative humidities the aerosols will be solid. However, if these aerosols were already effloresced they will remain in the solid phase up to their deliquescence points of 79.9% for ammonium sulphate and 75.3% for sodium chloride. In this work, solid aerosols were produced by passing aqueous aerosols, generated by the atomiser, through a diffusion dryer (consisting of silica gel) so that the relative humidity was below the efflorescence point of the aerosols (see Chapter 2 for more details). The relative humidity throughout the equipment was then kept below the deliquescence point of the aerosols and a phase test confirmed that they were effloresced (see Section 2.6.2). Figure 3.1 shows examples of the pseudo-first order rate constants measured in this work as a function of aerosol surface area for effloresced ammonium sulphate and sodium chloride aerosols.

Table 3.1 summarises the uptake coefficients of HO₂ onto solid aerosols that have been measured in this work and in previous studies. From Table 3.1, it can be noted that all of the uptake coefficients that have been measured in this work, and over a range of humidities, are below the limit of detection of 0.004. The uptake coefficients measured in this work were reproducible, with all experiments being below the limit of detection. For solid aerosols the HO₂ reactions would be limited to the surface of the aerosol as there is no aqueous bulk for the HO₂ to diffuse into. Therefore, no aqueous chemistry, as shown in Reactions 3.1 – 3.4, can occur, which means that the uptake coefficients should be small:



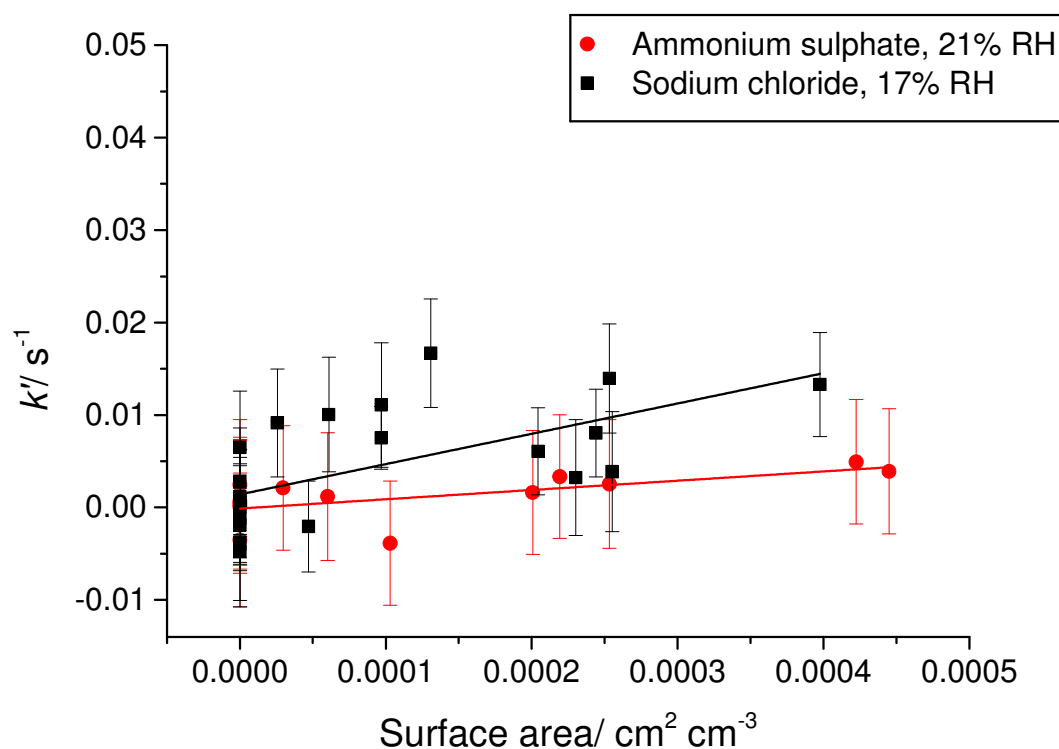


Figure 3.1: Examples of the pseudo-first order rate constant as a function of surface area for effloresced ammonium sulphate and sodium chloride aerosols at room temperature (293 ± 2 K in this work) and atmospheric pressure. The gradients of the lines were 10 and $32 \text{ s}^{-1} \text{ cm}^{-2} \text{ cm}^3$ and resulted in HO_2 uptake coefficients of 0.001 ± 0.003 and 0.003 ± 0.002 for ammonium sulfate and sodium chloride aerosols respectively. The error bars represent one standard deviation.

By comparing the HO_2 uptake coefficients measured in this work over a range of humidities ($\gamma < 0.004$) to other published work, shown in Table 3.1, it can be seen that the uptake coefficients in this work are only in agreement with the value measured by Loukhovitskaya et al. (2009). The differences in the measured uptake coefficients may be due to the different experimental conditions used by different groups. Taketani et al. (2008) used a similar experimental set up to the one used in this work. Aerosols were produced using an atomiser and an aerosol flow tube was coupled with a sensitive FAGE cell. However, the measurements published by Taketani et al. (2008) are at least an order of magnitude larger than the uptake coefficients measured in this work. One of the possible reasons for the difference in the measured uptake coefficient may be due to the higher flow rate of 10.4 L

min^{-1} that Taketani et al. (2008) used compared to a flow rate of approximately 5.4 L min^{-1} used for this work. These flow rates resulted in Taketani et al. (2008) working at reaction times of approximately 5 to 11 seconds compared to 10 to 20 seconds in this work. If the uptake was larger at shorter times, then any studies that were performed at shorter times would have larger observed uptake coefficients. Therefore, it may be the exposure time that the aerosols have to HO_2 which determines the uptake coefficient. Taketani et al. (2008) also used much lower initial HO_2 concentrations than were used in this work, and did not analyse solutions for metals. The HO_2 uptake coefficient dependence upon time and initial HO_2 concentration will be discussed in Sections 3.9 to 3.11.

Remorov et al. (2002) and Loukhovitskaya et al. (2009) used very high volumetric flow rates of approximately 300 L min^{-1} (0.4 - 1.2 slpm) whereas Gershenzon et al. (1995) used a flow rate of approximately 200 L min^{-1} (0.3 - 0.8 slpm). Therefore, the reaction times for these experiments were limited to a few milliseconds compared to about 10 to 20 seconds in this work and the difference in the measured uptake coefficient could be explained by a fast uptake followed by a slow uptake (as will be discussed in Sections 3.9 to 3.11 and in Chapter 8). Remorov et al. (2002) performed an experiment that showed that increasing the relative humidity decreases the uptake coefficient of HO_2 by solid NaCl surfaces as can be seen in Table 3.1. It was suggested that this may be due to water molecules being adsorbed onto the surface of the sodium chloride and therefore the number of free sites available for radical adsorption decreasing. Gershenzon et al. (1995), Loukhovitskaya et al. (2009) and Remorov et al. (2002), all carried out experiments in flow tubes which were coated with NaCl at very low pressures of 1-3 Torr and at a relative humidity of 0% whereas in this work all experiments were performed at atmospheric pressure and at much higher relative humidities.

Salt	Relative humidity/ %	Initial [HO ₂]/ molecule cm ⁻³	Uptake coefficient	Reference
Ammonium sulphate	20	~10 ⁸	0.04 ± 0.02	Taketani et al. (2008)
	45	~10 ⁸	0.05 ± 0.02	Taketani et al. (2008)
	0	4 × 10 ⁹ - 3 × 10 ¹¹	0.011	Gershenson et al. (1995)
	21 - 54	1 × 10 ⁹	< 0.004	George et al. (2013) (this work)
Sodium chloride	20	~10 ⁸	< 0.01	Taketani et al. (2008)
	45	~10 ⁸	0.02 ± 0.01	Taketani et al. (2008)
	0	4 × 10 ⁹ - 3 × 10 ¹¹	0.016	Gershenson et al. (1995)
	0	(2 - 9) × 10 ¹¹	0.0018	Loukhovitskaya et al. (2009)
	0	4 × 10 ¹⁰	0.0116 ± 0.0022	Remorov et al. (2002)
	0	5 × 10 ¹¹	0.0117 ± 0.0008	Remorov et al. (2002)
	28	5 × 10 ¹¹	0.0102 ± 0.0008	Remorov et al. (2002)
	17 - 54	1 × 10 ⁹	< 0.004	(George et al., 2013) (this work)

Table 3.1: Summary of HO₂ uptake coefficients that have been measured for solid inorganic salt aerosols at room temperature (293 ± 2) K and at atmospheric pressure (in this work). The errors in this work represent two standard deviations.

3.3 Measurements of the HO₂ uptake coefficient onto aqueous inorganic aerosols at room temperature

Figure 3.2 shows examples of the pseudo-first order rate constants measured in this work as a function of aerosol surface area for aqueous sodium chloride, ammonium sulphate and ammonium nitrate aerosols. By comparing Figure 3.2 to Figure 3.1 it can be observed that the HO₂ uptake coefficients were larger onto deliquesced aerosols than onto effloresced aerosols by at least a factor of two as will be discussed in greater detail below.

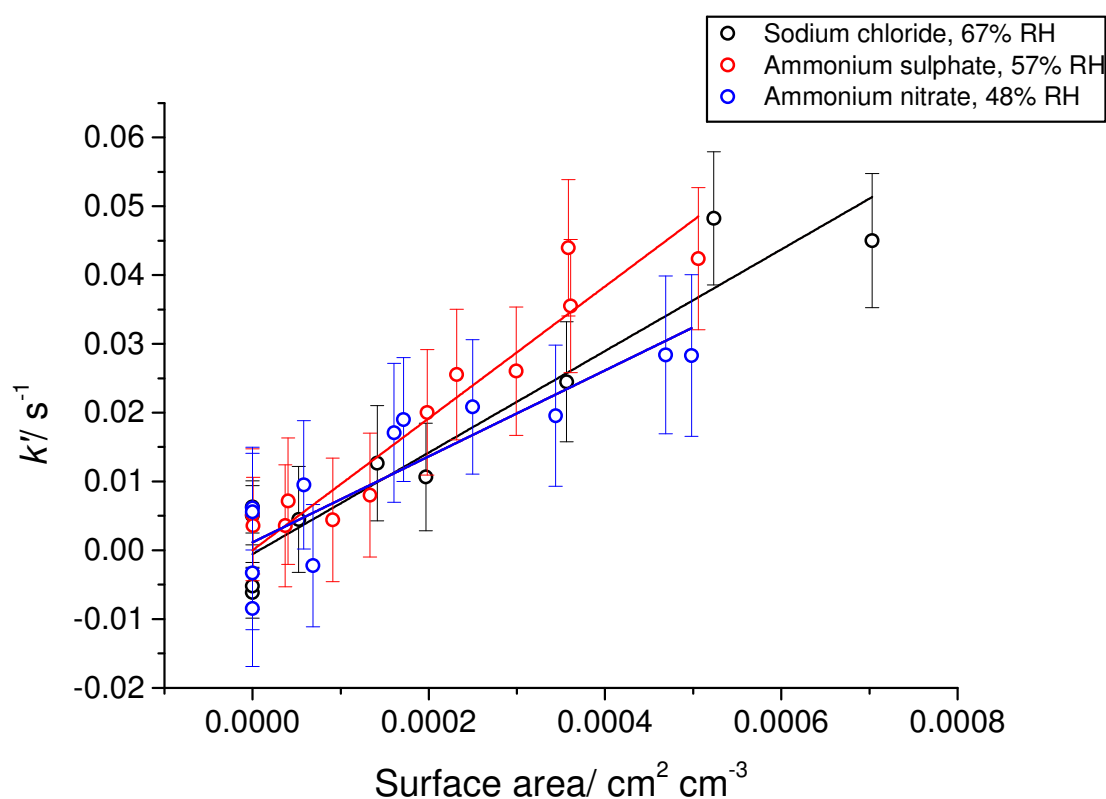


Figure 3.2: Examples of the pseudo-first order rate constant as a function of surface area for aqueous sodium chloride, ammonium sulphate and ammonium nitrate aerosols at 293 ± 2 K and atmospheric pressure. The gradients of the lines were 74 , 90 and 62 $\text{s}^{-1} \text{cm}^{-2} \text{cm}^3$ and resulted in HO₂ uptake coefficients of 0.007 ± 0.002 , 0.009 ± 0.002 and 0.006 ± 0.002 for sodium chloride, ammonium sulfate and ammonium nitrate aerosols, respectively. The error bars represent one standard deviation.

Table 3.2 summarises the uptake coefficients that have been measured for aqueous inorganic salt aerosols. For solid aerosols the HO₂ radicals are limited to diffusion to the surface of the

aerosol, adsorption, surface diffusion, desorption and reaction at the surface whereas for aqueous aerosols the HO₂ radicals could also diffuse into the bulk of the aerosol (Reaction 3.1) where the aqueous Reactions 3.2 to 3.4 (see Section 3.2) could subsequently occur (Jacob, 2000). Therefore, it was expected that the HO₂ uptake coefficient onto aqueous aerosols would be larger than onto solid aerosols. By comparing the values that were obtained in this work for the aqueous aerosols to the values for solid aerosols in Table 3.1, it can be noted that the uptake coefficients for aqueous aerosols are always larger than for solid aerosols. From the measurements obtained in this work, there does not seem to be any significant dependence on the relative humidity, if the aerosols remain aqueous, as the measured uptake coefficients are within the error bars of each other at different relative humidities. However, this will be discussed in further detail in Section 3.7.

Thornton and Abbatt (2005) measured a HO₂ uptake coefficient of ~ 0.1 onto ammonium sulphate aerosols that had been buffered to a pH of 5.1. This is approximately two orders of magnitude higher than the HO₂ uptake coefficients that were measured in this work. However, it should be noted that the initial HO₂ concentration was much larger than in this work (5×10^{10} molecule cm⁻³ compared to 1×10^9 molecule cm⁻³). The Thornton et al. (2008) uptake model predicts that increasing the HO₂ concentration by a factor of fifty would increase the HO₂ uptake coefficient by a factor of approximately 45 for aerosols at a pH of 5.1. This is due to the second order nature of the HO₂ self-reaction. Therefore the difference in the uptake coefficient between this work and the work by Thornton and Abbatt (2005) may be explained by the HO₂ concentration assuming known aqueous chemistry.

Salt	Relative humidity/ %	Initial [HO ₂]/ molecule cm ⁻³	Uptake coefficient	Reference
Ammonium sulphate	45	~10 ⁸	0.11 ± 0.03	Taketani et al. (2008)
	55	~10 ⁸	0.15 ± 0.03	Taketani et al. (2008)
	65	~10 ⁸	0.17 ± 0.04	Taketani et al. (2008)
	75	~10 ⁸	0.19 ± 0.04	Taketani et al. (2008)
	42	5 × 10 ¹⁰	~0.1	Thornton and Abbatt (2005)*
	55	1 × 10 ⁹	0.003 ± 0.005	George et al. (2013) (this work)
	65 - 75	1 × 10 ⁹	0.01 ± 0.01	George et al. (2013) (this work)
Sodium chloride	53	~10 ⁸	0.11 ± 0.03	Taketani et al. (2008)
	63	~10 ⁸	0.09 ± 0.02	Taketani et al. (2008)
	75	~10 ⁸	0.10 ± 0.02	Taketani et al. (2008)
	54	1 × 10 ⁹	0.016 ± 0.008	George et al. (2013) (this work)
	67 - 76	1 × 10 ⁹	0.01 ± 0.02	George et al. (2013) (this work)
Ammonium nitrate	29-70	1 × 10 ⁹	0.005 ± 0.002	George et al. (2013) (this work)

* This study was done with ammonium sulphate buffered to a pH of 5.1 by adding in malonate and bimalonate solutions

Table 3.2: Summary of HO₂ uptake coefficients that have been measured for aqueous inorganic salt aerosols at a temperature of 293 ± 2 K. The errors in this work represent two standard deviations.

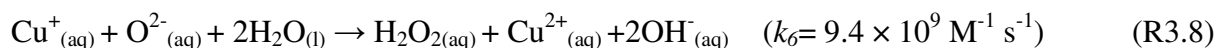
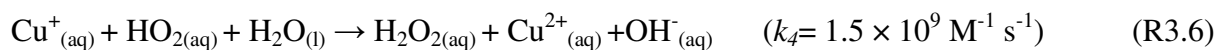
Taketani et al. (2008) also saw an increase in the uptake coefficient of HO₂ by aerosols when aqueous aerosols were being studied rather than solid aerosols. However, the results obtained by Taketani et al. (2008) were one to two orders of magnitude greater than the measurements obtained in this work. The reason for this difference is not known but may be related to the presence of trace metals in aerosols, the reaction time or the initial HO₂ concentration (see the discussion in Sections 3.9 to 3.11). Using the experimental setup used in this work it is not possible to probe this experimentally as using a higher flow rate, which would reduce reaction time, causes problems with the mixing in the flow tube with laminar flow only developing much further along the flow tube (see Section 2.5.2). However, it should be noted that the values obtained in this work were reproducible as they were always within error of each other. The average radius of the aqueous aerosols were also measured, and found to be larger than the average radius of the aerosols for the solid aerosols (see Section 2.6.2). The shift in the average radius showed that the aerosols must have been aqueous. Freshly prepared solutions were always added into the atomiser and all of the tubing, impactor and neutraliser were cleaned whenever the type of aerosol was changed in order to avoid transition metal ion contamination which could cause much higher HO₂ uptake coefficients to be measured.

3.4 Measurements of the HO₂ mass accommodation onto copper-doped inorganic aerosols at room temperature

Ions of copper and iron have been observed in ambient aerosols in a range of field studies (e.g. Allen et al. (2001); Sun et al. (2004)). The sources of the copper and iron found in aerosols are the Earth's crust and combustion (e.g. fossil fuel burning). The concentrations observed in aerosols have varied from 3 – 300 ng m⁻³ for copper and from 55 – 14500 ng m⁻³ for iron (Schroeder et al., 1987). However, copper is completely soluble in aerosols that have a pH < 5 (Deguillaume et al., 2005) whereas the solubility of iron varies from about 1 % to about 81 % depending on the source of the iron (Schroth et al., 2009).

The mass accommodation (α) is the probability of a molecule being adsorbed or absorbed upon collision with the surface of an aerosol. If an aerosol contained 0.1 M of copper (II) the

lifetime of HO₂ in the aerosol would be approximately one nanosecond based on the reaction scheme shown below:



Due to the short lifetime of HO₂ once it has been adsorbed into an aqueous copper-doped aerosol, it could therefore be assumed that the measured uptake coefficient would only be limited by the mass accommodation. Figure 3.3 shows the large increase in rate constants and therefore in the uptake coefficient (from $\gamma = 0.004 \pm 0.004$ to 0.47 ± 0.06) that was measured during an experiment in this work for copper-doped ammonium sulphate compared to ammonium sulphate aerosols. The measured HO₂ uptake coefficient in Figure 3.3 increased by two orders of magnitude when copper (II) sulphate was added to ammonium sulphate aerosols at a 20:1 ammonium sulphate to copper (II) sulphate molar ratio. In Section 3.5 the HO₂ uptake coefficient will be investigated as a function of copper (II) sulphate concentration.

Table 3.3 shows the mass accommodation coefficients that were measured for copper-doped aerosols. A range of conditions were used with the molarity of copper in the aerosols varying from approximately 0.003 to 0.38 M, and the initial HO₂ concentration varying from 10⁸ to 10¹⁰ molecule cm⁻³. The molarities were estimated from the ratio of copper sulphate to ammonium sulphate and the relative humidity at which the experiment was performed using the following equation:

$$\text{Estimated Cu molarity} = \frac{[\text{Cu}]_{1 \text{ mole AS}}}{\text{AWC}_{1 \text{ mole AS}}} \quad (\text{E3.1})$$

where $[\text{Cu}]_{1 \text{ mole AS}}$ is the copper concentration that would be expected if there was 1 mole of ammonium sulphate based on the copper sulphate: ammonium sulphate ratio and $\text{AWC}_{1 \text{ mole AS}}$ is the aerosol water content that would be expected at a given humidity for one mole of

ammonium sulphate based on the Aerosol Inorganic Model (Clegg et al., 1992; Wexler and Clegg, 2002) (<http://www.aim.env.uea.ac.uk/aim/aim.php>).

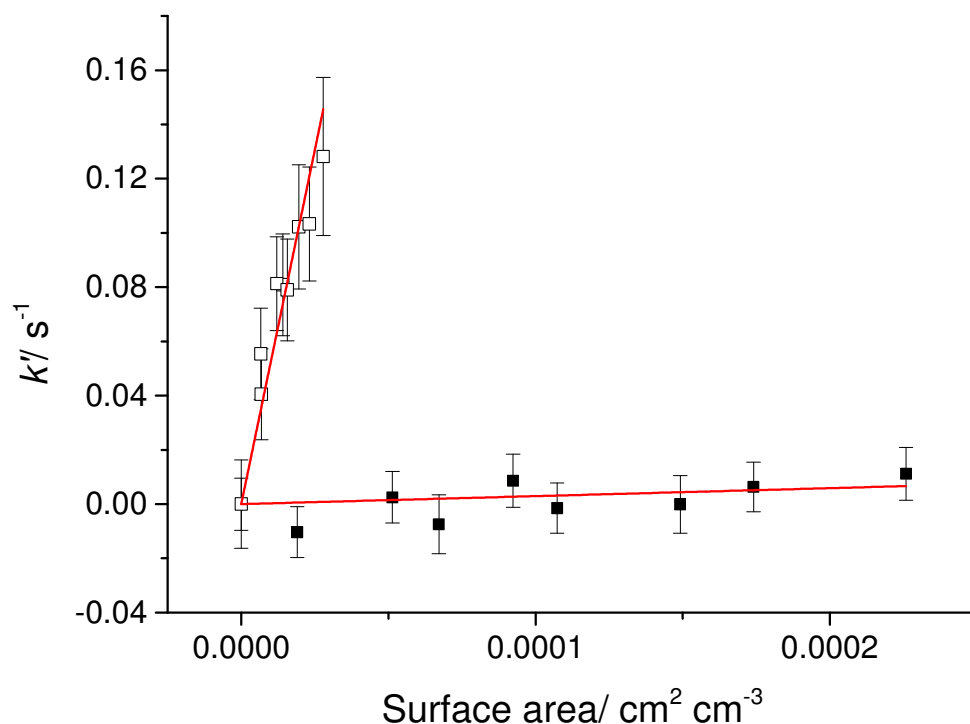


Figure 3.3: The pseudo-first order rate constant as a function of surface area for ammonium sulphate aerosols (closed symbols) and copper doped ammonium sulphate (open symbols) at a relative humidity of 57 % and at 293 ± 2 K. The error bars represent 1 standard deviation. These experiments gave HO_2 uptake coefficients of 0.004 ± 0.004 and 0.47 ± 0.06 for the non-copper doped and copper-doped ammonium sulphate aerosols, respectively.

Although the experimental conditions varies between different groups, it was not expected that the HO_2 concentration would affect the mass accommodation, as the reaction should be first order in terms of HO_2 and the HO_2 radical would have an extremely short lifetime once it had entered the aerosol bulk. The lifetime for the range of copper molarities meant that HO_2 should have a lifetime of between 0.3 ns (for $[\text{Cu}] = 0.38$ M) and 35 ns (for $[\text{Cu}] = 0.003$ M) once it had been absorbed into the aerosol bulk. Indeed, the mass accommodations that were measured between different groups were in agreement with each other. In this work the mass accommodation was measured as 0.5 ± 0.3 . Although the error bar on individual

experiments were much smaller, for example 0.06 in Figure 3.3, there was variability between the HO₂ uptake coefficient between experiments, possibly due to slightly different experimental conditions. It should also be noted that Thornton and Abbatt (2005) stated that the value 0.5 ± 0.1 was actually a lower limit of the mass accommodation. This may be the case if, for example, the HO₂ uptake was limited by gas phase diffusion.

Molar ratio of CuSO ₄ ·5H ₂ O : (NH ₄) ₂ SO ₄	Relative humidity/%	Estimation of [Cu] in the aerosol/M	Initial [HO ₂]/molecule cm ⁻³	Mass accommodation	Reference
Unknown*	75	0.003 and 0.006	Estimated at 10 ⁸ - 10 ⁹	> 0.2	Mozurkewich et al. (1987)
1 : 20	45	0.38	~10 ⁸	0.53 ± 0.12	Taketani et al. (2008)
1 : 50	42	0.16	(2.5 – 5.0) × 10 ¹⁰	0.5 ± 0.1	Thornton and Abbatt (2005)
1 : 20	55	0.34	~ 1 × 10 ⁹	0.5 ± 0.3	This work

* This experiment was with NH₄HSO₄ rather than (NH₄)₂SO₄.

Table 3.3: Summary of HO₂ uptake coefficients that have been measured for aqueous copper-doped aerosols at a temperature of 293 ± 2 K.

3.5 The HO₂ uptake coefficient dependence upon copper and iron concentrations

Mozurkewich et al. (1987) made measurements of the ratio of the HO₂ signal with aerosol to the signal without any aerosols by placing the HO₂ injector in a single position in a flow tube and varying the copper (II) concentration in the aerosols whilst keeping all of the other experimental conditions the same as shown in Figure 3.4. As the copper (II) in the aerosol increases, the HO₂ concentration in the flow tube decreases since the uptake coefficients begin to only be limited by the mass accommodation. Mozurkewich et al. (1987) showed that the HO₂ uptake coefficient started to increase at a copper molality of approximately 10⁻⁴ M, and that the uptake was fully limited by the mass accommodation when the copper (II) molality was greater than 10⁻² M.

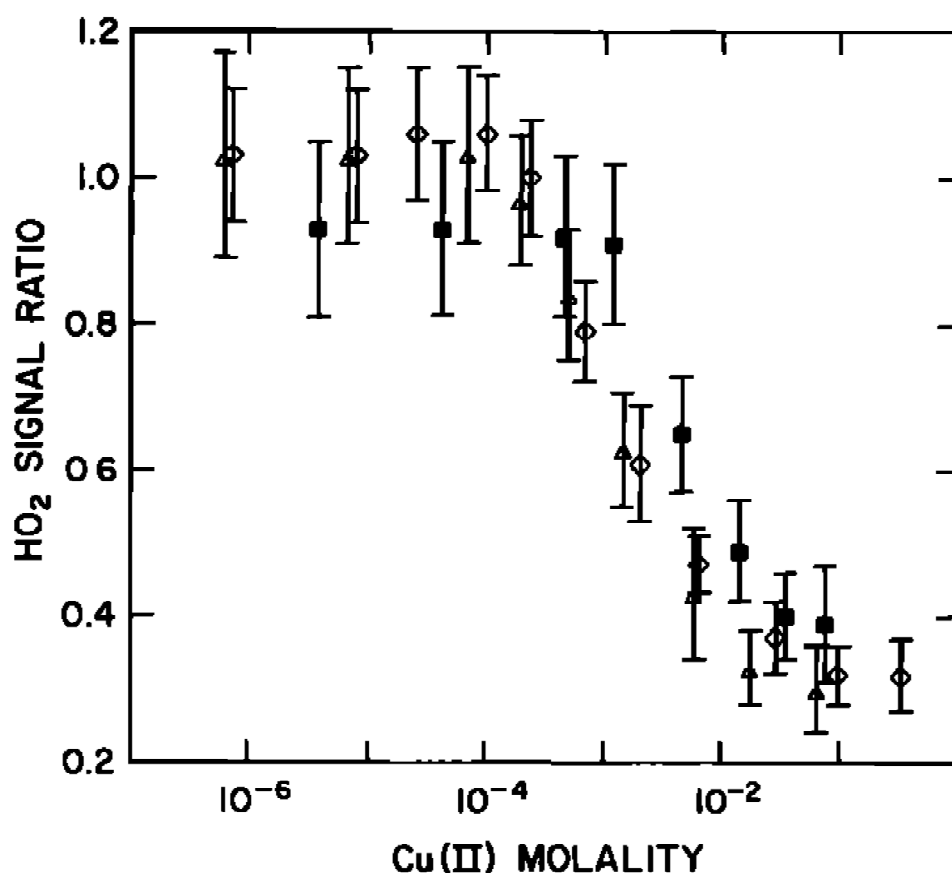


Figure 3.4: The HO₂ signal with aerosols to that without aerosols as a function of copper (II) concentrations within the aerosols measured by Mozurkewich et al. (1987). The measurements with the injector in a fixed position were made for NH₄HSO₄ (57,000 particles cm⁻³, radius = 0.064 μm), squares, LiNO₃ at pH 7 (58,000 cm⁻³, 0.064 μm), triangles, and LiNO₃ at pH 5 (52,000 cm⁻³, 0.069 μm), diamonds. This figure is reproduced from Mozurkewich et al. (1987).

Thornton et al. (2008) modelled the effect of varying the copper concentration in the aerosol on the uptake coefficient using the known aqueous chemistry shown in Reactions 3.5 to 3.8 and Equation 3.2, which was introduced in Section 1.13.3. A similar equation could also be utilised for aerosols containing iron:

$$\frac{1}{\gamma^{HO_2}} = \frac{1}{\alpha^{HO_2}} + \frac{w}{H_{eff}RT\sqrt{k^{II}[Cu]D_{aq}Q}} \quad (E3.2)$$

However, the model that was used predicted that the uptake coefficient would start to increase at a concentration of ~ 10⁻⁹ M and would be fully limited by mass accommodation at

a copper concentration greater than 10^{-4} M. As shown in Section 1.13.3, this is at least two orders of magnitude different to the experimental data obtained by Mozurkewich et al. (1987).

In this work, HO_2 uptake coefficients were measured as the copper concentration in the atomiser was varied. The copper concentrations in the aerosols were then estimated using Equation 3.1. Figure 3.5 shows that the uptake coefficient increased with increasing Cu (II) concentrations in the aerosols. The uptake coefficient increased from a copper (II) molality of approximately 10^{-4} M, and was fully limited by the mass accommodation at a copper molality of 10^{-2} M. The observed increase is in agreement with the work by Mozurkewich et al. (1987) but does not agree with the modelling performed by Thornton et al. (2008). It has been estimated from measured aerosol size distributions, and by making an assumption that all of the copper is soluble that a typical concentration of 3.1 ng m^{-3} of copper in the troposphere could lead to concentrations 2.9×10^{-3} M in aerosols in rural regions (Mao et al., 2013; Ross and Noone, 1991). Therefore, it is possible that for some aerosols the uptake coefficient would be equal to the mass accommodation.

The best fitting to the copper concentration dependence (shown by the red line in Figure 3.5) was found to follow the following equation:

$$\frac{1}{\gamma} = \frac{1}{\alpha} + \frac{1}{A[\text{Cu}]} \quad (\text{E3.3})$$

where α was found to be 0.26 and A was found to be 197 M^{-1} . A good fitting of the data could not be achieved using the Thornton et al. (2008) model in Equation 3.2 (the effect of square rooting the copper term in Equation 3.2 is shown by the blue line in Figure 3.5). It should be noted that at low copper concentrations the relationships shown in Equations 3.2 and 3.3 start to deviate from measurements as shown by Figure 3.6 where the inverse of the HO_2 uptake coefficient is plotted against the inverse of the copper concentration in the aerosol. The data cannot be described by Equation 3.3 at low copper concentrations as Equation 3.3 does not contain a term for the HO_2 self-reaction which is the dominant reaction

at low copper concentrations. However, in Chapter 8 the HO₂ uptake coefficient dependence upon copper concentration will be investigated by the KM-SUB model.

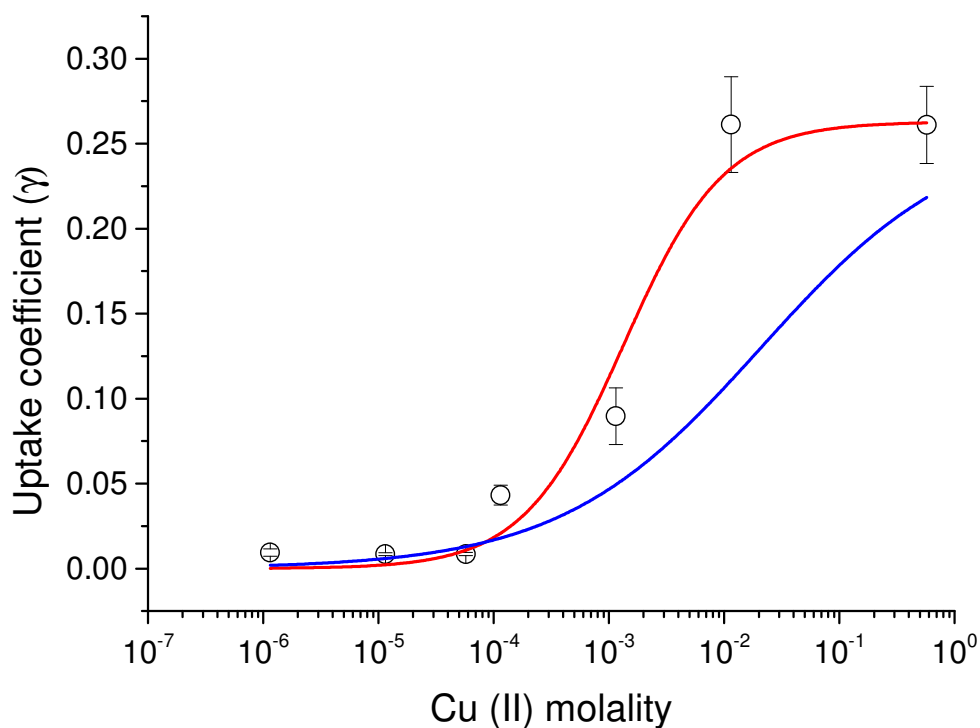


Figure 3.5: The HO₂ uptake coefficient as a function of the estimated Cu(II) molality in the ammonium sulphate aerosols at 65 % RH and 293 ± 2 K. The error bars are 2 standard deviations. The experimental data shown in this figure were obtained by Dr. Ingrid George. The red line represents a fitting of $1/\gamma = 1/\alpha + 1/(A \times [\text{Cu}])$. α was found to be 0.26 and A was found to be 197 M^{-1} . The blue line represents a fitting of $1/\gamma = 1/0.26 + 1/(B \times [\text{Cu}]^{0.5})$ where B was found to be $1.8 \text{ M}^{(1/2)}$.

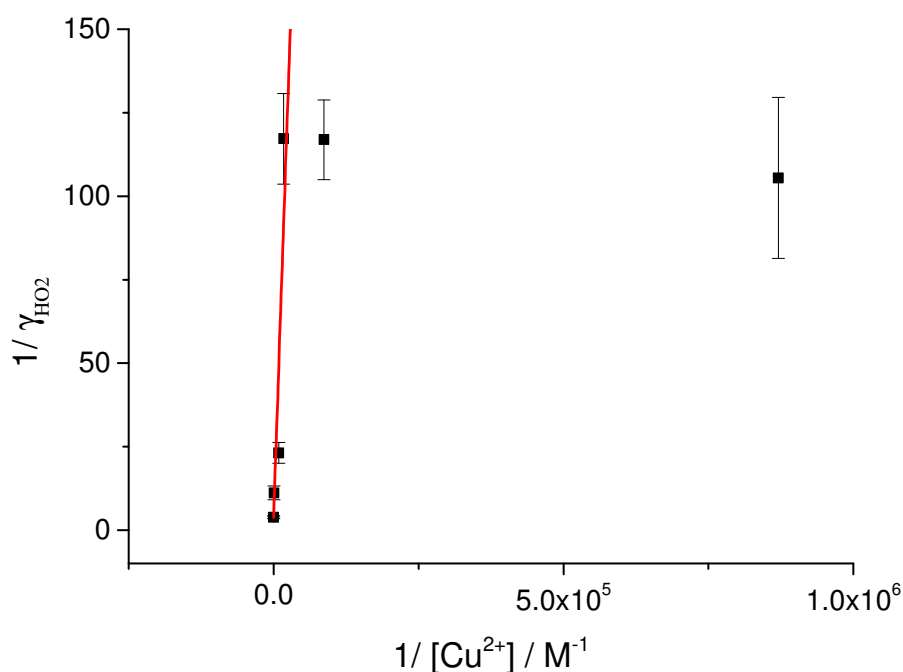


Figure 3.6: The inverse HO_2 uptake coefficient as a function of the inverse of the estimated Cu(II) molality in the ammonium sulphate aerosols at 65 % RH and 293 ± 2 K. The error bars are 2 standard deviations. The red line represents a fitting of $1/\gamma = 1/\alpha + 1/(A \times [\text{Cu}])$. α was found to be 0.26 and A was found to be 197 M^{-1} .

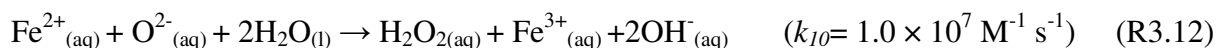
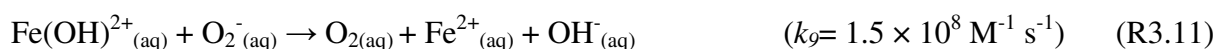
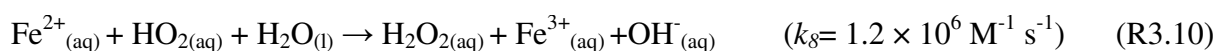
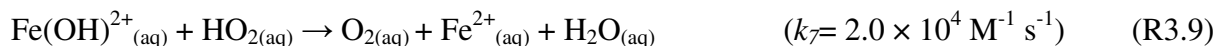
The reason for the experimental data measured in this work and by Mozurkewich et al. (1987) reaching a mass accommodation value at a copper concentration of 10^{-2} M compared to at a concentration of 10^{-4} M predicted by Thornton et al. (2008) is currently uncertain. Although there are several studies of the rate constants of Cu^{2+} with HO_2 and O_2^- it is unclear what the error bars on these rate constants are (Bielski et al., 1985; Cabelli et al., 1987; Rabani et al., 1973; Vonpiechowski et al., 1993). Another uncertainty could arise from the HO_2 Henry's Law constant which has been estimated using the following equation:

$$H = \exp(-\Delta G_{\text{sol}} / RT) \quad (\text{E3.4})$$

Schwartz (1984) estimated $\Delta G_{\text{sol}}(\text{HO}_2)$ to be $-4.2 \text{ kcal mol}^{-1}$ whereas Golden et al. (1990) calculated a value of $-4.9 \pm 0.5 \text{ kcal mol}^{-1}$. A range of $-4.2 \text{ kcal mol}^{-1}$ to $-5.4 \text{ kcal mol}^{-1}$ produces Henry's Law constants in the range of 1200 to 9000 M atm^{-1} . The HO_2 uptake

coefficient dependence upon the copper concentration will be investigated in greater detail using the KM-SUB model in Section 8.7.

Iron behaves in a similar way to copper by catalysing HO_2 into H_2O_2 via the following reactions:



By comparing the rate constants of the iron reactions to those of the copper reactions (Reactions 3.5 to 3.8), it can be noted that iron (II and III) is a less efficient catalyst than copper in the destruction of HO_2 . However, it was expected that similarly to copper, with increasing iron (II and III) concentrations the HO_2 uptake coefficient would increase as the HO_2 lifetime in the aerosol decreased. Therefore, an experiment was performed to investigate the effect of increasing concentrations of iron on the uptake coefficient. Similarly to increasing the copper concentration in the aerosol, the uptake coefficient increased as the iron concentration increased in the atomiser as shown in Figure 3.7. However, it should be noted that when iron (II or III) and ammonium sulphate were mixed together in the atomiser solution some precipitation occurred although it remains unclear as to the exact composition of the precipitate. Therefore, the concentrations shown in Figure 3.7 are upper estimates of the actual concentration. For the uptake coefficient shown at the highest estimated molarity of $\sim 1 \text{ M}$, no ammonium sulphate was added into the atomiser solution, and no precipitation formed although these concentrations were corrected to take into account the solubility of the iron species. For these high concentrations an uptake coefficient of 0.12 ± 0.03 was obtained, which is lower than the mass accommodation value of 0.26 ± 0.03 that was measured as the highest uptake coefficient for the copper (II) concentration graph shown in Figure 3.5.

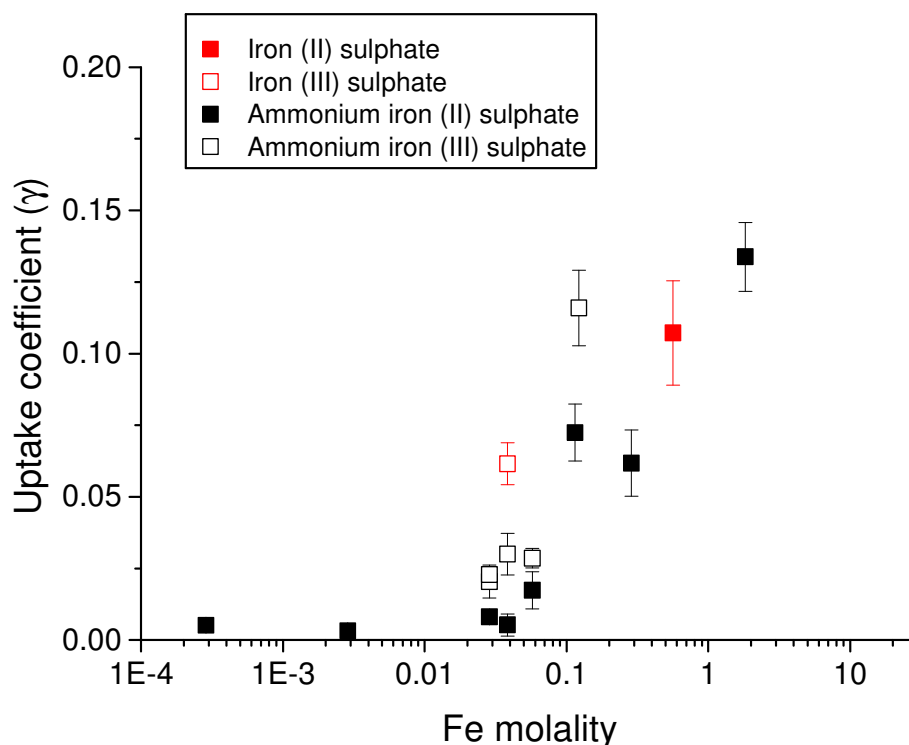
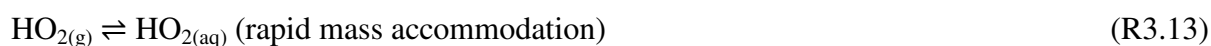


Figure 3.7: The HO_2 uptake coefficient as a function of the estimated Fe molality in the ammonium sulphate aerosols at 293 ± 2 K and at 66 ± 2 % RH. The ammonium sulphate aerosols were doped with iron (II) sulphate (red, closed), iron (III) sulphate (red, open), ammonium iron (II) sulphate (black, closed) and ammonium iron (III) sulphate (black, open). The error bars are 2 standard deviations.

3.6 The HO_2 uptake coefficient dependence upon the pH of the aerosol

The HO_2 uptake coefficient for non-copper doped aqueous aerosols is expected to be pH dependent. At room temperature the pK_a of HO_2 is approximately 4.7 which means that it is a weak acid (Jacob, 2000). When the aerosol pH increases there is greater dissociation of HO_2 into H^+ and O_2^- , which means that there is a greater solubility of HO_2 :



The solubility dependence of HO₂ on pH has been defined by an effective Henry's law constant (H_{eff}) (Thornton and Abbatt, 2005):

$$H_{eff} = H_{HO_2} \left(1 + \frac{K_{eq}}{[H^+]} \right) \quad (E3.5)$$

where H_{HO_2} is the physical Henry's law constant estimated to be 3900 M atm⁻¹, $[H^+]$ is the concentration of H⁺ ions, and K_{eq} is the equilibrium constant in Reaction 3.2.

There is currently only one experiment in the literature where the effect of pH on HO₂ uptake coefficients has been investigated. Thornton and Abbatt (2005) buffered ammonium sulphate aerosols to a pH of 5.1 by adding malonate and bimalonate solutions to the atomiser solution. Thornton and Abbatt (2005) measured an uptake coefficient of ~ 0.1 onto the buffered aerosol compared to an uptake coefficient of < 0.01 onto sulphuric acid aerosols (which would have an extremely low but unknown pH) with a HO₂ concentration of 5×10^{10} molecule cm⁻³.

In this work the initial pH of sodium chloride aerosols was altered by adding either hydrochloric acid or sodium hydroxide into the atomiser solution. The pH of the atomiser solution was measured using a pH meter (Martini instruments Mi150, accuracy ± 0.01 pH). It should be noted that as the aerosols are more concentrated than the atomiser solution (as the relative humidity decreases) and therefore the pH of the aerosols should be slightly different to the pH of the atomiser solutions. In this experiment the aerosols were not buffered. Higher uptake coefficients were measured at the very low pHs, however, after analysis of the atomiser solutions high iron (II or III) concentrations (~ 140 ppb) were measured in these solutions which could lead to iron molarities of $\sim 2 \times 10^{-4}$ M in the aerosols. It is believed that the high acidity of the solutions may have caused leaching of iron in the atomiser.

Figure 3.8 shows that no change in uptake was observed over the range of unbuffered pH experiments that were not affected by elevated iron concentrations. A quick calculation estimated that at a HO₂ concentration of 1×10^9 molecule cm⁻³ and a typical aerosol volume density of 1×10^{-13} L cm⁻³, the maximum HO₂ concentration that would enter the aerosol would be 0.017 M. If a thousandth of the total HO₂ entered the aerosols and dissociated into

H^+ and O_2^- another calculation shows that the pH of a neutral aerosol would decrease to a value of 5.7. Therefore, it is likely that the actual aerosol pH is much lower in the experiments than their initial pH. Therefore, the effective Henry's law would be smaller and the uptake coefficients would also be smaller than would be expected than if only the initial aerosol pH was taken into account.

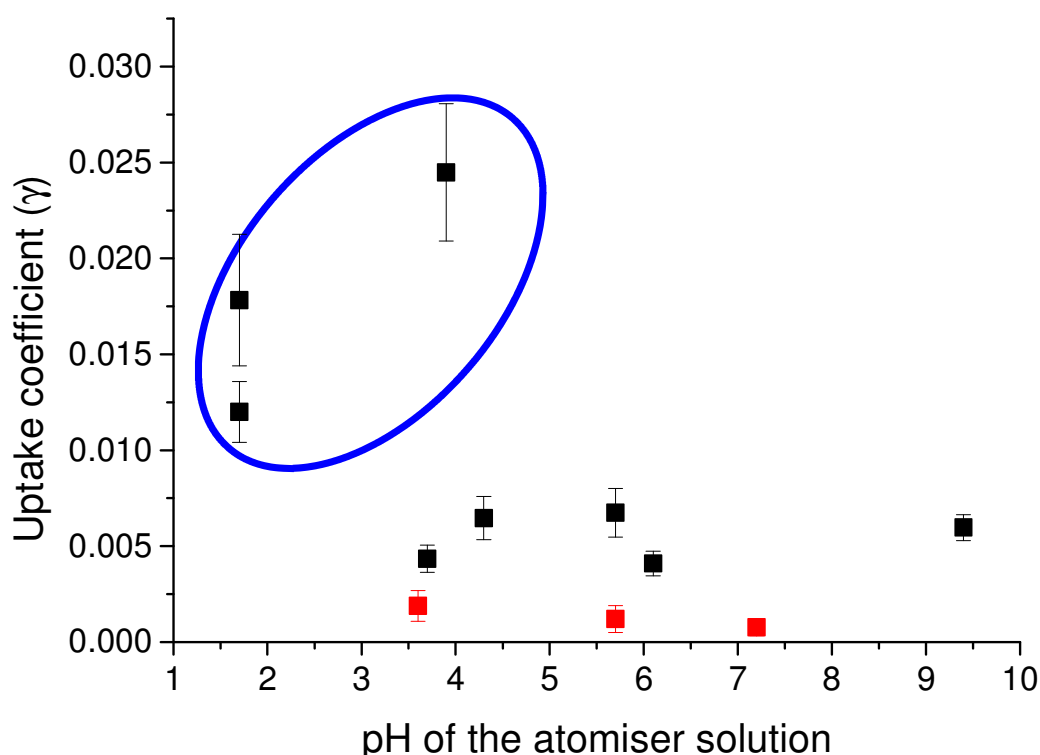


Figure 3.8: The HO_2 uptake coefficient for sodium chloride aerosols with hydrochloric acid or sodium hydroxide added into the atomiser solutions (black points) and ammonium sulphate aerosols containing a mixture of potassium hydrogen phthalate or potassium dihydrogen orthophosphate (red points). These experiments were performed at 293 ± 2 K and at 55 ± 2 % RH. The circled points had elevated iron concentrations in the atomiser solutions, possibly as a result of leaching from the atomiser. The error bars are 2 standard deviations.

Another experiment was performed with ammonium sulphate aerosols and buffers composed of either potassium hydrogen phthalate or potassium dihydrogen orthophosphate and either hydrochloric acid or sodium hydroxide. The molarities of these buffers was estimated at 0.6 M. Therefore, there should have been enough buffer for the pH of the aerosol to remain

stable. However, the uptake coefficient did not change over a pH range of 3.6 to 7.2. The Thornton et al. (2008) model predicts that the uptake coefficient should increase by approximately three orders of magnitude over this range of pH. There is also some field evidence that the HO₂ uptake coefficient onto cloud particles (which are larger than the aerosols used here) is dependent on the pH of the cloud (Whalley et al., 2014). It is unclear as to the reason for the lack of increase in the uptake coefficient for the buffered aerosols as the pH increases in this work. However, possible reasons for the constant uptake coefficient over the pH range could be if the buffer acted as a surfactant or changed the viscosity of the aerosol. However, there is currently no information about the effect of potassium hydrogen phthalate or potassium dihydrogen orthophosphate in aerosols available in the literature.

3.7 The HO₂ uptake coefficient dependence upon relative humidity for aqueous aerosols

It has already been shown in Section 3.2 and 3.3 that solid aerosols have much lower uptake coefficients than aqueous aerosols. Therefore, the relative humidity can affect the uptake coefficient if it causes the aerosol to effloresce or deliquesce. Remorov et al. (2002) also showed that the adsorption of water to solid surfaces may block the reactive sites on the surface to incoming HO₂ radicals thereby lowering the HO₂ uptake coefficient. In this work and in the work by Taketani et al. (2008) an increase in uptake coefficient for aqueous aerosols was observed when increasing the humidity for ammonium sulphate although this trend was not observed for sodium chloride. However, it should be noted that for this work, the increase in uptake coefficient with RH was within the error bars.

As the size of an aerosol increases, the uptake coefficient should also increase assuming that all other factors remain the same. The reacto-diffusive length (l) is a measure of the distance from the interface at which the reaction happens and is given by:

$$l = \sqrt{\frac{D}{k_r}} \quad (\text{E3.6})$$

where D is the aqueous phase diffusion coefficient and k_r is the first order rate constant for the HO_2 reaction in the bulk. Hanson and Lovejoy (1995) stated that the uptake coefficient can be given by the following equation:

$$\frac{1}{\gamma} = \frac{1}{\alpha} + \frac{w}{4HRT\sqrt{Dk_r}} \left(\coth(q) - \frac{1}{q} \right)^{-1} \quad (\text{E3.7})$$

where $q = r_s / l$ and r_s is the radius of the aerosol. If r_s is much larger than l then the reaction will occur at the surface of the aerosol and the size dependent term $[\coth(r_s / l) - (l/r_s)]$ approaches unity. In this case, the uptake coefficient is not dependent upon the size of the aerosol. However, if l is much larger than r_s the uptake coefficient will occur throughout the volume of the aerosol and the size dependent term tends towards $r/3l$ and Equation 3.7 can be written as:

$$\frac{1}{\gamma} = \frac{1}{\alpha} + \frac{w}{4HRT\left(\frac{V}{S}\right)k_r} \quad (\text{E3.8})$$

A typical volume to surface ratio in the experiments performed in this work is 2×10^{-6} cm. If an uptake coefficient of 0.005 is assumed then a value of approximately 300 s^{-1} for k_r can be calculated. The typical diffusion coefficient of HO_2 is assumed to be $10^{-5} \text{ cm}^2 \text{ s}^{-1}$ (Schwartz, 1984) and therefore the reacto-diffuso length can be calculated to be approximately 2000 nm. Comparing the reacto-diffuso length to an average particle radius of about 50 nm shows that the uptake coefficient should be volume limited and therefore dependent upon the radius of the aerosol.

The size of a deliquesced aerosol should be dependent upon the relative humidity of its surroundings. As the humidity increases, the aerosol will grow. The following equation that was developed by Thornton et al. (2008) and is based upon Equation 3.8 shows that the HO_2 uptake coefficient is expected to be dependent upon the size of the aerosol. This was explored in more detail in Section 1.13.3.

$$\frac{1}{\gamma^{\text{HO}_2}} = \frac{1}{\alpha^{\text{HO}_2}} + \frac{3wN_A}{8000(H_{eff}RT)^2 k_{eff}[\text{HO}_2(g)]r_p} \quad (\text{E3.9})$$

In order to be able to work over a large range of humidities, ammonium nitrate aerosols were studied as these do not effloresce down to a relative humidity of 0%. The average radius of the ammonium nitrate aerosols varied from 42.6 nm at 30% RH to 47.7 nm at 77 % RH determined from the SMPS data. However, the uptake coefficient remained at a constant value of 0.005 ± 0.002 over this range as shown in Figure 3.9.

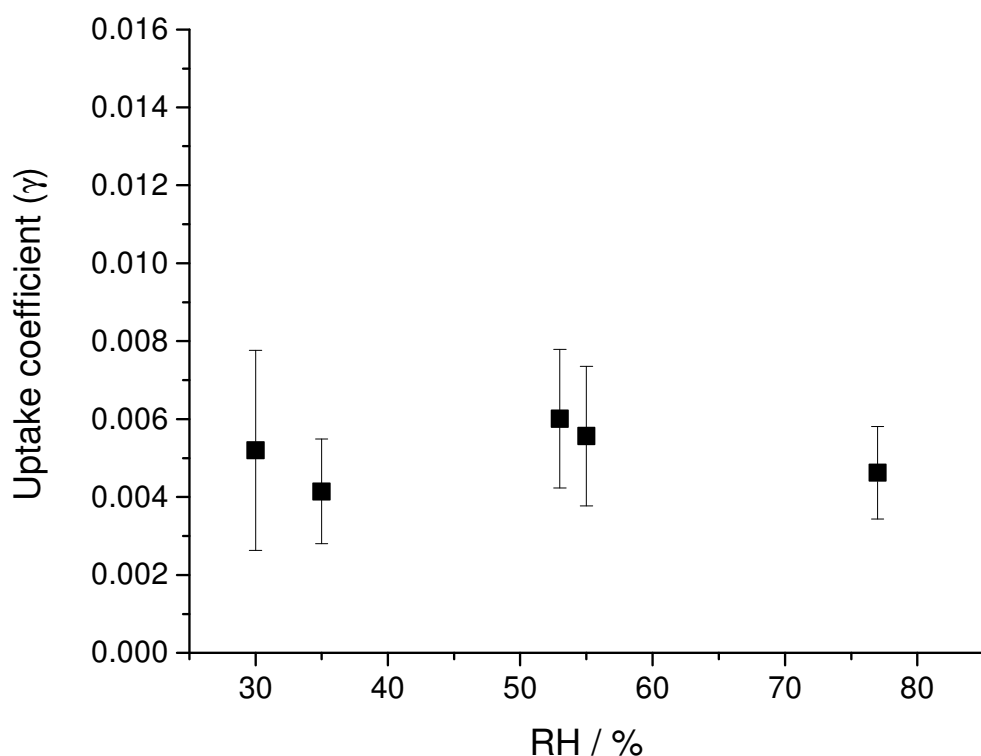


Figure 3.9: HO₂ uptake coefficients for aqueous ammonium nitrate aerosols as a function of relative humidity for an initial [HO₂] = 1×10^9 molecule cm⁻³ and at 293 ± 2 K. The error bars represent 2 standard deviations.

Thornton et al. (2008) predict using Equation 3.9 that increasing the average radius of an aerosol from 42.6 nm to 47.7 nm would increase the uptake coefficient by a factor of approximately 10%. Therefore, it was not expected that the uptake coefficient would increase significantly over the range of humidities that were studied. Any increase in uptake coefficient that would be observed would be below the precision of the experiment. For an observable change in the uptake coefficient, for example if it were to double from 0.005 to

0.010, the radius of the aerosols would also have needed to have doubled. In the work by Taketani et al. (2008) the increase in the uptake coefficient (from $\gamma = 0.11 \pm 0.03$ to $\gamma = 0.19 \pm 0.04$) for ammonium sulphate from 45 % to 75% RH, the aerosol radius increased from 90 nm to 110 nm. However, the Thornton model predicts a 20 % increase in the HO₂ uptake coefficient for this increase in the radius which is much smaller than the increase observed by Taketani et al. (2008) (Table 3.1).

3.8 The dependence of uptake coefficients upon reaction time and initial radical concentration

Many previous laboratory studies have observed both a time dependence and a dependence on the initial concentration of the radical or molecule that is being studied on the measured uptake coefficient. For example, both NO₂ and ozone uptake onto soot have been shown to depend upon exposure time of the molecule to the soot and also on the initial concentration of the molecule. The uptake coefficients were modelled by Ammann and Pöschl (2007) using the KM-SUB model described in Section 1.8.2 (and in Chapter 8). For NO₂ the mechanism was modelled as:



For ozone a similar scheme was used:



where X₁, X₂ and Y₁ were reactants on the surface of the soot.

For both the NO_2 uptake and the ozone uptake, the initial uptake was fast due to a reaction with a very reactive species (X_2 for NO_2 and Y_1 for O_3). For NO_2 the uptake then further decreased as reactant X_1 was consumed. Similarly for ozone, once the reactant Y_1 has been consumed Reaction 3.22 became dominant. Both NO_2 uptake and ozone uptake onto soot had been shown to be dependent on their respective concentrations during laboratory studies with larger uptake coefficients at lower radical concentrations. The dependence on the initial concentration of the molecule was due to the reactants (X_1 , X_2 and Y_1) being consumed at a faster rate when there was more of the molecule present. Figure 3.10 shows the NO_2 uptake coefficient dependence upon time and upon the NO_2 concentration measured in laboratory studies and modelled assuming the mechanism shown in Reactions 3.15 – 3.18 (Ammann and Pöschl, 2007). Similar time and molecule concentration dependences have also been measured for the nitration of aerosolised protein by ozone and nitrogen dioxide (Shiraiwa et al., 2012b; Shiraiwa et al., 2012c).

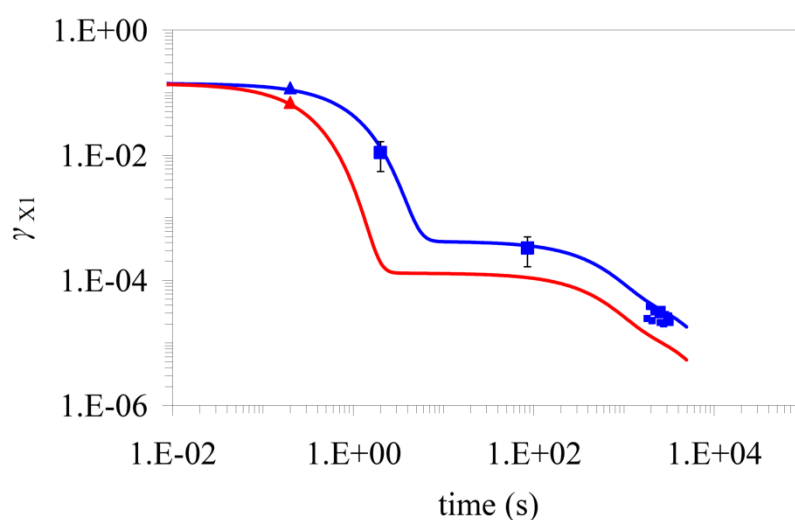
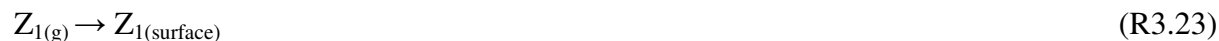


Figure 3.10: The NO_2 uptake coefficient onto soot surfaces measured by Ammann et al. (1998) (small squares), Ammann et al. (1997) (large squares) and by Gerecke et al. (1998) (triangles). The two NO_2 concentrations were $[\text{NO}_2] = 3 \times 10^{11} \text{ cm}^{-3}$ (blue) and $[\text{NO}_2] = 1 \times 10^{12} \text{ cm}^{-3}$ (red). The data were modelled using Reactions 3.15 – 3.18 and the KM-SUB model output is represented by the red and blue lines. This figure was reproduced from Ammann and Pöschl (2007).

Another example of a time and radical concentration dependence was for SO_2 uptake into acidic aerosols. This was also modelled by Ammann and Pöschl (2007) with the parameters

being based upon experimental data by Jayne et al. (1990). It was assumed that the SO_2 undergoes reversible adsorption and surface to bulk transport but that no reactions occur. The experimental scheme was as follows (where Z could represent SO_2):



In this case, the uptake coefficient is equal to the mass accommodation at time zero but rapidly drops to zero as the surface and bulk of the aerosol become saturated. The uptake coefficient drops to zero due to there not being a net removal of Z_1 . There is also a dependence of the uptake coefficient upon the initial concentration of Z_1 . At higher Z_1 concentrations the aerosol surface starts to saturate at a faster rate meaning that the surface accommodation (and therefore the uptake coefficient) at a given time is smaller than with lower Z_1 concentrations.

Slade and Knopf (2013) observed an OH concentration dependence for OH uptake coefficients onto levoglucosan, abietic acid, and nitroguaiacol with higher uptake coefficients at lower OH concentrations. Slade and Knopf (2013) modelled the uptake coefficient using a Langmuir Hinshelwood mechanism (described in Section 1.10), with more adsorption sites being filled at high OH concentrations, making them unavailable to incoming OH radicals.

3.9 Laboratory studies for the time dependence of the HO_2 uptake coefficient onto aqueous aerosols

The HO_2 uptake coefficient time dependence was investigated using the methodology described in Section 2.9. Figure 3.11 shows that as the reaction time increases (due to the HO_2 injector being moved backwards along the flow tube) the uptake coefficient decreases. These uptakes are the average uptake between time zero and the given reaction time. By comparing these uptake coefficients with the uptake coefficients given in

Table 3.2, it can be seen that these uptake coefficients are approximately an order of magnitude larger than those for moving injector experiments (equivalent to the average uptake between 10 and 20 seconds). These results suggest that there must be a large initial HO_2 uptake coefficient which decreases with time. Figure 3.11 also shows that a higher uptake coefficient is measured at a lower HO_2 concentration for two sodium chloride experiments at the same humidity.

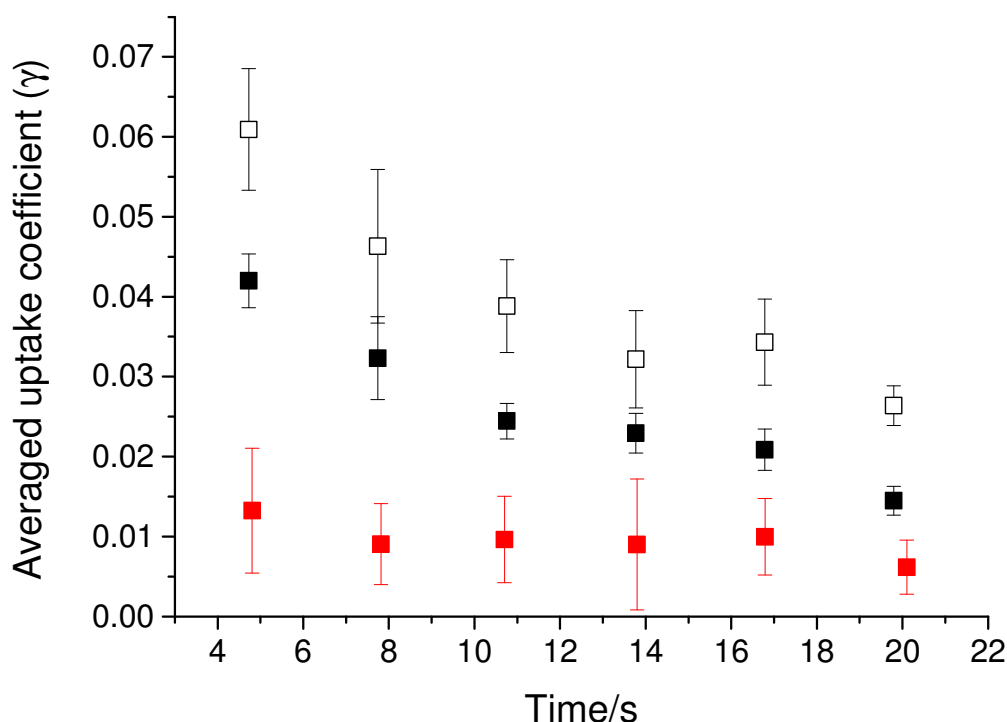


Figure 3.11: The average uptake coefficient between time zero and the given time for ammonium nitrate aerosols at an initial $[\text{HO}_2] = 1 \times 10^9$ molecule cm^{-3} and at 20 % RH (red symbols), sodium chloride aerosols at an initial $[\text{HO}_2] = 2.1 \times 10^9$ molecule cm^{-3} and at 59 % RH (closed black symbols) and sodium chloride aerosols at an initial $[\text{HO}_2] = 7.1 \times 10^8$ molecule cm^{-3} and at 59 % RH (open black symbols) at a temperature of 293 ± 2 K. Each point was obtained using the fixed injector methodology described in Section 2.9. The error bars represent one standard deviation.

Loukhovitskaya et al. (2009) reported a time dependence for the uptake of HO_2 onto solid sodium chloride and sodium bromide surfaces. However, the time dependence was attributed to the deactivation of the solid surface due to adsorption of HF which was one of the byproducts of their method of HO_2 production. In this work HO_2 is formed by the photolysis

of water and therefore no HF is formed. Therefore, the time dependence that was observed in this work cannot be explained by the surface deactivation that was observed in the work by Loukhovitskaya et al. (2009).

There are several possible explanations for the HO₂ uptake coefficient time dependence that was observed in this work. These explanations will be explored in greater detail in Chapter 8 where the HO₂ chemistry is explored using the KM-SUB model. However, some of the potential explanations are summarised below. The first possibility would be if the aerosol were becoming saturated over time. The mechanism for this potential explanation is described by Reactions 3.23 – 3.26 and is similar to the SO₂ uptake onto acidic aerosols described in Section 3.8. The surface and bulk of the aerosol may have been becoming saturated by HO₂ therefore reducing the uptake coefficient from an initial value of the mass accommodation. Once the aerosol is fully saturated the uptake coefficient could potentially decrease to a stable value. If there was no reaction of HO₂ in the aerosol the uptake coefficient would tend to zero over time. However, in the case of HO₂ uptake the measured uptake coefficient would then be controlled by the known aqueous chemistry. This explanation will be explored in detail using the KM-SUB model in Chapter 8.

The second possible explanation would be if a reactant in the aerosol was being used up over time. Examples of time dependences due to a reactant being used up were given in Section 3.8. There may be a trace contaminant in the aerosols which reacts with HO₂ and is used up over time. The contaminant would have to be highly reactive towards HO₂ but would be rapidly used up over time. A potential contaminant in this work could be iron or copper ions which have been measured as less than 0.2 μM and 0.1 μM respectively by ICP-MS in the atomiser solutions used for these experiments. These concentrations would lead to copper concentrations of less than 10 μM of copper and less than 20 μM of iron in sodium chloride aerosols at 65% RH (using Equation 3.1 in Section 3.4). However, these concentrations are less than the concentrations that have been found to affect the uptake coefficient in Figure 3.5 and Figure 3.7. Therefore, it is unlikely that the time dependence is due to trace copper and iron in the aerosol becoming used up or deactivated. The mechanism if metals were becoming deactivated is also unknown although could be due to complexation which is explored further in Sections 4.5 and 4.6.

A third possible explanation would be if the aerosol was becoming more viscous over time. If this were the case the HO_2 Henry's Law Constant would reduce so that less HO_2 would be entering the aerosol phase and reacting. If the aerosols were viscous the saturation time would also increase. However, it seems unlikely that the aerosols would become more viscous over time as this would require a mechanism that increased the viscosity of the aerosols. The effect of viscosity will be investigated further in Section 4.4.

A final explanation for the observed time dependence is the second order nature of the HO_2 self-reaction. The HO_2 concentration has been measured to decrease in the flow tube at longer injector positions (or times) due to the HO_2 loss to the walls of the flow tube and also due to HO_2 having been converted to H_2O_2 in the aerosols. As there is less HO_2 in the gas phase at longer times in the flow tube there will also be less HO_2 in the aqueous phase due to the Henry's law constant. Therefore, if there is less HO_2 in the aerosol, the HO_2 self-reaction is reduced and the uptake coefficient appears smaller. The KM-SUB model will be used in Chapter 8 to explore some of these explanations.

3.10 Laboratory studies for the HO_2 uptake time dependence onto aqueous copper doped aerosols

The time dependence was also explored for copper-doped ammonium sulphate aerosols. Figure 3.12 shows that, similarly to the aqueous salts, the uptake coefficient (or mass accommodation) appears to decrease over time. If the uptake coefficient was solely limited by mass accommodation a change in the measured uptake coefficient should not change over time but should instead remain at the mass accommodation value.

Similarly to the time dependence observed for the aqueous salts, the time dependence for copper-doped aerosols may be due to the saturation of the aerosol, a change in the aerosol viscosity or due to the copper ions in the aerosol becoming deactivated over time. However, it seems unlikely that the viscosity would change or that the copper would deactivate over time. The final explanation for aqueous salt aerosols was that the second order nature of the

HO₂ self-reaction was causing the time dependence due to the reduction in HO₂ concentrations along the flow tube. However, the HO₂ catalytic destruction by copper ions is a first order process in terms of HO₂ and therefore the reduction in the HO₂ uptake coefficient cannot be due to a decrease in HO₂ along the flow tube.

There is another explanation for the time dependence for aerosols containing metals ions. The gaseous and aerosol H₂O₂ concentrations in the flow tube should increase along the flow tube with larger concentrations at longer injector positions (or times) due to the formation of H₂O₂ from the reaction of HO₂. The H₂O₂ could then reform HO₂ in the presence of iron or copper in the aerosol phase via the Fenton reactions shown below:



Therefore, as the H₂O₂ concentrations in the flow tube increase there would also be an expectation that the rate of the back reaction reforming HO₂ would also increase. However, it is unknown as to whether the H₂O₂ formed along the flow tube would be at a high enough concentration to significantly affect the HO₂ uptake coefficient. This will be explored in further detail in Chapter 8.

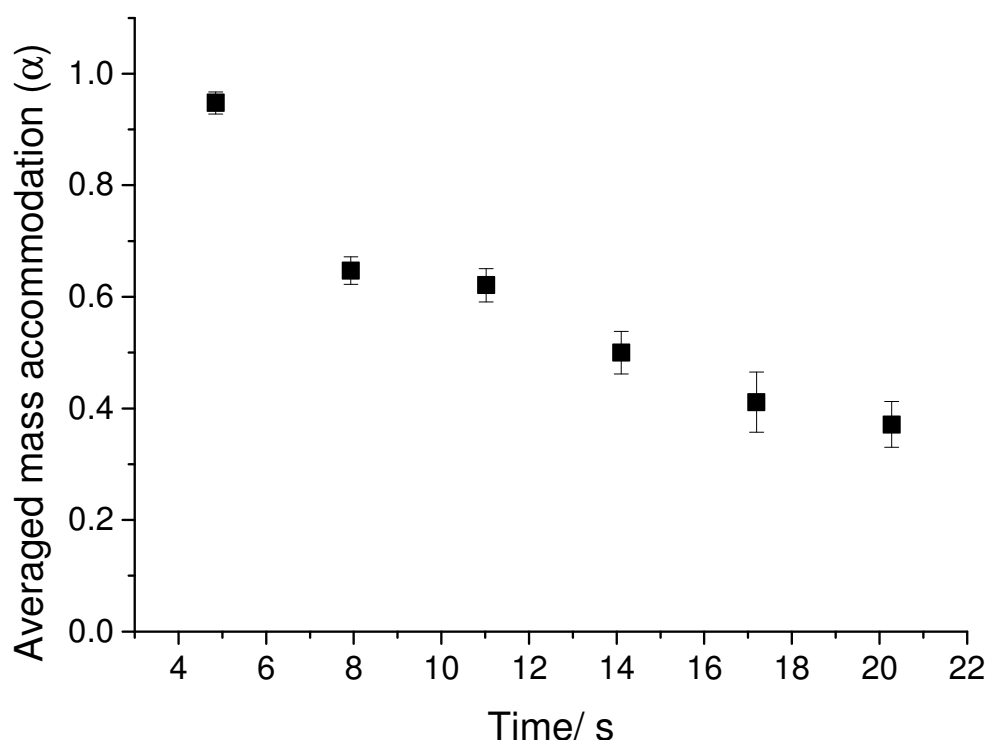


Figure 3.12: The average mass accommodation between time zero and the given time for copper-doped ammonium sulphate aerosols at an initial HO_2 concentration of 1×10^9 molecule cm^{-3} , at 59% RH and at 293 ± 2 K. The estimated copper concentration in the aerosol is 0.4 M. Each point was obtained using the fixed injector methodology described in Section 2.9. The error bars represent 1 standard deviation.

3.11 Laboratory studies for the dependence of the HO_2 uptake coefficient upon the initial HO_2 concentration

As discussed in Section 3.8 many studies that have observed a time dependence have also observed a dependence on the concentration of the radical or molecular species that is being investigated. Therefore, the effect of the initial HO_2 concentration upon the HO_2 uptake coefficient was investigated in greater detail by varying the current of the lamp that photolyses water vapour to form HO_2 . Figure 3.11 showed that for sodium chloride the uptake was larger for lower HO_2 concentrations (7.1×10^8 molecule cm^{-3}) and smaller for higher HO_2 concentrations (2.1×10^9 molecule cm^{-3}). This apparent dependence on HO_2 concentration was investigated in greater detail by doing experiments using the moving

injector method instead of the fixed injector method. An example of the results of one of these experiments is shown in Figure 3.13. The experiment was performed with ammonium nitrate aerosols and uptake coefficients of 0.009 ± 0.004 and 0.004 ± 0.002 were obtained for initial HO_2 concentrations of 1.1×10^9 molecule cm^{-3} and 2.7×10^9 molecule cm^{-3} , respectively. Although these uptake coefficients are within error of each other, all experiments that were performed on the same day using the same atomiser solution but with different lamp currents consistently showed the trend of larger uptakes at lower HO_2 concentrations. The trend was also investigated for copper-doped aerosols and a similar trend was observed with larger uptake coefficients measured at lower HO_2 concentrations.

The observed HO_2 concentration trend was consistent with the majority of the explanations that have been described in Section 3.9. For example, the HO_2 concentration dependence may be due to a saturation mechanism as at higher HO_2 concentrations the aerosol would saturate at a much faster rate. Therefore, at a given time the uptake for the lower HO_2 concentration would be larger as the aerosol would be less saturated than if the HO_2 concentration was higher. The HO_2 concentration dependence is also consistent with the hypothesis that a trace reactant in the aerosol is either being used up or deactivated. If this were the case then at higher HO_2 concentrations the reactant would be used up faster leading to smaller observed uptake coefficients.

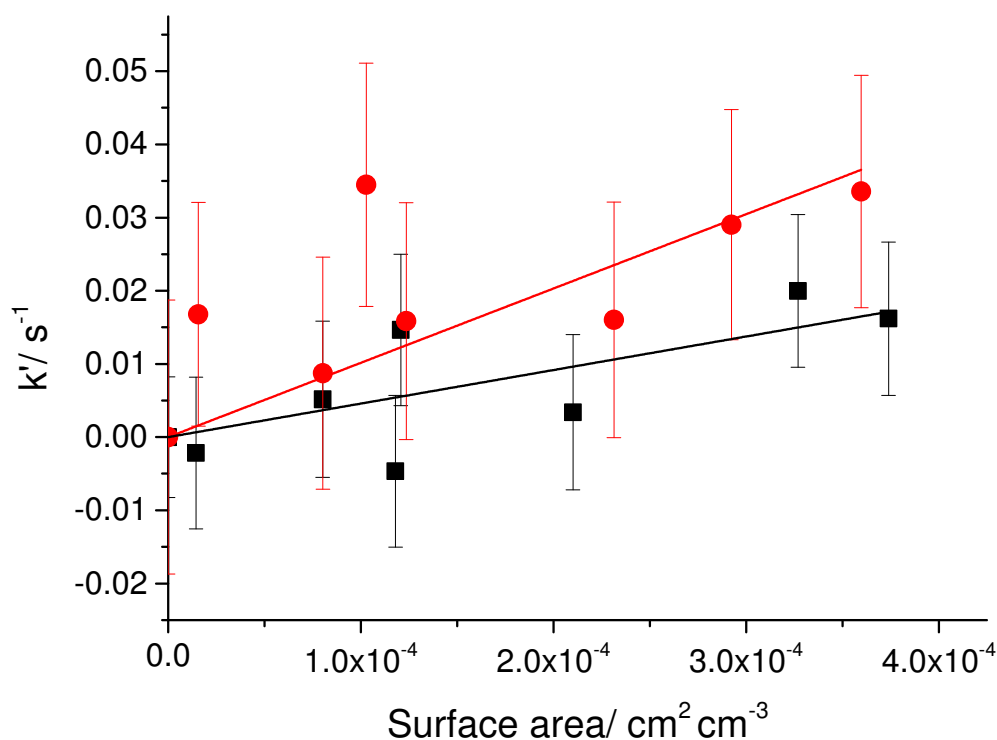


Figure 3.13: The pseudo-first order rate constant as a function of aerosol surface area for ammonium nitrate aerosols at 30% RH and 293 ± 2 K and at an initial HO_2 concentration of $1.1 \times 10^9 \text{ cm}^{-3}$ (red points) and $2.7 \times 10^9 \text{ cm}^{-3}$ (black points). The gradients of the lines were 102 ± 20 and $46 \pm 11 \text{ s}^{-1} \text{ cm}^{-2} \text{ cm}^3$ and HO_2 uptake coefficients of 0.009 ± 0.004 and 0.004 ± 0.002 were obtained. The error bars represent one standard deviation.

If the HO_2 entering the aerosol was causing it to become more viscous then the HO_2 concentration dependence would be consistent with this. However, it is unlikely that HO_2 causes any change in the viscosity of the aerosol. The HO_2 entering the aerosol could affect its pH, with higher HO_2 concentrations in the gas phase leading to more HO_2 entering the aerosol and therefore causing more acidic aerosols. A more acidic aerosol would cause the HO_2 uptake coefficient to be smaller as discussed in Section 3.6. However, the acidity hypothesis is not consistent with the time dependence. At longer injector distances (and longer times in the flow tube) the HO_2 concentration is smaller due to wall losses and the reaction of HO_2 in the aerosols. A smaller HO_2 concentration would lead to less acidic aerosols and therefore to higher HO_2 uptake coefficients. Therefore, if the HO_2 concentration

dependence was solely due to the pH of the aerosols the expectation would be that the uptake coefficient might increase over time (see Section 3.6).

It should also be noted that although the time dependence for aqueous aerosols could potentially be explained due to the second order nature of the HO₂ self-reaction, this is inconsistent with the observed HO₂ concentration dependence, as for second order reactions the rate of reaction should increase with increasing reactant concentrations. Another explanation that could explain the apparent HO₂ concentration dependence would be the conversion of H₂O₂ back to HO₂ via the Fenton reactions (Reactions 3.27 – 3.30) which could occur in the presence of trace metals. At higher mercury lamp currents more HO₂ comes out of the injector, but also higher H₂O₂ concentrations will also exit the injector (at 2.5 mA 40ppt H₂O₂ and at 20 mA 230 ppt), see Section 2.13 for the methodology that was used to determine H₂O₂ concentrations. Therefore, at higher lamp currents more H₂O₂ could be released into the flow tube and converted into HO₂, which would lead to a lower observed HO₂ uptake coefficient than if the H₂O₂ concentration had been lower. This will be investigated in greater detail using the KM-SUB model in Chapter 8.

3.12 Atmospheric Implications

In order to estimate the impact of aerosols containing inorganic salt ions on HO₂ concentrations in the troposphere the box model that was described in Section 2.14 was run. Cape Verde is primarily affected by marine aerosol, and therefore predominantly consists of sodium and chloride ions although metal species and organics would also be expected to be present in the aerosols. However, for simplicity the model was run assuming three different HO₂ uptake coefficients. Firstly, an uptake of 0.01, was used which was typical of the uptake coefficient measured in this work for aqueous aerosols containing no metals. Secondly, a HO₂ uptake coefficient of 0.5 was inputted into the model, which was a typical uptake coefficient for aqueous copper-doped aerosols and is representative of a mass accommodation value. Lastly, a HO₂ uptake coefficient of 1 was entered into the model, which is the largest possible uptake and provides an upper limit to the effect that the aerosols can have on the HO₂ concentrations. A typical aerosol surface to volume concentration of $1 \times$

$10^{-6} \text{ cm}^2 \text{ cm}^{-3}$ was also inputted into the model (Allan et al., 2009). The uptake coefficients of all other species in the model were set to zero.

A reduction of the HO_2 concentration at solar noon was observed from 1.88×10^8 molecule cm^{-3} to 1.87×10^8 molecule cm^{-3} , 1.50×10^8 molecule cm^{-3} and 1.25×10^8 molecule cm^{-3} for HO_2 uptake coefficients of 0.01, 0.5 and 1, respectively, as shown in Figure 3.14. This is equivalent to a 0.5 %, 20% and 33% reduction in the initial HO_2 concentration. Whalley et al. (2010) stated that in order to obtain a good agreement between the modelled and observed HO_2 concentrations during the RHaMBLe field campaign, an average reduction of ~23 % in the predicted concentrations was necessary. This indicates that aerosols containing no metals could not account for the discrepancy between predicted and observed concentrations. However, if the HO_2 uptake coefficient was approximately equal to the mass accommodation then the difference could be accounted for.

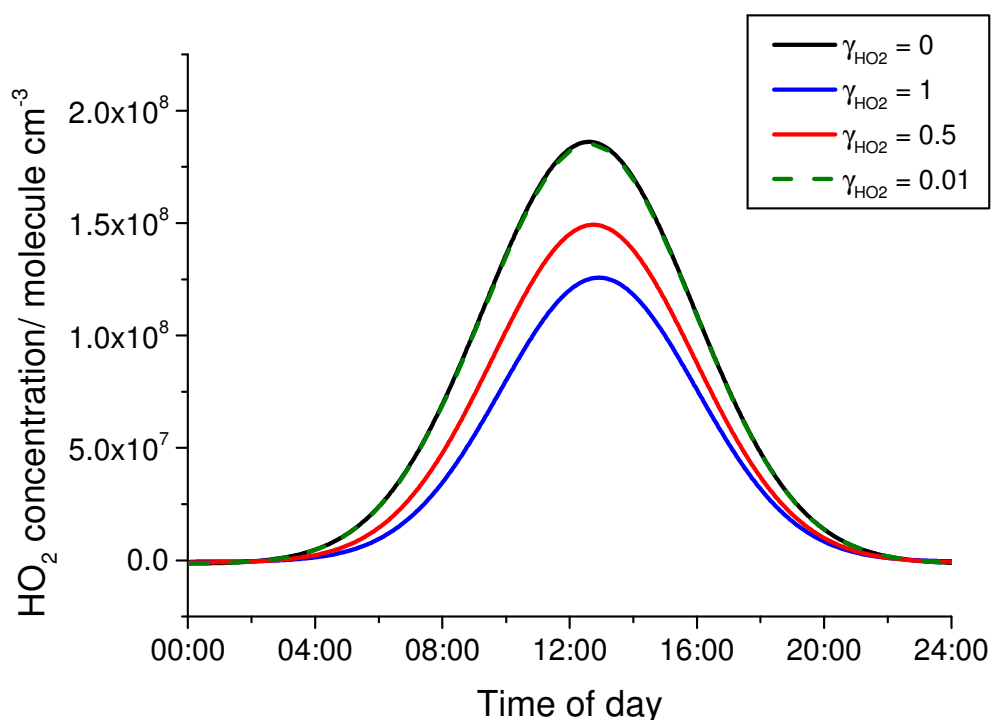


Figure 3.14: The effect of varying the HO_2 uptake coefficient upon the HO_2 gas phase concentrations under Cape Verde conditions (described in the text and in Section 2.14).

According to this work, and the work by Mozurkewich et al. (1987), a copper molality of $\sim 10^{-2}$ M or higher would be necessary in order to obtain a HO_2 uptake coefficient that was equal to its mass accommodation. Mao et al. (2013) stated that a concentration of 3.1 ng of copper ions in a cubic metre of air could provide a copper concentration of 2.9×10^{-3} M. By propagating this, in order to achieve a concentration of 10^{-2} M, necessary to achieve the mass accommodation value, the copper concentration in air would have to be $\sim 10 \text{ ng m}^{-3}$. Although it remains unclear as to the concentrations of transition metals in tropospheric aerosols, several studies have observed copper concentrations of $\sim 10 \text{ ng m}^{-3}$ in a variety of environments (e.g Bukowiecki et al. (2009); Formenti et al. (2003)). As the majority of aerosols in Cape Verde are marine aerosols, the concentration of transition metal ions in the aerosols would be very much dependent upon the metal concentrations in the seawater around Cape Verde. Although measurements of copper concentrations have not been reported during the RHaMBLe field campaign, subsequent measurements showed that the highest copper concentrations that were measured in Cape Verde were 0.81 ng m^{-3} and were in air masses originating from North Africa (Fomba et al., 2013). However, this concentration would be unlikely to affect the HO_2 uptake coefficient.

It should also be noted that although no pH dependence upon the HO_2 uptake coefficient was observed in this work, if known aqueous chemistry is controlling the uptake process then smaller uptake coefficients would be observed for more acidic aerosols. The uptake coefficient would also be dependent upon humidity, with higher uptake coefficients for deliquesced aerosols and for larger aerosols. Finally, the HO_2 uptake coefficient should be dependent upon the HO_2 concentration. If the HO_2 uptake is a second order process, as predicted by known aqueous chemistry, then the uptake coefficient should increase with increasing HO_2 concentration. However, in this work the opposite trend was observed and a time dependence was also observed. Until the HO_2 concentration dependence and time dependence are fully understood, it is difficult to relate these to implications for HO_2 concentrations in the troposphere. Therefore, in Chapter 8, the KM-SUB model will be used to try and fully understand the chemistry occurring in the flow tube in order to relate this to the chemistry occurring in the troposphere.

3.13 Summary

The HO₂ uptake coefficients were measured for different aqueous and solid salts that are commonly found in tropospheric aerosols. For solid salts the uptake coefficient was below the limit of detection ($\gamma < 0.004$) whereas for aqueous salts the uptake coefficient was measurable ($\gamma = 0.003 - 0.016$). The HO₂ uptake coefficients are larger for aqueous aerosols than for solid aerosols as reactions can occur within the bulk of the aerosol and are not limited to the surface of the aerosol. These HO₂ uptake coefficients were much smaller than had been measured in previous studies and only in agreement with the measurement made by Loukhovitskaya et al. (2009). However, for copper doped aerosols the measured HO₂ mass accommodation measured in this work ($\alpha = 0.5 \pm 0.3$) was in agreement with previous studies.

The HO₂ uptake coefficient dependence upon the copper concentration in the aerosols was also investigated and it was found that the uptake coefficient started to increase at a copper concentration of approximately 10^{-4} M and was fully limited by the mass accommodation at a copper concentration of 10^{-2} M. This was in agreement with the experimental work by Mozurkewich et al. (1987) but not with the modelling of the known aqueous chemistry that was done by Thornton et al. (2008). Doping the aerosols with iron (II or III) also produced a similar trend with higher HO₂ uptake coefficients measured at higher iron molarities. By running an atmospheric box model constrained to conditions encountered at Cape Verde, it was shown that in order to obtain agreement between predicted and measured HO₂ concentrations, the aerosols would need to contain transition metals and the uptake coefficient would have needed to be equal to the mass accommodation value.

The pH of the aerosols was also varied in this work. It was expected that the uptake into the aerosols would increase at higher pH due to the effective Henry's law as predicted by the Thornton et al. (2008) model. However, no change in the uptake coefficient was observed over a range of aerosol pH. The reason for this may be the HO₂ entering the aerosol and making it more acidic, although no dependence was observed with buffered aerosol either. The dependence upon the aerosol size was also investigated for ammonium nitrate by varying

the relative humidity. However, no change was observed over a range of 42.6 to 47.7 nm, which was consistent with the Thornton model.

Finally, time and HO₂ concentration dependences were observed in this work with larger uptake coefficients at shorter times and lower HO₂ concentrations. These dependences may help to explain the difference in magnitude for the uptake coefficients that were measured in this work compared to those measured by Taketani et al. (2008) who worked at shorter reaction times and lower HO₂ concentrations. Although, the reason for the time and HO₂ concentration is unknown there may be several different explanations. Aerosol saturation, a trace reactant being used up, the second order nature of the HO₂ self-reaction, a change in viscosity, a change in pH and a reaction of H₂O₂ reforming HO₂ have all been suggested as possible reasons for the time and/or the HO₂ concentration dependence. These explanations will be investigated in greater detail using the KM-SUB model in Chapter 8.

Chapter 4: Measurements of the HO₂ uptake coefficient onto organic aerosols at room temperature and atmospheric pressure

4.1 The importance of organic aerosols in the troposphere

Organic aerosols are ubiquitous throughout the troposphere with 20 – 90 % of the submicron particulate mass being attributable to organics (Murphy et al., 2006; Zhang et al., 2007). Organic aerosols can be classified by their formation mechanism as either primary or secondary. Primary organic aerosols are directly emitted into the atmosphere mainly by fossil fuel combustion and biomass burning. The composition of these aerosols can then be altered by chemical processing in the atmosphere. Secondary organic aerosols are formed by the oxidation of volatile organic compounds (VOCs) in the troposphere, and will be discussed in greater detail in Chapter 5.

There are many classes of organic species that have either been observed or are predicted to be present in tropospheric aerosols. These include water insoluble organics, for example, *n*-alkanes, *n*-alkanoic acids, diterpenoid acids, aromatic polycarboxylic acids and polycyclic aromatic hydrocarbons, ketones and quinones, and water soluble organics, for example, dicarboxylic acid, glyoxal, ketoacids, polyols, hydroxyamines, amino acids and nitrophenol (Rogge et al., 1993; Saxena and Hildemann, 1996).

Organic aerosols could affect the HO₂ uptake coefficient in several different ways. For example, if components of the organic aerosols were reactive towards HO₂ this would increase the uptake coefficient. Organics can also act as surfactants, form ligands with metal ions and increase the viscosity of the aerosols. All of these factors would be expected to lower the HO₂ uptake coefficient. In this work, the HO₂ uptake coefficient onto several different single component organic aerosols that are representative of tropospheric aerosol components were measured in order to compare these uptake coefficients to those measured for inorganic salt aerosols. The effect of increasing the viscosity of aerosols by using sucrose

that forms glasses at low relative humidity (Power et al., 2013) was also investigated as well as the effect of surfactants and ligands on the HO₂ uptake coefficient.

4.2 Measurements of the HO₂ uptake coefficient onto single component organic aerosols

Figure 4.1 shows the pseudo-first order rate coefficient as a function of aerosol surface area for some of the HO₂ uptake measurements on single component organic aerosols carried out in this study. The gradients of the graphs in Figure 4.1 were much larger for humic acid than for the other aerosols. Figure 4.2 and Table 4.1 summarise the HO₂ uptake coefficients that were measured in this work onto a variety of single component aqueous and effloresced organic aerosols (glutaric acid, glyoxal, malonic acid, stearic acid, oleic acid, squalene, two brands of humic acid and two different iminium salts (mono ethanol amine sulphate – H₂SO₄ (MEA-H₂SO₄) and mono methyl amine sulphate (MMS))). Table 4.1 also contains the HO₂ uptake coefficients measured by Taketani et al. (2010, 2013) onto single component organic aerosols. In this work, the phase of each type of aerosol was determined using the efflorescence and deliquescence points of a particular organic as shown in Table 2.1 in Section 2.6.2. Uptake coefficients were measured in this work from below the detection limit ($\gamma < 0.004$) to $\gamma = 0.008 \pm 0.004$ for all of the single component aerosols apart from humic acid. Humic acid displayed much larger uptake coefficients of $\gamma = 0.007 - 0.06$ over a relative humidity range of 32 – 76 % for the Acros organics humic acid and $\gamma = 0.043 - 0.09$ over a relative humidity range of 33 – 75 % for Leonardite humic acid. The relative humidity dependence will be discussed in Section 4.3. Acros organics humic acid, is obtained by mining and is the product of the decomposition of organic matter, especially plants, and can be found in soil, peat and soft coal. Leonardite humic acid is produced by the oxidation of lignite which is a coal and is mined from the Gascoyne mine in North Dakota (Pope et al., 2010). Due to the large uptake coefficients observed for the humic acid solutions, a large number of the atomiser solutions were analysed for metals using ICP-MS.

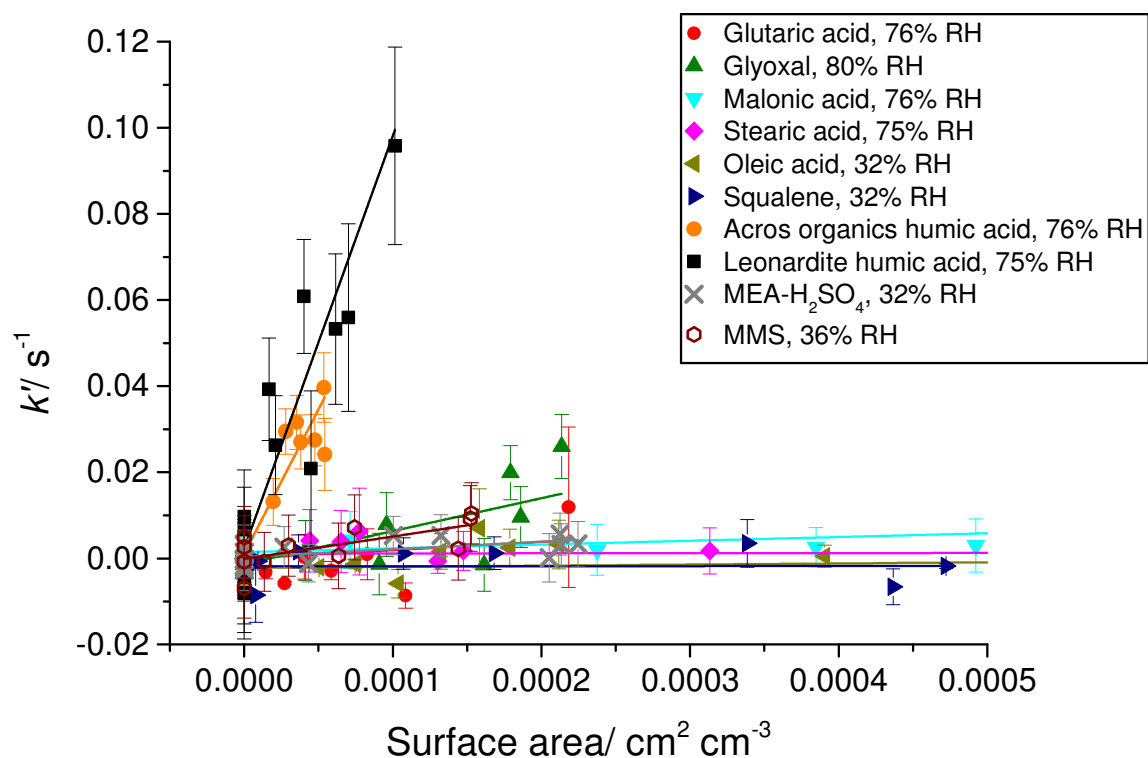


Figure 4.1: The pseudo first order rate coefficient for HO_2 loss as a function of aerosol surface area for different single component organic aerosols measured in this work. Atomiser solutions were prepared by dissolving 5 grams (or 1 gram for Leonardite humic acid) of the organic in 500 ml mQ water. The humic acid solutions were then filtered. Aerosols from organics that were insoluble in water (stearic acid, oleic acid and squalene) were formed by homogeneous nucleation. The initial HO_2 concentration was 1×10^9 molecule cm^{-3} and the experiments were performed at 293 ± 2 K. Error bars are 2 standard deviations (2σ).

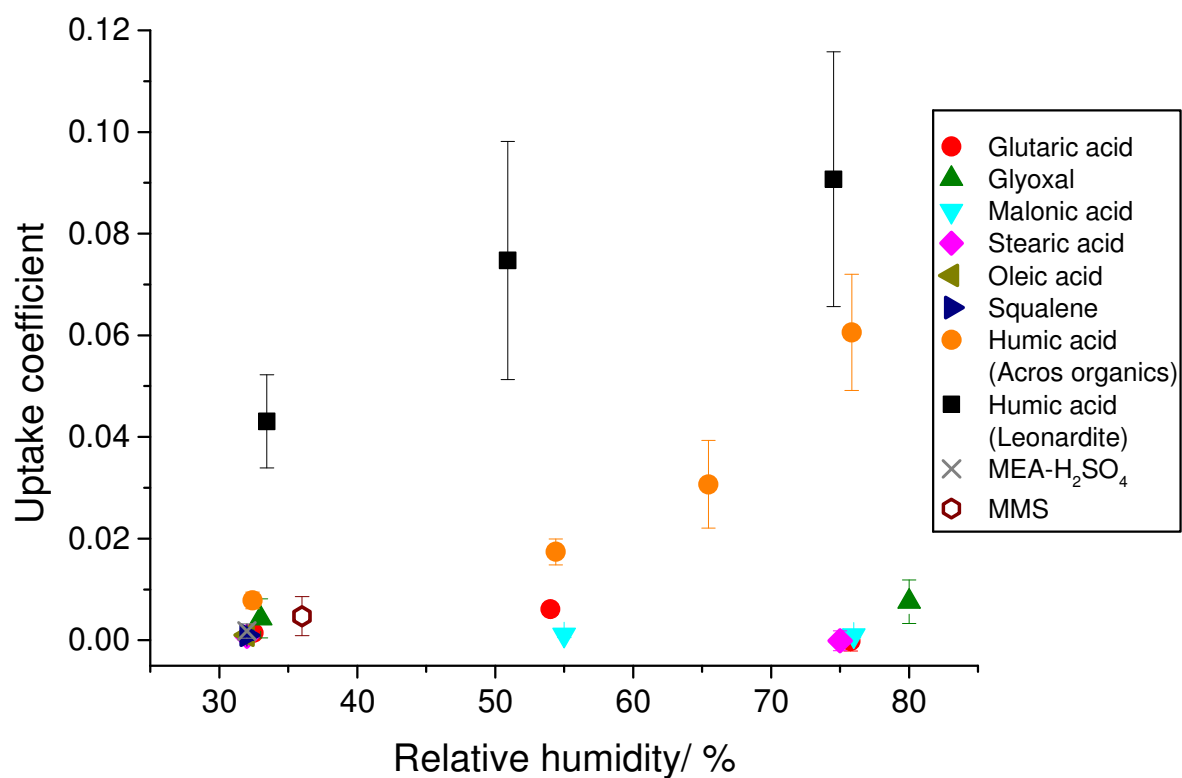


Figure 4.2: The HO₂ uptake coefficient as a function of humidity for different single component organic aerosols measured in this work. The initial HO₂ concentration was 1×10^9 molecule cm⁻³ and the experiments were performed at 293 ± 2 K. The error bars are 2σ .

Compound	RH/ %	Aqueous or Solid	Initial [HO ₂]/ molecule cm ⁻³	Uptake coefficient (γ)	Reference
Succinic acid	28	Solid	~10 ⁸	0.07 ± 0.02	Taketani <i>et al.</i> (2013)
	68	Aqueous	~10 ⁸	0.18 ± 0.07	Taketani <i>et al.</i> (2013)
Glutaric acid	28	Solid	~10 ⁸	0.07 ± 0.02	Taketani <i>et al.</i> (2013)
	68	Aqueous	~10 ⁸	0.15 ± 0.04	Taketani <i>et al.</i> (2013)
	32	Aqueous	1 × 10 ⁹	< 0.004	This work
	54	Aqueous	1 × 10 ⁹	0.006 ± 0.002	This work
	76	Aqueous	1 × 10 ⁹	< 0.004	This work
Adipic acid	28	Solid	~10 ⁸	0.02 ± 0.01	Taketani <i>et al.</i> (2013)
	68	Solid	~10 ⁸	0.06 ± 0.01	Taketani <i>et al.</i> (2013)
Pimelic acid	28	Solid	~10 ⁸	0.06 ± 0.03	Taketani <i>et al.</i> (2013)
	68	Aqueous	~10 ⁸	0.13 ± 0.04	Taketani <i>et al.</i> (2013)
Levoglucosan	20	Aqueous	~10 ⁸	< 0.01	Taketani <i>et al.</i> (2010)
	40	Aqueous	~10 ⁸	0.01 ± 0.01	Taketani <i>et al.</i> (2010)
	55	Aqueous	~10 ⁸	0.05 ± 0.01	Taketani <i>et al.</i> (2010)
	75	Aqueous	~10 ⁸	0.09 ± 0.02	Taketani <i>et al.</i> (2010)
	92	Aqueous	~10 ⁸	0.13 ± 0.03	Taketani <i>et al.</i> (2010)

Table continued on next page

Table continued from previous page

Compound	RH/ %	Aqueous or Solid	Initial [HO ₂]/ molecule cm ⁻³	Uptake coefficient (γ)	Reference
Glyoxal	33	Aqueous	1×10^9	0.003 ± 0.003	This work
	80	Aqueous	1×10^9	0.008 ± 0.004	This work
Malonic acid	55 - 76	Aqueous	1×10^9	< 0.004	This work
Stearic acid	32 - 75	Solid	1×10^9	< 0.004	This work
Oleic acid	32	Solid	1×10^9	< 0.004	This work
Squalene	32	Solid	1×10^9	< 0.004	This work
Humic acid (Acros organics)	32	Aqueous	1×10^9	0.007 ± 0.002	This work
	54	Aqueous	1×10^9	0.017 ± 0.003	This work
	65	Aqueous	1×10^9	0.031 ± 0.009	This work
	76	Aqueous	1×10^9	0.06 ± 0.01	This work
Humic acid (Leonardite)	33	Aqueous	1×10^9	0.043 ± 0.009	This work
	51	Aqueous	1×10^9	0.07 ± 0.02	This work
	75	Aqueous	1×10^9	0.09 ± 0.03	This work
MEA-H₂SO₄	32	Aqueous	1×10^9	< 0.004	This work
MMS	36	Aqueous	1×10^9	0.005 ± 0.004	This work

Table 4.1: The HO₂ uptake coefficient onto single component organic aerosols measured in this work and published in the literature at 293 ± 2 . The HO₂ uptake coefficients measured in this work for glutaric acid, stearic acid, oleic acid and squalene were obtained by Dr. Ingrid George.

The copper and iron concentrations in the atomiser solutions were measured using ICP-MS. However, in order to relate these concentrations to the concentration that would be expected in the aerosol the following equation was used which assumes that the aerosol volume for the organic aerosols is the same as for ammonium sulphate aerosols:

$$\text{Estimated Cu or Fe molarity} = \frac{[AS]_{aerosol, RH} [M]_{atomiser}}{[organic]_{atomiser}} \quad (\text{E4.1})$$

where $[organic]_{atomiser}$ is the molarity of the organic in the atomiser, $[AS]_{aerosol, RH}$ is the ammonium sulphate molarity in an aerosol at a given relative humidity based on the AIM model, and $[M]_{atomiser}$ is the metal molarity in the atomiser. Although, the growth of organic aerosols is not the same as for ammonium sulphate, the average radius of the size distributions, as measured using the SMPS, of glyoxal, glutaric acid and malonic acid were within 20 % of the ammonium sulphate aerosols under the same conditions. However, for the humic acids the comparison was harder to make as the exact amount of humic acid in the atomiser solution was unknown as some components of the humic acid did not dissolve. Although either one or five grams were added to 500 ml mQ water the sample was then filtered, removing some of the humic acid which means that only a lower limit of the copper and iron concentrations could be estimated.

Table 4.2 and Table 4.3 show the estimated iron (II and III) and copper (I and II) concentrations in the aerosols, respectively, based on the ICP-MS measurements on the atomiser solutions. Figures 2 and 3 in Section 3.5 showed that the uptake coefficient starts to increase when the copper (II) molarity is greater than $\sim 10^{-4}$ molar and when the iron (II or III) concentration in the aerosol is greater than 10^{-1} molar. Therefore, it seems likely that the higher HO_2 uptake coefficients that were measured for both types of humic acids was due to the elevated copper and iron concentrations whereas the copper and iron concentrations for the other organics were too low to affect the measured HO_2 uptake coefficient as shown in Table 4.2 and Table 4.3. As the humidity increased for the humic aerosols the copper and iron concentrations decreased due to the aerosol water content increasing (in accordance with AIM model). However, the HO_2 uptake coefficient increased with increasing humidity. Therefore, the uptake coefficient was not solely controlled by the metal ion concentrations and there must have been another process affecting the uptake. This will be explored in greater detail in Section 4.3.

Organic	Iron concentration in 500 ml mQ water/ ppb	Estimated iron (II and III) molarity in the aerosol/ M
Humic acid (Acros organics)	51000 ± 3000	> 1.1×10^{-1} (32 % RH) > 5.3×10^{-2} (76 % RH)
Humic acid (Leonardite)	600 ± 30	> 6.3×10^{-3} (33 % RH) > 3.2×10^{-3} (75 % RH)
Glyoxal	12 ± 2	~ 2.5×10^{-5} (33 % RH) ~ 1.1×10^{-5} (80 % RH)
Glutaric acid	1620 ± 70	~ 3.4×10^{-3} (32 % RH) ~ 1.7×10^{-3} (76 % RH)
Malonic acid	46 ± 3	~ 7.2×10^{-5} (55 % RH) ~ 4.8×10^{-5} (76 % RH)

Table 4.2: Iron (II and III) concentrations that were measured in the atomiser solutions using ICP-MS for different organics dissolved in mQ water. Atomiser solutions were made by dissolving 5.0 g of the organic into 500 ml mQ water with the exception of Leonardite humic acid where 1.0 g was dissolved into 500 ml mQ water. The humic acid solutions were also filtered before experiments were performed.

Organic	Copper concentration in 500 ml mQ water/ ppb	Estimated copper (I and II) molarity in the aerosol/ M
Humic acid (Acros organics)	380 ± 20	> 7.2×10^{-4} (32 % RH) > 3.5×10^{-4} (76 % RH)
Humic acid (Leonardite)	16 ± 1	> 1.5×10^{-4} (33 % RH) > 7.6×10^{-5} (75 % RH)
Glyoxal	5 ± 1	~ 9.4×10^{-6} (33 % RH) ~ 4.2×10^{-6} (80 % RH)
Glutaric acid	0.7 ± 0.1	~ 1.3×10^{-6} (32 % RH) ~ 6.5×10^{-7} (76 % RH)
Malonic acid	5 ± 1	~ 7.0×10^{-6} (55 % RH) ~ 4.7×10^{-6} (76 % RH)

Table 4.3: Copper (I and II) concentrations that were measured in the atomiser solutions using ICP-MS for different organics dissolved in mQ water. Atomiser solutions were made by dissolving 5.0 g of the organic into 500 ml mQ water with the exception of Leonardite humic acid where 1.0 g was dissolved into 500 ml mQ water. The humic acid solutions were also filtered before experiments were performed.

Taketani et al. (2013) also measured HO₂ uptake coefficients onto a variety of organic aerosols (succinic acid, glutaric acid, adipic acid, pimelic acid and levoglucosan). For solid organic aerosols the HO₂ uptake coefficients ranged from 0.02 to 0.07 whereas for aqueous organic aerosols the uptake coefficient ranged from less than 0.01 to 0.18. The uptake coefficients measured by Taketani et al. (2013) are significantly higher than the uptake coefficients measured in this work. In both studies the HO₂ uptake onto aqueous glutaric acid aerosols were determined. In this work, the uptake coefficient was measured from below the limit of detection ($\gamma < 0.004$) to 0.006 ± 0.002 , whereas Taketani et al. (2013) measured an uptake coefficient of $\gamma = 0.15 \pm 0.04$ for aqueous glutaric acid at a relative humidity of 68 %. Therefore, similarly to the salt aerosols, the HO₂ uptake coefficients measured by Taketani et al. (2013) were approximately two orders of magnitude different to those measured in this work.

Another interesting point is that the solid organics tended to have a smaller uptake coefficient than the aqueous organics. In this work the solid organic aerosols always had an uptake coefficient below the limit of detection ($\gamma < 0.004$) whereas aqueous organic aerosols had an uptake coefficient of between $\gamma < 0.004$ and 0.008 ± 0.004 . This is comparable to the behaviour of solid salts in Table 3.1 in Section 3.2 where the HO₂ uptake coefficient was always below the limit of detection and the aqueous salts in Table 3.2 in Section 3.3 where the HO₂ uptake coefficients were in the range of 10^{-2} to 10^{-3} . The uptake coefficients obtained by Taketani et al. (2013) for both solid organic and salt aerosols were 10^{-2} (with the exception of sodium chloride at 20 % RH which had an uptake coefficient of less than 0.01). Taketani et al. (2013) also measured higher uptake coefficients for both aqueous salt, and organic aerosols of 10^{-1} with the exception of levoglucosan, which varied from $\gamma < 0.01$ to $\gamma = 0.13 \pm 0.03$, and was strongly dependent on humidity. It was expected that the HO₂ uptake coefficient would be larger for aqueous aerosols than for solid aerosols as the HO₂ cannot enter the bulk of the aerosol to react, as discussed in greater detail in Section 3.3.

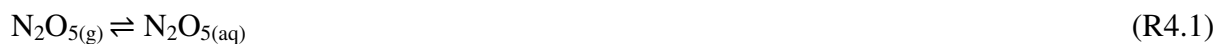
The uptake coefficients that were measured for organic aerosols were a similar magnitude to those measured for salt aerosols, although in this work, in the case of malonic acid and glutaric acid, the uptake coefficients appeared to be slightly smaller. The similarities in the uptake coefficients for salt aerosols and organic aerosols suggest that HO₂ is not reacting with

the organic components of the aerosols, but instead is limited by the HO₂ self-reaction as was the case for the inorganic salt aerosols.

The humidity dependence observed by Taketani et al. (2013) for HO₂ uptake onto levoglucosan aerosols can be explained in several ways. Levoglucosan was aqueous over the range of humidities that was explored. Taketani et al. (2013) suggested that the water concentration in the aerosol might be the cause of the increase in the uptake coefficient. The increase in the size of the aerosol could also cause the uptake coefficient (as discussed in Section 3.7). The viscosity of the aerosol, the Henry's law coefficient and the mass accommodation could change with changing humidity. Although levoglucosan was not studied in this work, a significant increase in HO₂ uptake coefficient with increasing humidity was observed with humic acid aerosols, and will be explored further in Section 4.3.

4.3 The uptake coefficient dependence upon humidity for humic acid aerosols

As discussed in Section 4.2, the HO₂ uptake coefficient onto humic acid aerosols has been observed to be strongly dependent on humidity. For comparison with this work, the N₂O₅ uptake for humic acid aerosols which has been studied previously by Badger et al. (2006b) and was also found to be dependent upon humidity will be discussed below. Badger et al. (2006b) reported an increase in uptake coefficient from 2×10^{-4} to 9×10^{-4} from 25 to 75% RH. The following mechanism was suggested by Thornton et al. (2003) for N₂O₅ in aqueous aerosols:

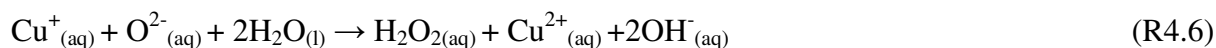
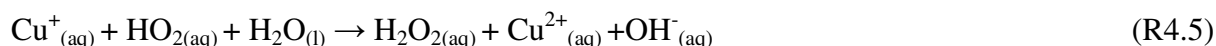


Thornton et al. (2003) suggested that at water activities of less than 0.4 (or relative humidities of less than 40%) the uptake would be limited by Reaction 4.3. The uptake coefficient was therefore expected to increase as the humidity increased up to approximately 40% RH due to the liquid water content of the aerosol increasing (Badger et al., 2006a). However, above 50%

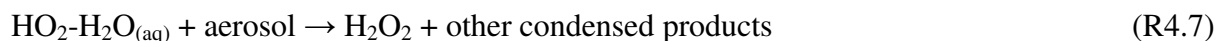
RH the uptake coefficient would be limited by either the formation of the H_2ONO_2^+ intermediate or by the mass accommodation.

Badger et al. (2006b) also reported a decrease in the N_2O_5 uptake coefficient for humic acid aerosols of one to two orders of magnitude compared to ammonium sulphate aerosols. Folkers et al. (2003) made measurements of N_2O_5 uptake using organic coatings and observed a relative humidity dependence. Humic acid is also known to have surfactant properties. Several studies have shown that humic acid will form micelles at the surface of aqueous solutions (Davies and Ghabbour, 1999; Wershaw, 1993). On one hand, as the relative humidity increases there is a greater chance of water at the surface of the aerosol. Therefore, the mass accommodation may increase. On the other hand, a coating at the surface of the aerosol may act as a diffusion barrier especially at low relative humidities when there is less water at the surface of the aerosol and would cause a decrease in the HO_2 uptake coefficient. Alternatively, humic acid may also decrease the Henry's law constant at the surface of the aerosol thereby leading to slower initial solvation into the aerosol and therefore to lower N_2O_5 uptake coefficients.

In this work, a large humidity dependence was observed for HO_2 uptake onto humic acid aerosols. Similarly to N_2O_5 , some of the HO_2 reactions that occur in the aerosol are dependent on the water concentration in the aerosol (Reactions 4.4 – 4.6) (Jacob, 2000):



Therefore, it seems likely that analogously to N_2O_5 , at low relative humidities (< 40 % RH) the uptake coefficient would be limited by low water concentrations within the aerosols. It has also been suggested that HO_2 might form a complex with water which could then take part in the heterogeneous reaction shown in Reaction 4.7 (Aloisio et al., 2000):



If this reaction was significantly faster than the uncomplexed HO₂ reactions, it may be expected that the rate of reaction would increase with humidity due to the increase in liquid water content of the aerosols. However, there is currently no evidence to suggest that reactions with HO₂-H₂O in the aerosol phase would be significantly faster than the analogous uncomplexed reactions.

The HO₂ uptake coefficient dependence upon relative humidity at humidities above 40 % could be due to a change in the mass accommodation, a change in the Henry's law constant or a combination of both of these changing as was suggested for N₂O₅ which was discussed above. If the humic acid was acting as a surfactant at the surface of the aerosol, this could cause a diffusion barrier. There could also be more water at the surface of the aerosol at higher humidities causing a higher mass accommodation. The humic acid could also affect the Henry's law which could vary with humidity causing less HO₂ to enter the aerosol bulk at low humidities and leading to a lower HO₂ uptake coefficient.

4.4 Measurements of the HO₂ uptake coefficient onto copper doped sucrose aerosols

Glassy aerosols can be defined as amorphous, non-crystalline solids that have a viscosity of greater than 10¹² Pa s (Debenedetti and Stillinger, 2001). These aerosols are ubiquitous throughout the atmosphere. Recently, Virtanen et al. (2010) were able to show that secondary organic aerosols (SOA) can be defined as glassy. Virtanen et al. (2010) observed a bounce factor as a function of aerosol radius as SOA impacted onto a smooth plate. If the aerosols were liquid they would impact, and would not bounce whereas solid or glassy aerosols would bounce upon impact. The bounce factor for SOA formed from VOCs emitted from pine seedlings was similar to that of amorphous polystyrene, suggesting that the SOA was a glassy aerosol. High aerosol viscosities can affect heterogeneous chemistry due to slow diffusion of the reacting species into the bulk of the aerosol. Due to the prevalence of glassy aerosols in the troposphere, measurements of the HO₂ uptake coefficient onto a glassy aerosol were made over a range of humidities in this work and will be discussed below.

The viscosity of sucrose and the diffusion of water into sucrose have been fairly well studied (He et al., 2006; Power et al., 2013; Price et al., 2013; Zobrist et al., 2011). Power et al. (2013) measured the viscosity of sucrose by coalescing two particles using optical tweezers and measuring the time that it took for the resulting particle to relax to a sphere. The viscosity was parameterised as varying from $\sim 10^{12}$ to $\sim 10^0$ Pa s from 20 to 80 % RH. He et al. (2006) parameterised the diffusion coefficient of water into a sucrose solution using the free volume model. The diffusion coefficient was parameterised as varying from $\sim 10^{-16}$ to $\sim 10^{-6}$ cm² s⁻¹ between 20 and 80 % RH. Zobrist et al. (2011) measured the adsorption and desorption of water into a suspended aqueous sucrose aerosol as the humidity was changed. Optical techniques were utilised to measure the change in radius of the aerosol from which a diffusion coefficient of water could be determined. The diffusion coefficients were determined as varying from $\sim 10^{-12}$ to $\sim 10^{-7}$ cm² s⁻¹ between 10 and 80 % RH. Price et al. (2013) measured the diffusion coefficient of water into sucrose by measuring the D₂O that had diffused into a water droplet over time at different relative humidities using Raman spectroscopy. The diffusion coefficient was parameterised and increased from $\sim 10^{-15}$ to 10^{-7} cm² s⁻¹ between 10 and 90 % RH.

The parameterisations of the diffusion coefficient of water into sucrose are shown in Figure 4.3. The parameterisations agree quite well above 50 % RH but start to deviate below this humidity. For example, at 20 % RH the parameterised diffusion coefficient varies by five orders of magnitude from $\sim 10^{-16}$ to $\sim 10^{-11}$ cm² s⁻¹. The measured HO₂ uptake coefficient in this work is also shown in Figure 4.3 and increased from 0.012 ± 0.007 at 17 % RH to 0.20 ± 0.06 at 71 % RH. Although, the diffusion coefficient of water into the copper doped sucrose is unlikely to be the same as the diffusion coefficient of HO₂, there are currently no measurements of the HO₂ diffusion coefficients into sucrose aerosols. Therefore, due to the similar structures of HO₂ and H₂O the diffusion coefficient of water into sucrose solutions is the best estimate that there is of how the diffusion coefficients of HO₂ will vary over a range of humidities. These diffusion coefficients will be inputted into the KM-SUB model in Chapter 8 to see whether changing diffusion coefficients can explain the changing HO₂ uptake coefficients. However, it should also be noted that the viscosity of aerosols at low relative humidities in this work is likely to be lower than predicted by the parameterisations due to the dehydration of sucrose being slow and the aerosols only having ~ 10 seconds in the conditioning flow tube in which to equilibrate before entering the reaction flow tube (Bones

et al., 2012). For example, Bones et al. (2012) estimated that for 100 nm diameter sucrose aerosols the equilibration time was more than 10 seconds when the viscosity increased above $\sim 10^5$ Pa s, which would occur at ~ 43 % RH (Power et al., 2013).

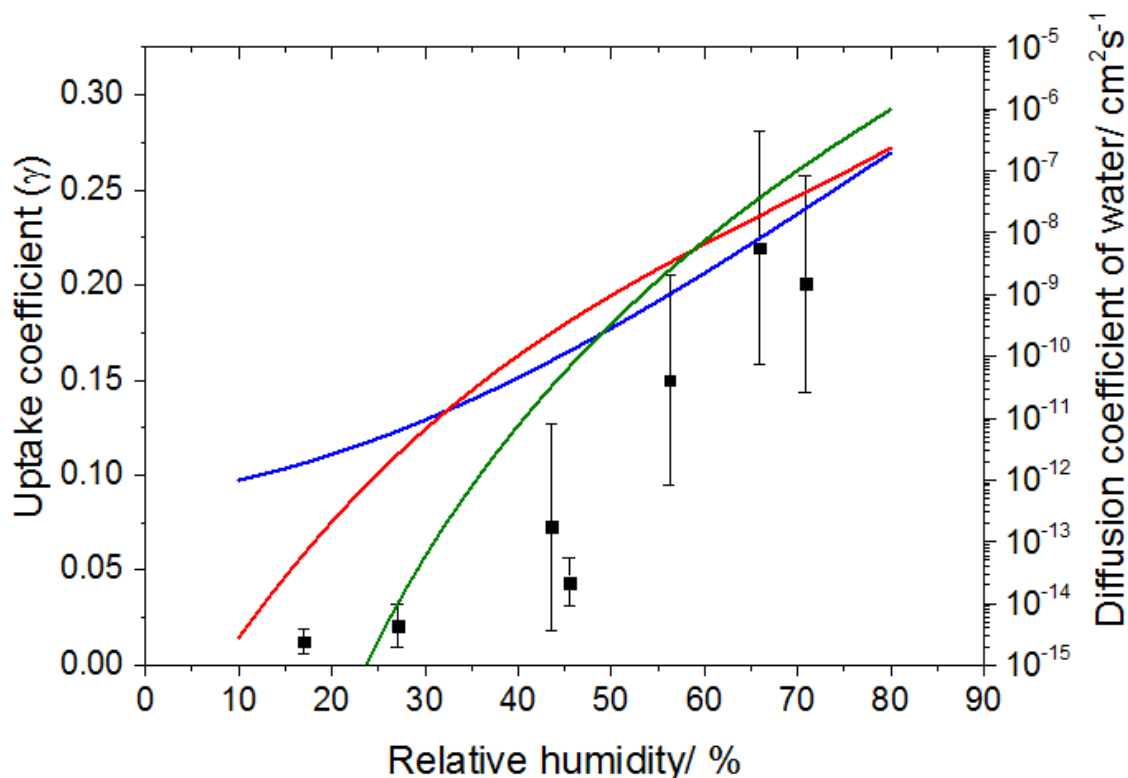


Figure 4.3: The HO_2 uptake coefficient as a function of relative humidity for aerosols containing a 20 to 1 sucrose to copper sulphate molar ratio at 293 ± 2 K. The error bars are 2σ . The blue, red and green lines represent the parameterisation of the diffusion coefficient of water into sucrose solutions given by Zobrist et al. (2011), Price et al. (2013) and He et al. (2006) respectively.

It is likely that the HO_2 uptake coefficient measurements for copper doped sucrose increase due to the decreasing viscosity with increasing relative humidity. At high relative humidities the uptake coefficient is only limited by mass accommodation due to the aerosols containing high copper concentrations (~ 0.3 M) meaning that the HO_2 has a lifetime of less than one nanosecond once it enters the aerosol bulk. However, at the lower relative humidities the aerosols are much more viscous and the HO_2 uptake coefficient will be limited by diffusion into the bulk of the aerosol. If the HO_2 radicals cannot enter the aerosol bulk or only enter it on a slow timescale, then there is much less HO_2 in the aerosols for the copper to catalytically convert into hydrogen peroxide and therefore the uptake coefficient would be lower. The KM-SUB model will be used to test the hypothesis that the change in the uptake coefficient is

due to a change in the rate of diffusion of HO₂ into the bulk of the aerosol. The results from the model will be discussed in Section 8.9.

4.5 Measurements of the HO₂ uptake coefficient onto copper doped ammonium sulphate aerosols containing EDTA

Several publications have suggested that organic components in aerosols may act as ligands towards any metal species in the aerosols (Okochi and Brimblecombe, 2002; Spokes et al., 1996). If this were the case the HO₂ uptake coefficient would decrease compared to the expected uptake for aerosols containing transition metals as the metal ions would no longer be available to catalyse the HO₂ into hydrogen peroxide or water. However, there have been no studies to ascertain whether the HO₂ uptake coefficient decreases for metal containing aerosols if the metals are bound to organic ligands.

Ethylenediaminetetraacetic acid (EDTA) is an extremely strongly binding hexadentate ligand with a stability constant ($\log K_1$) of 18.8 towards copper (Flaschka, 1959) (see Figure 4.4) and each EDTA molecule will bind with one copper ion. Therefore, it was ideal to test the hypothesis that ligands binding to copper may affect the measured HO₂ uptake coefficient by making the copper unavailable to catalyse HO₂ to hydrogen peroxide. In this set of experiments a 20 to 1 molar ratio of ammonium sulphate to copper sulphate was used. The aerosols were then also doped with different molar ratios of EDTA and the HO₂ uptake coefficient was measured. Figure 4.5 shows that the uptake coefficient started to reduce from the mass accommodation value of 0.21 ± 0.04 when the molar ratio of EDTA to copper was greater than 0.5. At a molar ratio of 1, the uptake coefficient was 0.009 ± 0.009 and at a molar ratio of 1.2 the uptake coefficient was 0.005 ± 0.005 . This behaviour is expected as the EDTA binds strongly to the copper making it unavailable for catalysis. A one to one ratio would be required for all of the copper to be strongly bound at which stage the uptake coefficient should be controlled by the HO₂ self-reaction. The uptake coefficient at the one to one ratio is similar that measured for aqueous salts in Section 3.3.

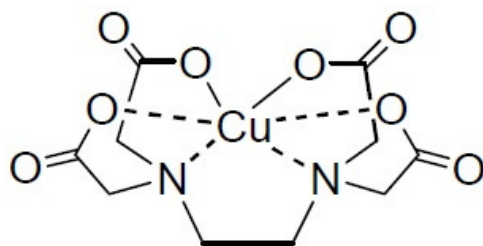


Figure 4.4: The Cu : EDTA complex.

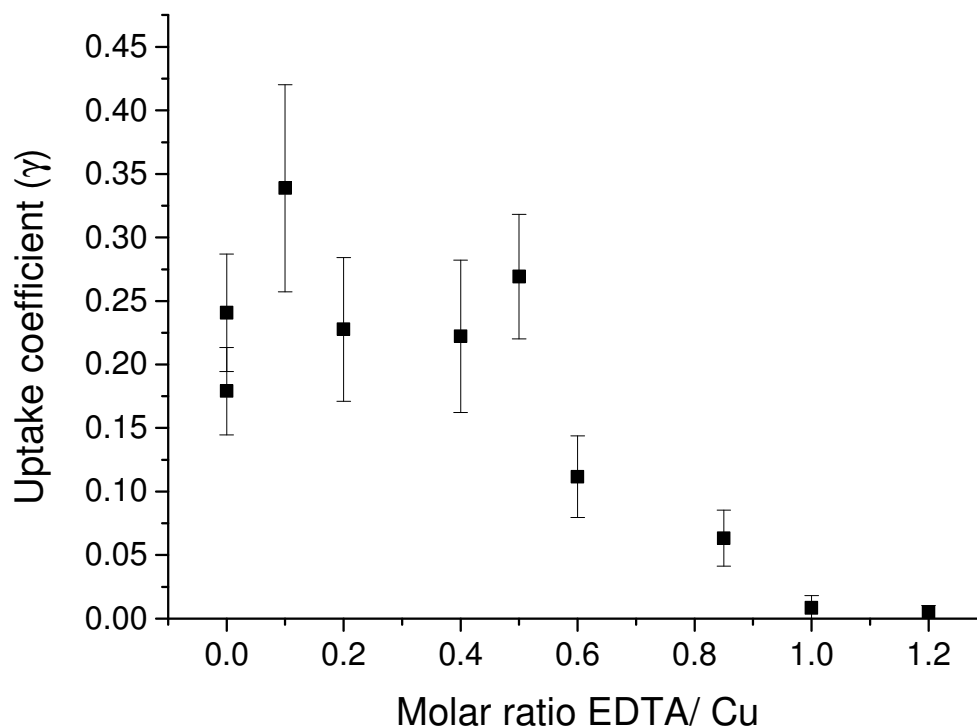


Figure 4.5: The HO_2 uptake coefficient for aerosols containing a 20 to 1 ammonium sulphate to copper molar ratio as a function of the molar ratio of EDTA to copper in the aerosols at a humidity of $72 \pm 4\%$ and at $293 \pm 2\text{ K}$. The error bars represent two standard deviations.

However, it remained unclear as to whether the EDTA binding to the copper ions was the reason for the decrease in the uptake coefficient or whether other factors might be playing a role. Therefore, the estimated unbound copper was calculated by assuming that each EDTA molecule would bind to one copper ion (see Figure 4.4). In Section 3.5 it was shown that the

HO₂ uptake coefficient dependence upon copper (II) could be fitted quite well with the following:

$$\frac{1}{\gamma} = \frac{1}{\alpha} + \frac{1}{197[Cu(II)]} \quad (E4.2)$$

However, as shown in Figure 4.6, when Equation 4.2 was plotted against the estimated unbound copper concentration it was found that it did not fit the data very well (Figure 4.6), suggesting that the EDTA binding to the copper and making it unavailable as a catalyst for destruction of HO₂ is not the only reason for a decrease in the uptake coefficient. Therefore, Equation 4.2 was modified to:

$$\frac{1}{\gamma} = \frac{1}{\alpha} + \frac{1}{197[Cu(II)]} + \frac{1}{A[Cu(II)]} \quad (E4.3)$$

where A is a constant reducing term which may be due to either an increase in viscosity with increasing EDTA or to the EDTA exhibiting surfactant properties. Therefore, although the hypothesis of ligands binding to copper and reducing the uptake coefficient cannot be proven, the EDTA experiments have provided another example of a reduction in the uptake coefficient due to an organic being present in the aerosol.

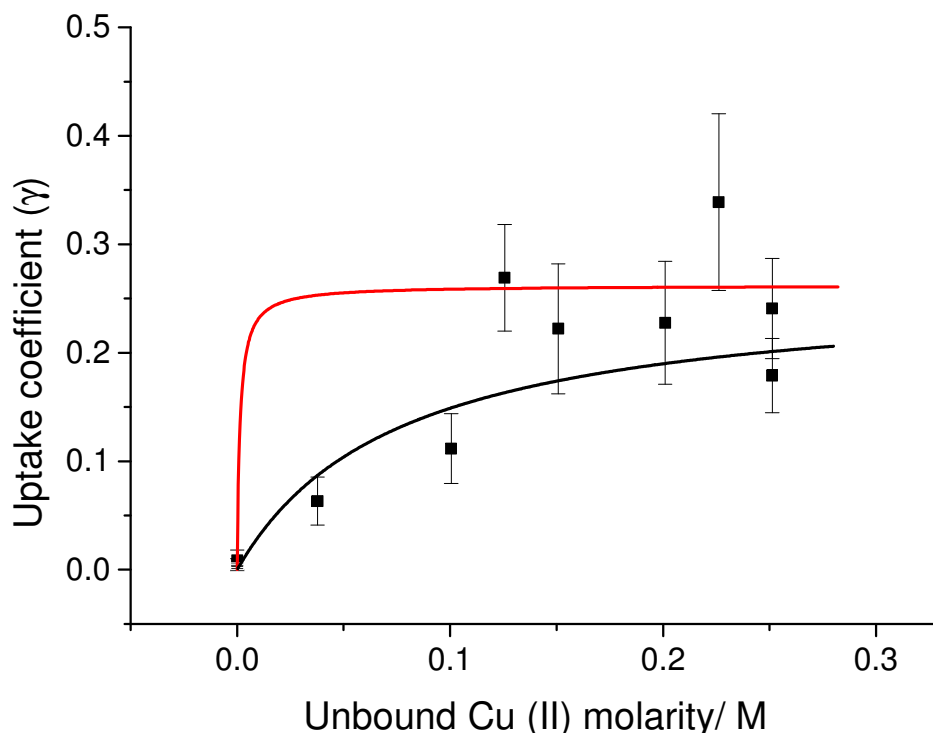


Figure 4.6: The HO_2 uptake coefficient as a function of copper molarity for aerosols containing a 20 to 1 ammonium sulphate to copper molar ratio and different concentrations of EDTA. An assumption was made that the EDTA would bind to copper in a 1 to 1 ratio, making it unavailable in the catalytic destruction of HO_2 . The red line represents the expected change in uptake coefficient controlled only due to changing copper concentrations as given by Equation 4.2 and the black line is the best fit of equation 4.3 to the data, which assumes that another process is also controlling the change in the HO_2 uptake coefficient.

4.6 Measurements of the HO_2 uptake coefficient onto copper doped ammonium sulphate aerosols also containing different atmospherically relevant organic compounds

In Sections 4.3 - 4.5 it was shown that the HO_2 uptake coefficient may reduce under some conditions if organics are present in the aerosol. However, although humic acid and sucrose are atmospherically relevant, EDTA has not been observed in tropospheric aerosols. Therefore, a range of other organic components that are found in the tropospheric aerosols were tested to determine their effects on the uptake coefficient. The organics that were chosen (malonic acid, citric acid, 1,2 diaminoethane, tartronic acid and oxalic acid) were chosen because of their likelihood to bind with metals in the aerosol based upon their Henry's

law constant and their binding constant with copper (II) (Okochi and Brimblecombe, 2002). All experiments were performed at an atmospherically relevant humidity of 60 % RH and with copper doped ammonium sulphate aerosols. Figure 4.7 shows the uptake coefficients that were measured for twenty to one ammonium sulphate to copper sulphate molar ratios with different molar ratios of organics at 60 % RH. The HO₂ uptake coefficient values are summarised in Table 4.4. The HO₂ uptake coefficient measured in this work decreased slightly when oxalic acid was added in a two to one molar ratio with copper (II) sulfate and significantly when the ratio was ten to one. No observable decrease was measured when malonic acid, citric acid, 1,2 diaminoethane or tartronic acid was added to the aerosol. It should be noted that Okochi and Brimblecombe (2002) calculated the concentration of a ligand that would be needed for 50 % complexation of copper in aerosols based on binding constants and the Henry's law constants of the organic ligand. The concentration for oxalic acid was given as 1.9 ppt whereas the concentration for tartronic acid was 2.3×10^{-3} ppt. However, although these values are extremely similar a decrease in the HO₂ uptake coefficient was not observed upon the addition of tartronic acid but was observed when oxalic acid was added to the aerosols suggesting that the reason for the decrease in the HO₂ uptake coefficient is not due to a complex forming and making the copper unavailable for HO₂ catalytic destruction. However, oxalic acid and its effect on the properties of an aerosol has been studied and will be discussed below.

A recent study showed that the addition of oxalic acid to aerosols containing inorganics (e.g CaCl₂, MgCl₂ and ZnCl₂) could have a large effect on both the volatility of the oxalic acid and the hygroscopicity of the aerosol (Drozd et al., 2013). Drozd et al. (2013) measured the effect of oxalic acid on the hygroscopicity of aerosols by exposing aerosols at low relative humidity to oxalic acid vapour and then increasing the relative humidity to 10 % RH above the deliquescence point of the aerosol. The size of the aerosols was then measured using an SMPS and provided information about the amount of oxalic acid that had been absorbed. Cloud condensation nuclei (CCN) activity was then measured using a CCN Counter from which a hygroscopicity could be calculated. Drozd et al. (2013) measured the volatility of oxalate in aerosols using a Temperature Programmed Desorption Aerosol-Chemical Ionization Mass Spectrometer. The oxalic acid in the gas phase was reacted with I⁻ ions and the clusters that formed were detected by the mass spectrometer as a function of temperature.

By applying the Clausius-Clapeyron equation the enthalpy of vaporisation of the oxalate in the aerosol could be determined.

Drozd et al. (2013) showed that the formation of metal-oxalate complexes caused a large decrease in the measured hygroscopicity compared to the predicted hygroscopicity. This could either be due to a large increase in the viscosity of the aerosol or to the formation of insoluble metal-oxalate complexes forming a coating at the surface of the aerosol. The volatility of the oxalate bound to metals in the aerosols was also measured to be much lower than pure oxalic acid aerosols.

The large decrease that was observed for the 10:1 oxalic acid: copper sulphate molar ratio in this work could be due to a number of factors. As discussed, the hygroscopicity of the aerosol decreases with the formation of metal-oxalate complexes. Therefore, the viscosity may have increased so that the uptake is limited by HO₂ diffusion into the bulk of the aerosol. Drozd et al. (2013) also claimed that the metal oxalate complex could precipitate out of the aerosol. Although no precipitate was observed in the atomiser solutions, it may be possible that precipitation occurs in the much more concentrated aerosols. This would make the copper unavailable for the catalytic destruction of HO₂. Finally, if the metal oxalate complex was forming a coating, this could also affect the uptake coefficient by forming a diffusion barrier into the bulk of the aerosol.

However, Figure 4.7 and Table 4.4 show that the HO₂ uptake coefficients do not change significantly and are within error for a two to one or ten to one organic to copper (II) sulphate molar ratio when the organic component is malonic acid, citric acid, 1,2 diaminoethane or tartronic acid. This suggests that these organics are not as efficient in either binding to the copper in the aerosol causing it to precipitate out, affecting the viscosity or changing the HO₂ diffusion into the aerosol by forming a coating at the surface. However, it remains unclear as to the reason for the large decrease observed for oxalic acid, but not observed for the other organics and further investigation is needed.

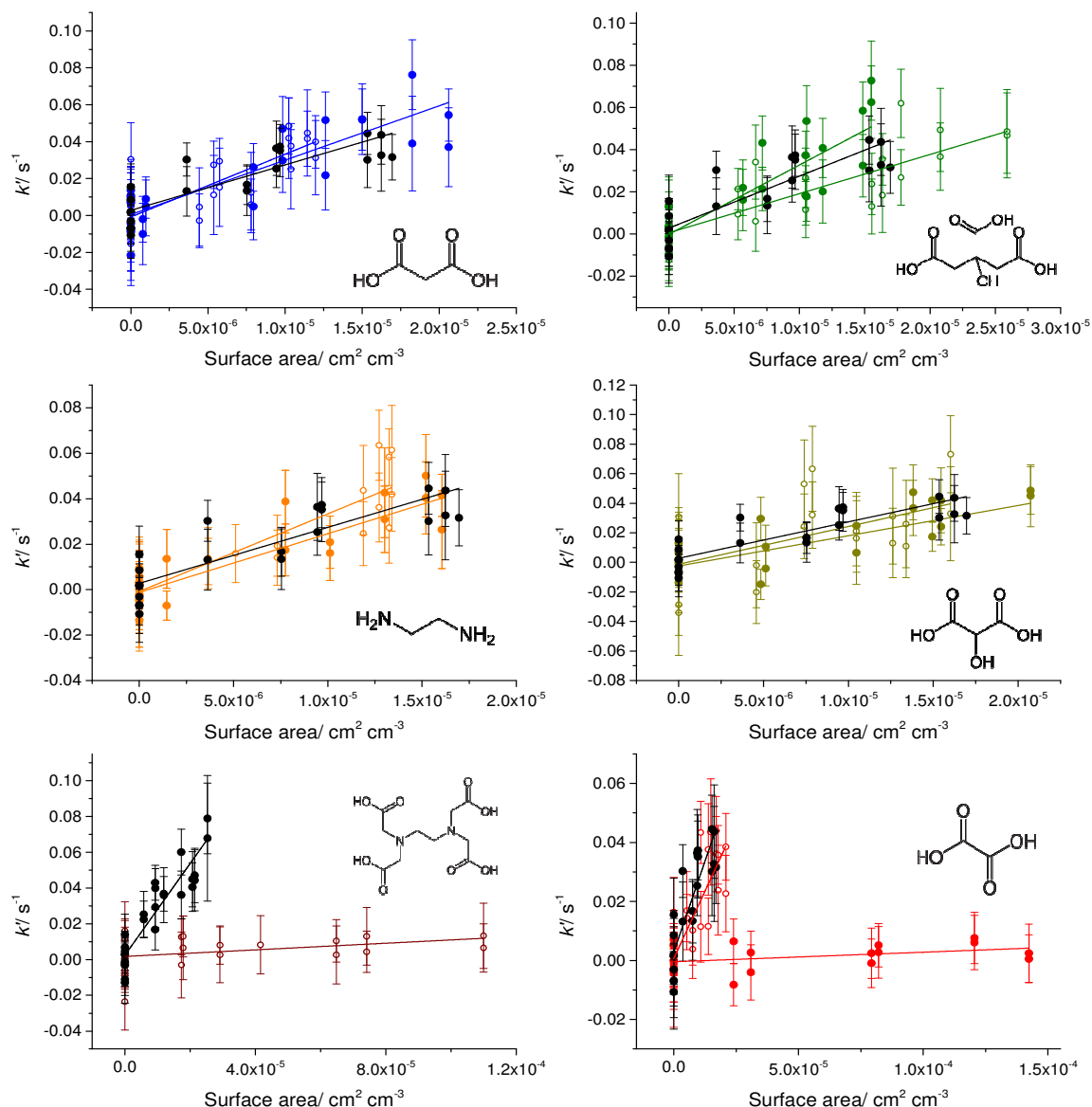


Figure 4.7: The pseudo first order rate coefficients as a function of aerosol surface area for copper doped ammonium sulfate aerosols (black) and with malonic acid (blue), citric acid (green), 1,2 diaminoethane (orange), tartronic acid (dark yellow), EDTA (maroon) and oxalic acid (red) added. A 20 to 1 molar ratio of ammonium sulphate to copper sulphate was used. The open symbols represent a 2 to 1 molar ratio of the organic to the copper, with the exception of EDTA which is in a 1 to 1 ratio. The closed symbols represent a 10 to 1 molar ratio of the organic to the copper. The two points for a given surface area represent repeat experiments. All experiments were performed at 60 ± 3 % RH and at 293 ± 2 K. The error bars represent one standard deviation.

Organic	Uptake coefficient for a given organic : copper sulphate molar ratio	
	2:1	10:1
Malonic acid	0.32 ± 0.09	0.28 ± 0.06
Citric acid	0.17 ± 0.05	0.31 ± 0.08
1,2 diaminoethane	0.32 ± 0.07	0.24 ± 0.05
Tartronic acid	0.24 ± 0.15	0.19 ± 0.07
Oxalic acid	0.17 ± 0.05	0.003 ± 0.004

Table 4.4: The uptake coefficients that were measured for copper (II) sulphate doped ammonium aerosols containing either a 2 to 1 or 10 to 1 organic to copper molar ratio. All experiments were performed at 60 ± 3 % RH and at 293 ± 2 K. The error bars represent one standard deviation. The mass accommodation value obtained when no organics were present in the aerosols was 0.23 ± 0.07 .

4.7 Atmospheric implications

The impact of organic aerosols on HO₂ concentrations in the troposphere is likely to be small. In Section 3.12 it was stated that the percentage decrease in HO₂ concentrations due to aqueous aerosols containing no metals would be approximately 0.5 % using a box model initiated for Cape Verde conditions. The decrease was calculated using a HO₂ uptake coefficient of 0.01. The HO₂ uptake coefficients for single component organic aerosols were similar to the aqueous and solid salts and would therefore have a similar impact on tropospheric HO₂ concentrations. The measured uptake coefficients for single component organic aerosols that did not contain copper or iron ions were all less than 0.01 and therefore would be expected to have an impact of less than 0.5%. However, in urban areas the aerosol loadings would be a lot higher than in the marine boundary layer (and are likely to contain more organic species) and therefore the impact would be expected to be much greater (Finlayson-Pitts and Pitts, 2000).

The HO₂ uptake measurements onto copper doped sucrose aerosols were very dependent upon the relative humidity and the viscosity of the aerosols. Glassy aerosols are ubiquitous throughout the atmosphere and recent measurements on the bouncing of secondary organic aerosols have shown that these are likely to be very viscous or glassy. For example,

Abramson et al. (2013) have estimated the viscosity of α -pinene derived aerosols to be $\sim 10^8$ Pa s. The uptake coefficients onto copper doped sucrose aerosols suggested that at low aerosol viscosities the HO₂ uptake coefficient would be small. Therefore, it is likely that in regions with glassy aerosols there will be very little impact upon the HO₂ uptake coefficient even if the aerosols contain elevated metal concentrations.

Dicarboxylic acids contribute approximately 15% of the total marine organic aerosol with oxalic acid contributing more than 50% of the total dicarboxylic acids (Fu et al., 2013; Myriokefalitakis et al., 2011; Neusüss et al., 2000). During the RHaMBLe field campaign oxalate was measured by collecting aerosols using impactors and filters. The total oxalate was measured as 78 – 151 ng m⁻³ (Mueller et al., 2010). However, the copper concentration in the aerosols is not stated. The impact of the measured oxalate during the RHaMBLe field campaign is unclear. However, in this work a 10 to 1 oxalic acid to copper molar ratio decreased the uptake coefficient by approximately three orders of magnitude. Therefore, if copper was the only metal ion that could bind with oxalate a concentration in Cape Verde of 5.6 – 10.9 ng m⁻³ or less would be unable to catalytically destroy HO₂ either due to the precipitation of copper-oxalate complexes or due to an increase in aerosol viscosity. However, in Cape Verde there were also other metals such as iron and magnesium that could also potentially bind with oxalate. Therefore, further laboratory studies with different salt, metal, pH and oxalic acid ratios would be required in order to definitively know the effect of oxalate in aerosols and to relate this to atmospheric aerosols.

Humic acid is also a major component of aerosols. Humic like substances have been measured in several field campaigns in a variety of aerosol types including marine, dust from soil and aerosols from biomass burning (Baduel et al., 2010; Cavalli et al., 2004; Decesari et al., 2000; Havers et al., 1998; Mayol-Bracero et al., 2002). These humic substances may decrease the HO₂ uptake coefficient by either changing the liquid water content of the aerosols, by forming a surfactant layer which would change the mass accommodation or by affecting the Henry's law constant of the HO₂ into the aerosol.

4.8 Summary

The HO₂ uptake coefficients onto several different single component organic aerosols were measured. The HO₂ uptake coefficients were measured to be $\gamma < 0.004$ for solid aerosols and $\gamma < 0.004$ to $\gamma = 0.006 \pm 0.002$ for aqueous organic aerosols. These values are of a similar order of magnitude to the uptake coefficients that were measured in this work for inorganic salt aerosols. However, the HO₂ uptake coefficients that were measured for single component organic aerosols by Taketani et al. (2010, 2013) were up to two orders of magnitude larger than in this work. Possible reasons for this difference could be due to the different experimental conditions used in this work compared to in the work by Taketani et al (2010, 2013), such as reaction time and initial HO₂ concentration which will be explored further in Chapter 8.

The humic acid aerosols had much larger HO₂ uptake coefficients than the other organic aerosols that were tested. However, after ICP-MS analysis the copper (I and II) and iron (II and III) concentrations in the atomiser solutions were found to be 16 - 380 ppb and 600 - 51000 ppb for copper and iron respectively. A calculation showed that this would be expected to lead to copper (I and II) and iron (II and III) concentrations in the aerosols that could increase the HO₂ uptake coefficient due to the catalytic destruction of HO₂. The copper (I and II) concentration in the aerosols decreases with increasing humidity and it was therefore expected that the uptake coefficient would decrease. However, the HO₂ uptake coefficient onto humic acid aerosols was measured to be strongly dependent upon humidity with higher uptake coefficients at higher humidities. Several possible reasons were suggested for the increase in the HO₂ uptake coefficient with increasing humidity. First, it was suggested that at low relative humidities, the uptake coefficient might be limited by the low water concentrations in the aerosols as some of the reactions involve water. Secondly, it was suggested that at higher humidities there would be more HO₂-H₂O complex formed due to an increase in the liquid water content of the aerosol. If the reaction of this complex with itself was faster than the equivalent uncomplexed reactions then an increase in the uptake coefficient would be observed at higher humidities. Thirdly, it was suggested that humic acid can act as a surfactant causing a diffusion barrier and decreasing the mass accommodation.

At higher humidities there would be more water at the surface and therefore the mass accommodation would increase. Finally, the humic acid could have an effect on the Henry's law constant with a smaller Henry's law constant at lower humidities.

The HO₂ uptake coefficient was measured onto copper doped sucrose over a relative humidity range of 17 % to 71 %. The HO₂ uptake coefficient increased from 0.012 ± 0.007 at 17 % RH to 0.20 ± 0.06 at 71 % RH. The increase in the uptake coefficient was attributed to a change in the viscosity of the copper (II) sulphate doped sucrose aerosols and therefore a change in the diffusion of the HO₂ into the aerosol. If the diffusion into the aerosol is slower, there will be less HO₂ in the bulk of the aerosol that can be catalytically destroyed by copper and therefore, the uptake coefficient will be lower. The effect of diffusion will be investigated in greater detail using the KM-SUB model in Chapter 8.

The HO₂ uptake coefficient onto copper (II) doped ammonium sulphate aerosols containing different amounts of EDTA was also investigated. The uptake coefficient was measured as decreasing from a mass accommodation value of 0.21 ± 0.04 when no EDTA was present to a value of 0.009 ± 0.009 when a one to one molar ratio of EDTA and copper was present in the aerosols. The EDTA may be binding to the copper making it unavailable to catalytically destroy HO₂. However, it was shown that another process must also be having an effect on the uptake coefficient and it is likely that the EDTA is also acting as a surfactant or changing the viscosity of the aerosol.

Finally, the HO₂ uptake coefficient was measured onto copper (II) doped ammonium sulphate aerosols containing a variety of atmospherically relevant organic species at different concentrations and at an atmospherically relevant relative humidity of 60 %. Although, no significant change was observed in the HO₂ uptake coefficient upon the addition of malonic acid, citric acid, 1,2 diaminoethane and tartronic acid, a decrease of three orders of magnitude was observed when a ten to one ratio of oxalic acid to copper was in the aerosols. The suggested reasons for this decrease in the HO₂ uptake coefficient included a change in viscosity of the aerosols and a precipitation out of the aerosol of a copper-oxalate complex.

Although with the current data it is difficult to quantify the magnitude of effects of organic compounds in atmospheric aerosols, it is likely that they will reduce the HO₂ uptake

coefficient in the atmosphere. It has been demonstrated that organics can act as surfactants, can increase the viscosity of the aerosol and could potentially bind to copper so that it cannot catalytically destroy HO₂. Humic acid and oxalic acid have both been observed in atmospheric aerosols and have been shown in this work to decrease the HO₂ uptake coefficient. There are also many glassy aerosols present in the atmosphere such as SOA, and due to the large viscosity of these aerosols a low uptake coefficient may be observed as the uptake coefficient may be limited by diffusion into the bulk of the aerosol. Experiments onto SOA are the subject of Chapter 5.

Chapter 5: Measurements of the HO₂ uptake coefficient onto secondary organic aerosols at room temperature

5.1 The importance of secondary organic aerosols

Measurements of the composition of particulate mass have shown that secondary organic aerosol (SOA) accounts for a large proportion of the organic matter in the troposphere (Kanakidou et al., 2005). In urban areas SOA can account for up to 90 % of the organic aerosol mass (Lim and Turpin, 2002). SOA is formed from the oxidation of volatile organic compounds (VOCs), typically monoterpenes and aromatic compounds, by radicals such as OH, O₃ and NO₃ (Kanakidou et al., 2005).

Several factors determine whether the oxidation of a VOC will lead to SOA formation. First, the precursor VOC must be relatively abundant in the atmosphere. Secondly, the VOC must be reactive, it must be oxidised rapidly (compared to its dilution rate) for products to accumulate and reach high concentrations. Lastly, the volatility of the products must be low so that they may either condense onto surrounding particles, (or homogeneously nucleate), once gas phase saturation has been reached (Donahue et al., 2013; Kanakidou et al., 2005).

There are currently no laboratory measurements of HO₂ uptake coefficients onto SOA. However, due to its abundance in the troposphere it is very important to know the HO₂ uptake coefficient onto SOA so that it can be included into atmospheric models. Two precursor VOCs were used in this work to form aerosols: α -pinene and trimethylbenzene (TMB). α -pinene is a biogenic gaseous precursor to SOA. It is an alkene which is released into the atmosphere by coniferous trees, especially pine trees, and has an estimated flux of 50 Tg C yr⁻¹ (Chung and Seinfeld, 2002; Guenther et al., 1995). Trimethylbenzene (TMB) is an anthropogenic gaseous precursor to SOA and is emitted into the atmosphere by automobiles, waste treatment plants and coal fired power stations. The oxidation of both VOCs by OH is shown in Figure 1.

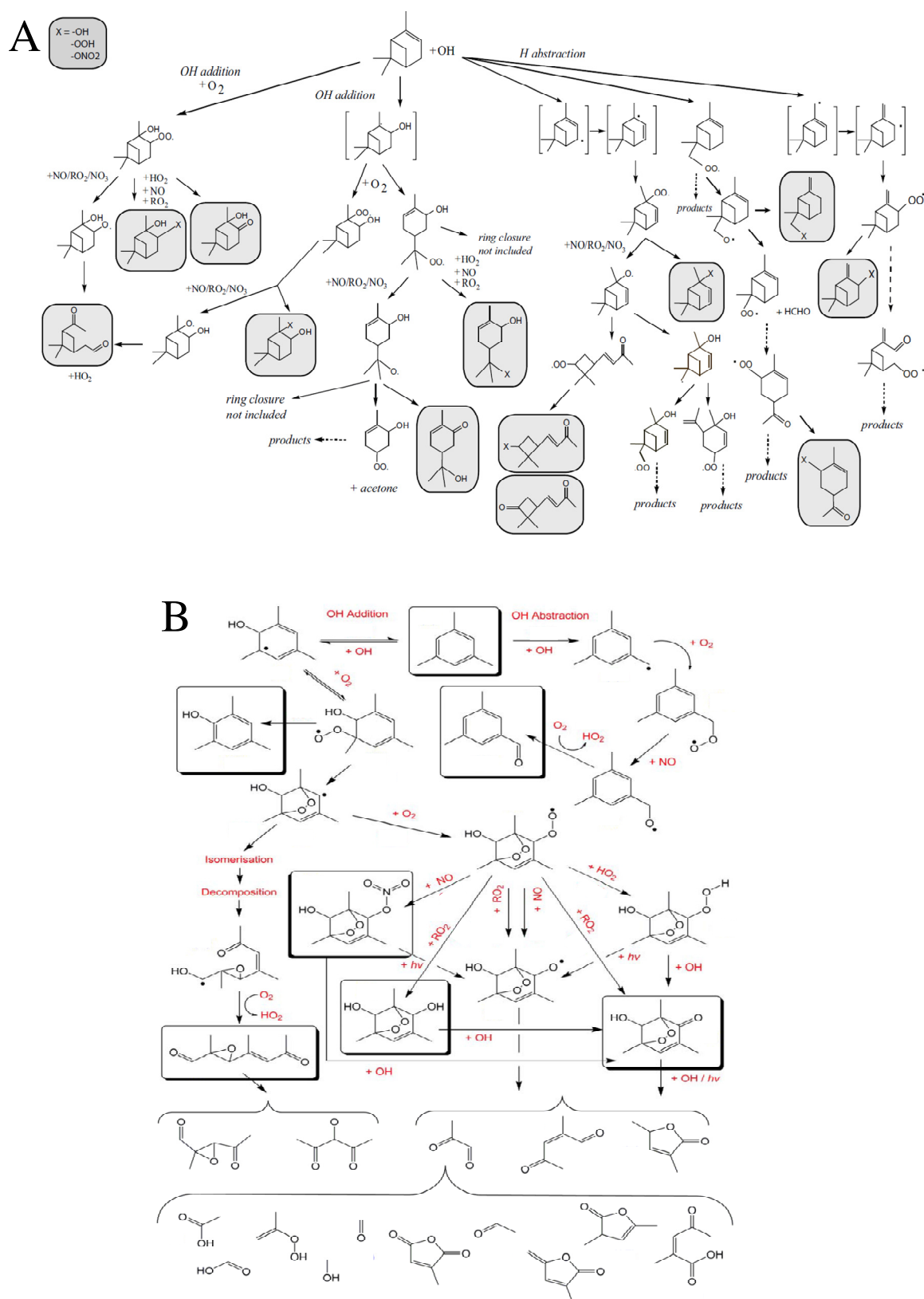


Figure 5.1: The oxidation of (A) α -pinene and (B) 1,3,5 trimethylbenzene by OH. Figures are reproduced and adapted from Valorso et al. (2011) and Wyche et al. (2009).

5.2 Comparison of instrument performance between the experimental setups at Leeds and PSI

The HO₂ uptake coefficient measurements onto SOA were performed at the Paul Scherrer Institute (PSI) in Switzerland. Therefore, the first experiment compared the uptake coefficients that were obtained in Switzerland with those that were obtained in Leeds for the same aerosol type. The main difference between the experiments was the SMPS that was used (described in Chapter 2). Two experiments were performed, the first experiment was with ammonium sulphate aerosols at 60 % RH and the second experiment was with copper sulphate doped ammonium sulphate aerosols at 57 % RH. The pseudo-first-order rate constants as a function of aerosol surface area are shown in Figure 5.2. HO₂ uptake coefficients of 0.008 ± 0.002 and 0.20 ± 0.04 were measured for the ammonium sulphate aerosols and copper sulphate doped ammonium sulphate aerosols, respectively. The HO₂ uptake coefficient values were within error of the values obtained in Leeds of 0.003 – 0.01 for ammonium sulphate and 0.5 ± 0.3 for copper doped ammonium sulphate for moving injector experiments at $\sim 1 \times 10^9$ molecule cm⁻³.

During smog chamber experiments, the flow passed through a charcoal denuder (~ 20 cm long, 2 cm diameter, honeycomb shaped charcoal) and two or three cobalt oxide denuders (~ 1 metre long, 2 cm diameter glass tube with a cobalt oxide coating). The pressure within the flow tube was also measured and was found to be below atmospheric pressure, which was due to pumping the flow through the flow tube rather than pushing it through and the presence of a flow restriction (due to the denuders) before the flow tube. Therefore, a test was performed on ammonium sulphate aerosols to ensure that neither the denuders nor the lower pressure in the flow tube were affecting the measured HO₂ uptake coefficients. The pressure was lowered by placing an obstruction just before the flow tube and the flow was passed through the denuders. An uptake coefficient of 0.004 ± 0.002 was measured for the ammonium sulphate aerosols at 60% RH and at 915 mbar which agrees within error of the previous measurement and with the measurements obtained in Leeds at atmospheric pressure (see Table 3.2 in Section 3.3), thereby giving confidence that the setup had been successfully reproduced at PSI.

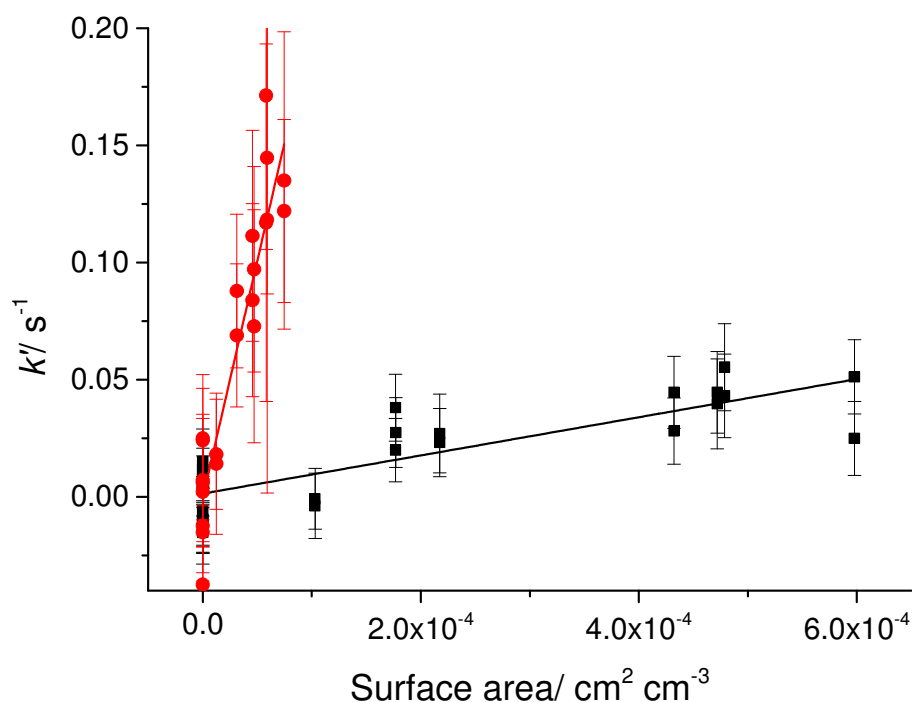


Figure 5.2: The pseudo-first order rate constant as a function of aerosol surface area for ammonium sulphate aerosols (black) and copper sulphate doped ammonium sulphate aerosols (red) at relative humidities of 60 % RH and 57 % RH, respectively, and at 293 ± 2 K. The error bars are 1 standard deviation. These experiments gave HO_2 uptake coefficients of 0.008 ± 0.002 and 0.20 ± 0.04 for the non-copper doped and copper sulphate doped ammonium sulphate aerosols respectively.

5.3 Measurements of HO_2 uptake coefficient measurements onto α -pinene and trimethylbenzene derived aerosols

Two different types of denuder were used during the experiments. A charcoal denuder was used in order to remove oxidising gases such as ozone and cobalt oxide denuders were used to remove NO_x species (Ammann, 2001; Lee and Davidson, 1999). Although most radicals should have been removed by these denuders, during TMB experiments an interference was observed in the FAGE cell. A FAGE interference is due to a species that reacts with NO to produce either HO_2 or OH. FAGE interferences (the degree of which depends on the experimental configuration and operating conditions) can occur for certain RO_2 species via the following mechanism (Fuchs et al., 2011; Whalley et al., 2013):



FAGE interferences due to RO_2 were until recently believed to be unimportant as Reaction 5.2 is slow due to a combination of a low pressure in the FAGE cell, and the short residence time between the NO injection and the OH detection area. However, Fuchs et al. (2011) observed a FAGE interference for HO_2 from certain alkenes, aromatics and isoprene derived RO_2 . The mechanism for the interference due to alkenes was attributed to the following scheme of reactions:



The exact species causing the FAGE interference when performing TMB derived SOA experiments remains unknown, however, for these experiments, regular measurements of the background signal with the NO on and the mercury lamp off were made in order to subtract the signal due to RO_2 species. The interference disappeared when the NO flow to the FAGE cell was removed, indicating that production of secondary OH was not the cause of the interference. However, when the mercury lamp in the aerosol flow tube injector was turned off the FAGE signal was still often half to three quarters of the signal with the mercury lamp on. On a couple of occasions it was also noted that the signal with the mercury lamp off was higher than the signal with it on. This may indicate that the RO_2 was reacting with HO_2 that exited the injector. However, a FAGE interference was not observed for the α -pinene aerosols.

As discussed previously in Chapter 2, two different chambers were utilised during these experiments, a smog chamber and a potential aerosol mass (PAM) chamber, which are shown

in Figure 5.3. The smog chamber was 27 cubic metres and was made from 125 μm Teflon fluorocarbon film (FEP) (Paulsen et al., 2005). For the photochemical gas phase reactions four xenon arc lamps (4 kW rated power, 1.55×10^5 lumens each, XBO 4000 W/HS, OSRAM) similar to the solar radiation were switched on. For ozonolysis experiments, ozone was generated by irradiation of pure air in quartz tubes with UV lamps. The purified air in the chamber was obtained using an AADCO (737-250 series, AADCO Instruments, Inc., USA) pure air generation system. Either α -pinene or TMB were injected into a glass bulb that was wrapped in a silicon heater at 80 °C and flushed with 10 L min^{-1} of purified air. The humidity was controlled using a commercial clothes steamer (J-4000 series, Jiffy Steamer Company, LLC, USA) with mQ water and was monitored using a humidity sensor (Rotronic Hygro Clip SCO5) (Paulsen et al., 2005).

The potential aerosol mass (PAM) chamber was a small Teflon chamber with an internal volume of 15 litres. It was attached to the smog chamber using copper tubing during many of the experiments and the flow passing through this chamber was 4 lpm. It contained Teflon coated lamps which emitted mostly 185 nm and 254 nm light. The 185 nm light photolysed water vapour in air to produce OH and HO₂ and also photolysed O₂ to produce O atoms and hence O₃ whereas the 254 nm light could photolyse O₃ to produce OH. The concentrations of O₃, OH and HO₂ that were produced in the PAM chamber were expected to be several orders of magnitude higher than would be expected in the atmosphere, although the exact concentrations during these experiments were unknown. However, the OH / HO₂ and OH / O₃ ratios should be similar to tropospheric concentrations (Kang et al., 2007). The larger radical concentrations should be equivalent to a few days' worth of exposure in terms of tropospheric oxidation whereas in the PAM chamber the oxidation occurs within a few minutes.

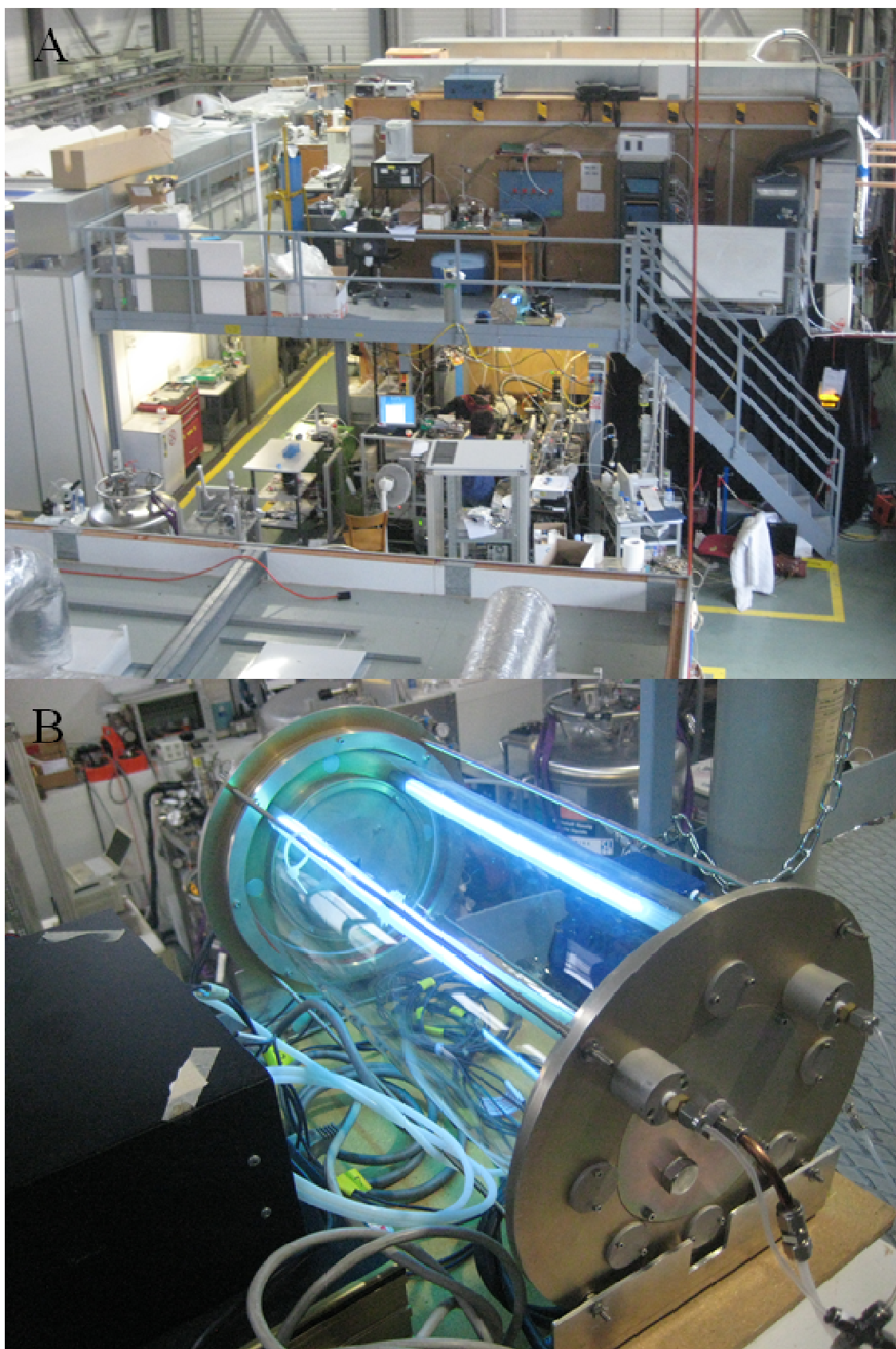


Figure 5.3: (A) The PSI smog chamber housed in the wooden enclosure and (B) the PSI PAM chamber.

For all experiments, either the PAM chamber or the smog chamber was attached to the rest of the equipment using copper tubing and a 4 lpm flow from the chamber(s) was pulled through the equipment using a pump (KnF vacuum pump), see Chapter 2 for more details. Four different experiments were performed and are described below (it should be noted that TMB ozonolysis was also attempted in the smog chamber but did not produce a large enough aerosol surface to volume ratio ($< 5 \times 10^{-5} \text{cm}^2 \text{cm}^{-3}$) over a period of approximately 8 hours to perform an experiment).

1) α -pinene precursor and ozone in the smog chamber.

For these experiments α -pinene vapour entered the smog chamber at initial concentrations of between 200 and 600 ppb and at 50 or 80% RH. Ozone was injected at initial concentrations of between 280 and 310 ppb. The ozone oxidised the α -pinene to form SOA.

2) α -pinene precursor and NO_2 with the UV lights switched on in the smog chamber.

For this experiment α -pinene vapour entered the smog chamber at an initial concentration of 500 ppb and NO_2 was injected at an initial concentration of 500ppb. The NO_2 then photolysed via the following reaction:



The O atom can then react with O_2 to form ozone. Photolysis of water vapour was also expected in the smog chamber, resulting in OH radicals. The reaction of OH with NO_2 could form HNO_3 which could then form NO_3 by reaction with OH radicals. The oxidation of α -pinene by O_3 , OH and NO_3 formed SOA. However, the relative concentrations of the O_3 , OH and NO_3 were not recorded.

3) α -pinene precursor and UV lights switched on in the PAM chamber.

In these experiments α -pinene vapour entered the smog chamber at an initial concentration of either 500 ppb or 1 ppm and at a RH of either 50 or 80% RH. The chamber air was then passed through the PAM chamber where the TMB was oxidised by OH and O_3 to form SOA.

4) TMB and UV lights switched on in the PAM chamber.

For these experiments TMB vapour entered the smog chamber at an initial concentration of 2 ppm and at 50% RH. The chamber air was then passed through the PAM chamber where the TMB was oxidised by OH and O₃ to form SOA.

The pseudo-first-order rate constant plotted against the aerosol surface area for α -pinene and TMB derived aerosols for experiments performed in the PAM chamber is shown in Figure 5.4. The results from HO₂ uptake experiments onto α -pinene derived aerosols and TMB derived aerosols are summarised in Table 5.1. The average HO₂ uptake coefficient for α -pinene derived aerosols was measured as $\gamma < 0.001$ and for TMB derived aerosols $\gamma = 0.004 \pm 0.003$ at an initial HO₂ concentration of $\sim 1 \times 10^9$ molecule cm⁻³. These uptake coefficients are very similar to the uptake coefficients measured for laboratory generated organic aerosols that were shown in Chapter 4. In Chapter 4 it was shown that there was no observable dependence of the HO₂ uptake coefficient upon the composition of the organic and therefore other factors are likely to influence the uptake (as will be discussed in Section 5.4). It should be noted that the method of formation of α -pinene derived aerosols, as outlined above did not affect the uptake coefficient that was measured, with no measurable uptake observed for any of the experiments. However, the upper limit for the HO₂ uptake coefficient was lower with the PAM chamber experiments due to higher aerosol surface areas.

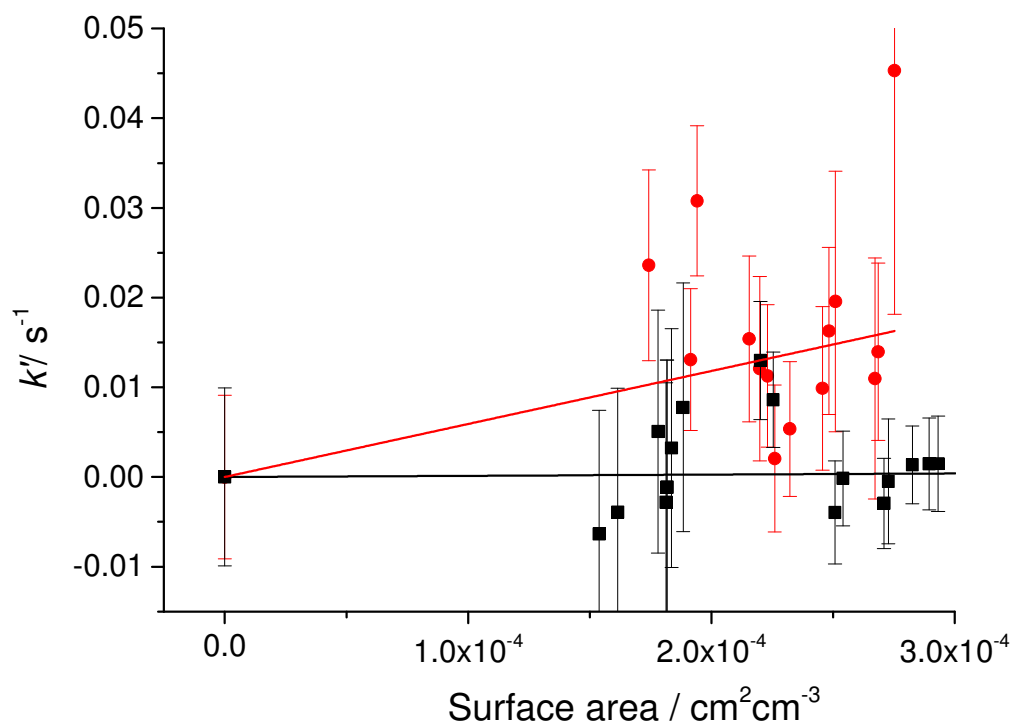


Figure 5.4: The pseudo-first-order rate constants as a function of aerosol surface area for α -pinene derived aerosols (black) and trimethylbenzene derived aerosols (red) at a pressure of 904 – 929 mbar and at 293 ± 2 K. These experiments were performed using the PAM chamber and HO_2 uptake coefficients of < 0.001 and 0.004 ± 0.002 were measured for α -pinene and TMB derived aerosols, respectively. The error bars represent one standard deviation.

Experiment number	Reaction type	Initial precursor concentrations	UV	Relative humidity in the chamber/ %	Pressure in the flow tube/ mbar	Maximum surface to volume ratio in the flow tube/ $\text{cm}^2 \text{cm}^{-3}$	HO_2 uptake coefficient (γ)
1	α -pinene ozonolysis	[α -pinene] = 600 ppb [O_3] = 280 ppb	Off	50	987	6.30×10^{-5}	< 0.01
2	α -pinene ozonolysis	[α -pinene] = 600 ppb [O_3] = 280 ppb	Off	50	965	1.30×10^{-4}	< 0.004
3	α -pinene ozonolysis	[α -pinene] = 200 ppb [O_3] = 310 ppb	Off	80	939	7.10×10^{-5}	< 0.006
4	α -pinene photochemistry	[α -pinene] = 500 ppb [NO_2] = 350 ppb	On	50	940	6.30×10^{-5}	< 0.018
5	α -pinene photochemistry	[α -pinene] = 500 ppb	On	50	929	2.93×10^{-4}	< 0.001
6	TMB photochemistry	[TMB] = 2 ppm	On	50	923	2.75×10^{-4}	0.004 ± 0.002
7	TMB photochemistry	[TMB] = 2ppm	On	50	918	2.32×10^{-4}	0.004 ± 0.003
8	α -pinene photochemistry	[α -pinene] = 500 ppb	On	50	927	1.88×10^{-4}	< 0.005
9	α -pinene photochemistry	[α -pinene] = 1 ppm	On	80	904	3.90×10^{-4}	< 0.001

Table 5.1: Summary of the reactants and conditions that were utilised for the HO_2 uptake coefficient experiments that were carried out at the Paul Scherrer Institute. Experiments 1 – 4 were performed using the smog chamber whereas experiments 5 – 9 were performed using the PAM chamber.

5.4 Discussion of the HO₂ uptake coefficient measurements onto α -pinene and trimethylbenzene derived aerosols

One possibility for the smaller measured HO₂ uptake coefficient for α -pinene derived aerosols is a larger viscosity than for TMB derived aerosols. If α -pinene aerosols were much more viscous, the diffusion of HO₂ into the bulk of the aerosol might become rate limiting. There have been several studies that have made measurements with α -pinene derived aerosols to determine its phase. Saukko et al. (2012) and Kannosto et al. (2013) observed that the aerosols bounce on impact with a hard surface suggesting the aerosols must be rigid. However, Saukko et al. (2012) also noticed that the bouncing reduced slightly with increasing relative humidity. Vaden et al. (2011) observed that SOA derived from the ozonolysis of α -pinene exhibited much slower evaporation kinetics than would be expected for liquid droplets and Kuwata and Martin (2012) observed much larger ammonia uptake onto these aerosols when the relative humidity was larger than 94 % compared to when it was less than 5% suggesting a transition from semi-solid to liquid particles at higher humidities. Abramson et al. (2013) have estimated the viscosity of α -pinene derived aerosols as 10⁸ Pa s (a typical viscosity for a liquid is 10⁻² to 10³ Pa s). The estimated viscosity is consistent with the observations that have been made that the aerosols are solid enough to bounce, although this viscosity would also allow the surface tension to produce spheres on a time scale of minutes.

Zhou et al. (2013) used benzo[a]pyrene (BaP) ammonium sulphate particles that were coated with SOA formed from the ozonolysis of α -pinene to investigate the kinetics of BaP with ozone. The reaction time was up to 66 seconds and the loss of BaP was measured using an aerosol mass spectrometer. A higher loss of BaP was observed (~ a 30 % increase at an ozone concentration of 6 × 10¹⁴ molecule cm⁻³) at 70 % RH compared to 50 % RH. The increase in the loss of BaP could be attributed to an increase in the diffusion of ozone through the SOA due to the SOA being less viscous at a higher humidity. This is in agreement with the low HO₂ uptake coefficients observed for α -pinene derived SOA in this work. In this work, a change in uptake coefficient with changing humidity was not observable, although this may be due to the difference between the relative humidities not being large enough.

The estimated viscosity of 10^8 Pa s for α -pinene derived aerosols is comparable to a value of $\sim 10^8$ Pa s measured by Power et al. (2013) for sucrose aerosols at 30 % RH. In Section 4.3 it was shown that the HO₂ uptake coefficient was greatly reduced onto copper doped sucrose aerosols from a mass accommodation value of 0.20 ± 0.06 at 71% to a HO₂ uptake coefficient value of 0.02 ± 0.01 at a relative humidity of ~ 30 % RH. Therefore, it seems likely that the low HO₂ uptake coefficient measurements onto α -pinene derived aerosols is due to the high viscosity of the aerosols. Due to the high viscosity of the aerosols, the diffusion of HO₂ into the aerosols would be slow and therefore there would be less HO₂ in the aerosol bulk to react with itself. The diffusion of HO₂ into aerosols will be investigated in detail using the KM-SUB model in Chapter 8.

Although it seems likely that the low HO₂ uptake coefficients observed for α -pinene derived aerosols is due to their high viscosity, it should be noted that the diffusion coefficient into α -pinene aerosols is high enough for mixing to occur on a timescale of one minute. Robinson et al. (2013) formed SOA from the oxidation of α -pinene in a 100 litre sample bag and formed SOA from the OH oxidation of toluene in a 10 m³ chamber. The α -pinene derived SOA was then added to the chamber containing the toluene derived SOA. Robinson et al. (2013) then used single particle mass spectroscopy to assess mixing between the aerosols. Mixing could either have occurred by coagulation of the aerosols (where aerosols collide with each other) or by condensational mixing (where mixing occurs through gas phase diffusion). Coagulation was ruled out because for a similar experiment with docosane/docosane-d46 the two types of aerosol were found not to mix and the mass spectra did not evolve over time. The aerosol number concentrations used for the α -pinene SOA/ toluene SOA were similar to the docosane/docosane-d46 concentrations and therefore coagulation can be ruled out as a significant mixing process. On a time scale of a minute toluene oxidation products were found to be present in the α -pinene derived aerosols at a mass fraction of 40%, indicating a strong absorption of these toluene oxidation products into the α -pinene derived SOA. This experiment is not necessarily in disagreement with this work, as the timescales of experiments in this work were between 10 – 20 seconds and it is possible that the HO₂ uptake coefficient is limited by diffusion into the bulk of the aerosol at short times.

Unfortunately, there are no estimations of the viscosity of TMB derived aerosols published in the literature. Therefore, until experiments have been performed to estimate the viscosity of TMB aerosols, it is impossible to state whether the larger HO₂ uptake that is observed is due to a lower viscosity of the aerosol. However, if the viscosity in the aerosol were higher for α -pinene than for TMB, the gas to particle partitioning would be limited by aerosol diffusion which would mean lower HO₂ concentrations in the aerosol and therefore lower reaction and a lower uptake coefficient.

A second possibility for the lower HO₂ uptake coefficients measured for α -pinene derived aerosols would be if these aerosols had a lower liquid water content than TMB derived aerosols. Cocker et al. (2001) measured that the absorbed water mass divided by the secondary organic aerosol mass at ~ 50% RH was ~ 0.1. In comparison, the same ratio for ammonium sulphate gives a value of ~ 0.3 at 50 % RH (Clegg et al., 1998; Wexler and Clegg, 2002) (<http://www.aim.env.uea.ac.uk/aim/aim.php>). However, no data are available for TMB derived aerosols. The liquid water content of the aerosols could affect the HO₂ uptake coefficient due to the following reaction being dependent upon the water concentration in the aerosol:



Therefore, as the liquid water content decreases, the uptake coefficient may decrease due to a decrease in the rate of Reaction 5.11. This was suggested as being one of the possible reasons for the observed HO₂ uptake coefficient humidity dependence onto humic acid aerosols in Section 4.3.

Another possibility exists for the larger HO₂ uptake coefficients observed for TMB compared to α -pinene. During the experiments with TMB, an interference was observed in the FAGE cell which is likely due to RO₂. Therefore, when the aerosol enters the flow tube it is reasonable to assume that it contains high concentrations of RO₂ as well as there being large RO₂ concentrations in the gas phase. HO₂ is known to react with RO₂ via the following reaction (although for some species such as R = CH₃C(O) there is a yield of OH):



Therefore, it is feasible that both α -pinene and TMB derived aerosols have large viscosities and that in fact the larger uptake that is observed for TMB derived aerosols is due to HO_2 reacting with RO_2 either at the surface or in the bulk of the aerosol. If the reaction is faster in the aqueous phase than in the gas phase then the uptake coefficient will be higher when RO_2 is present. Further experiments are necessary to investigate this hypothesis further.

5.5 Atmospheric Implications

The low HO_2 uptake coefficients of < 0.001 and 0.004 ± 0.002 measured for α -pinene and TMB derived aerosols, respectively, were inputted into the Cape Verde model. The Cape Verde model predicted a decrease of less than 0.05 % and of 0.20 % with the two HO_2 uptake coefficients assuming an aerosol surface area of $1 \times 10^{-6} \text{ cm}^2 \text{ cm}^{-3}$. Therefore, the impact of SOA on atmospheric HO_2 gas phase concentrations is small and insignificant compared to aqueous salt aerosols and to copper doped aerosols under the same conditions. However, in urban areas the SOA concentrations would be expected to be much higher than in Cape Verde and therefore the SOA would have a greater impact upon gaseous HO_2 concentrations.

The reaction of HO_2 with RO_2 has also been shown to potentially be an important heterogeneous process. RO_2 radicals are present in the troposphere at concentrations of $\sim 10^8$ molecule cm^{-3} (e.g. Salisbury et al. (2002)). It seems likely that RO_2 and HO_2 could react in the aqueous aerosol phase, and the results of the TMB experiment are a first indication that the HO_2 uptake coefficient may be enhanced in the presence of RO_2 . However, more experiments with different RO_2 species as well as different RO_2 and HO_2 concentrations would be required to estimate an enhanced rate of loss of HO_2 in the presence of aerosols and to estimate the impact on tropospheric HO_2 concentrations.

5.6 Summary

For the first time, HO₂ uptake coefficients have been measured onto SOA. It has been shown that the HO₂ uptake coefficient measured onto laboratory generated ammonium sulfate and copper doped ammonium sulfate aerosols were within error bars of the HO₂ uptake coefficients measured in Leeds. Four different types of SOA experiment were then performed: α -pinene ozonolysis in the smog chamber, α -pinene photochemistry in the smog chamber, α -pinene photochemistry in the PAM chamber and TMB photochemistry in the PAM chamber. The HO₂ uptake coefficients were $\gamma < 0.001$ for α -pinene derived aerosols and $\gamma = 0.004 \pm 0.002$ for TMB derived aerosols.

The low HO₂ uptake coefficient for α -pinene derived aerosols may be due to the high viscosity of the aerosol, with the uptake being affected by diffusion into the bulk of the aerosol. The higher HO₂ uptake coefficient for TMB derived aerosols could either be due to the viscosity of TMB derived aerosols being lower than for α -pinene derived aerosols, the liquid water content of α -pinene derived aerosols being lower than for TMB derived aerosols or due to HO₂ reacting with RO₂ on the surface or in the bulk of the aerosol. However, until the viscosity and the liquid water content of TMB derived aerosols has been estimated, it is not possible to definitely say with confidence whether the higher uptake is due to viscosity, the aerosol water concentration, or a RO₂ reaction. Future laboratory measurements could investigate the effect of the presence of RO₂ in the flow tube upon the HO₂ uptake coefficient in a more controlled fashion, which could then be extended to measuring RO₂ uptake coefficients.

Chapter 6: Measurements of the HO₂ uptake coefficient onto inorganic salts at temperatures between 263 and 314 K and at atmospheric pressure

6.1 The importance of measuring the HO₂ uptake coefficient over a range of temperatures

The temperature in the troposphere varies from approximately 20°C (293K) near the Earth's surface to around -57°C (216 K) at the tropopause. However, at the equator average temperatures near the Earth's surface tend to be approximately 30°C (303K). There have also been several instances of much higher temperatures being recorded, for example, in June 2013 an air temperature of 47°C was recorded in Phoenix, Arizona whilst a temperature of almost 51°C was recorded in Death Valley in California (B.B.C. News, 2013). Therefore, due to the range in the temperatures throughout the troposphere, it is important to know how the HO₂ uptake coefficient varies as the temperature changes.

Mao et al. (2010) measured HO₂ concentrations in the Arctic at temperatures of 256 K at altitudes between 0 and 3 km, 243 K between 3 and 6 km and 226 K between 6 and 9 km during the ARCTAS field campaign. The measured HO₂ was up to a factor of two lower than the concentrations predicted by a global 3-D chemical transport model (GEOS-Chem) with the largest discrepancy occurring at the highest altitudes and lowest temperatures. Therefore, it is extremely important to understand how the HO₂ uptake coefficient varies with temperature.

There are currently only a few studies that have measured HO₂ uptake coefficients onto surfaces over a range of temperatures, but there are no studies that have investigated the change in the HO₂ uptake by aerosols as the temperature varies. Remorov et al. (2002) and Loukhovitskaya et al. (2009) measured the HO₂ uptake coefficient onto solid sodium chloride surfaces over a range of temperatures (345 – 240 K). These studies showed an increase in the uptake coefficient with decreasing temperature (this will be discussed in greater detail in

Section 6.2). There have also been several studies of the HO₂ uptake coefficient onto sulphuric acid aerosols at room temperature (Thornton and Abbatt, 2005) as well as onto surfaces coated with sulphuric acid at lower temperatures (Cooper and Abbatt, 1996; Gershenson et al., 1995; Hanson et al., 1992). The HO₂ uptake coefficient onto sulphuric acid also appeared to be temperature dependent with an uptake coefficient of < 0.01 and > 0.2 measured at 295 K and 243 K, respectively. In this work, HO₂ uptake coefficients were measured onto effloresced ammonium sulphate and sodium chloride aerosols and onto deliquesced ammonium nitrate and copper doped ammonium nitrate aerosols in the temperature range of 263 - 314 K.

6.2 Measurements of HO₂ uptake coefficients onto effloresced sodium chloride and ammonium sulphate aerosols over a range of temperatures

Examples of the pseudo-first order rate coefficients as a function of aerosol surface area measured in this work are shown in Figure 6.1 for effloresced sodium chloride and effloresced ammonium sulphate aerosols at the two extreme temperatures utilised in this work (263 K and 314 K). The average HO₂ uptake coefficients measured in this work over the 263 to 314 K temperature range onto effloresced aerosols are summarised in Table 6.1. The uptake coefficients ranged from 0.000 ± 0.001 to 0.004 ± 0.003 and appeared to increase slightly with increasing temperature (this will be discussed in greater detail below). The average initial HO₂ concentrations and the average relative humidities of the experiments are also summarised in Table 6.1.

Ideally, both the relative humidity and the initial HO₂ concentrations would have remained the same at the different temperatures used in this work. However, due to the setup used the flow tube and DMA were at different temperatures, which meant that it was not possible to keep the relative humidity constant for the range of temperatures. See Chapter 2 for more information about the experimental setup. It was important that the deliquescence relative humidity was not reached either in the flow tube or in the DMA where the aerosols were size selected to obtain a size distribution. Sodium chloride aerosols deliquesce at 75 ± 1 to 77 ± 3 % RH between 298 K and 263 K whereas ammonium sulphate aerosols deliquesce at 79 ± 1

% to 82 ± 3 % RH between 298 K and 263 K (Cziczo and Abbatt, 1999, 2000; Cziczo et al., 1997). A relative humidity of 9 % at 314 K would lead to a relative humidity of 30 % in the DMA at 293 K. However, a relative humidity of 22 % at 314 K would have led to a relative humidity of 75 % which is the deliquescence point of sodium chloride. The relative humidity in the flow tube at low temperatures was higher than in the DMA that was maintained at room temperature. However, it was difficult to decrease the relative humidity due to the method of HO₂ production being the photolysis of water vapour. The initial HO₂ concentrations would also ideally have been kept constant. However, at lower temperatures lower HO₂ concentrations exited the injector. The lower HO₂ concentrations coming out of the injector at lower temperatures may be due to the faster rate of the HO₂ self-reaction at lower temperatures in the injector (Kircher and Sander, 1984; Stone and Rowley, 2005). The HO₂ loss to the walls of the injector could also have potentially increased.

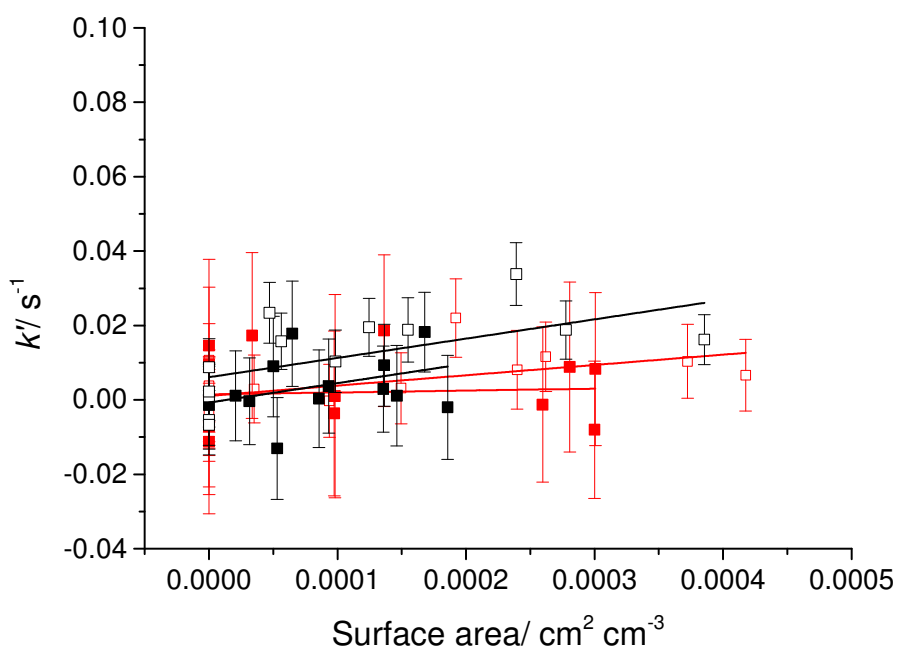


Figure 6.1: Examples of the pseudo-first order rate constant as a function of aerosol surface area for effloresced sodium chloride (black points) and effloresced ammonium sulphate (red points) at 263 K (open symbols) and 314 K (closed symbols). The uptake coefficients from these graphs were measured as 0.003 ± 0.003 and 0.006 ± 0.003 at 314 K for ammonium sulphate at 7 % RH and sodium chloride at 5 % RH respectively and as 0.001 ± 0.002 and 0.001 ± 0.003 at 263 K for ammonium sulphate at 56 % RH and sodium chloride at 30 % RH respectively.

Temperature/ K	Sodium chloride HO ₂ uptake coefficient	Ammonium sulfate HO ₂ uptake coefficient	Average initial HO ₂ concentration/ molecule cm ⁻³	Average relative humidity in the flow tube/ %
314	0.004 ± 0.002	0.002 ± 0.003	9.7 × 10 ⁸	9
304	0.002 ± 0.003	0.003 ± 0.002	9.2 × 10 ⁸	19
292	0.004 ± 0.003	0.001 ± 0.002	8.8 × 10 ⁸	31
284	0.001 ± 0.002	0.001 ± 0.001	1.3 × 10 ⁹	39
274	0.001 ± 0.002	0.000 ± 0.002	4.2 × 10 ⁸	62
263	0.000 ± 0.002	0.000 ± 0.001	2.5 × 10 ⁸	43

Table 6.1: The HO₂ uptake coefficient onto effloresced sodium chloride and ammonium sulphate aerosols over a range of temperatures and at atmospheric pressure. The errors represent two standard deviations.

In contrast to this work, Remorov et al. (2002) and Loukhovitskaya et al. (2009) observed a temperature dependence for HO₂ uptake to solid coatings of sodium chloride with larger HO₂ uptake coefficients at lower temperatures (Figure 6.2). Remorov et al. (2002) parameterised the HO₂ uptake coefficient as the following Arrhenius equation:

$$\gamma = (5.66 \pm 3.62) \times 10^{-5} \exp [(1560 \pm 140) / T] \quad (\text{E6.1})$$

whereas Loukhovitskaya et al. (2009) parameterised the HO₂ uptake coefficient as:

$$\gamma = (2.2 \pm 0.7) \times 10^{-8} \exp [(3340 \pm 90) / T] \quad (\text{E6.2})$$

Both of these parameterisations show a negative activation energy which may be due to a variety of reasons. The mass accommodation is likely to be temperature dependent as will be discussed below for copper doped aerosols. The HO₂ uptake coefficients measured by Remorov et al. (2002), Loukhovitskaya et al. (2009) and in this work onto effloresced sodium chloride surfaces and aerosols are shown in Figure 6.2 alongside the parameterisations shown in Equations 6.1 and 6.2.

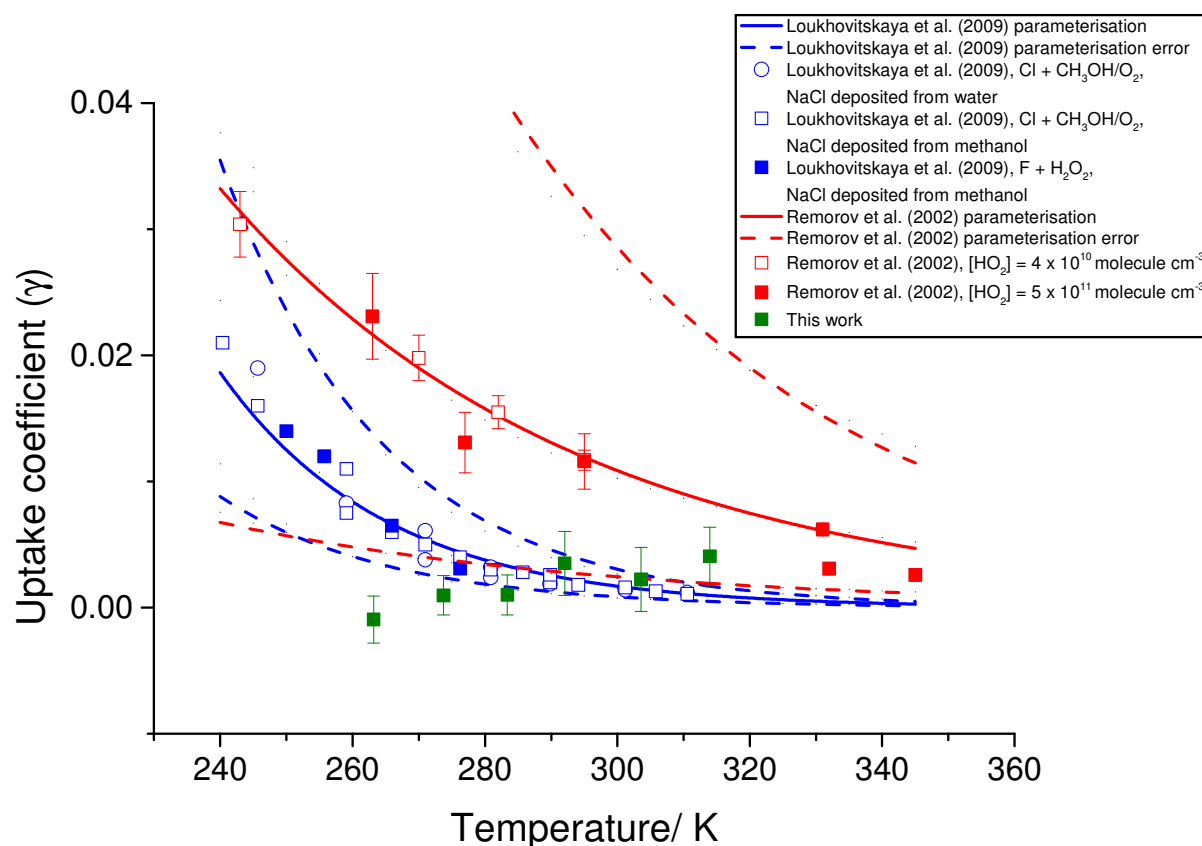


Figure 6.2: The HO₂ uptake coefficient measured onto effloresced sodium chloride aerosols in this work and onto surfaces coated with effloresced sodium chloride by Remorov et al. (2002) and Loukhovitskaya et al. (2009) over a range of temperatures. Remorov et al. (2002) measured the HO₂ uptake coefficient at two different initial HO₂ concentrations of 4×10^{10} molecule cm⁻³ and 5×10^{11} molecule cm⁻³. Loukhovitskaya et al. (2009) measured the HO₂ uptake coefficient with Cl + CH₃OH/O₂ and F + H₂O₂ sources of HO₂ and with NaCl deposited from water and methanol solutions. The red and blue solid lines represent the parameterisations in Equations 6.1 and 6.2 with the dashed lines represent the errors in the parameterisations.

In this work, the HO₂ uptake coefficient did not increase with decreasing temperature. Both Remorov et al. (2002) and Loukhovitskaya et al. (2009) worked at 0 % RH. However, when Remorov et al. (2002) increased the water vapour in their flow tube from $[\text{H}_2\text{O}] = 0$ molecule cm⁻³ to $[\text{H}_2\text{O}] = 3 \times 10^{15}$ the uptake coefficient decreased by 13 and 21% at 295 K (RH ~ 0.5 %) and 243 K (RH ~ 28%) respectively. Therefore, the lower uptake coefficients observed in this work may be due to the higher relative humidities that were utilised meaning that this work is not inconsistent with the work by Remorov et al. (2002) and Loukhovitskaya et al.

(2009). The relative humidity of the experiments performed in this work varied from 5 % to 62 % as shown in Table 6.1. However, it should also be noted that Loukhovitskaya et al. (2009) also investigated the impact of humidity and observed no difference in the HO₂ uptake coefficient when working at 0 and 28% RH at 243 K which appeared to be in contrast with the work by Remorov et al. (2002). However, Loukhovitskaya et al. (2009) stated that their results were not in disagreement with those of Remorov et al. (2002) and that the dependence upon the relative humidity might be masked by other species such as CH₃OH, HCl, Cl₂, H₂O₂ and HF causing surface deactivation present in the flow tube. However, Loukhovitskaya et al. (2009) did observe a factor of two decrease in uptake at 18 % RH compared to 0 % RH for MgCl₂·6H₂O.

It should also be noted that in contrast to the work by Remorov et al. (2002) and Loukhovitskaya et al. (2009), Taketani et al. (2008) observed an increase in uptake coefficient of $\gamma < 0.01$ to $\gamma = 0.02 \pm 0.01$ from 20 to 53 % RH. Taketani and Kanaya (2010) also observed an increase in the HO₂ uptake coefficient from 0.01 ± 0.01 to 0.03 ± 0.01 between 22 and 92 % RH onto solid polystyrene latex beads. Taketani et al. (2008) and Taketani and Kanaya (2010) stated that the increase in uptake coefficient with increasing humidity could be due to the formation of a HO₂-H₂O complex (Hamilton and Lii, 1977):



If the HO₂-H₂O complex had a larger uptake coefficient than HO₂, this would manifest itself by a larger HO₂ uptake coefficient onto aerosols at higher humidities (Aloisio et al., 2000). However, there is currently no evidence for the HO₂-H₂O complex having a higher uptake coefficient than HO₂.

The HO₂ uptake coefficients over a range of temperatures were also measured in this work for effloresced ammonium sulphate aerosols. The measured uptake coefficients for both ammonium sulphate and sodium chloride are shown in Figure 6.3. Similarly to sodium chloride, there was no observable change in uptake coefficient as the temperature decreased. However, this could be due to the increase in relative humidity leading to fewer active sites on the surface of the aerosols, or may be due to the lower HO₂ concentrations at lower

temperatures if the uptake coefficient is controlled by HO₂ self-reaction at the surface of the aerosol at which the work was done. It is possible that the changes in humidity are masking a change in the uptake coefficient due to a change in temperature.

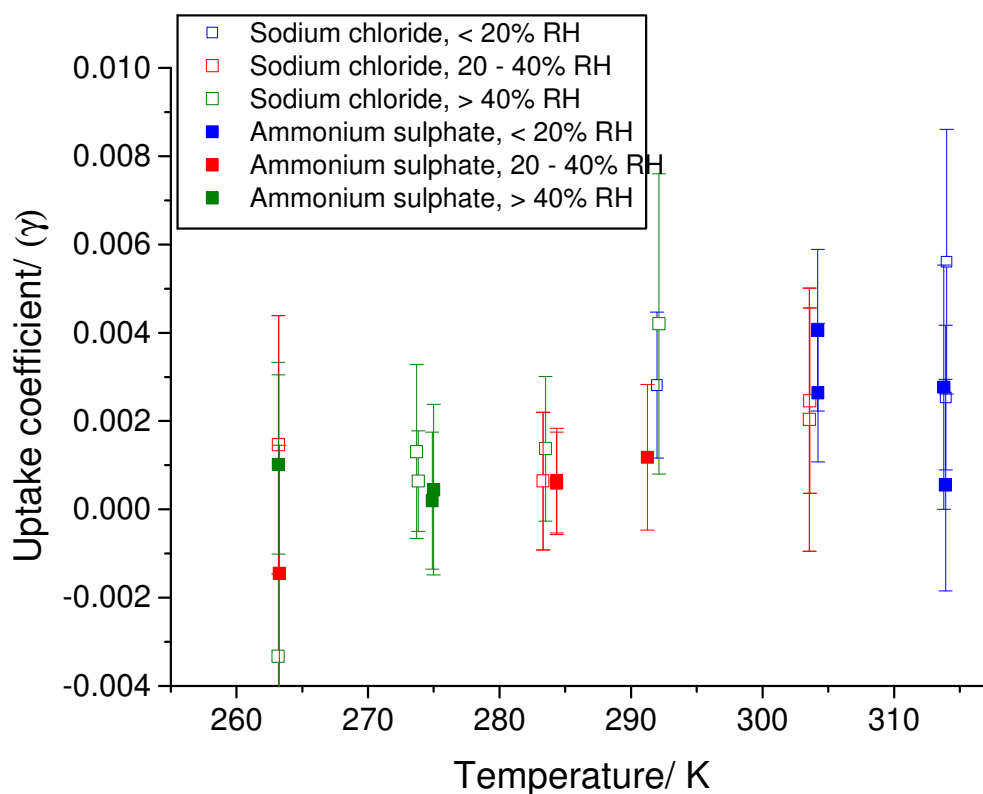
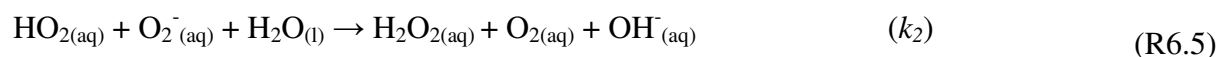


Figure 6.3: The HO₂ uptake coefficient onto effloresced sodium chloride aerosols and effloresced ammonium sulphate aerosols measured in this work over as a function of temperature. The error bars represent two standard deviations.

6.3 Measurements of HO₂ uptake coefficients onto deliquesced ammonium nitrate aerosols over a range of temperatures

The HO₂ uptake coefficient in aqueous aerosols is expected to be affected by temperature in several different ways. First, the rate coefficients of different reactions are dependent upon temperature (Reaction 31 and 32):





The Thornton et al. (2008) model that was described in Section 1.13.3 estimated an activation energy of $-4.7 \text{ kcal mol}^{-1}$ (or $-19.7 \text{ kJ mol}^{-1}$) for Reaction 6.4 and -3 kcal mol^{-1} (or $-12.6 \text{ kJ mol}^{-1}$) for Reaction 6.5 (Jacob, 2000). Thornton et al. (2008) therefore parameterised k_1 and k_2 (in $\text{M}^{-1} \text{ s}^{-1}$) using the following equations where T is the temperature in units of Kelvin:

$$k_1 = 2.4 \times 10^9 \exp\left(\frac{-2.36 \times 10^3}{T}\right) \quad (\text{E6.3})$$

$$k_2 = 1.6 \times 10^{10} \exp\left(\frac{-1.51 \times 10^3}{T}\right) \quad (\text{E6.4})$$

Thornton et al. (2008) also calculated the Henry's law (in M atm^{-1}) constant using Equation 6.5 below which was based upon an estimation by Hanson et al. (1992). Hanson et al. (1992) based their estimation for the Henry's law constant upon a ΔG_{sol} value of $-4.9 \pm 0.5 \text{ kcal mol}^{-1}$ calculated by Golden et al. (1990) and a value of ΔS_{sol} of $-23 \pm 3 \text{ cal K}^{-1} \text{ mol}^{-1}$. However, the error on the Henry's law constant from Equation 6.5 is at least a factor of 2.5.

$$H_{\text{HO}_2} = 9.4 \times 10^{-6} \exp\left(\frac{5.92 \times 10^3}{T}\right) \quad (\text{E6.5})$$

The Henry's law constant decreases with increasing temperature due to the solvation of HO_2 being an exothermic process. Therefore, due to Le Chatelier's principle which states that the position of an equilibrium will move to counteract a change, when the temperature increases the solubility of HO_2 will decrease. Overall, in the Thornton et al. (2008) model it was found that the effect of the Henry's law constant dominated over the rate constants to increase the HO_2 uptake coefficient as the temperature decreased. Therefore, as temperature increased the

uptake coefficient should decrease due to a smaller HO₂ concentration being in the bulk of the aerosol and available for self-reaction.

Although there are currently no measured HO₂ uptake coefficients onto aerosols over a range of temperatures reported in the literature, several different studies have measured the HO₂ uptake coefficient onto aqueous sulphuric acid surfaces at low temperatures and onto aqueous sulphuric acid aerosols at room temperature. The HO₂ uptake coefficient was measured to be < 0.01 at 295 K (Thornton and Abbatt, 2005), > 0.05 at 249 K (Hanson et al., 1992), > 0.2 at 243 K (Gershenzon et al., 1995) and 0.055 ± 0.020 at 223 K (Cooper and Abbatt, 1996). Overall, there appears to be an increase in the HO₂ uptake coefficient with decreasing temperature. However, no study has systematically measured the HO₂ uptake coefficient over a range of temperatures.

Griffiths and Cox (2009) measured N₂O₅ uptake coefficients between 263 and 303 K onto aqueous ammonium sulphate and aqueous ammonium bisulphate aerosols at a relative humidity of 50%. The uptake coefficients varied from 0.005 ± 0.002 at 303 K to 0.036 ± 0.002 at 263 K for ammonium sulphate and from 0.003 ± 0.001 at 303 K to 0.036 ± 0.009 at 263 K for ammonium bisulphate. The temperature dependence in these experiments were believed to be limited by mass accommodation (which will be discussed in greater detail in Section 6.4). However, in this work, it has already been shown that the HO₂ uptake coefficient is only limited by mass accommodation when aqueous aerosols are doped with copper. The limiting factors for HO₂ uptake into non-copper doped aqueous ammonium nitrate aerosols is likely to be solubility and the rate of reaction, both of which are temperature dependent.

In this work, the HO₂ uptake coefficient was measured over a range of temperatures (263 K – 312 K) for deliquesced ammonium nitrate aerosols. Ammonium nitrate aerosols were chosen because they do not effloresce down to humidities of 0 % and therefore, a correction could be made for their surface area between the flow tube and the DMA (as described in Section 2.12.1.) which will have different relative humidities. Examples of the pseudo-first order rate coefficients as a function of humidity are shown in Figure 6.4 at the two extreme

temperatures in this work (263 K and 312 K). The average HO₂ uptake coefficients that were measured in this work over the range of temperatures are summarised in Table 6.1.

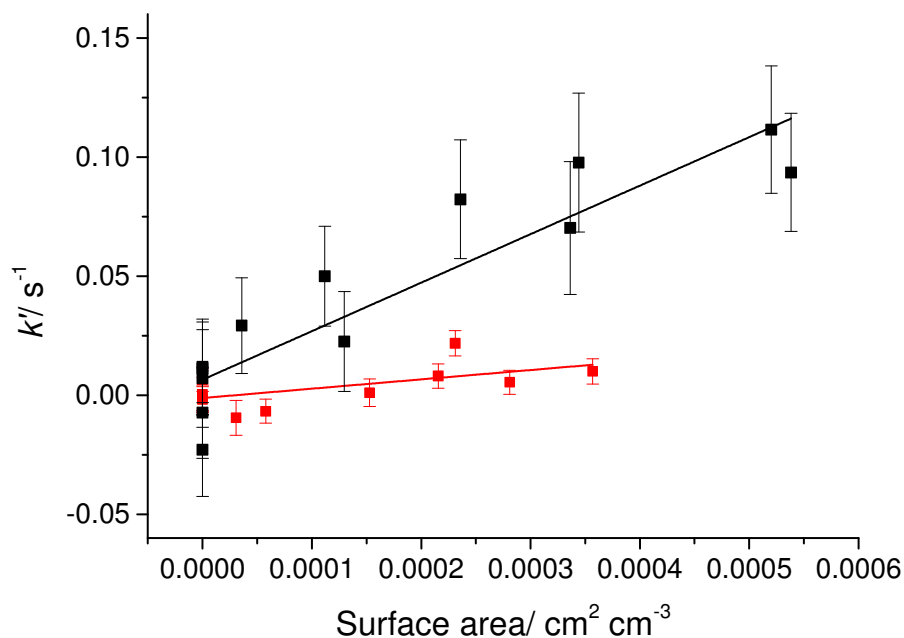


Figure 6.4: Examples of the pseudo first order rate constant as a function of aerosol surface area for aqueous ammonium nitrate aerosols at 263 K and 69 % RH (black points) and 312 K and 17 % RH (red points). The error bars represent one standard deviation. The gradients of the graphs were 207 ± 45 and $46 \pm 27 \text{ s}^{-1} \text{ cm}^{-2} \text{ cm}^3$ which yielded HO₂ uptake coefficients of 0.020 ± 0.004 and 0.004 ± 0.002 for 263 K and 312 K respectively. A correction was made to the surface area to account for the humidity in the DMA being different to the relative humidity in the flow tube as described in Section 2.12.1.

Temperature/ K	Uptake coefficient	Average initial HO ₂ concentration/ molecule cm ⁻³	Average HO ₂ concentration at 40 cm	Average relative humidity in the flow tube/ %
312	0.005 ± 0.002	4.7 × 10 ⁸	2.3 × 10 ⁸	18
302	0.007 ± 0.002	9.7 × 10 ⁸	5.0 × 10 ⁸	36
292	0.005 ± 0.001	1.3 × 10 ⁹	9.1 × 10 ⁸	45
284	0.007 ± 0.003	1.2 × 10 ⁹	5.2 × 10 ⁸	50
275	0.010 ± 0.002	6.1 × 10 ⁸	2.6 × 10 ⁸	52
263	0.016 ± 0.005	3.8 × 10 ⁸	1.3 × 10 ⁸	53

Table 6.2: The HO₂ uptake coefficient onto aqueous ammonium nitrate aerosols over a range of temperatures and at atmospheric pressure. The errors represent two standard deviations.

Ideally, the conditions for all of the experiments would have remained constant. However, as shown in Table 6.2 this was not the case. The humidity varied due to the different temperatures in the flow tube. At lower temperatures the relative humidity would be much higher in the flow tube compared to the DMA whereas at higher temperatures the humidity in the flow tube was lower than in the DMA. For example, a relative humidity of 18 % in the flow tube at 312 K would mean a relative humidity of 54 % in the DMA that was at 293 K. If the relative humidity had been increased to 33 % then this would have led to a relative humidity of 100 % in the DMA which would have made measuring the aerosol surface distribution impossible. Unfortunately, it was also not possible to decrease the humidity at the lower temperatures as the HO₂ production methodology involved the photolysis of water vapour which led to higher relative humidities at lower temperatures. To reduce the relative humidity coming out of the injector would have led to lower HO₂ concentrations hence low signals that were too low to perform an experiment.

It was also difficult to keep the initial HO₂ concentration constant. At lower temperatures much less HO₂ exited the injector. This may be due to the rate coefficient of the HO₂ self-reaction increasing, the loss to the injector walls increasing and a decrease in the absolute

water vapour concentrations. In order to be able to directly compare the measurements at the highest and lowest temperatures, the current to the UV lamp in the injector at 312 K was decreased in order to decrease the HO₂ concentration to be similar to the HO₂ concentration at 263 K.

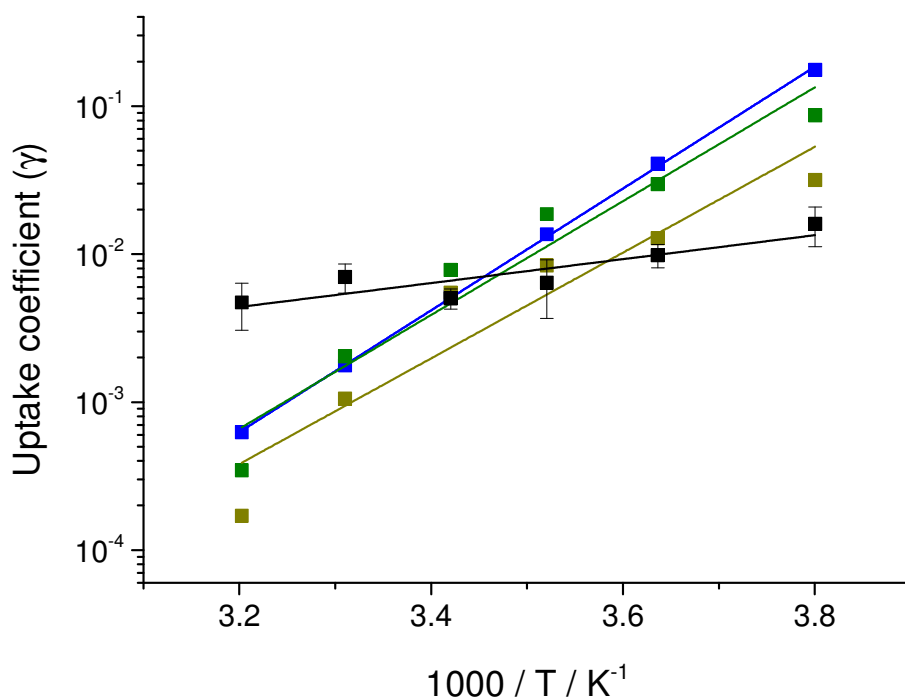


Figure 6.5: The average HO₂ uptake coefficients of several determinations measured in this work onto aqueous ammonium nitrate aerosols as a function of temperature (black points). The error bars represent two standard deviations of the averaged data. The Thornton et al. (2008) model (equation 1.18 in Section 1.13.3) expected uptake coefficient onto the aqueous aerosols assuming an average aerosol diameter of 100 nm and an aerosol pH of 5.5 over a range of temperatures and with a constant HO₂ concentration of 8.4×10^8 molecule cm⁻³ (blue points), at the initial HO₂ concentrations measured in this work (green points) and at the HO₂ concentrations measured at 40 cm along the flow tube (dark yellow points). See Table 6.2 for specific HO₂ concentrations.

Figure 6.5 shows that the HO₂ uptake coefficient measured in this work increased with decreasing temperature from 0.005 ± 0.002 at 312 K to 0.016 ± 0.005 at 263 K. However, the Thornton et al. (2008) model, shown by equation 1.18 in Section 1.13.3, predicts a change in the uptake coefficient of more than two orders of magnitude (from 0.18 to 0.0006 between 263 K and 312 K) if an aerosol pH of 5.5 is estimated and the HO₂ concentration is set to 8.4

$\times 10^8$ molecule cm^{-3} (the average initial HO_2 concentration in this work). However, as the HO_2 concentration was not constant in this work, the initial HO_2 concentrations measured in this work were also inputted into the model as well as the HO_2 concentrations measured at 40 cm along the flow tube. The model results are shown in Figure 6.5 and show that if the actual HO_2 concentrations used in our experiments are inputted the HO_2 uptake coefficient will change by slightly less than if the HO_2 concentration is kept constant. However, the change in the HO_2 uptake coefficient still changes by about two orders of magnitude between 263 K and 312 K which is a much larger change than observed in this work. Several possible explanations for the differences between the results obtained in this work and predicted by the Thornton et al. (2008), are explored below.

The copper (I and II) and iron (II and III) concentrations in the atomiser solutions for all experiments were measured using ICP-MS and it was found that for all of the solutions the copper (I and II) and iron (II and III) concentrations were less than 5 ppb. An individual analysis of each experiment using equation 3.1 in Section 3.4, showed that the estimated copper molarity in the aerosols was always less than 5×10^{-5} M for both copper (I and II) and iron (II and III) over the range of temperatures and humidities. The observed uptake coefficients should therefore not be affected by these levels of trace metals as was demonstrated in Section 3.5, and trace metals can be ruled as an explanation for the difference between the measurements in this work and predicted by the Thornton et al. (2008) model.

It should be noted that the different average relative humidities could have also affected the HO_2 uptake coefficients. At higher relative humidities, the aerosols would have a higher water content than at low relative humidities. As discussed previously in Sections 4.3 and 5.4 the HO_2 uptake coefficient may be dependent upon the liquid water content of the aerosol with higher uptake coefficients at higher liquid water contents. The higher water content of the aerosol at higher relative humidities would also lead to more dilute ammonium nitrate, which is a weak acid, and therefore to less acidic aerosols. As discussed in Section 3.6, it is expected that at higher pH the uptake coefficient would increase. The increase in the radius of the aerosol would be expected to have a negligible effect on the HO_2 uptake coefficient as investigated in Section 3.7. However, the fact that at higher relative humidity the uptake

coefficient should increase cannot explain the discrepancy between the Thornton et al. (2008) model and the HO₂ uptake coefficients measured in this work. In order to explain the difference at higher relative humidities the uptake coefficient would have needed to decrease.

One possible reason for the discrepancy between the HO₂ uptake coefficients measured in this work and modelled by Thornton et al. (2008) is the uncertainty in the HO₂ Henry's law coefficient. This was briefly discussed in Section 3.5 and also earlier in this section. If the Henry's law coefficient did not increase to the extent predicted by Thornton et al. (2008) with decreasing temperature, then it would be expected that between 312 and 263 K the uptake coefficient would decrease by a smaller amount. Similarly, if the rate constants of the reactions had a larger dependence on the temperature a smaller decrease in the HO₂ uptake coefficient between 312 and 263 K would be expected.

Another possible reason for the discrepancy between the HO₂ uptake coefficient measurements made in this work and predicted by Thornton et al. (2008) is the release of hydrogen peroxide from the injector reforming HO₂ in the aerosols via the Fenton reactions. This was previously discussed in Section 3.10. At lower temperatures it might be expected that there would be a greater HO₂ self-reaction in the gas phase in the injector. Therefore, it would be predicted that at the lowest temperature there would be the most hydrogen peroxide whereas at the highest temperature there would be the least hydrogen peroxide exiting the injector. If the hydrogen peroxide was then converted to HO₂ within the aerosol, the observed uptake coefficient would be reduced with the biggest reduction occurring at the highest HO₂ concentrations (and the highest temperatures). However, there are currently no measurements of the hydrogen peroxide concentration exiting the injector at different temperatures, and therefore it would currently be difficult to model this. In Chapter 8 the HO₂ uptake coefficients are modelled using the KM-SUB model to show the effect of different hydrogen peroxide experiments that were performed at room temperature.

6.4 Measurements of HO₂ uptake coefficients onto copper doped ammonium nitrate aerosols over a range of temperatures

The mass accommodation of different species onto aerosols is expected to be dependent upon temperature with higher mass accommodations at higher temperatures as explained below. Jayne et al. (1991) derived the temperature dependence of the mass accommodation (Equation 6.9) using Equations 6.6 – 6.8 shown below. The mass accommodation can be split into a thermal adsorption term and a solvation term (as discussed in 1.8.1.3). However, an assumption can be made that the thermal accommodation is equal to one, and therefore only the solvation into the bulk needs to be considered (Nathanson et al., 1996; Pöschl et al., 2007). The maximum flux of the gas species into the aerosol is equal to the net flux of the incoming and outgoing fluxes into the aerosol as shown below:

$$\frac{\alpha n_g \omega}{4} = \frac{n_g \omega}{4} - n_s k_d \quad (\text{E6.6})$$

where α is the mass accommodation, n_g is the gas phase concentration of the species, n_s is the concentration of the surface adsorbed species, ω is the average molecular speed of the species and k_d is the rate coefficient of desorption from the surface of the aerosol. If the net flux of the incoming gas phase species is equal to the flux into the liquid phase then:

$$\frac{\alpha n_g \omega}{4} = n_s k_{sol} \quad (\text{E6.7})$$

where k_{sol} is the rate coefficient of solvation (the transfer of the species from the surface into the bulk of the aerosol). Equations 6.6 and 6.7 can then be combined to give:

$$\alpha = \frac{k_{sol}}{k_{sol} + k_d} \quad (\text{E6.8})$$

Equation 8 can then be written in terms of a Gibbs free energy (Jayne et al., 1991):

$$\frac{\alpha}{1 - \alpha} = \frac{k_{sol}}{k_d} = \exp \left(-\frac{\Delta G^\ddagger_{obs}}{RT} \right) \quad (\text{E6.9})$$

where k_{sol}/k_d is the equilibrium constant between the species in the solvated aqueous phase and the gaseous phase, R is the gas constant, T is the temperature and ΔG^\ddagger_{obs} is the Gibbs free energy barrier of the transition state between the gaseous and solvated phases given by:

$$\Delta G^\ddagger_{obs} = \Delta H^\ddagger_{obs} - T\Delta S^\ddagger_{obs} \quad (\text{E6.10})$$

where ΔH^\ddagger_{obs} is the change in enthalpy and ΔS^\ddagger_{obs} is the change in entropy.

Nathanson et al. (1996) suggested a new model to explain ΔG^\ddagger_{obs} which is based on classical nucleation theory. An incoming gas molecule would strike the surface of the aerosol and would then become a loosely bound species (n_s). These loosely bound species could then become more tightly bound, forming aggregates or clusters (n^*_s), which are more liquid-like than the more loosely bound molecules. It would be expected that clusters below a critical size (N^*) would fall apart whereas larger clusters would continue to grow until they merge into the aerosol bulk. The energy difference (ΔG^\ddagger_{obs}), which is related to the mass accommodation via Equation 6.9, can be given by the difference in the free energy of the vapour (ΔG_{vap}) and the critical cluster (ΔG^*_s) as shown in Figure 6.6.

Several studies have studied the changing mass accommodation with changing temperature. Griffiths and Cox (2009) measured $\Delta H^\ddagger_{obs} = -33 \text{ kJ mol}^{-1}$ and $\Delta S^\ddagger_{obs} = -152 \text{ J K}^{-1} \text{ mol}^{-1}$ for the enthalpy and entropy of accommodation for uptake of N_2O_5 onto aqueous ammonium sulphate. Another example is hydrogen peroxide where Worsnop et al. (1989) measured $\Delta H^\ddagger_{obs} = -23 \text{ kJ mol}^{-1}$ and $\Delta S^\ddagger_{obs} = -94 \text{ J K}^{-1} \text{ mol}^{-1}$ onto water using a droplet train flow reactor. Similar values of ΔH^\ddagger_{obs} and S^\ddagger_{obs} have also been observed for a variety of organic species onto water surfaces (Davidovits et al., 2006). However, the magnitude of ΔH^\ddagger_{obs} and ΔS^\ddagger_{obs} for radical species is currently unknown (Davidovits et al., 2006).

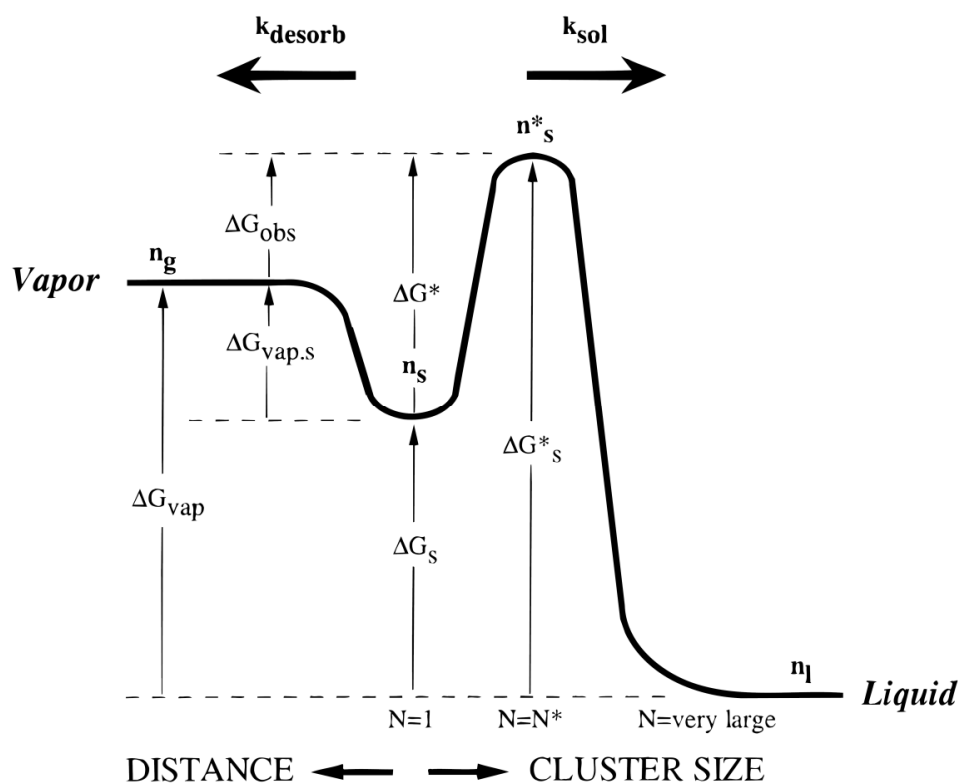


Figure 6.6: The free energy diagram first postulated by Nathanson et al. (1996) for the liquid vapour interface. This figure is reproduced with permission from Nathanson et al. (1996).

In this work, HO_2 uptake coefficients were measured onto copper-doped ammonium nitrate aerosols over a temperature range of 263 to 312 K. However, at 302 and 312 K the aerosols were effloresced, as determined by recording a humidogram (shown in Section 2.6.2) which showed that at 302 and 312 K the radius of the aerosols were approximately 50 % smaller than the average radius at other temperatures. At temperatures lower than 263 K there was not enough HO_2 signal to do an experiment. Therefore, unfortunately it was only possible to measure mass accommodation values between 263 and 292 K. Examples of the pseudo-first order rate constants as a function of aerosol surface area at 263 and 292 K are shown in Figure 6.7. The measured HO_2 mass accommodation values between 263 and 292 K are summarised in Table 6.3.

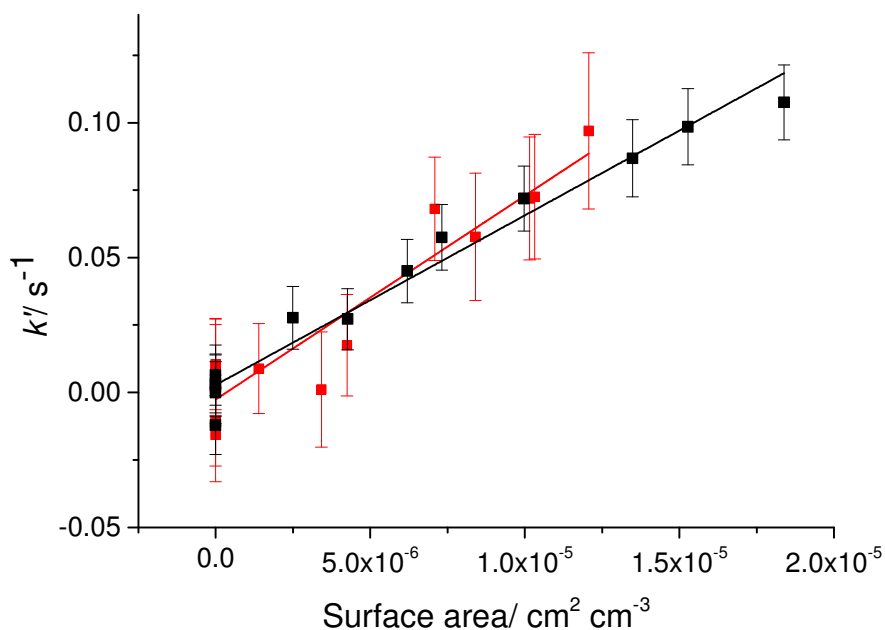


Figure 6.7: Examples of the pseudo-first order rate constant as a function of aerosol surface area for aqueous copper doped ammonium nitrate aerosols at 263 K and 38 % RH (red points) and 292 K and 50 % RH (red points). The aerosol copper (II) concentration was estimated as ~ 0.7 M. The gradients of the graphs were $(7600 \pm 1400) \text{ s}^{-1} \text{ cm}^{-2} \text{ cm}^{-3}$ and $(6300 \pm 800) \text{ s}^{-1} \text{ cm}^{-2} \text{ cm}^{-3}$, which yielded HO_2 uptake coefficients of 0.80 ± 0.07 and 0.61 ± 0.07 for 263 K and 292 K respectively. Although, the gradients of the two graphs were similar and within error, the differences in the HO_2 thermal molecular speed and the gas phase diffusion coefficient of HO_2 meant that the uptake coefficients were not within error (see Section 2.8).

Temperature/ K	Uptake coefficient	Average initial HO ₂ concentration/ molecule cm ⁻³	Average relative humidity in the flow tube/ %
292	0.62 ± 0.05	1.2 × 10 ⁹	33
284	0.71 ± 0.03	1.3 × 10 ⁹	33
275	0.65 ± 0.03	9.7 × 10 ⁸	42
263	0.71 ± 0.06	6.1 × 10 ⁸	43

Table 6.3: The HO₂ mass accommodation onto aqueous copper-doped ammonium nitrate aerosols over a range of temperatures and at atmospheric pressure. The aerosol copper (II) concentration was estimated as ~ 0.7 M. The errors represent two standard deviations.

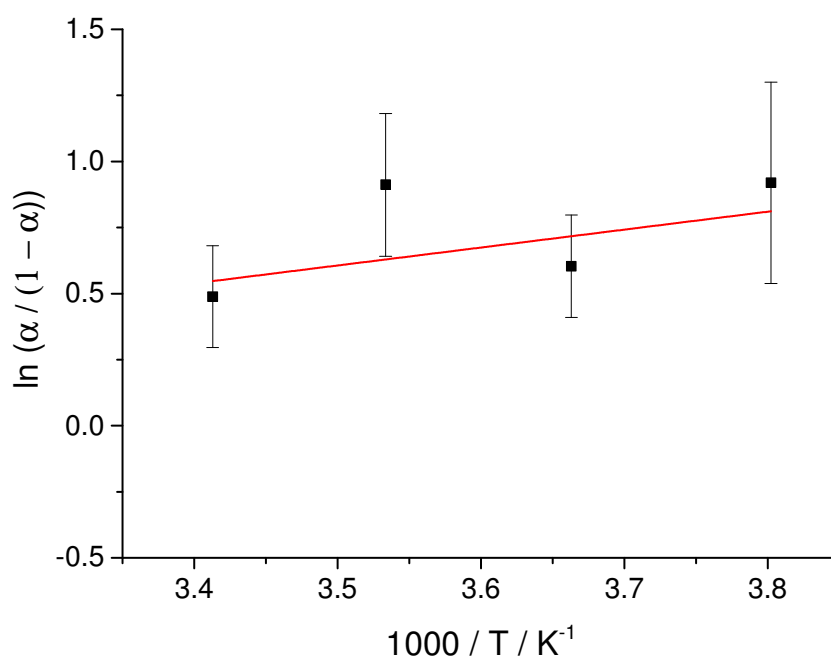


Figure 6.8: $\ln (\alpha / (1 - \alpha))$ as a function of $1000 / T$ for copper doped ammonium nitrate aerosols. The error bars represent two standard deviations. The gradient of the graph was 680 ± 790 K and the intercept was -1.8 ± 2.8 .

The gradient of the graph of $\ln(\alpha / (1-\alpha))$ plotted against $1 / T$ gave a gradient of (680 ± 790) K and an intercept of (-1.8 ± 2.8) (Figure 6.8). The gradient and intercept allowed values of ΔH^\ddagger_{obs} and ΔS^\ddagger_{obs} of (-5600 ± 6600) J mol⁻¹ and (-15 ± 23) J K⁻¹ mol⁻¹ to be calculated, respectively. However, ideally more temperatures would have been studied in order to reduce the error on these measurements, as currently the errors are larger than the actual values. It should also be noted that, similarly to ammonium nitrate aerosols, the results might have been affected by the different experimental conditions.

The different average relative humidities of the experiments would lead to different liquid water contents of the aerosols that could affect the rate of the HO₂ catalytic reaction with copper. The different relative humidities would also affect the concentration of the copper in the aerosol. For example, it can be estimated that at 292 K and 33 % RH the copper molarity in the aerosol would be ~ 0.8 M. The copper molarity in the aerosol at 263 K and 43 % RH was also estimated to be ~ 0.8 M. Both of these copper molarities would lead to HO₂ lifetimes of less than one nanosecond once it had accommodated. Therefore, it is unlikely that the 10 % change in relative humidity has an impact on the HO₂ mass accommodation.

Unlike the HO₂ uptake coefficients onto undoped ammonium nitrate aerosols, the HO₂ mass accommodation should not vary with varying HO₂ concentrations as the catalytic destruction of HO₂ is a first order reaction in terms of HO₂. However, as previously discussed in Section 3.11 an apparent HO₂ concentration dependence has been observed for copper-doped aerosols. Therefore, it could be hypothesised that although the HO₂ concentration does not affect the mass accommodation, the different hydrogen peroxide concentrations exiting the injector for different HO₂ concentrations could potentially affect the observed mass accommodation. At higher hydrogen peroxide concentrations there would be a greater reformation of HO₂ in the aerosol from the Fenton reactions, and therefore a smaller observed HO₂ uptake coefficient. At lower temperatures it might be expected that more hydrogen peroxide would exit the injector (hence the greatest reformation of HO₂ in the aerosol) and that this would mean the largest decrease in the observed HO₂ concentrations would occur at the lowest temperatures. If this were the case, the gradient of the graph in Figure 6.8 would increase at low temperatures leading to a greater value of ΔH^\ddagger_{obs} . The intercept would also change, although the extent of this would depend on the extent to which the hydrogen

peroxide was affecting the results. However, hydrogen peroxide measurements exiting the injector at different temperatures are required in order to test this hypothesis.

6.5 Atmospheric Implications

In order to estimate the impact that decreasing temperatures would have on tropospheric HO₂ gas phase concentrations, the Cape Verde model that was described in Section 2.14 was run. The largest HO₂ uptake coefficient measured onto effloresced salt was 0.004 ± 0.003 at 314 K. This HO₂ uptake coefficient would lead to a decrease in atmospheric HO₂ concentrations from 1.75×10^8 molecule cm⁻³ to 1.74×10^8 molecule cm⁻³ or a decrease of 0.19% assuming a typical aerosol surface to volume concentration of 1×10^{-6} cm² cm⁻³ (Allan et al., 2009). At lower temperatures, smaller HO₂ uptake coefficients were measured which would lead to a lower impact upon tropospheric HO₂ gas phase concentrations. However, as discussed in Section 6.2, the observed decrease in the uptake coefficient may be due to the higher humidities of the experiments with water blocking the reactive sites on the surface of the effloresced salts. Therefore, at low temperatures and low relative humidities, the uptake coefficient could potentially be larger, but these conditions were not studied owing to HO₂ signals being too small.

An increase in the HO₂ uptake coefficient was observed for aqueous ammonium nitrate aerosols from 0.005 ± 0.002 to 0.016 ± 0.005 between 312 to 263 K. The impact on gas phase HO₂ concentrations for a HO₂ uptake coefficient of 0.004 and 0.018, and with the temperature in the model set to 312 and 263 K respectively, would be to decrease the HO₂ gas phase concentration by 0.19 % and 1.01 % for an aerosol surface to volume concentration of 1×10^{-6} cm² cm⁻³ compared to if no aerosols were present. The prediction by Thornton et al. (2008) of an uptake coefficient of 0.049 at 263 K, an aerosol pH of 5.5, 100 nm diameter aerosols and a HO₂ concentration of 2×10^8 molecule cm⁻³ would decrease the HO₂ gas phase concentration by 2.7 % which is larger than the decrease in this work. Finally, the HO₂ mass accommodation increased slightly in this work from 0.62 ± 0.05 to 0.71 ± 0.06 between 292 and 263 K. These HO₂ uptake coefficients would decrease the HO₂ gas phase concentrations

by 23 % and 28 % respectively, but would require an aerosol containing a high concentration of copper ions.

Overall, it has been shown that the HO₂ uptake coefficient is dependent upon temperature and could potentially have a larger effect on the HO₂ gas phase concentrations at low temperatures. The HO₂ uptake coefficient dependence upon temperature could help to explain the discrepancies between HO₂ field measurements at low temperatures and model predictions. For example, Mao et al. (2010) made HO₂ measurements during the ARCTAS field campaign and observed a larger discrepancy occurring at the lowest temperatures of 226 K. However, as discussed previously, in this work, the decreasing HO₂ concentrations at lower temperatures and the potentially larger hydrogen peroxide exiting the injector may have been decreasing the observed HO₂ uptake coefficient at low temperatures. More work would be needed in order to be able to accurately determine the HO₂ uptake coefficients, and how they are affected by different hydrogen peroxide concentrations. This will be investigated at room temperature using the KM-SUB model in Chapter 8. Once the effect of hydrogen peroxide upon HO₂ uptake coefficients is better understood, and hydrogen peroxide measurements have been made at different temperatures in the flow tube, the laboratory studies would be able to more accurately related to tropospheric measurements.

6.6 Summary

The first temperature dependent measurements of the HO₂ uptake coefficient onto effloresced sodium chloride and ammonium sulphate aerosols and deliquesced ammonium nitrate and copper-doped ammonium nitrate have been reported in this work. The HO₂ uptake coefficients onto effloresced sodium chloride and ammonium sulphate aerosols varied from 0.004 ± 0.002 to 0.000 ± 0.002 and 0.002 ± 0.003 , respectively, between 314 and 263 K. However, Remorov et al. (2002) and Loukhovitskaya et al. (2009) measured increases in the HO₂ uptake coefficient onto solid sodium chloride surfaces with decreasing temperature. Remorov et al. (2002) and Loukhovitskaya et al. (2009) parameterised the HO₂ uptake coefficient as increasing from 0.008 to 0.021 and from 0.0009 to 0.007 respectively between 314 and 263 K. One of the possible reasons for the larger HO₂ uptake coefficients observed

by Remorov et al. (2002) and Loukhovitskaya et al. (2009) was the low relative humidity (0%) used by these groups compared to the higher relative humidities (9 – 62 %) used in this work. The water molecules could potentially be binding to the active sites on the sodium chloride surface making them unavailable to HO₂. This could also explain the smaller HO₂ uptake coefficients measured at lower temperatures in this work as at the lower temperatures the relative humidity, and hence the water surface coverage, was higher.

The HO₂ uptake coefficient onto deliquesced ammonium nitrate aerosols was measured as significantly increasing from 0.004 ± 0.002 to 0.018 ± 0.006 between 312 K and 263 K. The HO₂ uptake coefficient into aqueous aerosols was expected to be temperature dependent due to the Henry's law coefficient increasing with decreasing temperature. Therefore, at lower temperatures there would be more HO₂ in the bulk of the aerosol and therefore a greater loss of HO₂ due to self-reaction. However, although an increase in the HO₂ uptake coefficient was observed, the Thornton et al. model predicted that between 312 K and 263 K the HO₂ uptake coefficient should have changed by approximately two orders of magnitude which was a much larger change than measured in this work. There are a couple of possible reasons for this discrepancy. First, the uncertainty in the Henry's law constant dependence upon temperature is large. If the change in the Henry's law coefficient was smaller over a range of temperatures the HO₂ uptake coefficients would not increase by the two orders of magnitude between 312 and 263 K predicted by Thornton et al. (2008) and the increase could potentially be similar to the measurements made in this work. Secondly, if there was more hydrogen peroxide exiting the injector at lower temperatures due to a faster HO₂ self-reaction rate in the gas phase, the measurements made in this work could be affected. If more hydrogen peroxide were exiting the injector, there could potentially be more reformation of HO₂ in the aerosols via the Fenton reactions. The HO₂ could then partition to the gas phase and decrease the observed HO₂ uptake coefficient. However, there are currently no measurements of how the hydrogen peroxide concentrations exiting the injector vary with temperature. Future work measuring H₂O₂ concentrations exiting the injector and along the flow tube would be highly beneficial.

The HO₂ mass accommodation onto deliquesced copper-doped ammonium nitrate aerosols measured as varying from 0.62 ± 0.05 to 0.71 ± 0.06 between 292 K and 263 K. The mass

accommodation was expected to be temperature dependent due to the Gibbs free energy barrier of the transition state between the gaseous and solvated phases being temperature dependent. However, although a small increase in the mass accommodation was observed at lower temperatures, ΔH_{obs} and ΔS_{obs} were calculated as $(-5600 \pm 6600) \text{ J mol}^{-1}$ and $(-15 \pm 23) \text{ J K}^{-1} \text{ mol}^{-1}$ respectively from the mass accommodation measurements. The large error bars were due to measurements being made at only four temperatures owing to efflorescence of the aerosols, as indicated by the large reduction in the radius of the aerosols. It should also be noted that, again, hydrogen peroxide exiting the injector could also have potentially affected these results.

The increasing HO_2 uptake coefficient with decreasing temperature observed in this work for deliquesced aerosols could help to explain the discrepancy between field measurements and modelled HO_2 concentrations at low temperatures. For example, Mao et al. (2010) observed the largest discrepancies between predicted and observed HO_2 concentrations at the lowest temperatures during the ARCTAS field campaign. However, more laboratory measurements would be needed in order to understand to what extent the changing relative humidity and the hydrogen peroxide in the flow tube were affecting the laboratory results, in order to better understand the mechanism and apply it to field campaigns. The relative humidity could be better controlled in the flow tube if all of the equipment was at the same temperature and there was therefore no issue with aerosols deliquescing or efflorescing in the DMA. If all of the equipment were at the same temperature this would also allow a range of aerosols to be studied, and would allow the copper-doped ammonium nitrate aerosols to be studied over a larger range of temperatures.

Chapter 7: Measurements of the HO₂ uptake coefficient onto dust aerosols at room temperature

7.1 The importance of dust aerosols in the troposphere

Mineral dust has an estimated flux of 2000 Tg year⁻¹ into the atmosphere making it one of the most abundant aerosols in the troposphere (Textor et al., 2006). It is formed by wind erosion over soils and deserts, and is therefore mainly composed of mineral oxides and carbonates found in the Earth's crust. The main removal path of mineral dust is dry deposition and it has an average lifetime of approximately four days, which allows it to be carried thousands of kilometres from its sources, notably the North African and Asian deserts (Textor et al., 2006). Although mineral dust is extremely important for radiative forcing, visibility and air quality, it has also been shown to provide an active surface for heterogeneous chemistry (Dentener et al., 1996; Seinfeld and Pandis, 2006). For example, McNaughton et al. (2009) made measurements of dust and NO_y (NO, NO₂, HNO₃, peroxy nitrates and alkyl- and hydroxyalkyl nitrates) concentrations in the spring of 2006 over Mexico and the Eastern North Pacific. McNaughton et al. (2009) measured that without dust NO_y accounted for more than 85 % of the total nitrogen, whereas when dust exceeded 10 μg m⁻³, NO_y only accounted for 60 - 80% of total nitrogen due to heterogeneous reaction on the surface of the dust.

The majority of HO₂ uptake coefficient measurements performed in this work were made using Arizona Test Dust (ATD, 0 – 3 μm, Powder Technology Inc.). ATD contains many of the same minerals as naturally occurring mineral dust and consists of SiO₂ (68-76%), Al₂O₃ (10-15%), Fe₂O₃ (2-5%), Na₂O (2-4 %), CaO (2-5%), MgO (1-2%), TiO₂ (0.5-1.0%) and K₂O (2-5%) (Karagulian et al., 2006). Although the mineralogy of ATD is different to Saharan dust, previous uptake coefficient measurements onto both types of dust have yielded almost identical values for NO₂ and NO₃, whereas the uptake coefficients for N₂O₅ and HNO₃ have been a factor of 1.5 to 2 higher for Saharan dust (Crowley et al., 2010; Tang et al., 2014). ATD was chosen in this work rather than Saharan dust due to its availability, and its smaller size distribution which reduces the risk of dust deposition along the flow tube.

There is currently only one study that has measured HO₂ uptake onto ATD surfaces but no studies exist onto any other types of dust or onto aerosols rather than surfaces (Bedjanian et al., 2013). Therefore, in this work HO₂ uptake coefficient measurements were made onto ATD aerosols over a range of humidities and HO₂ concentrations. HO₂ uptake coefficients were also measured onto a proxy for cosmic dust aerosols (FeMgSiO₄) for comparison purposes to ATD.

7.2 Measurements of the HO₂ uptake coefficient onto ATD aerosols

The HO₂ uptake coefficients were measured in this work over a range of relative humidities (6 – 76 %) and at two different initial HO₂ concentrations ($\sim 1 \times 10^9$ molecule cm⁻³ and $\sim 3 \times 10^8$ molecule cm⁻³). The time dependence of the uptake coefficient was also investigated. Examples of the raw data obtained in this work are shown in Figure 7.1, and the experimental methodology and data analysis for these experiments is described in detail in Chapter 2. The surface area of one aerosol (A_d) was obtained using the dust size distributions shown by Figure 2.12 in Section 2.6.1 as being 9.4×10^{-9} cm² for ATD using the methodology also described in Section 2.6.1. The methodology to obtain the graphs of $0.25\gamma\omega A_d t$ as a function of time shown in Figure 7.1 was described in Section 2.10 where more raw data (including an example of the anticorrelation between the HO₂ signal and the aerosol number concentration and pseudo first order decays) are also shown.

The measurements of the HO₂ uptake coefficient onto ATD aerosols measured in this work and published in the literature are shown in Table 7.1. There are several differences in the experimental methodology used in this work and the work by Bedjanian et al. (2013). Bedjanian et al. (2013) used an injector coated with ATD, whereas in this work aerosols were used. Bedjanian et al. (2013) also measured initial HO₂ uptake coefficients (i.e. the uptake coefficient onto fresh ATD before the uptake coefficient starts to drop due to surface deactivation), whereas in this work uptake coefficients were measured between $\sim 7 - 24$ seconds. The method of HO₂ formation was also different. In this work, HO₂ was formed by the photolysis of water vapour whereas Bedjanian et al. (2013) either reacted F atoms with hydrogen peroxide or reacted Cl atoms with methanol as shown in Reactions 7.1 – 7.3.

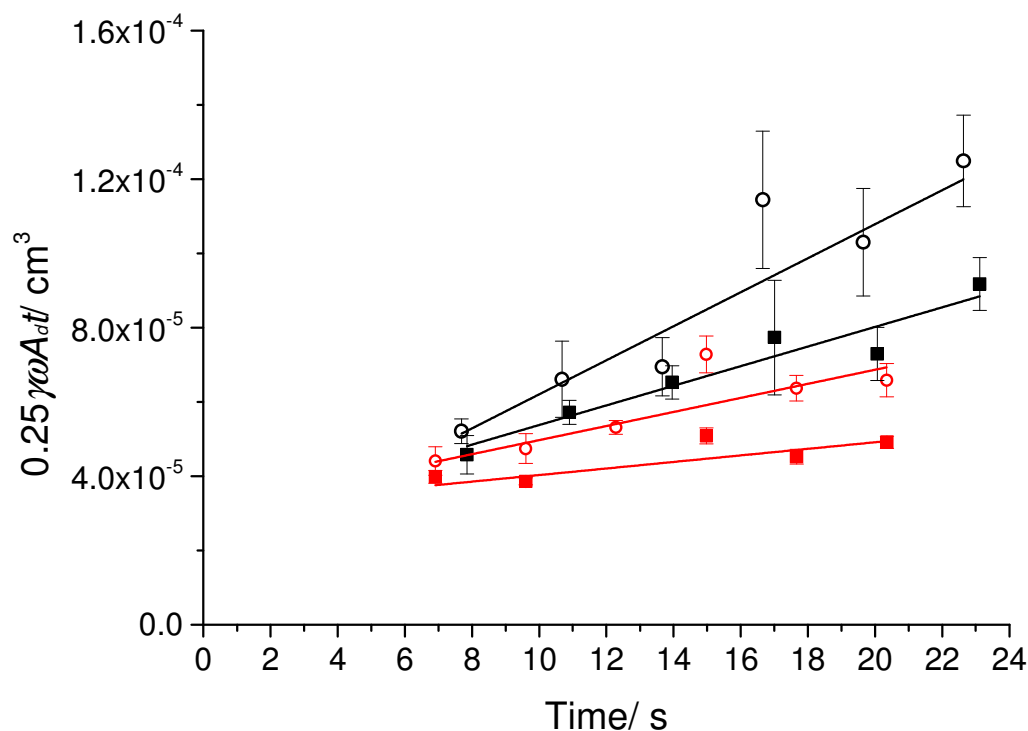


Figure 7.1: Examples of $0.25\gamma\omega A_d t$ as a function of time at initial HO_2 concentrations of $\sim 1 \times 10^9$ molecule cm^{-3} (red points) and $\sim 3 \times 10^8$ molecule cm^{-3} (black points) and at 10% RH (closed symbols) and 70 % RH (open symbols).

Finally, it should be noted that Bedjanian et al. (2013) measured HO_2 uptake coefficients using the Brunauer–Emmett–Teller (BET) surface area whereas in this work spherical aerosols were assumed in order to calculate the surface area. The BET surface area is the specific or true surface area of the dust and assumes that multi-layer adsorption of a species can occur on a surface or aerosol. The specific surface area can be measured by the physical adsorption of a gas onto the solid of a surface. The partial pressure of the adsorbing gas is varied and the volume of the adsorbed gas is measured, allowing the amount of adsorbate gas corresponding to a monolayer to be calculated and hence a specific surface area to be measured. However, atmospheric models do not utilise a BET surface area as this is usually

not available, and for this reason, an uptake coefficient onto a geometric surface area is a more useful parameter for modellers even though it may not represent the actual surface area. It is also extremely difficult to estimate the BET surface area of aerosols as this may be different to the BET surface area of the dust placed into the dust disperser. Therefore, in this work spherical particles were assumed and measurements of the surface area were made using an SMPS and APS as discussed in Section 2.6.1. However, a rough calculation of the difference in estimating spherical particles compared to using BET surface areas is made below.

By assuming a spherical geometry of the aerosols, the HO₂ uptake coefficient was overestimated compared to if the true surface area had been used. No assumption was made during the data analysis in this work as to whether monolayer or multilayer adsorption was possible and therefore this is not taken into consideration in the following calculation. In Section 2.6.1 the average radius of the ATD aerosols was calculated as being 273 nm. When assuming spherical particles (as measured by the SMPS and APS) on average each particle had a surface area of $9.4 \times 10^{-13} \text{ m}^2$ and the volume of one particle was $8.5 \times 10^{-14} \text{ cm}^3$. By assuming a density of ATD to be 2.7 g cm^{-3} , the mass of each particle would be equivalent to 2.3×10^{-13} grams. This would then produce a BET surface area of $2.0 \times 10^{-11} \text{ m}^2$ per particle if an assumption is made that the BET surface area measured by Bedjanian et al. (2013) onto ATD surfaces was the same as the BET surface area of the ATD aerosols in this work. Bedjanian et al. (2013) stated that the BET surface area of ATD was $85 \pm 10 \text{ m}^2 \text{ g}^{-1}$. By assuming spherical particles the volume would have been overestimated, which means that this number would be an upper estimate. However, this would lead to a surface area approximately 20 times larger than when assuming spherical particles (when measuring using an SMPS and APS) and therefore the HO₂ uptake coefficient would be approximately 20 times smaller. If this were the case the uptake coefficients would be similar to those measured for the solid salts in Chapter 3 of < 0.004 . However, in the following sections the HO₂ uptake coefficient will be reported assuming spherical particles.

Relative humidity/ %	Initial HO ₂ concentration / molecule cm ⁻³	Temperature / K	Uptake coefficient	Reference
7	$\sim 3 \times 10^8$	293 ± 2	0.022 ± 0.003	Matthews et al. (2014) (this work)
31	$\sim 3 \times 10^8$	293 ± 2	0.046 ± 0.009	Matthews et al. (2014) (this work)
53	$\sim 3 \times 10^8$	293 ± 2	0.028 ± 0.006	Matthews et al. (2014) (this work)
71	$\sim 3 \times 10^8$	293 ± 2	0.044 ± 0.007	Matthews et al. (2014) (this work)
7	$\sim 1 \times 10^9$	293 ± 2	0.008 ± 0.002	Matthews et al. (2014) (this work)
33	$\sim 1 \times 10^9$	293 ± 2	0.026 ± 0.002	Matthews et al. (2014) (this work)
51	$\sim 1 \times 10^9$	293 ± 2	0.019 ± 0.003	Matthews et al. (2014) (this work)
73	$\sim 1 \times 10^9$	293 ± 2	0.030 ± 0.006	Matthews et al. (2014) (this work)
0	0.35×10^{12}	300	0.067 ± 0.004	Bedjanian et al. (2013)
0	3.30×10^{12}	300	0.067 ± 0.004	Bedjanian et al. (2013)
10	$\sim 10^{12}$	300	0.038 ± 0.005	Bedjanian et al. (2013)
30	$\sim 10^{12}$	300	0.019 ± 0.004	Bedjanian et al. (2013)
65	$\sim 10^{12}$	300	0.009 ± 0.002	Bedjanian et al. (2013)
95	$\sim 10^{12}$	300	0.007 ± 0.001	Bedjanian et al. (2013)

Table 7.1: The HO₂ uptake coefficients onto Arizona Test Dust aerosols measured in this work and published in the literature for ATD coated solid surfaces at different relative humidities, initial HO₂ concentration and temperatures.

7.3 The HO₂ uptake coefficient onto ATD aerosols as a function of relative humidity

The results of the HO₂ uptake coefficient measurements assuming spherical particles over a relative humidity range of 5 – 76 % and at initial HO₂ concentrations of 1×10^9 molecule cm⁻³ are shown in Figure 7.2. Figure 7.2 shows that the measured HO₂ uptake coefficient onto ATD increases with humidity from 0.008 ± 0.002 to 0.030 ± 0.006 between 6 and 73 % RH.

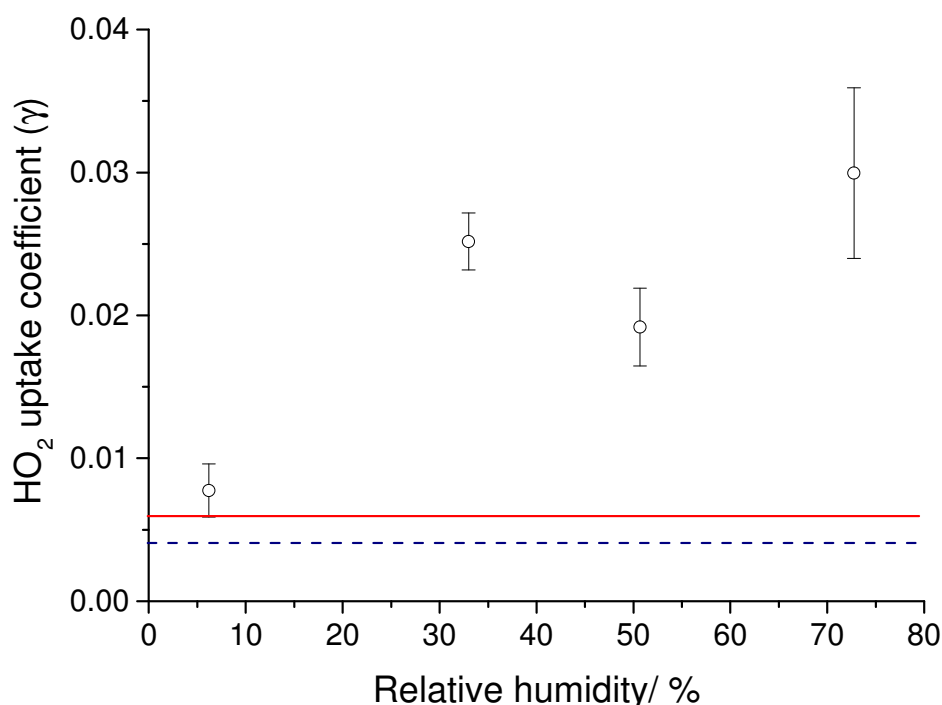


Figure 7.2: The measured HO₂ uptake coefficient onto Arizona Test Dust aerosols (open symbols) at an initial HO₂ concentration of 1×10^9 molecule cm⁻³. The red line represents the average HO₂ uptake coefficient that was observed for ammonium nitrate aerosols over a range of humidities and the dashed blue line represents the limit of detection below which all HO₂ uptake measurements for solid salts at an initial HO₂ concentration of 1×10^9 molecule cm⁻³ have been measured. The error bars are one standard deviation of a number of repeated experiments.

Taketani and Kanaya (2010) observed an increase in the HO₂ uptake coefficient onto polystyrene latex particles from 0.01 ± 0.01 to 0.03 ± 0.01 when increasing the humidity from 22 to 92 % RH. Taketani and Kanaya (2010) stated that the increase in the HO₂ uptake

coefficient may be due to a HO₂-H₂O complex reaction on the surface of the aerosols (Reaction 7.4) as first suggested by Aloisio et al. (2000):



It should also be noted that many minerals, such as SiO₂ and Al₂O₃, are hydroxylated in the presence of water vapour which results in OH groups at the surface of the aerosol. These OH groups could potentially bind to water or to HO₂. Therefore, the chemistry occurring at the surface of the aerosol may change with changing humidity. It also cannot be ruled out that although the dust aerosols are dry, at higher humidities a film of water could start to form at the surface of the aerosol leading a change in the chemistry at the surface of the aerosol.

In contrast to this work, Bedjanian et al. (2013) observed a factor of ten decrease in the initial HO₂ uptake coefficient (γ_0) when increasing the relative humidity from 0 to 95 % RH. The decrease in the HO₂ uptake coefficient was fitted to the following equation:

$$\gamma_0 = 1.2/(18.7 + RH^{1.1}) \quad (\text{E7.1})$$

The decrease in the HO₂ uptake coefficient with increasing relative humidity is in agreement with the work by Remorov et al. (2002) where an increase in relative humidity from 0 % to 28 % led to a 13 % decrease in the HO₂ uptake coefficient onto solid sodium chloride surfaces. However, Loukhovitskaya et al. (2009) did not observe a change in the HO₂ uptake coefficient when increasing the relative humidity from 0 to 28 % RH for either sodium chloride or sodium bromide, although the lack of an observable decrease could be due to the decrease being small and within the experimental uncertainties. Loukhovitskaya et al. (2009) did observe a factor of two decrease in the HO₂ uptake coefficient for MgCl₂·6H₂O when 2×10^{15} molecule cm⁻³ of water vapour was added to the flow tube compared to dry conditions, which may be due to MgCl₂·6H₂O having a larger water absorbing ability

The decrease in uptake coefficients with increasing humidity that have been observed onto solid salts (Remorov et al., 2002) and ATD surfaces (Bedjanian et al., 2013) can be attributed to water molecules binding to reactive sites on the surface of the solid. The water that is

bound to the reactive sites inhibits the HO₂ from reaching the sites and reacting. Therefore, the HO₂ uptake coefficient decreases as the humidity increases.

Another possible reason for the higher uptake coefficients at higher humidities observed in this work is due to the changing HO₂ concentration at different humidities. At higher humidities the observed wall loss is significantly higher. For example, it was observed that at 30 cm along the flow tube (~ 7 seconds) and at 7 % RH the HO₂ concentration was approximately double the HO₂ concentration at 75 % RH. This was observed for both initial HO₂ concentrations. A higher HO₂ concentration leading to a lower HO₂ uptake coefficient had already been observed for aqueous salt aerosols and was discussed in Section 3.11. Therefore, the effect of changing the HO₂ concentration upon the HO₂ uptake coefficient onto ATD aerosols was investigated and will be discussed in Section 7.4.

7.4 The HO₂ uptake coefficient onto ATD aerosols as a function of the initial HO₂ concentration

Figure 7.3 shows the HO₂ uptake coefficients that were measured in this work over a range of humidities and at initial HO₂ concentrations of $\sim 3 \times 10^8$ molecule cm⁻³ and $\sim 1 \times 10^9$ molecule cm⁻³. The uptake coefficient at the higher HO₂ concentration was ~ 30 to 70 % smaller than at the lower HO₂ concentration and the average HO₂ uptake coefficient over the range of humidities were 0.031 ± 0.008 and 0.018 ± 0.006 at $\sim 3 \times 10^8$ molecule cm⁻³ and $\sim 1 \times 10^9$ molecule cm⁻³, respectively. Figure 7.4 also shows an apparent dependence of the HO₂ uptake coefficient upon the HO₂ concentration with higher uptake coefficients observed at lower HO₂ concentrations. The HO₂ trend that is observed in this work is similar to the trend that was observed for aqueous salt aerosols in Section 3.11. Possible reasons for the HO₂ uptake coefficient dependence upon the initial HO₂ concentration were postulated in Section 3.11 to be due to a change in viscosity of the aerosol, a change in the pH of the aerosol, a trace reactant being used up, the saturation of the aerosol or the conversion of H₂O₂ to reform HO₂. However, for dust aerosols the uptake is limited to a solid surface and therefore the HO₂ uptake coefficient with changing HO₂ concentration must be due to saturation of the surface, a trace reactant being used up or the conversion of H₂O₂ to reform HO₂. These three possibilities will be investigated in greater detail below.

The first possible reason that the HO₂ uptake coefficient might vary with HO₂ concentration is due to saturation of the dust surface. It is likely that the HO₂ uptake mechanism follows either the Eley-Rideal mechanism (Reactions 7.5 – 7.6) or the Langmuir-Hinshelwood mechanism (Reactions 7.7 – 7.8) with the product of these reactions being either H₂O₂, water or a mixture of both:

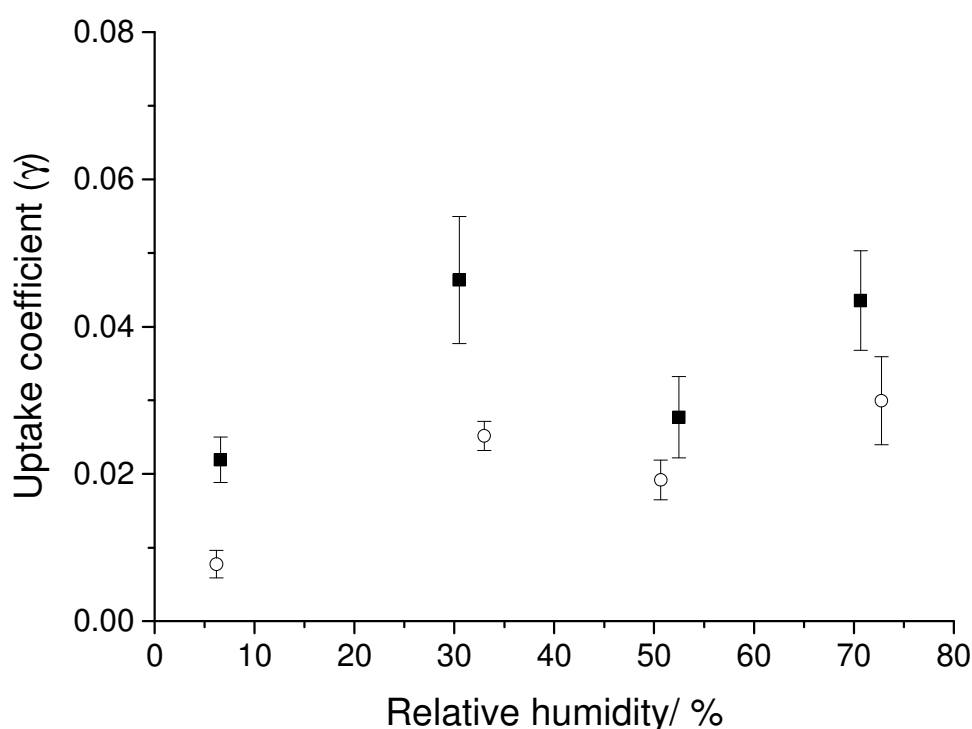


Figure 7.3: The HO₂ uptake coefficient as a function of relative humidity at an initial HO₂ concentration of $\sim 1 \times 10^9$ molecule cm^{-3} (open symbols) and $\sim 3 \times 10^8$ molecule cm^{-3} (closed symbols). The error bars represent one standard deviation of a number of repeated experiments.

The steady state surface coverage (θ_{HO_2}) of the aerosols can be estimated by assuming a Langmuir isotherm and by using the equation given by Pöschl et al. (2001):

$$\theta_{HO_2} = \frac{K_{HO_2}[HO_2]}{1 + K_{HO_2}[HO_2]} \quad (E7.2)$$

where K_{HO_2} is given by the following equation:

$$K_{HO_2} = \frac{S_{0,HO_2}\omega_{HO_2}\tau_{HO_2}}{4[SS]_s} \quad (E7.3)$$

where S_{0,HO_2} is the sticking probability when the surface coverage of HO_2 is zero, ω_{HO_2} is the mean molecular speed of HO_2 , τ_{HO_2} is the inverse of the mean residence time on the surface and $[SS]_s$ is the concentration of adsorption sites on the surface per square centimetre. By assuming a HO_2 diameter of 4×10^{-8} cm, an aerosol number concentration of $20,000 \text{ cm}^{-3}$ and an average aerosol radius of 273 nm, the number of adsorption sites can be estimated as $3.7 \times 10^{10} \text{ cm}^{-3}$ assuming spherical particles. The mean molecular speed at 293 K is approximately $43,000 \text{ cm s}^{-1}$, the mean residence time of HO_2 can be estimated as 0.2 seconds (assuming that it is similar to the mean residence time of O_3 on soot articles coated with Benzo[*a*]pyrene) and the sticking probability when the surface coverage is zero can be estimated as 0.001 (Pöschl et al., 2001). By making these assumptions about the values of the different parameters, and by ignoring reactions taking place at the dust surface, the steady state surface coverage can be estimated to be 59 % at a HO_2 concentration of 1×10^9 molecule cm^{-3} and 30 % at a HO_2 concentration of 3×10^8 molecule cm^{-3} . However, as the aerosols are not spherical, the steady state surface coverage would be less.

Slade and Knopf (2013) observed that the OH uptake coefficient onto surfaces coated with levoglucosan, abietic acid and nitroguaiacol decreased as the steady state surface coverage was greater than 10%, assuming spherical particles. However, in this work, there are many factors besides HO_2 surface coverage that could affect the uptake coefficient, such as relative humidity, reactions at the surface, and competitive surface coverage by products of the reactions, such as H_2O_2 . Therefore, a complex model would be required in order to assess the impact of surface coverage upon the uptake coefficient. This could be done in the future by

using the kinetic double-layer model of aerosol surface chemistry and gas-particle interactions (K2-SURF) (Shiraiwa et al., 2009).

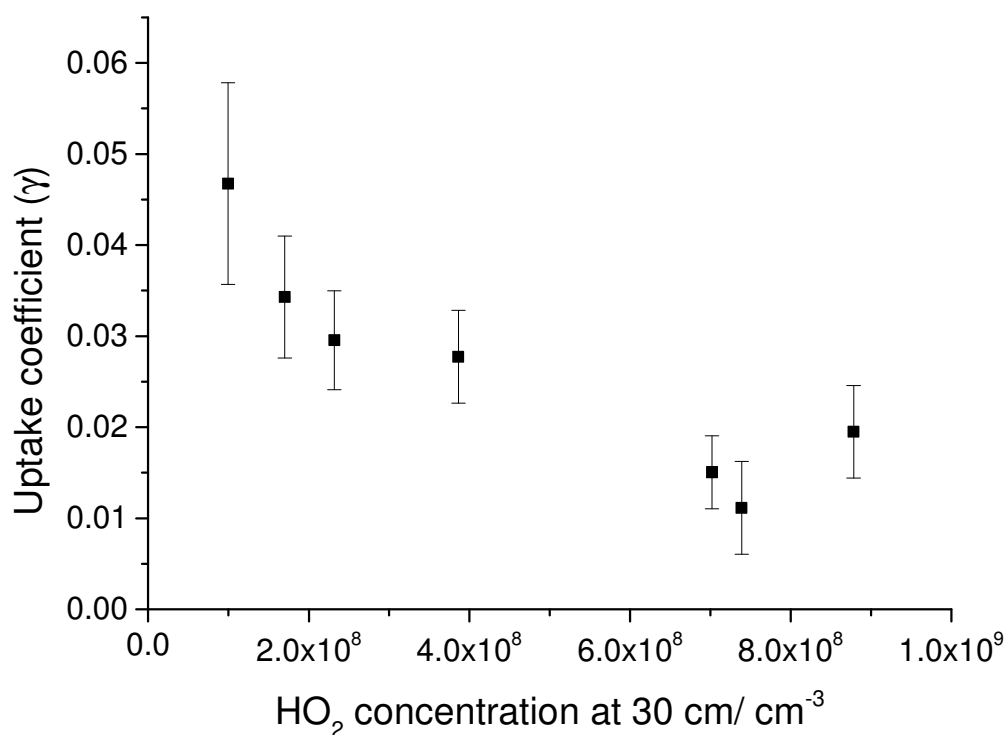


Figure 7.4: The average uptake coefficient measured along the flow tube as a function of the HO₂ concentration when the injector was placed at 30 cm along the flow tube. The error bars represent one standard deviation of the averaged values. The temperature was 293 ± 2 K.

The second possible explanation for the HO₂ uptake coefficient dependence upon the initial HO₂ concentration is if a trace reactant on the dust surface was being used up over time. In this case the mechanism could be described by Reactions 7.9 – 7.10:



where X is the trace reactant that is being used up. If this was the mechanism the rate of reaction could be described as:

$$\frac{d[HO_2]}{dt} = -k_{R9}[HO_2][S] + k_{-R-9}[HO_2 - S] \quad (E7.4)$$

$$\frac{d[Products]}{dt} = k_{R10}[HO_2 - S][X] \quad (E7.5)$$

where k_{R9} and k_{-R-9} are the forwards and backwards rate constants of the reactions shown in R9 and k_{R10} is the rate constant of reaction 7.10. At higher HO_2 concentrations the trace reactant would be used up at a faster rate, and therefore the uptake coefficient would decrease at a faster rate. Therefore, at a given moment in time the uptake coefficient for the lower HO_2 concentration would be higher than for the higher HO_2 concentration. However, this theory cannot currently be tested as neither the concentration of a potential trace reactant nor the rate of reaction with HO_2 are known.

The third possible reason for the HO_2 uptake coefficient dependence upon the initial HO_2 concentration is if hydrogen peroxide is reforming HO_2 . The experiments that were performed at an initial HO_2 concentration of 1×10^9 molecule cm^{-3} had the mercury lamp current in the injector set to 20 mA, whereas the experiments at an initial HO_2 concentration of 3×10^8 molecule cm^{-3} had the mercury lamp set to 2.5 mA. At PSI, in Switzerland the hydrogen peroxide concentrations coming out of the injector after mixing and with no aerosols present at 20 mA and 2.5 mA were measured as 230 ppt and 40 ppt, respectively. If the hydrogen peroxide was reforming HO_2 the measured uptake coefficient would be reduced, with a larger reduction observed at the higher HO_2 and hydrogen peroxide concentrations.

Several studies have observed HO_2 as the product of hydrogen peroxide uptake onto either dust or a component of dust. Romanias et al. (2012) and Pradhan et al. (2010) measured the H_2O_2 uptake coefficient onto TiO_2 which is a component of dust. Romanias et al. (2012) proposed the following mechanism based on the available literature data. First, the UV light activated the surface of the TiO_2 by promoting an electron to the conduction band and leaving a hole in the valence band (Reaction 7.11). The electrons and holes can then lead to the oxidation and reduction reactions shown by Reactions 7.12 – 7.15:



The reaction products, OH and HO₂ could then take part in further reactions as outlined in Reactions 7.16 – 7.20 below. It should be noted that HO₂ is formed by the uptake of hydrogen peroxide in Reactions 7.13 and 7.16:

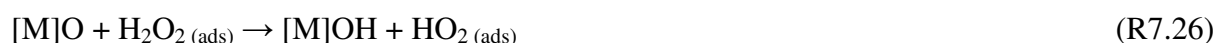


However, in this work, when measuring the HO₂ uptake coefficients onto ATD, there would have been very little UV light present in the flow tube that could cause the formation of HO₂ by H₂O₂ by the reaction mechanism suggested in Reactions 7.11 – 7.20. However, another mechanism that can result in HO₂ formation from H₂O₂ has been suggested by Zhao et al. (2011).

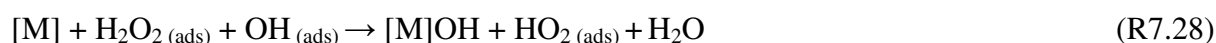
Zhao et al. (2011) made measurements of the H₂O₂ uptake coefficient onto both SiO₂ and α-Al₂O₃. Uptake coefficients assuming BET surface areas of ~ 8 × 10⁻⁹ and ~ 8 × 10⁻⁸ were measured onto SiO₂ and α-Al₂O₃ respectively at humidities of more than 21 %. The mechanism for the H₂O₂ uptake onto SiO₂ was suggested as Reactions 7.21 – 7.23 (Hiroki and LaVerne, 2005):



α -Al₂O₃ has been found to be highly reactive towards a variety of trace gases (Usher et al., 2003). Zhao et al. (2011) measured the H₂O₂ uptake coefficient onto α -Al₂O₃ to be approximately an order of magnitude higher than onto a relatively inactive SiO₂ surface. The following mechanism was suggested for the H₂O₂ uptake onto α -Al₂O₃ surfaces:



There are several possible destruction pathways for H₂O₂. Firstly, it could bind with a surface AlOH group which could then decompose to form HO₂ and water via Reactions 7.24 and 7.25 (Do et al., 2009; Lin and Gurol, 1998). Secondly, the oxygen atoms in α -Al₂O₃ may also be able to decompose H₂O₂ via Reaction 7.26. Lastly, it is also believed that Al may be reductive and can therefore destroy H₂O₂ via Reaction 7.27. Zhao et al. (2011) then suggested that the products of Reactions 7.24 – 7.27, HO₂ and OH could then rapidly react with H₂O₂ and each other via Reactions 7.28 – 7.31 (Do et al., 2009; Lin and Gurol, 1998). The net product of all of these reactions would be to form water:



Bedjanian et al. (2013) did not observe a dependence upon the HO₂ concentration that was being used. However, this may be due to the fact that Bedjanian et al. (2013) measured initial HO₂ uptake coefficients. The initial HO₂ uptake coefficient onto dust can be assumed to be the uptake coefficient onto fresh dust, i.e. onto dust for which the HO₂ surface coverage is initially zero and any trace reactant that could potentially be used up over time would still be present at high concentrations. Therefore, the HO₂ concentration would not affect the uptake coefficient. Finally, it is unclear as to what the initial H₂O₂ concentrations were in the work by Bedjanian et al. (2013).

Bedjanian et al. (2013) measured the H_2O_2 yield from the HO_2 uptake onto ATD. However, no change in the H_2O_2 concentration against a relatively high background due to oxygen was observed. An upper limit of 5 % production of H_2O_2 was reported, which suggested that the product of HO_2 uptake was not H_2O_2 or that any H_2O_2 that was formed rapidly decomposed or reacted to form HO_2 , OH and water. Bedjanian et al. (2013) also measured initial H_2O_2 uptake coefficients onto ATD surfaces and found that the H_2O_2 uptake coefficients of H_2O_2 were approximately two orders of magnitude lower than the initial HO_2 uptake coefficient onto ATD surfaces.

7.5 The HO_2 uptake coefficient onto ATD aerosols as a function of time

The HO_2 uptake coefficient was also measured as a function of aerosol exposure time. The time dependence at a relative humidity of 10 % for two initial HO_2 concentrations is shown in Figure 7.5. The HO_2 uptake coefficients were fitted with the following exponentially decaying functions:

$$\gamma = 0.58 \exp(-t/2.9) + 0.042 \quad [\text{HO}_2]_0 = 3 \times 10^8 \text{ molecule cm}^{-3} \quad (\text{E6})$$

$$\gamma = 0.11 \exp(-t/5.4) + 0.024 \quad [\text{HO}_2]_0 = 1 \times 10^9 \text{ molecule cm}^{-3} \quad (\text{E7})$$

The three possible explanations for the HO_2 concentration dependence were the saturation of the surface of the aerosol, a trace reactant being used up over time and H_2O_2 decomposition to reform HO_2 . These three explanations will now each be investigated in terms of the observed time dependence as well as the explanation that the decrease in HO_2 along the flow tube is responsible for the time dependence. The time dependence and apparent HO_2 concentration dependence are similar to the results obtained for aqueous aerosols in Chapter 3. Although the HO_2 uptake mechanisms will be different for dust and aqueous aerosols, some of the explanations for these trends may be similar. The time and apparent HO_2 concentration dependence for aqueous aerosols will be explored further in Chapter 8.

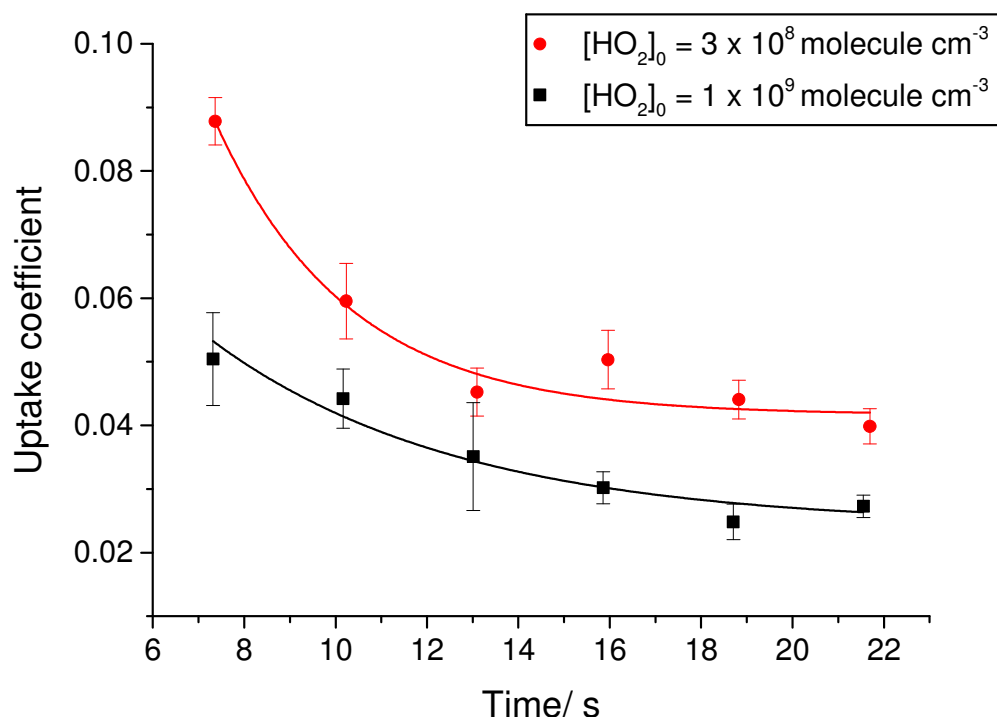


Figure 7.5: Average HO_2 uptake coefficient between time 0 and the given reaction time on the x-axis at a relative humidity of 10 % and at initial HO_2 concentration of $1 \times 10^9 \text{ molecule cm}^{-3}$ and $3 \times 10^8 \text{ molecule cm}^{-3}$. The temperature was $293 \pm 2 \text{ K}$. The error bars represent 1 standard deviation. Exponential decays with the equations $\gamma = 0.58 \exp(-t/2.9) + 0.042$ and $\gamma = 0.11 \exp(-t/5.4) + 0.024$ were fitted to the data for the lower and higher HO_2 concentration, respectively.

The time dependence could be explained if the surface of the dust or the reactive sites on the surface of the dust were becoming partially saturated by HO_2 or by the products of the surface reaction over time. At time zero, the surface of the dust would be fresh and the rate of adsorption of HO_2 onto the surface of the dust would be much faster than the rate of desorption. However, as the surface coverage of the dust increased, the adsorption would decrease over time until it equalled the rate of desorption of the HO_2 and products of HO_2 leading to a constant coverage. A time dependence has previously been modelled by Ammann et al. (2003) for the theoretical adsorption of gas uptake by solid atmospheric aerosols. Ammann et al. (2003) showed that surface saturation of solid aerosols could cause a decrease in the measured uptake coefficient. However, a model has not yet been developed for HO_2 uptake onto dust aerosols. In the future, the KM-SUB model could be adapted to test

the theory that partial saturation of the surface leads to the time dependence and the decay shapes shown in Figure 7.5.

The time dependence could also be explained if a reactive species was being used up over time. As the time increased the concentration of the reactive species would decrease and therefore the HO₂ uptake coefficient would also decrease. Such a dependence has already been observed for NO₂ and ozone uptake onto soot as described in Section 3.8. Figure 7.5, shows that the uptake coefficient does not tend to zero over time suggesting that if a trace reactant were being used up, this occurs within the first few seconds and the uptake coefficient is then controlled by other reactions.

The time dependence could potentially be explained by hydrogen peroxide reforming HO₂. However, for this to be the case the H₂O₂ concentration in both the aerosol and the gas phase along the flow tube would have to increase leading to more HO₂ being reformed in the aerosol, and therefore decreasing the observed uptake coefficient. It is currently not possible to know whether H₂O₂ increases along the flow tube as currently no measurements exist. The techniques to measure H₂O₂ such as the hydrogen peroxide monitor (AL-2021) described in Section 2.13, are unlikely to be sensitive enough to measure small changes (~ 1 ppt) in the hydrogen peroxide concentrations.

Finally, the observed time dependence may be due to a decrease in the gas-phase HO₂ concentration along the flow tube. If the main loss of HO₂ onto ATD aerosols is due to the self reaction of HO₂ on the surface of the ATD either via the Eley-Rideal or Langmuir-Hinshelwood mechanisms, the rate of HO₂ loss would be a second order process. Therefore, as HO₂ decreased along the flow tube, due to uptake to the aerosols and to the walls, the rate of HO₂ loss would decrease and therefore the uptake coefficient would decrease.

Bedjanian et al. (2013) also observed a decrease in the HO₂ uptake coefficient over a few minutes. However, Bedjanian et al. (2013) attributed this decrease to deactivation of the dust surface which could be due to the product of the reactions (such as water) remaining on the surface of the dust and blocking the reactive sites. The reactants used to make the HO₂ such as CH₃OH, HCl, Cl₂, H₂O₂ and HF could also potentially deactivate the surface over time by binding to the surface. Loukhovitskaya et al. (2009) had also observed the deactivation of

sodium chloride surfaces with these reactants, with the highest deactivation observed when experiments were performed with HF. In this work, the HO₂ was formed by the photolysis of water vapour in the presence of O₂ and therefore deactivation of the surface by reactants should not occur. However, H₂O₂ is formed as a by-product of HO₂ formation in the injector and could therefore potentially reduce the available reactive sites by binding to them.

7.6 The HO₂ uptake coefficient onto cosmic dust

There were several reasons to study the HO₂ uptake coefficient onto cosmic dust. First, cosmic dust enters the Earth's atmosphere at high concentrations of approximately 100 to 300 tonnes per day (Plane, 2012). Secondly, cosmic dust is believed to have the same chemical composition as the mineral olivine which is present in the Earth's crust (Saunders and Plane, 2011). Finally, HO₂ uptake coefficient measurements were made onto cosmic dust in order to be able to directly compare the result with ATD.

A proxy for cosmic dust was prepared by Mr. Sandy James at the University of Leeds using the methodology described below. MgCl₂ (8.5 grams) and (Fe(NH)₄)₂(SO₄)₂ (8.5 grams) were dissolved into water (500 ml). Na₄SiO₄ (14.6 grams) was also dissolved into water (500 ml) to form a separate solution. These two solutions were then mixed together, and left to react for two weeks, with nitrogen being bubbled through the solution. The reaction mechanism that occurs is unknown but results in the product FeMgSiO₄. The nitrogen was bubbled through the solution to avoid the formation of Fe₂O₃ which would be formed in the presence of oxygen. The salts and FeMgSiO₄ were then separated by Soxhlet extraction.

Due to the limited amount of cosmic dust that was available (~ 15 grams) HO₂ uptake experiments onto cosmic dust were only performed under one set of conditions. The initial HO₂ concentration was set to 1×10^9 molecule cm⁻³ and the relative humidity was 10 %. The HO₂ uptake coefficient was measured as 0.07 ± 0.01 . For comparison, the uptake coefficient of ATD at an initial HO₂ concentration of 1×10^9 molecule cm⁻³ and at 7 % RH was 0.008 ± 0.002 . Therefore, there was almost a factor of 10 increase when measuring the HO₂ uptake coefficient of cosmic dust compared to ATD under these conditions. The relationship between the HO₂ uptake coefficient and the reaction time is shown in Figure 7.6. It should be

noted that the average surface area of a single aerosol was $9.4 \times 10^{-9} \text{ cm}^2$ and $9.2 \times 10^{-9} \text{ cm}^2$ for ATD and cosmic dust, respectively. Therefore, the similarities of these two surface areas means that the gradients in Figure 7.6 can be directly compared.

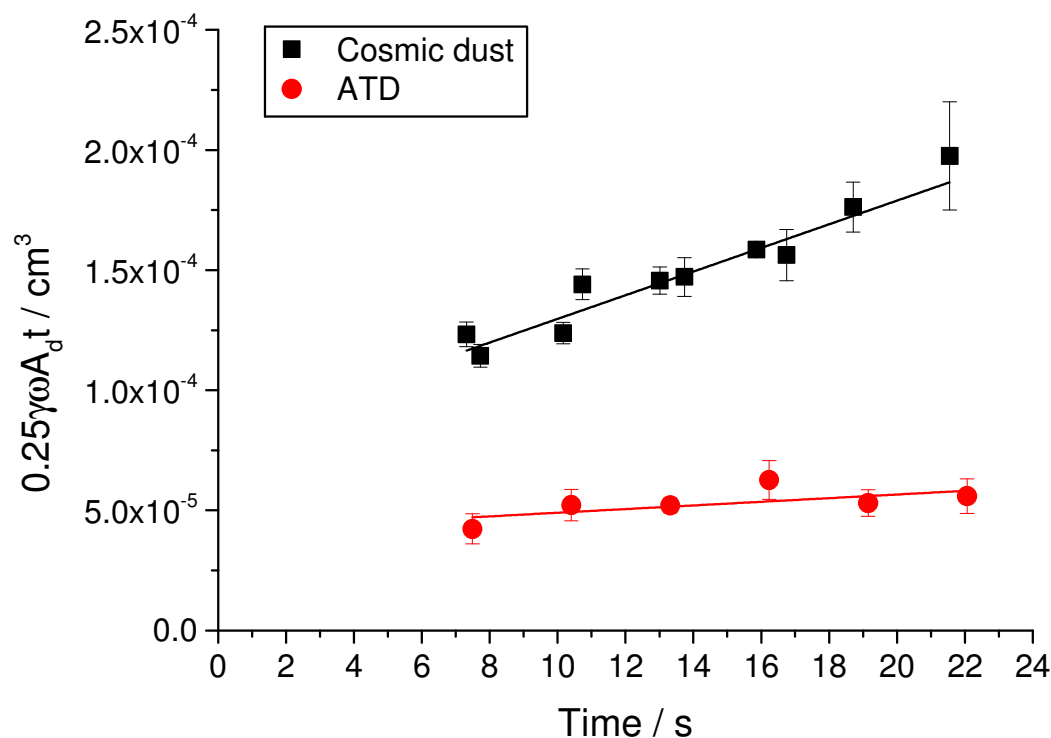


Figure 7.6: Examples of $0.25\gamma\omega A_d t$ as a function of time for ATD and cosmic dust at a relative humidity of 10%, at $293 \pm 2 \text{ K}$ and at an initial HO_2 concentration of $1 \times 10^9 \text{ molecule cm}^{-3}$. It should be noted that A_d was $9.4 \times 10^{-9} \text{ cm}^2$ for ATD and $9.2 \times 10^{-9} \text{ cm}^2$ for cosmic dust. The gradients of the plots were $(7.6 \pm 4.1) \times 10^{-7} \text{ cm}^3 \text{ s}^{-1}$ and $(4.9 \pm 0.4) \times 10^{-6} \text{ cm}^3 \text{ s}^{-1}$ for ATD and cosmic dust, respectively, leading to HO_2 uptake coefficients of 0.01 ± 0.01 and 0.07 ± 0.01 .

There are two possible reasons that could explain the larger HO_2 uptake coefficient for cosmic dust compared to ATD. First, the surface area of the aerosols were measured using an SMPS and APS and are therefore assumed to be spherical. However, the aerosols are non-spherical and the BET surface areas of the two types of aerosol may be significantly different. The BET surface area of ATD was measured as $85 \pm 10 \text{ m}^2 \text{ g}^{-1}$ by Bedjanian et al. (2013) whereas the BET of cosmic dust is $\sim 100 - 400 \text{ m}^2 \text{ g}^{-1}$ (Sandy James, personal communication). The density of ATD is 2.7 g cm^{-3} whereas for cosmic dust it is $\sim 3.3 \text{ g cm}^{-3}$. However, these BET surface areas were not measured for aerosols in the flow tube and might

therefore be different as smaller aerosols are more likely to be entrained into a flow than the larger aerosols. The actual surface area might be able to explain fully or partly explain the differences in the HO₂ uptake coefficient. The second possibility is if the HO₂ is destroyed faster on the surface of cosmic dust due to its composition. Some components of the cosmic dust, (such as the iron or magnesium), could potentially enhance the destruction of HO₂.

It is currently unclear as to whether the size of the HO₂ uptake coefficient onto dust aerosols is controlled solely by the surface area of the dust, or whether the composition of the dust also affects the uptake coefficient. In the future, further experiments could be performed with a range of dusts and minerals that have varying BET surface areas and compositions. If the HO₂ uptake coefficient was measured onto a large range of minerals and dusts, it would be possible to verify whether the uptake was solely due to surface area or also due to the presence of specific metals.

7.6 Atmospheric Implications

Although Cape Verde is mainly affected by marine aerosols, which contain salts and organics, it is also seasonally affected by Saharan dust. During the SAMUM-2 field campaign which took place in Cape Verde during the winter of 2008 dust concentrations ranged from ~10 - 200 µg m⁻³, whereas during the RHaMBLe field campaign which took place in May 2007 high dust concentrations of 40 – 69 µg m⁻³ were measured only during the first three days of the field campaign (Allan et al., 2009; Schladitz et al., 2011). During the remainder of the RHaMBLe campaign dust concentrations were less than 10 µg m⁻³. However, the week before the campaign started a concentration of 332 µg m⁻³ had been measured during a dust event. In order to be able to input the dust concentrations into the Cape Verde box model (described in Section 2.14), the geometric surface area of the dust particles was estimated by assuming spherical particles with an average aerosol diameter of 1 µm and a density of 2.7 g cm⁻³. By making these assumptions, concentrations of 10 µg m⁻³ to 332 µg m⁻³ would lead to a geometric surface areas of 2.2×10^{-7} to 7.4×10^{-6} cm² cm⁻³.

An uptake coefficient of $\gamma = 0.031 \pm 0.008$ (the average uptake coefficient measured for the lower initial HO₂ concentration in this work and reported in Section 7.4) was inputted into the

Cape Verde box model and the dust surface area was varied. The results of the model on the HO₂ concentrations are shown in Figure 7.7. For the range of surface areas of 2.2×10^{-7} to $7.4 \times 10^{-6} \text{ cm}^2 \text{ cm}^{-3}$, a decrease in HO₂ concentrations of 0.3 % to 10.5 % compared to when there are no aerosols was calculated. Whalley et al. (2010) stated that a decrease of 23 % due to HO₂ aerosol uptake would be necessary for the Cape Verde model predictions and observations to be in agreement. If the uptake coefficient was $\gamma = 0.031$ as measured then a dust surface area of $2 \times 10^{-5} \text{ cm}^2 \text{ cm}^{-3}$ would be needed to match with field measurements. However, during the majority of the RHaMBLe field campaign the geometric dust surface area was less than $2.2 \times 10^{-7} \text{ cm}^2 \text{ cm}^{-3}$ which would have led to a decrease in HO₂ of less than 0.3 %. However, the decrease in HO₂ concentrations may be larger if the uptake coefficient onto Saharan dust is larger than onto ATD as is the case for N₂O₅ and HNO₃ (Crowley et al., 2010; Tang et al., 2014). However, even if the uptake coefficient onto Saharan dust was 2 – 3 times larger it cannot explain the discrepancy between the model and predictions during the RHaMBLe field campaign. The discrepancy may be due to uptake onto marine aerosols, especially if these contain transition metal ions (as discussed in Section 3.12). Soot and silicate particles have also been observed in Cape Verde although the effect of these particles on HO₂ concentrations is unknown due to a lack of laboratory data. The reaction between HO₂ and RO₂ at the surface of the dust aerosol could also potentially decrease the HO₂ concentrations (as discussed in Sections 5.4 and 5.5).

However, there are also many other factors that could affect the HO₂ uptake coefficient in the troposphere onto dust. For example, atmospheric processing can change the composition of the dust. Inorganic and organic acids on the surface of the dust can lower the pH at the dust surface causing an increase in the solubility of the iron in the dust which causes the iron to enter an aqueous phase (Chen and Grassian, 2013; Shi et al., 2012). In Section 3.5 experiments were discussed showing that the uptake coefficient increased with increasing aqueous iron concentrations. Therefore, if acids were present on the surface of the dust the HO₂ uptake coefficient could be much higher than measured in this work. Another factor that would need to be considered in the troposphere is the impact of solar radiation. As has been discussed, UV light can influence the chemistry by activating the surface of TiO₂, leading to reformation of HO₂ from H₂O₂ and thereby decreasing the net loss of HO₂ to dust aerosols.

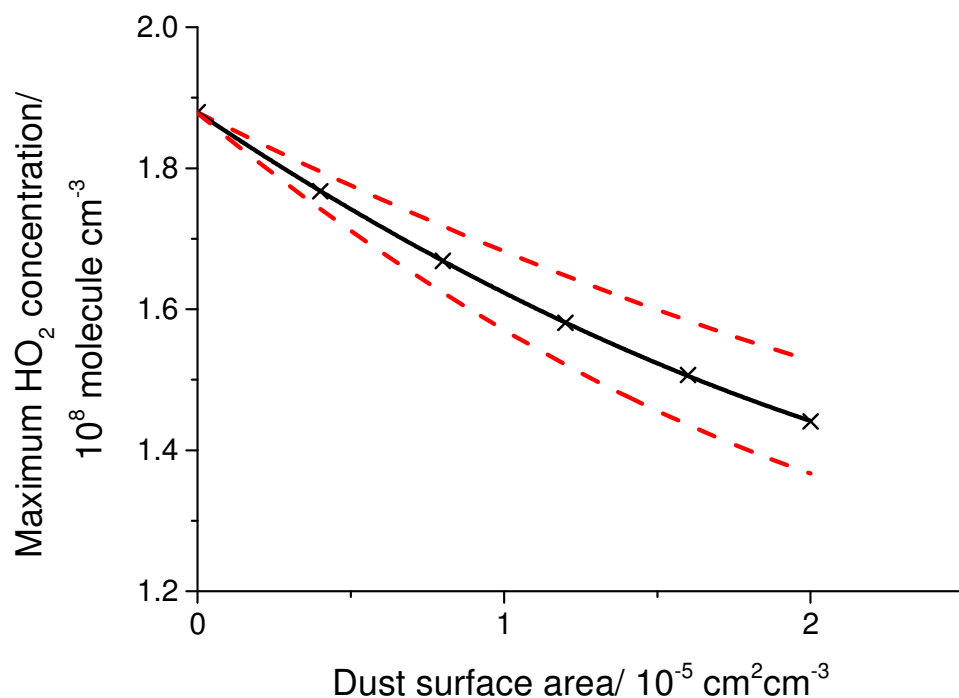


Figure 7.7: The decrease in the solar noon maximum HO_2 concentration using the Cape Verde model for different dust surface area concentrations and assuming a HO_2 uptake coefficient of 0.031 ± 0.008 . The red line represents the impact of the ± 0.008 error on the uptake coefficient.

In order to accurately be able to predict the effect of dust aerosols upon HO_2 concentrations several factors would need to be determined. First, the BET dust surface area would need to be accurately known during experiments and in the field. Secondly, the exact composition of the dust would also need to be known. As discussed in Section 7.4, different minerals have different effects on the reformation of HO_2 from H_2O_2 and may also have different HO_2 uptake coefficients which could also be the case for cosmic dust. Therefore, to fully understand the mechanism and to be able to relate it to the troposphere, HO_2 uptake coefficients should be measured onto a range of different dusts and minerals, with different BET surface areas and different initial HO_2 and H_2O_2 concentrations. The HO_2 concentrations in the flow tube could then be modelled using a model such as K2-SURF, to take into account the adsorption and desorption of different species, the surface coverage of the dust and the reactions in the gas phase and at the dust surface (Shiraiwa et al., 2009).

7.7 Summary

In this work the first measurements of the HO₂ uptake coefficients onto ATD aerosols were made. Experiments were performed at initial HO₂ concentrations of $\sim 1 \times 10^9$ and $\sim 3 \times 10^8$ molecule cm⁻³ and over a relative humidity range of 6 – 76 %. An increase in the HO₂ uptake coefficient was observed with increasing relative humidity, which may be due to (i) the hydroxylation of minerals in the dust leading to a different reactivity, (ii) the formation of HO₂-H₂O complexes which could potentially react at a faster rate than HO₂ at the dust surface (Li et al., 2014) or (iii) decreasing HO₂ concentrations at higher humidities due to a greater wall loss.

Higher HO₂ uptake coefficients were observed at the lower initial HO₂ concentrations, and the uptake coefficients were also observed to increase as the HO₂ concentration measured at 30 cm along the flow tube decreased. A time dependence was also observed with lower uptake coefficients observed at longer times. Several possible explanations could explain these observations. First, the surface may be becoming partially saturated over time, especially at the higher HO₂ concentrations, leading to a decrease in the adsorption of more HO₂ to the surface. Secondly, a trace reactant could potentially be used up over time. At higher HO₂ concentrations the trace reactant would be used up at a faster rate leading to lower observed uptake coefficients. Thirdly, the time dependence could also potentially be explained if the main destruction route of HO₂ was via the HO₂ self-reaction. At longer times (or greater injector distances) the HO₂ concentration decreases and therefore, the rate of the HO₂ self-reaction decreases leading to smaller uptake coefficients. Finally, the HO₂ concentration dependence and time dependence could also be potentially explained by there being more H₂O₂ in the flow tube at higher HO₂ concentrations. The H₂O₂ could potentially reform HO₂ on the dust, which could then desorb into the gas phase thereby decreasing the observed uptake coefficient. A similar reformation of HO₂ from H₂O₂ has been modelled in Chapter 8 for aqueous aerosols, however, no modelling has yet been done for dry dust aerosols although this could be done in the future by adapting the model.

The HO₂ uptake coefficient onto a proxy for cosmic dust was also investigated. It was measured as 0.07 ± 0.01 at 10 % RH and at an initial HO₂ concentration of 1×10^9 molecule

cm^{-3} . The HO_2 uptake coefficient obtained was approximately a factor of ten higher than measured for ATD aerosols under the same conditions. The difference in the HO_2 uptake coefficient for the two types of dust was attributed to a difference either in the BET surface area or due to the dust compositions with some components of the cosmic dust being more reactive towards HO_2 . More experiments could be done with different dusts that have a variety of compositions and BET surface areas in order to check whether any components of dust are highly reactive towards HO_2 .

In the future, the K2-SURF model (designed for solid aerosols) could be adapted to try to account for the HO_2 uptake coefficients and the observed trends. The main processes and reactions that would need to be included are summarised in Figure 7.8. These would include adsorption and desorption of HO_2 , H_2O_2 and water vapour to and from the surface of the dust as well as a rate constant for any reactions that occur at the surface of the dust. The reactions in the model would include reactions between adsorbed species which could be influenced by the composition of the dust. Some components of the dust could also be hydroxylated in the presence of water which could also affect the rates of some reactions at the surface. The adsorption and desorption of any products would also need to be included. The physical properties of the adsorption sites on the surface of the dust would have to be inputted into the model and the number of adsorption sites could be estimated from effective diameter of the adsorbing species and the total surface area of the dust. The total surface area of the dust would have to be estimated as the spherical surface area assumed in this work is an underestimation. Finally, a sticking probability of the different species to the surface of the dust would also have to be estimated. By using different dusts with different compositions and different BET surface areas each parameter could be optimised.

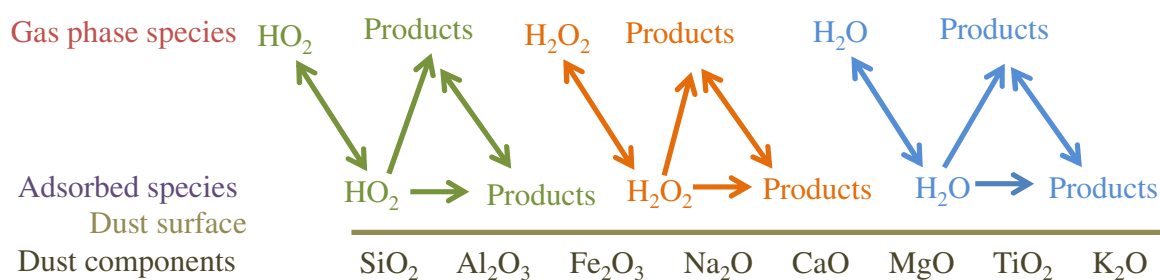


Figure 7.8: Schematic of the main reactions and processes that would need to be inputted into a model to understand HO_2 uptake to dust aerosols.

The effect of the HO₂ uptake coefficient onto dust aerosols was also investigated by using a box model operated for conditions encountered at Cape Verde in the tropical Atlantic ocean. The HO₂ uptake coefficient measured onto dust aerosols was larger than onto non-copper doped aqueous and solid aerosols. Therefore, the impact of the dust aerosols on gaseous HO₂ gas phase concentrations would be expected to be greater than onto non-copper doped aqueous and solid aerosols assuming the same surface area of both. By assuming a HO₂ uptake coefficient of 0.031, which was the uptake coefficient measured in this work at the smaller HO₂ concentration of 3×10^8 molecule cm⁻³, dust concentrations of 10 μg m⁻³ to 332 μg m⁻³ observed during the RHaMBLe field campaign were shown to decrease the HO₂ concentrations by 0.3 % to 10.5 % compared to when the HO₂ uptake coefficient was set to zero. However, the HO₂ uptake coefficient may be different for other types of dust that have different compositions or BET surface areas. Therefore, it is important in future to investigate several dust types in order to determine whether the magnitude of the HO₂ uptake coefficient is determined solely by the dust surface area, or whether it can be influenced by different dust components.

Chapter 8: Modelling of the HO₂ uptake coefficient using the KM-SUB model

8.1 The importance of modelling the HO₂ uptake coefficient

The modelling of aerosol uptake coefficients has enabled trends in time and concentration of species observed during laboratory measurements to be interpreted and explained (Ammann and Pöschl, 2007; Slade and Knopf, 2013). For example, the measured uptake coefficient of NO₂ and O₃ onto soot was measured to decrease with time and with increasing NO₂ or O₃ concentration. These observations were explained using the kinetic multi-layer model of aerosol surface and bulk chemistry (KM-SUB) as being due to a trace reactant on the surface of the soot being consumed over time by reaction with NO₂ or O₃ (Ammann and Pöschl, 2007). At higher O₃ or NO₂ concentrations, the trace reactant would be used up faster leading to lower uptake coefficients. The SO₂ uptake onto acidic aerosols was also shown to be dependent upon time and SO₂ concentration, although in this case these dependencies were due to the aerosol bulk becoming saturated with SO₂. The KM-SUB model also allows investigation of the effects of aerosol viscosity on the uptake coefficients (Shiraiwa et al., 2010).

In this work, a dependence of the HO₂ uptake coefficient upon time and the initial HO₂ concentration has been observed for aqueous aerosols and was discussed in Sections 3.9 – 3.11. Several explanations were suggested for these dependencies such as: (1) the saturation of the aerosol surface or bulk with HO₂, (2) a trace reactant being used up over time, (3) a change in the viscosity of the aerosol, (4) a decrease in HO₂ concentration along the flow tube leading to less HO₂ being destroyed by self-reaction, (5) a change in the aerosol pH and finally, (6) a reformation of HO₂ from hydrogen peroxide due to the Fenton reactions. However, in order to understand which of these processes may be causing the time dependence and is consistent with the apparent dependence upon the initial HO₂ concentration, modelling of the HO₂ uptake coefficient is required. Moreover, the change in the HO₂ uptake coefficient with changing aerosol viscosity as observed for copper doped

sucrose aerosols in Section 4.4 will also be investigated using the KM-SUB model. The effect of viscosity on the HO₂ uptake coefficient could also help to explain the low HO₂ uptake coefficients onto SOA measured in this work (Sections 5.3 and 5.4).

There has been a large variability in the HO₂ uptake coefficients published in the literature. However, the HO₂ uptake coefficients measured in this work have tended to be much smaller than measured by other groups using a similar experimental setup. In this work, HO₂ uptake coefficients of 0.003 ± 0.005 and 0.01 ± 0.01 were measured onto aqueous ammonium sulphate aerosols at 55% RH and at 65 – 75%, respectively. The initial HO₂ concentration was $\sim 1 \times 10^9$ molecule cm⁻³ and measurements were made between approximately 10 and 20 seconds. Taketani et al. (2008) measured a HO₂ uptake coefficient of 0.11 ± 0.03 to 0.19 ± 0.04 between 45 and 75 % RH which is at least an order of magnitude higher than in this work. However, Taketani et al. (2008) used a much lower initial HO₂ concentration ($\sim 10^8$ molecule cm⁻³) and measured uptake coefficients at shorter times of about 5 to 11 seconds. Thornton and Abbatt (2005) also measured a much larger HO₂ uptake coefficient (~ 0.1) onto buffered ammonium sulphate aerosols at 42 % RH than measured in this work. Thornton and Abbatt (2005) used an initial HO₂ concentration of $\sim 10^{12}$ molecule cm⁻³ and made measurements between approximately 7 and 16 seconds. Once a model has been developed to explain the trends observed in this work, progress will also be made towards explaining the different HO₂ uptake coefficients measured by different groups.

8.2 A description of the KM-SUB model developed to calculate the HO₂ uptake coefficient

The KM-SUB model was briefly described in Section 1.8.2 but will be described in greater detail below. The KM-SUB model splits the aerosol into several layers. For the HO₂ uptake version of this model, these layers consist of a gas phase, a near surface gas phase, a sorption layer, a near surface bulk layer and several bulk layers as shown in Figure 8.1. For the majority of this work the number of bulk layers was set to five. However, when investigating viscosity effects in Section 8.9, the bulk layer number was set to one hundred as the diffusion between the bulk layers becomes an important process. Several processes were also included into the model including gas phase diffusion, adsorption and desorption to and from the

surface of the aerosol, surface to bulk transport, transport between each bulk layer and reactions in the gas phase and reactions in the aerosol bulk (Pöschl et al., 2007; Shiraiwa et al., 2010). These processes are illustrated in Figure 8.1 for the version of the model written specifically to investigate the HO₂ uptake. The code was modified by Thomas Berkemeier and Manabu Shiraiwa of the Max Planck Institute für Chemie in Mainz.

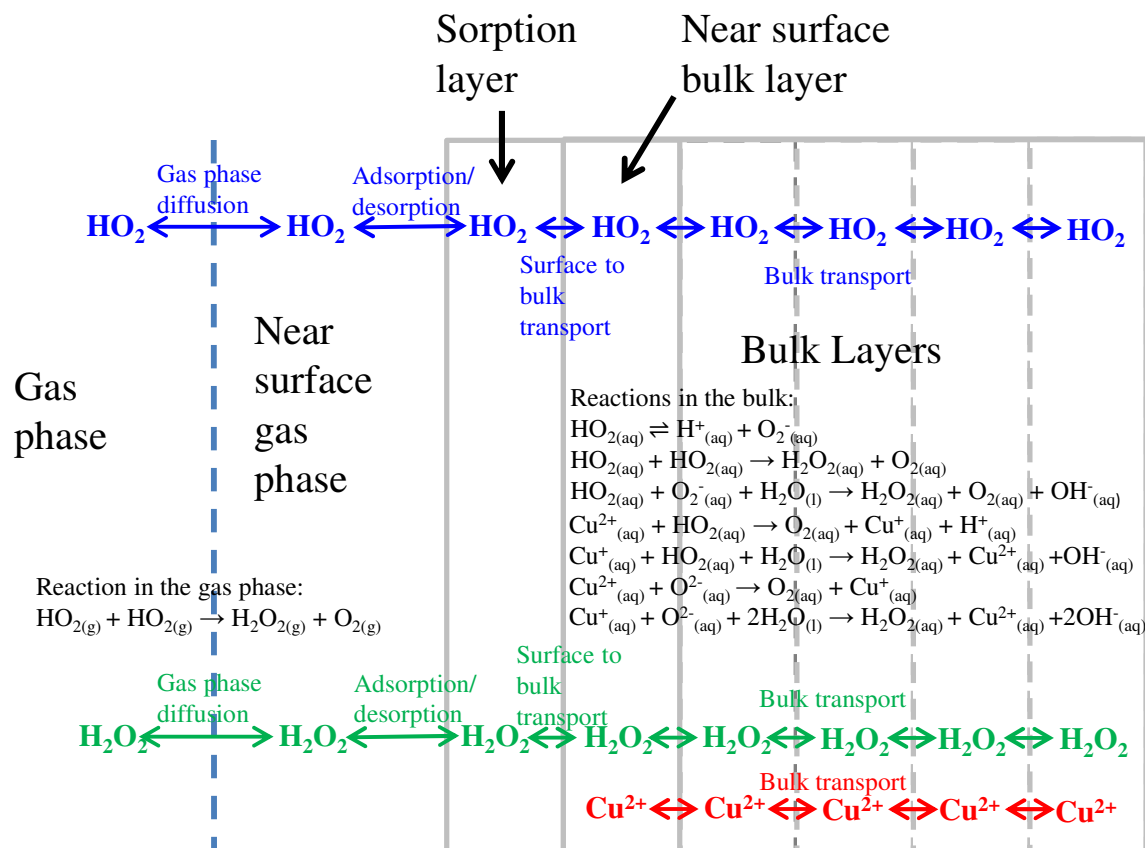


Figure 8.1: A schematic of the KM-SUB model adapted for HO₂ uptake.

The gas phase diffusion flux to the near surface gas phase (J_{diff}) in the KM-SUB model was given by

$$J_{diff} = 4\pi(mfp_X + r_p)D_{g,X}([X]_g - [X]_{gs}) \quad (\text{E8.1})$$

where $D_{g,X}$ is the gas phase diffusion coefficient of X (where X represents either HO₂ or H₂O₂), r_p is the particle radius, $[X]_g$ is the gas phase concentration of X, $[X]_{gs}$ is the gas phase concentration of X near the surface of the aerosol and mfp_X is the mean free path of X in air or nitrogen given by:

$$mfp_X = \frac{1.7D_{g,X}}{\omega_X} \quad (\text{E8.2})$$

where ω_X is the mean thermal velocity of ω_X calculated as below:

$$\omega_X = \sqrt{\frac{8RT}{\pi M_X}} \quad (\text{E8.3})$$

where R is the gas constant, T is the temperature and M_X is the molar mass of X.

The adsorption rate of a gas phase species, X, to the surface of the aerosol was given by:

$$J_{ads} = J_{coll,X} \alpha_{s,0} [X]_{gs,X} = \frac{\alpha_{s,0} [X]_{gs,X} \omega_X}{4} \quad (\text{E8.4})$$

where $J_{coll,X}$ is the flux of collisions of X with the surface of the aerosol, $\alpha_{s,0}$ is the surface accommodation of X at time zero, $[X]_{gs,X}$ is the gas phase concentration of X near the surface of the aerosol and ω_X is the mean thermal velocity of X.

The desorption rate from the surface of the aerosol was described by the following equation:

$$J_{des} = k_{des,X} [X]_s = \tau_{d,X}^{-1} [X]_s \quad (\text{E8.5})$$

where $k_{des,X}$ is the desorption rate coefficient from the surface of the aerosol, $\tau_{d,X}$ is the desorption lifetime of X from the surface of the aerosol and $[X]_s$ is the concentration of X at the surface of the aerosol (i.e. the concentration in the sorption layer).

The bulk to surface flux ($J_{b,s,X}$) was given by:

$$J_{b,s,X} = k_{b,s,X} [X]_{b1} \quad (\text{E8.6})$$

where $[X]_{b1}$ is the concentration of X in the first bulk layer and $k_{b,s,X}$ is the rate coefficient of bulk to surface transport given by:

$$k_{b,s,X} = \frac{2D_{b,X}}{(\delta + \delta_X)} \quad (\text{E8.7})$$

where $D_{b,X}$ is the bulk diffusion coefficient of X, δ is the thickness of the bulk layers and δ_X is the effective diameter of X. It should be noted that $(\delta + \delta_X)/2$ is the average distance that X needs to travel from the first bulk layer of the aerosol to the surface of the aerosol (Atkins, 1997; Pfrang et al., 2010; Shiraiwa et al., 2010).

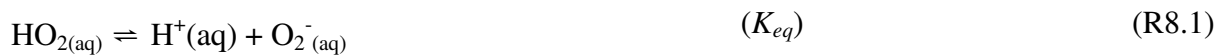
The surface to bulk transport ($J_{b,s,X}$) was described as:

$$J_{s,b,X} = k_{s,b,X}[X]_s \quad (\text{E8.8})$$

where $[X]_s$ is the concentration of X at the surface of the aerosol and $k_{s,b,X}$ is the rate coefficient of bulk to surface transport given by:

$$k_{s,b,X} = \frac{4k_{b,s,X}H_{eff,X}k_{des,X}}{\alpha_{s,X}w_X} \quad (\text{E8.9})$$

where H_{eff} is the effective Henry's law coefficient. For H_2O_2 an assumption was made that the Henry's law coefficient remained constant for different aerosol pH, whereas for HO_2 a correction was made to the physical Henry's law coefficient (H_{HO_2}) to account for an enhanced solubility of HO_2 at higher pH due to dissociation as shown below:



Therefore, the effective Henry's law coefficient was defined as (Thornton et al., 2008):

$$H_{eff} = H_{\text{HO}_2} \left(\frac{K_{eq}}{[H^+]} \right) \quad (\text{E8.10})$$

where $[H^+]$ is the concentration of H^+ ions in the aerosol.

The transport between each bulk layer was described as:

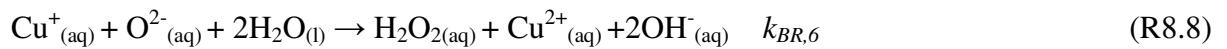
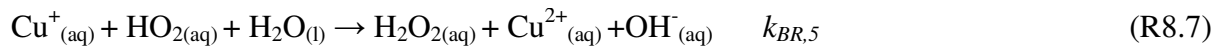
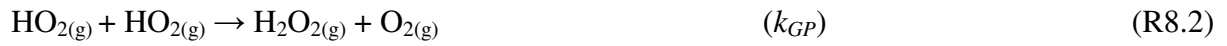
$$J_{b,b\pm 1,X} = k_{b,b,X}[X]_b \quad (\text{E8.11})$$

where $[X]_b$ is the concentration of X in a particular bulk layer and $k_{b,b,X}$ is the rate coefficient of transport between the bulk layers given by (Shiraiwa et al., 2010):

$$k_{b,b,X} = \frac{D_{b,X}}{\delta} \quad (\text{E8.12})$$

In this case the average travel distance is the thickness of the bulk layer which can be calculated from the number of bulk layers and the diameter of the aerosol.

The KM-SUB model was also modified by Thomas Berkemeier and Manabu Shiraiwa, of the Max Planck Institute für Chemie in Mainz, to include the HO₂ gas phase and aqueous reactions shown below (Jacob, 2000):



The initial parameters used in the model are summarised in Table 8.1.

Parameter	Value at 293 K	Reference
$k_{BR,1}$	$1.3 \times 10^{-15} \text{ cm}^3 \text{ s}^{-1}$	Thornton et al. (2008)
$k_{BR,2}$	$1.5 \times 10^{-13} \text{ cm}^3 \text{ s}^{-1}$	Thornton et al. (2008)
$k_{BR,3}$	$1.7 \times 10^{-13} \text{ cm}^3 \text{ s}^{-1}$	Jacob (2000)
$k_{BR,4}$	$1.3 \times 10^{-11} \text{ cm}^3 \text{ s}^{-1}$	Jacob (2000)
$k_{BR,5}$	$2.5 \times 10^{-12} \text{ cm}^3 \text{ s}^{-1}$	Jacob (2000)
$k_{BR,6}$	$1.6 \times 10^{-11} \text{ cm}^3 \text{ s}^{-1}$	Jacob (2000)
k_{GP}	$3 \times 10^{-12} \text{ cm}^3 \text{ s}^{-1}$	Sander et al. (2003)
K_{eq}	$2.1 \times 10^{-5} \text{ M}$	Thornton et al. (2008)
H_{HO_2}	5600 M atm^{-1}	Thornton et al. (2008)
$H_{H_2O_2}$	$1.65 \times 10^5 \text{ M atm}^{-1}$	Staffelbach and Kok (1993)
$D_{b,all}$	$1 \times 10^{-5} \text{ cm}^2 \text{ s}^{-1}$	Thornton et al. (2008)
τ_d	$3.5 \times 10^{-11} \text{ s}$	Shiraiwa et al. (2012a)
$\alpha_{s,0}$	1	
D_{g,HO_2}	$0.25 \text{ cm}^2 \text{ s}^{-1}$	Thornton et al. (2008)
δ_X	$4 \times 10^{-8} \text{ cm}$	
T	293 K	

Table 8.1: The initial parameters used in the KM-SUB HO₂ uptake model.

The HO₂ and H₂O₂ concentrations at a given time in each layer could then be calculated by integrating the loss and production terms of HO₂ and H₂O₂ (described above) over time. The uptake coefficient was then calculated for each time position using the following equation:

$$\gamma = \frac{J_{ads,X} - J_{des,X}}{J_{coll}} \quad (\text{E8.13})$$

Although the model has been described in this section, further changes were made as the model development evolved that will be described in the following sections.

The model is closely connected to the experimental measurements. The total aerosol surface area and volume inputted into the model were the same as the maximum total aerosol surface

area and volume used during experiments. The concentrations of species such as copper in the aerosols and the initial HO₂ concentration in the gas phase were also able to be changed within the model to replicate the experimental concentrations. The wall loss could also be included into the model as well as a changing HO₂ concentration along the flow tube as will be discussed in Section 8.5. However, there are a few differences between the experimental measurements and the modelling all of which are discussed below. First, the average aerosol radius was inputted into the model whereas in reality a range of aerosol radii are present within the aerosol flow tube. Secondly, the measurements were corrected for gas phase diffusion effects whereas in the model the HO₂ became depleted near the surface of the aerosol resulting in slightly lower HO₂ uptake coefficients. Finally, it should be noted that mixing was not included in the KM-SUB model. However, it was estimated from the KM-SUB model and by running the model at different HO₂ concentrations (such that each aerosol was exposed to more or less HO₂) that the HO₂ uptake coefficient during fixed injector experiments due to the mixing would be less than 10 % for all of the injector positions utilised during the experiments. It should also be noted that close to the injector (~ 1 cm) aerosol number concentrations were approximately 25 % higher in the centre of the flow tube compared to the sides of the flow tube whereas HO₂ concentrations were approximately 25 % lower in the centre of the flow tube compared to the sides of the flow tube. However, by ~ 6 - 7 cm from the injector measurable differences in aerosol and HO₂ concentrations across the flow tube were not observed.

8.3 Comparing the KM-SUB model to uptake coefficients measured during fixed injector and moving injector experiments

The KM-SUB model outputted the true or actual uptake coefficient at a given time. However, the HO₂ uptake coefficient for aqueous aerosols was measured in two different ways in this work as described in Sections 2.8 and 2.9. Fixed injector experiments measured the average uptake coefficient between time zero (when the flows initially mixed) and a given exposure time (determined by the position of the injector in the flow tube) whereas for moving injector experiments the HO₂ uptake coefficient was measured from HO₂ decays taken between approximately 10 and 20 seconds after initial mixing. For fixed injector experiments, the

uptake coefficient was determined in the model by numerical integration using the trapezoid method which averages two subsequent data points as shown by Equation 8.14:

$$Z = \int_{t_a}^{t_{a+1}} \gamma_{HO_2}(t) dt \approx (t_{a+1} - t_a) \left[\frac{\gamma(a) + \gamma(a+1)}{2} \right] \quad (\text{E8.14})$$

where t_a and t_{a+1} are two subsequent time points in the KM-SUB model and $\gamma(a)$ and $\gamma(a+1)$ are the HO₂ uptake coefficients at time t_a and time t_{a+1} respectively.

The time integrated uptake coefficients were then added together between time zero and the total time elapsed (t_x) as shown by Equation 8.15 in order to give a cumulative HO₂ uptake coefficient ($\gamma_{cumulative}$):

$$\gamma_{cumulative} = \sum_{t_0}^{t_x} Z \quad (\text{E8.15})$$

Finally, the cumulative HO₂ uptake coefficient was divided by the total time elapsed to give the average uptake coefficient between time zero and the total time elapsed ($\gamma_{avg,t_x,0}$) as shown in Equation 8.16:

$$\gamma_{avg,t_x,0} = \frac{\gamma_{cumulative}}{t_x} \quad (\text{E8.16})$$

An example of the KM-SUB output showing both the actual HO₂ uptake coefficient at each time point and the average HO₂ uptake coefficient between time zero and each given time point (which is equivalent to the fixed injector experiments) using the methodology described above is shown in Figure 8.2. The dependence of the HO₂ uptake coefficient upon time shown in Figure 8.2 will be described in further detail in Section 8.5.

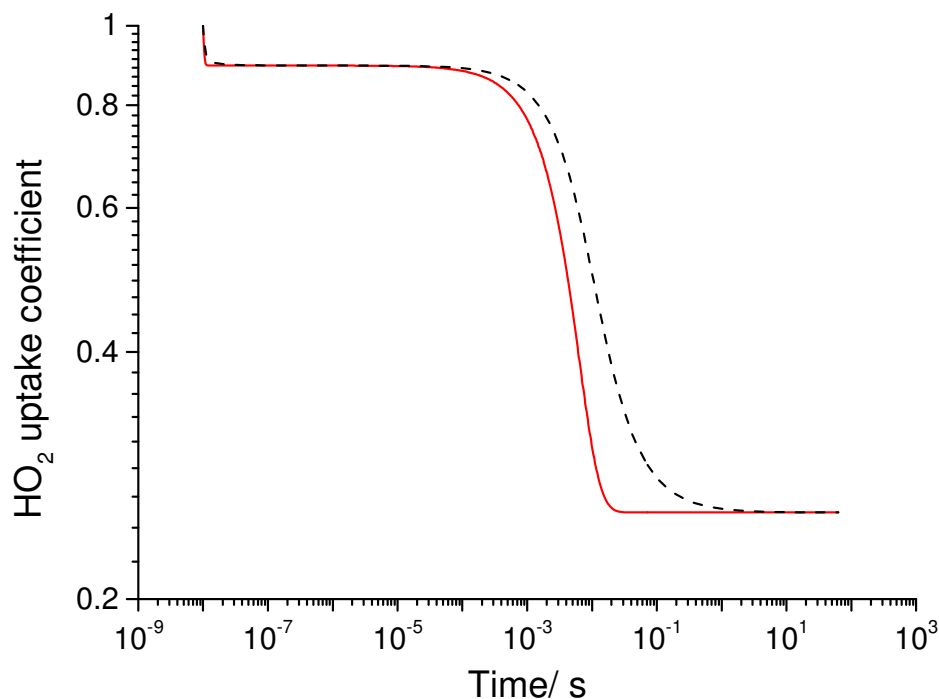


Figure 8.2: An example of the actual HO₂ uptake coefficient outputted by the model at each time point (red line) and the average HO₂ uptake coefficient between time zero and each time point (dashed black line) outputted by the KM-SUB model for an aqueous aerosol and at a HO₂ concentration of 1×10^9 molecule cm⁻³.

For comparison to data from the moving injector experiments the uptake coefficient was assumed to be given by the average HO₂ uptake coefficient between 10 and 20 seconds (γ_{10-20} seconds) as shown by Equation 8.17:

$$\gamma_{10-20 \text{ seconds}} = \frac{20\gamma_{0-20 \text{ seconds}} - 10\gamma_{0-10 \text{ seconds}}}{10} \quad (\text{E8.17})$$

where $\gamma_{0-20 \text{ seconds}}$ is the average uptake between 0 and 20 seconds and $\gamma_{0-10 \text{ seconds}}$ is the average uptake between 0 and 10 seconds which are calculated by the KM-SUB model using Equations 8.14 – 8.16 discussed earlier in this Section. Equation 8.17 was derived using a simplified relationship between the fixed injector experiments and moving injector experiments shown in Figure 8.3. Figure 8.3 is a simplification of the relationship between the fixed injector and moving injector experiments as it assumes that the uptake coefficients

can be described by a fast initial uptake coefficient followed by a constant uptake coefficient after 10 seconds. However, during the data analysis the moving injector analysis implicitly assumes a constant uptake coefficient between 10 and 20 seconds and for this reason Equation 8.17 can be considered a good approximation of the HO₂ uptake coefficient for moving injector experiments.

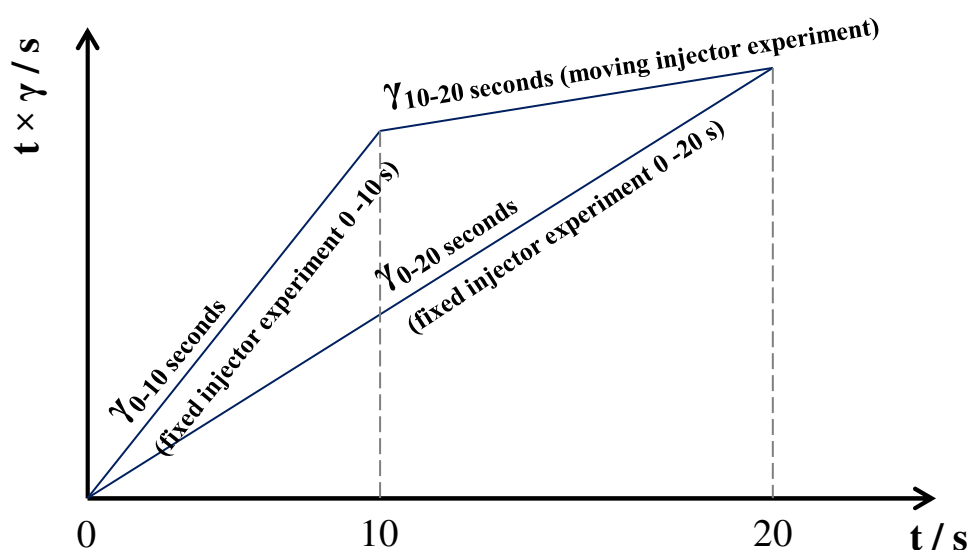


Figure 8.3: The simplified relationship between fixed injector experiments that measure an uptake coefficient between time zero and a given exposure time and the moving injector experiments that measure an uptake coefficient between approximately 10 and 20 seconds. The gradient of these lines represent the uptake coefficients measured by the different experiments.

8.4 Intercomparison of the Thornton et al. expression with the KM-SUB model

The Thornton et al. (2008) expression was described in Section 1.13.3 and is given by Equation 8.18. It is based on the resistor model that was described in Section 1.8.1 and is currently the only HO₂ uptake expression based on well understood HO₂ chemistry in the aqueous phase:

$$\frac{1}{\gamma^{HO_2}} = \frac{1}{\alpha^{HO_2}} + \frac{3wN_A}{8000(H_{eff}RT)^2 k_{eff}[HO_{2(g)}]r_p} \quad (E8.18)$$

where γ^{HO_2} is the uptake coefficient of HO_2 , α^{HO_2} is the mass accommodation coefficient, w is the molecular thermal speed of HO_2 , N_A is Avogadro's number, H_{eff} is the effective Henry's law constant defined in Equation 8.9 in Section 8.2, R is the universal gas constant, T is the temperature, $[HO_{2(g)}]$ is the concentration of HO_2 , r_p is the particle radius and k_{eff} is the effective second order rate constant defined in equation 8.19 (Thornton et al., 2008):

$$k_{eff} = \frac{k_{BR1} \left(\frac{K_{eq}}{[H^+]_{aq}} \right) k_{BR2}}{\left(1 + \frac{K_{eq}}{[H^+]_{aq}} \right)^2} \quad (E8.19)$$

Thornton et al. (2008) also modelled the HO_2 uptake coefficient for copper doped aerosols using Equation 8.20:

$$\frac{1}{\gamma^{HO_2}} = \frac{1}{\alpha^{HO_2}} + \frac{w}{H_{eff}RT \sqrt{k^I D_{aq} Q}} \quad (E8.20)$$

where k^I is the pseudo first order rate constant equivalent to $k^{II}[TMI]$, and k^{II} is the second order rate constant for the reaction between $HO_2 + Cu^{2+}$ and $O_2^- + Cu^{2+}$ obtained using the rate constants for Reaction 8.5 and 8.6 and equation 8.19. Q is given by the following equation and accounts for aqueous-phase diffusion limitations (Hanson and Lovejoy, 1995):

$$Q = \left(\coth(q) - \frac{1}{q} \right) \quad (E8.21)$$

where q is the reacto-diffusive parameter and is given by the following equation:

$$q = r \sqrt{\frac{k^I}{D_{aq}}} \quad (E8.22)$$

where r is the radius of the aerosols and D_{aq} is the HO_2 diffusion in the aerosol.

The rate constants and Henry's law constant shown in Table 8.1 were used in both the Thornton et al. (2008) expression and the KM-SUB model. There were three main

differences between the KM-SUB model and the Thornton et al. (2008) expression. First, the KM-SUB model split the aerosol and gas phase into different layers and had terms for the diffusion between each layer. This allowed the concentrations in each layer to be estimated. Secondly, the KM-SUB model included hydrogen peroxide as a product and allowed the release of hydrogen peroxide from the aerosol phase to be estimated. Thirdly, the KM-SUB model allowed the evolution of the HO₂ uptake coefficient to be monitored with time whereas the Thornton et al. (2008) expression outputted an equilibrated uptake coefficient. For example, Figure 8.4 shows an example of the output of the KM-SUB model with a changing HO₂ uptake coefficient over time. The HO₂ uptake coefficient starts at a value of 1 which is the mass accommodation. The uptake coefficient then drops to a value of ~ 0.8 due to depletion of HO₂ near the surface of the aerosol. Between 10⁻⁸ and 10⁻² seconds the HO₂ uptake coefficients decreases further as the bulk of the aerosol becomes saturated. The actual shape of the plot will be discussed in detail in Section 8.5. However, after ~ 0.1 seconds the HO₂ uptake coefficient no longer changes with time suggesting an equilibrated value which is the relevant value for the atmosphere. The equilibrated HO₂ uptake coefficient outputted by the KM-SUB model can therefore be directly compared with the HO₂ uptake coefficient outputted by the Thornton et al. (2008) expression enabling validation and verification of the KM-SUB model as shown below.

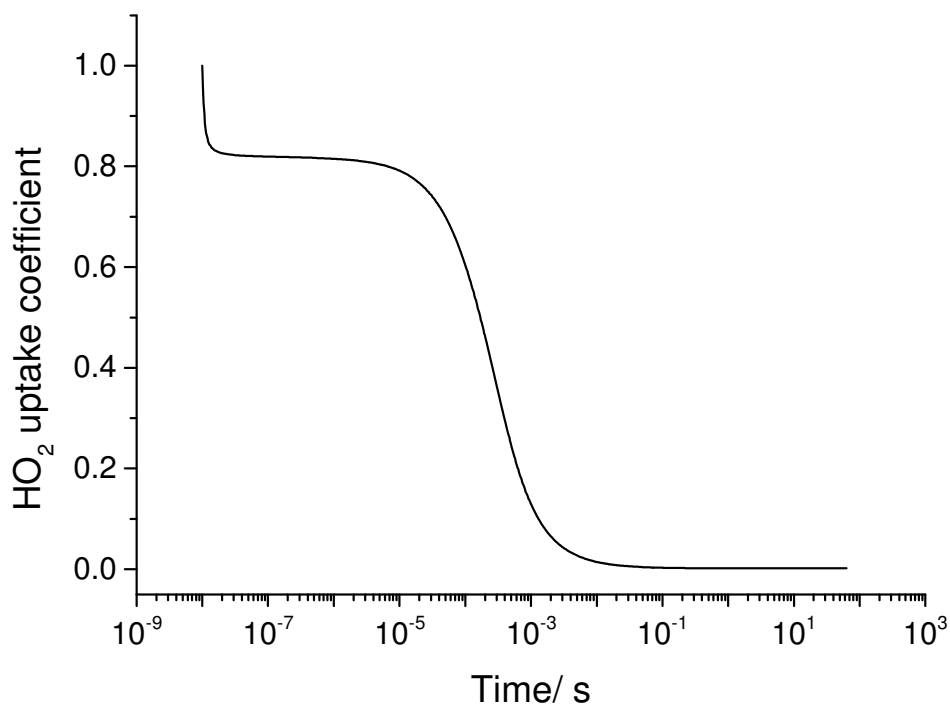


Figure 8.4: The KM-SUB model output for the HO₂ uptake coefficient as a function of time for 100 nm aqueous aerosols at a pH of 5 and with the gas phase HO₂ concentration set to a constant concentration of 5×10^8 molecule cm⁻³ and the temperature set to 293 K.

Figure 8.5 shows good agreement between the HO₂ uptake coefficients predicted by the Thornton et al. (2008) model and the KM-SUB model with changing aerosol pH, aerosol radius, HO₂ concentration and temperature. However, the HO₂ uptake coefficients start to deviate at larger uptake coefficients. For example, in Figure 8.5A the uptake coefficient at an aerosol pH of 12 for the KM-SUB model is 0.8 compared to an uptake coefficient of 1.0 for the Thornton et al. (2008) model. The slightly smaller HO₂ uptake coefficients for the KM-SUB model compared to the Thornton et al. (2008) model when the uptake coefficient is large can be explained by a depletion of HO₂ near the surface of the aerosol. Therefore, the flux of HO₂ to the surface of the aerosol decreases. An example of how the gas phase concentrations near the surface of the aerosol changes is shown in Figure 8.6.

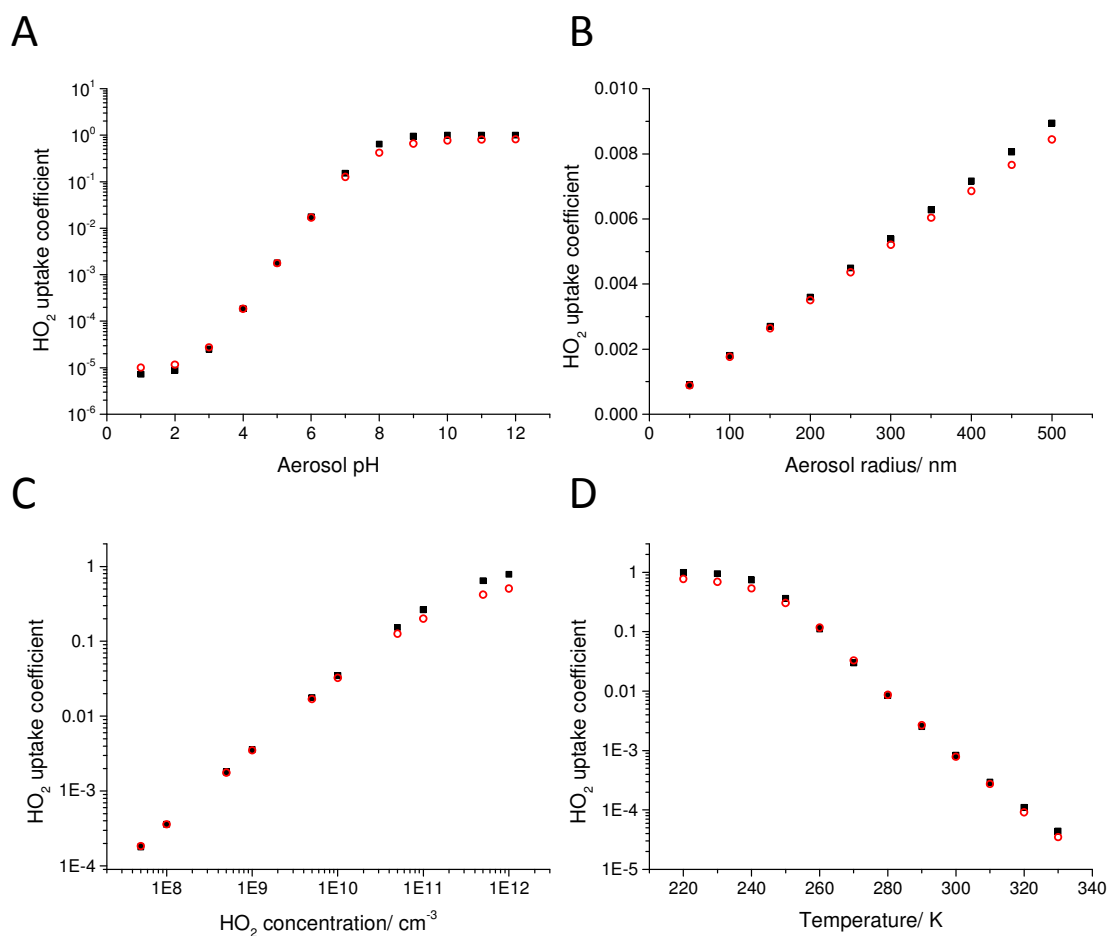


Figure 8.5: A comparison between the HO_2 uptake coefficients predicted by the Thornton et al. model (black squares) and from the KM-SUB model (red open circles) for aqueous aerosols as a function of (A) aerosol pH, (B) aerosol radius, (C) HO_2 concentration and (D) temperature. The pH of the aerosol was set to 5, the aerosol radius was 100 nm, the HO_2 concentration was 5×10^8 molecule cm^{-3} and the temperature was 293 K unless otherwise stated.

Figure 8.6 shows that at very short times ($\sim 10^{-8}$ seconds) the HO_2 gas phase concentration near the surface of the aerosol is depleted as the uptake coefficient is high and the diffusion to the near surface gas phase is slow compared to the loss of HO_2 once at the surface due to the high uptake. In these circumstances, the HO_2 uptake coefficient is limited only by gas phase diffusion to the aerosol. However, as the HO_2 concentration near the surface of the aerosol increases the uptake coefficient becomes less limited by gas phase diffusion. When the uptake coefficient is small, for example, at an aerosol pH of 1 (the black line in Figure 8.6) the gas phase diffusion limitations will be negligible. However, when the uptake coefficient is larger, for example, at an aerosol pH of 7 and 12 (the green and blue lines in Figure 8.6)

the gas phase diffusion limitations become larger and this results in the discrepancy between the Thornton et al. (2008) model and the KM-SUB model.

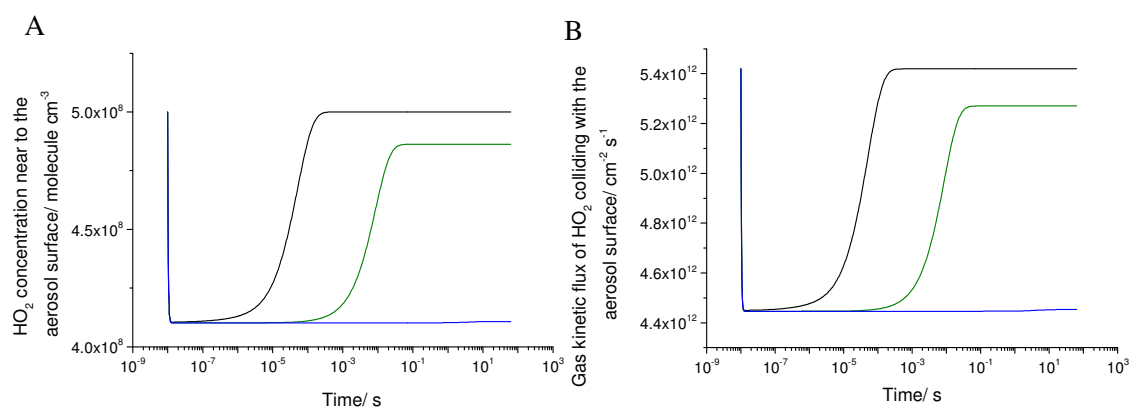


Figure 8.6: (A) The HO₂ concentration near the surface of the aerosol as a function of time and (B) the flux of HO₂ colliding with the surface of the aerosol (J_{coll}) as a function of time. The pH of the aerosol was set to 1 (black line), 7 (green line) and 12 (blue line), the aerosol radius was 100 nm, the gas phase HO₂ concentration was 5×10^8 molecule cm⁻³ and the temperature was 293 K.

The agreement between the Thornton et al. (2008) model and the KM-SUB model was also investigated for aqueous aerosols containing a variety of copper concentrations. Similarly to the comparison shown in Figure 8.5, at large HO₂ uptake coefficients the KM-SUB model outputted smaller uptake coefficients than the Thornton et al. (2008) model due to a depletion of the HO₂ near the surface of the aerosol. Whereas the Thornton et al. (2008) model reached the mass accommodation of 1 the KM-SUB model was limited by gas phase diffusion when the uptake coefficient was very large. However, overall the shape of the KM-SUB graph was very similar to the Thornton et al. (2008) model although there was some disagreement at copper molarities of 10⁻⁸ to 10⁻⁶ M. However, this may be due to the non-inclusion of reactions between Cu⁺ and HO₂ or O₂⁻ in the Thornton et al. (2008) model which is a product of the reactions of Cu²⁺ with HO₂ or O₂⁻. In the KM-SUB model reaction of HO₂ with both Cu⁺ and Cu²⁺ are included.

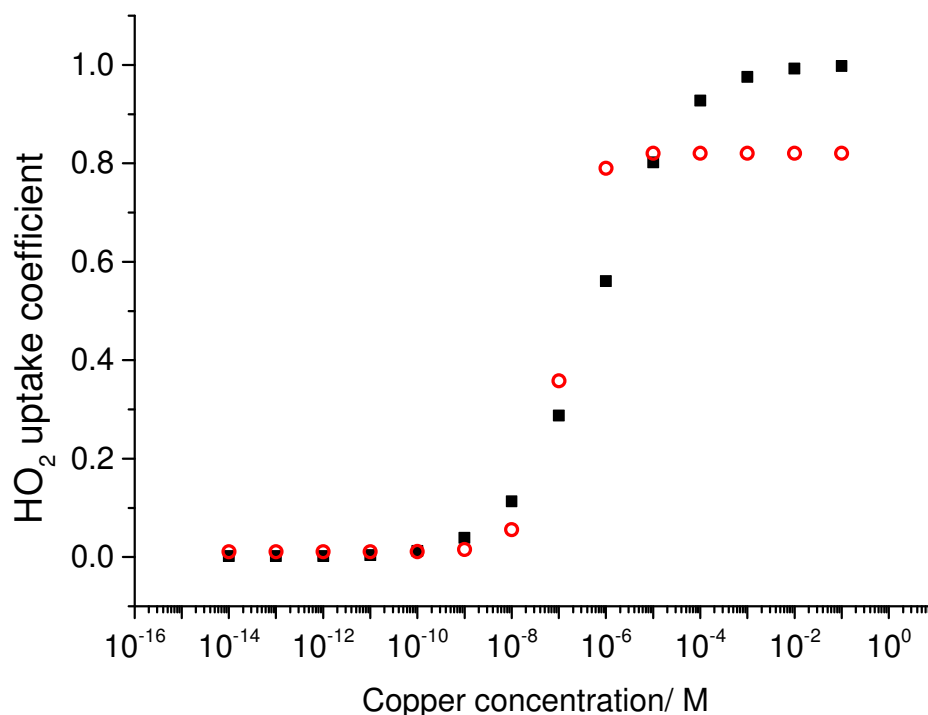


Figure 8.7: A comparison between the equilibrated HO₂ uptake coefficients predicted by the Thornton et al. model (black squares) and from the KM-SUB model (red open circles) as a function of aerosol copper molarity. The pH of the aerosol was set to 5, the aerosol radius was 100 nm, the HO₂ concentration was set to a constant concentration of 5×10^8 molecule cm⁻³ and the temperature was 293 K.

8.5 Modelling of the HO₂ uptake coefficient time dependence onto aqueous aerosols

As previously described in this work in Section 3.9, HO₂ uptake coefficients were observed to decrease over time for aqueous sodium chloride and ammonium nitrate aerosols. Several possible explanations were suggested in Section 3.9 for this time dependence. The explanations that were discussed included a saturation mechanism, a trace reactant being used up over time, a change in aerosol viscosity over time, or a decrease in the HO₂ concentration along the flow tube leading to a decrease in the rate of the HO₂ self-reaction. However, it seems unlikely that a trace reactant would be being used up over time. As discussed in Section 3.9, the most likely reactant that would be used up would be copper or iron, however, ICP-MS analysis has shown that these two reactants are not present at high enough

concentrations to affect the uptake coefficient and the deactivation mechanism is unknown. It also seems unlikely that the aerosols would be becoming more viscous over time as this would require a mechanism that would increase the viscosity of the aerosols. However, viscosity will be explored in greater detail in Section 8.8.

The first possible explanation that was explored was that the aerosols were becoming saturated by HO_2 over time. If the bulk of the aerosol became fully saturated over time (i.e. by reaching the HO_2 solubility limit), the HO_2 uptake coefficient would decrease (as discussed in Section 3.9). Once the aerosol was fully saturated the uptake coefficient would stabilise to an uptake coefficient that would be controlled by HO_2 chemistry within the aerosol which irreversibly removes HO_2 . In order to test the hypothesis that saturation was causing the time dependence the KM-SUB model was run under the experimental conditions of a sodium chloride experiment that has been performed in this work. Figure 8.8 shows that indeed the HO_2 uptake coefficient does decrease with time, but the KM-SUB model predicted that the aerosol would be fully saturated by approximately 0.1 seconds and that this could not explain the time dependence shown by the experimental data at longer times. It can also be seen that the model predicts that the HO_2 uptake coefficient would be approximately an order of magnitude larger than measured in this work. However, in Figure 8.8 the HO_2 concentration along the flow tube (or with time) was kept constant in the KM-SUB model which is unrealistic (others model runs are described below in which HO_2 is allowed to change).

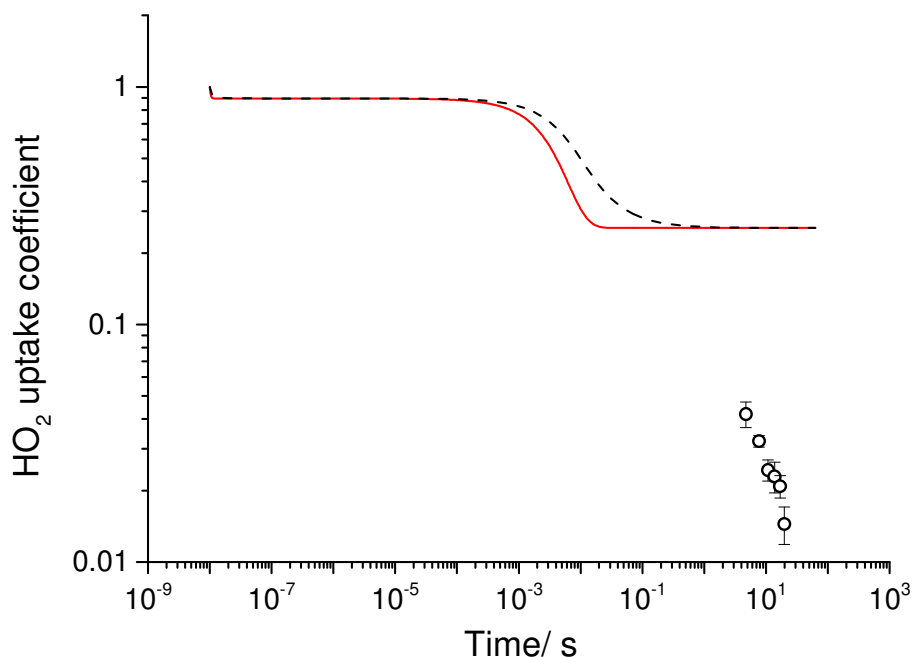


Figure 8.8: The HO₂ uptake coefficient measured in this work for aqueous sodium chloride aerosols at a maximum aerosol concentration of $1 \times 10^6 \text{ cm}^{-3}$ and with an average radius of 67 nm with an initial HO₂ concentration of $2.1 \times 10^9 \text{ molecule cm}^{-3}$ as a function of time. The HO₂ uptake coefficient (red line) and time averaged HO₂ uptake coefficient (dashed black line) outputted by the KM-SUB model assume that the aerosol pH is 7 and does not change with time and also assumes for this run that the gas phase HO₂ concentration does not change with time.

The second possible explanation was that the decrease in HO₂ along the flow tube due to removal of HO₂ by uptake and by wall losses was the cause of the time dependence. As the HO₂ in the gas phase decreased, less HO₂ would partition to the aerosols and therefore there would be a decrease in the rate of the HO₂ self-reaction shown below. A reduction in the HO₂ self-reaction in the aerosols would then lead to a decrease in the HO₂ uptake coefficient:



In order to test this hypothesis, the model was set up so that the HO_2 concentration along the flow tube was allowed to decrease instead of being kept constant. The decrease in the gas phase HO_2 concentration was due to both reactions in the aerosols (irreversible uptake) leading to lower HO_2 concentrations in the aerosol and also due to a wall loss term that was inputted based on the observed HO_2 uptake to the wall multiplied by the wall surface area and multiplied by the flux of HO_2 collisions with the flow tube wall ($J_{collwall}$):

$$J_{collwall} = \frac{[\text{HO}_2]\omega}{4} \quad (\text{E8.23})$$

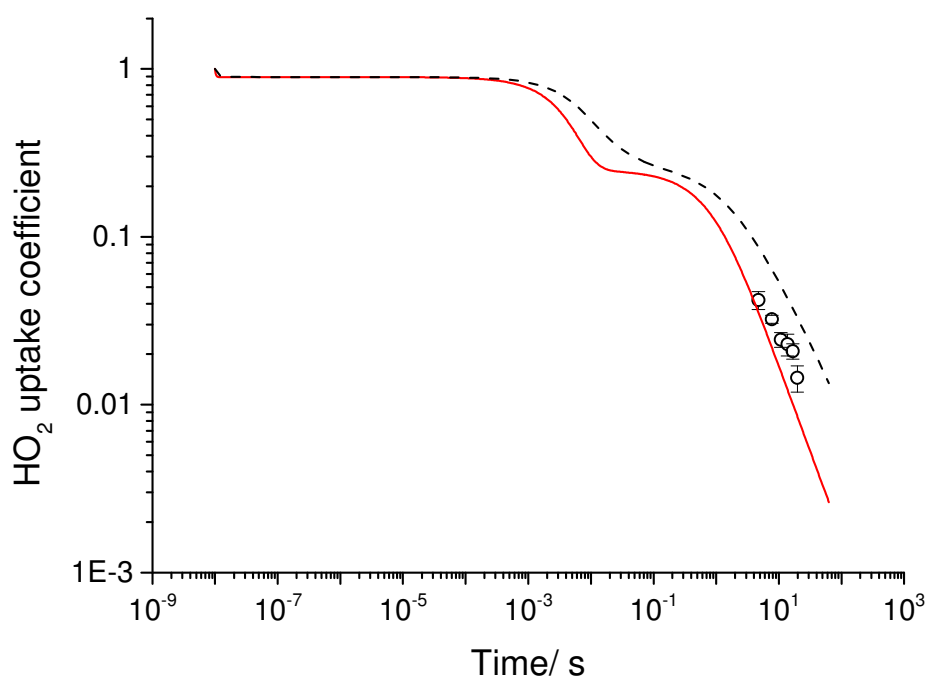


Figure 8.9: The HO_2 uptake coefficient measured in this work for aqueous sodium chloride aerosols during fixed injector experiments at a maximum aerosol concentration of $1 \times 10^6 \text{ cm}^{-3}$ and with an average radius of 67 nm with an initial HO_2 concentration of $2.1 \times 10^9 \text{ molecule cm}^{-3}$ as a function of time. The HO_2 uptake coefficient (red line) and time averaged HO_2 uptake coefficient (dashed black line) outputted by the KM-SUB model assume that the aerosol pH is 7 and does not change with time. The HO_2 concentration in the aerosol was recalculated at each time point so that it decreased with time due to loss by reaction. The model conditions were chosen to match those of the experiment as closely as possible.

Figure 8.9 shows that once the HO₂ concentrations were allowed to decrease over time in the KM-SUB model due to aerosol and wall losses there was quite good agreement between the HO₂ uptake coefficients measured over time in this work for aqueous aerosols and the HO₂ uptake coefficients predicted by the KM-SUB model. This agreement suggests that the HO₂ uptake coefficient for aqueous aerosols is controlled by the second order HO₂ self-reaction in the aerosol phase. It would also mean that reaction time, wall loss and initial HO₂ concentration could all potentially affect the measured HO₂ uptake coefficient. It should also be noted that a check was performed to make sure that although a second order uptake mechanism was assumed in the KM-SUB model, the HO₂ decay with time outputted by the KM-SUB model would indeed be pseudo first order, as is observed experimentally. Figure 8.10 shows that a log plot of the HO₂ concentration against time did still appear first-order (i.e. is linear) and that the pseudo-first-order assumption made during the data analysis (Section 2.8) was valid.

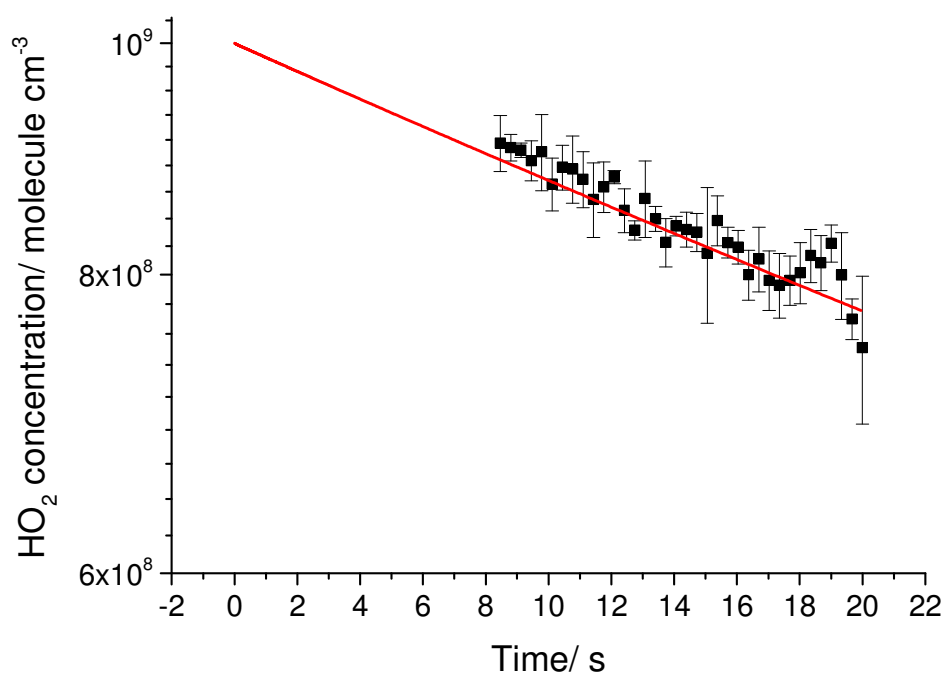


Figure 8.10: The HO₂ concentration decay over time obtained in this work for sodium chloride aerosols (black points) and predicted by the KM-SUB model (red line) for an initial HO₂ concentration of 1×10^9 molecule cm⁻³, an average aerosol radius of 56 nm, an aerosol number concentration of 1.8×10^6 cm⁻³ and an aerosol pH of 7. The KM-SUB model conditions were chosen to match those of the experiment as closely as possible.

8.6 Modelling the observed initial HO₂ concentration dependence of the HO₂ uptake coefficient onto aqueous aerosols

As previously discussed in Section 3.11, as well as observing a time dependence of the uptake coefficient for aqueous aerosols in this work, an apparent HO₂ concentration dependence was also observed with larger HO₂ uptake coefficients measured at lower initial HO₂ concentrations. This trend was consistently observed for aqueous aerosols for both moving injector experiments and fixed injector experiments. However, when running the KM-SUB model, the opposite trend was observed, as shown in Figure 8.11. Two potential explanations for the larger HO₂ uptake coefficients experimentally observed at lower HO₂ concentrations will be explored in Sections 8.6.1 and 8.6.2.

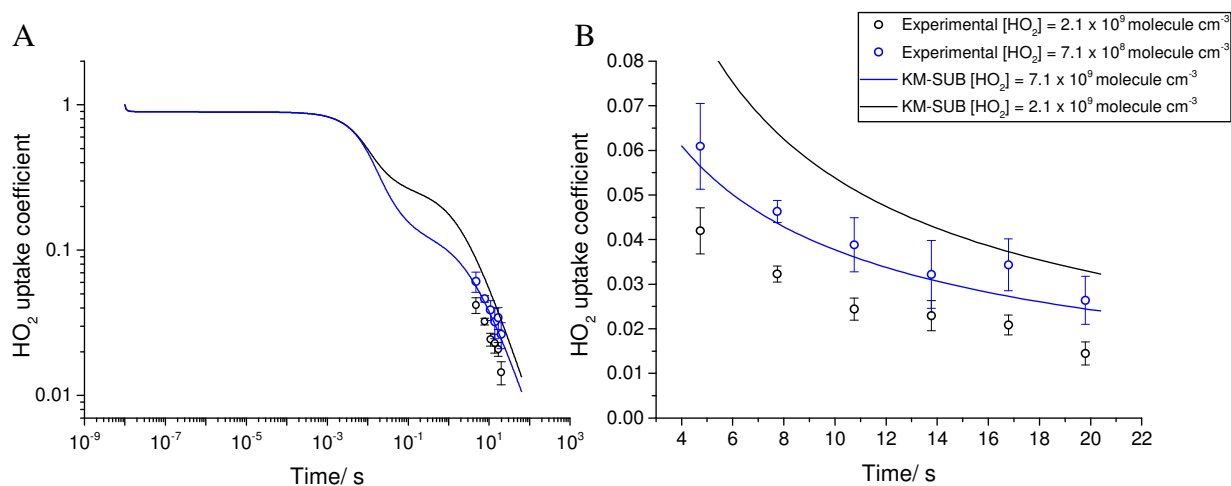


Figure 8.11: The measured HO₂ uptake coefficient onto aqueous sodium chloride aerosols at a maximum aerosol concentration of $1 \times 10^6 \text{ cm}^{-3}$ and with an average radius of 67 nm with an initial HO₂ concentration of $2.1 \times 10^9 \text{ molecule cm}^{-3}$ (black points) and at an initial HO₂ concentration of $7.1 \times 10^8 \text{ molecule cm}^{-3}$ (blue points) as a function of time. The HO₂ uptake coefficient outputted by the KM-SUB model under the same conditions as the experiments are shown for an initial HO₂ concentration of $2.1 \times 10^9 \text{ molecule cm}^{-3}$ (black line) and at an initial HO₂ concentration of $7.1 \times 10^8 \text{ molecule cm}^{-3}$ (blue line) assuming a constant aerosol pH of 7. B is an expanded version of A between 4 – 20 seconds.

8.6.1 Investigating the effect of the changing aerosol pH due to dissociation of HO₂ in the aerosol

One of the potential explanations given for the observed experimental HO₂ concentration dependence in Section 3.11, and shown in Figure 8.11, was the possibility that at higher HO₂ concentrations there would be more HO₂ in the aerosol and therefore more H⁺ from dissociated HO₂, since HO₂ is a weak acid with a pK_a of 4.7 (Jacob, 2000). More acidic aerosols would lead to a smaller HO₂ uptake coefficient as was shown in Figure 8.5A. Therefore, the HO₂ uptake coefficient would be lower at larger HO₂ concentrations, as seen experimentally. Another interesting observation that could be explained by changing the aerosol pH within the KM-SUB model would be the much lower HO₂ uptake coefficients that were observed for ammonium nitrate aerosols. Ammonium nitrate is a weak acid whereas sodium chloride aerosols should have a pH of 7.

The initial pH of the aerosol was inputted into the model. For sodium chloride the initial pH was inputted as 7 whereas for ammonium nitrate the initial pH was estimated as 4.9, although there is some uncertainty in this as it is not possible to directly probe the pH of the aerosols within the flow tube. An iterative method was then included in the model that captures the interaction of dissolved HO₂, its dissolution into H⁺ and O₂⁻ and the feedback on dissolved HO₂.

The effect of the two different initial HO₂ concentrations on the aerosol pH for the aqueous sodium chloride experiments was investigated, as well as for the ammonium nitrate aerosols. Figure 8.12 shows the change in pH of the aerosols over time and the changing HO₂ uptake coefficient over time. Figure 8.12A shows that for sodium chloride aerosols, as the HO₂ enters the aerosol this causes the aerosol to become much more acidic due to dissociation into H⁺. However, as the HO₂ decreases along the flow tube there is also less HO₂ partitioning to the aerosol phase and dissociating, and therefore the pH of the aerosol starts to increase. However, the pH of the ammonium nitrate aerosols does not change very much due to the much lower initial pH of the aerosols which means that the effective Henry's law constant is lower and less HO₂ enters the bulk of the aerosols and dissociates.

The effect of aerosol pH was suggested as a possible reason for the observed HO_2 concentration dependence. However, Figure 8.12B shows that the changing aerosol pH due to the dissociation of HO_2 cannot explain the experimental dependence of the HO_2 uptake coefficient upon the initial HO_2 concentration as shown in Figure 8.11. The predicted HO_2 uptake coefficient from the KM-SUB model still remains larger for the larger initial HO_2 concentrations. This suggests that the rate of the HO_2 self-reaction in the aerosol dominates the observed uptake coefficient with larger uptake coefficients measured at larger HO_2 concentrations. If the pH term had instead been dominant, it might have been expected that the uptake coefficient would have increased over time as the aerosols became less acidic, which is not observed experimentally.

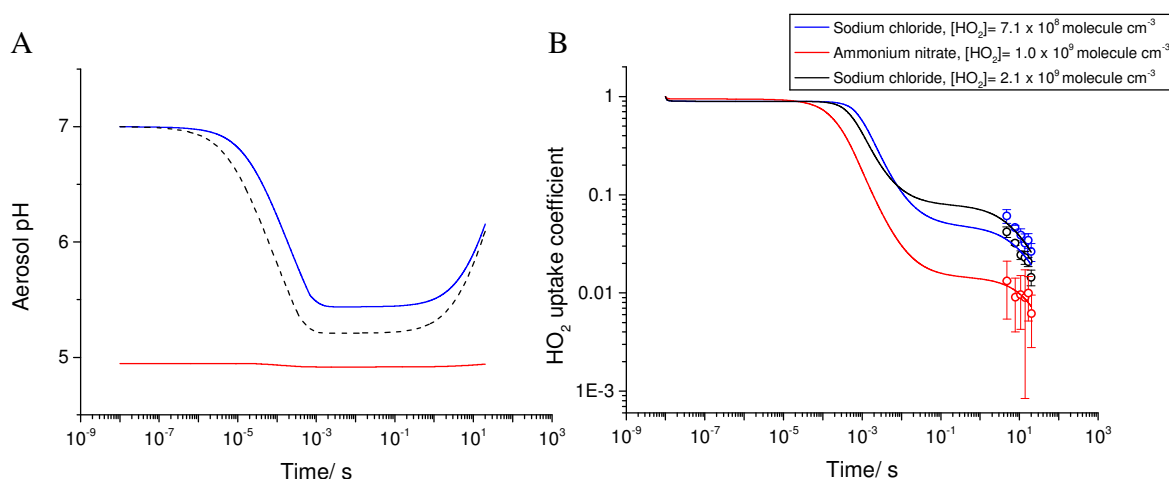


Figure 8.12: The change in (A) the aerosol pH and (B) the HO_2 uptake coefficient as a function of time for sodium chloride aerosols at a maximum aerosol concentration of $1 \times 10^6 \text{ cm}^{-3}$, with an average radius of 67 nm with an initial HO_2 concentration of $2.1 \times 10^9 \text{ molecule cm}^{-3}$ (black) and at an initial HO_2 concentration of $7.1 \times 10^8 \text{ molecule cm}^{-3}$ (blue) as a function of time. The data for ammonium nitrate aerosols at a maximum aerosol concentration of $1 \times 10^6 \text{ cm}^{-3}$ and with an average radius of 44 nm with an initial HO_2 concentration of $1 \times 10^9 \text{ molecule cm}^{-3}$ (red) is also shown. The HO_2 uptake coefficient outputted by the KM-SUB model under the same conditions as the experiments are shown for the data assuming the rate constants shown in the second column of Table 8.3 but with a Henry's law coefficient of $1.5 \times 10^4 \text{ M atm}^{-1}$.

Figure 8.12B does show that the different initial pH of the sodium chloride aerosols and ammonium nitrate aerosols can explain the difference in the magnitude of the HO_2 uptake coefficient between the ammonium nitrate and sodium chloride aerosols. The much lower uptake coefficient for the ammonium nitrate aerosols is due to a much lower effective

Henry's law coefficient at low pH, and therefore a decrease in the surface to bulk rate constant. The time dependence of ammonium nitrate experimental data is also modelled well.

Figure 8.13 shows that by including the change in aerosol pH due to the dissociation of HO_2 into H^+ and O_2^- , the lack of an increase in the HO_2 uptake coefficient at high pH can be explained. The pH experiments were discussed in Section 3.6 and it was expected that at a pH of approximately 10, the HO_2 uptake coefficient would only be limited by mass accommodation as shown in Figure 8.5A. However, the model cannot explain the HO_2 uptake coefficients at low pH that were measured as being much larger than predicted by the model. A possible explanation is that these aerosols contained trace amounts of metals (from the original salt or possibly leached from the atomiser) that were in large enough concentrations to increase the HO_2 uptake coefficients.

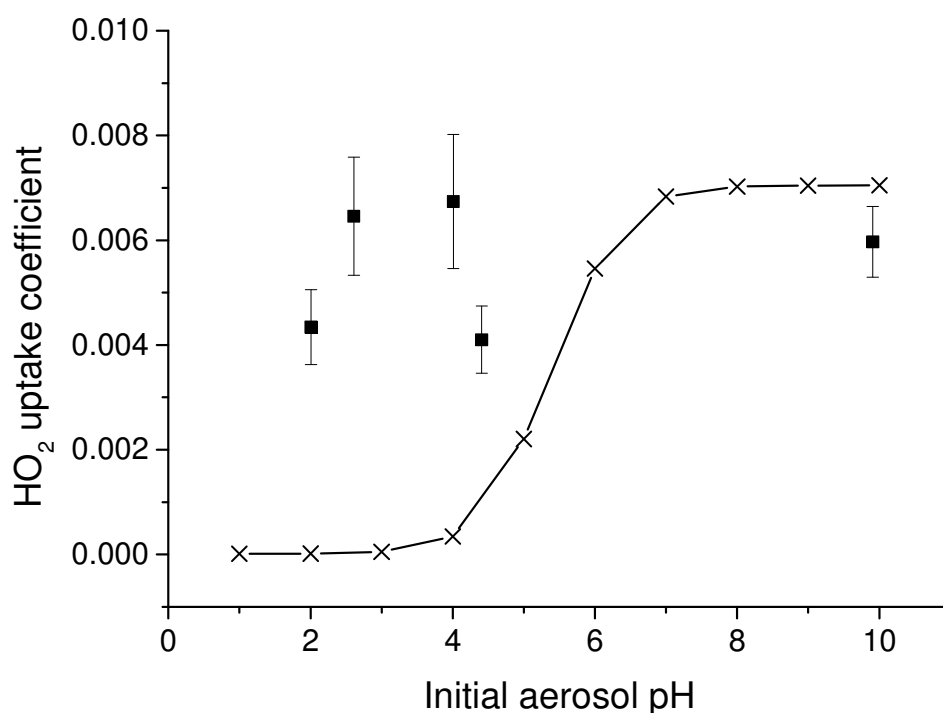


Figure 8.13: The HO_2 uptake coefficient for sodium chloride aerosols with hydrochloric acid or sodium hydroxide added into the atomiser solutions measured in this work (black points). The line represents the change in the HO_2 uptake coefficient predicted by the KM-SUB model when also including changes to the aerosol pH due to the dissociation of HO_2 to H^+ and O_2^- .

8.6.2 Investigating the effect of a Fenton-like reaction

Up to now, in this chapter the copper and iron concentrations in the aerosols have been set to zero. However, ICP-MS measurements have shown that the copper and iron concentrations tend to be around 1 ppb ($\sim 3 \times 10^{13}$ molecule cm^{-3} , although there is some variability in the concentrations), even if all possible care is taken in preparing and not storing solutions. By measuring the concentrations of copper ions in the sodium chloride and ammonium nitrate solutions using ICP-MS (for the experiments shown in Figure 8.12) the copper ion concentrations were estimated as 3×10^{13} molecule cm^{-3} for ammonium nitrate aerosols and 6×10^{12} molecule cm^{-3} for sodium chloride aerosols. These copper concentrations are equivalent to copper molarities of 1×10^{-8} M and 5×10^{-8} M for ammonium nitrate and sodium chloride aerosols respectively. These concentrations would be expected to increase the uptake coefficient from a value that would be obtained with no copper present (see Figure 8.7) making the relatively good agreement shown in Figure 12 much worse.

The inclusion of a Fenton-like reaction could potentially reduce the modelled HO_2 uptake coefficient by converting H_2O_2 back to HO_2 , thereby lowering the modelled HO_2 uptake coefficient. It could also potentially explain the lower HO_2 uptake coefficients observed at higher HO_2 concentrations. H_2O_2 concentrations were measured during the experiments at the Paul Scherrer Institute in Switzerland when the mercury lamp used to generate HO_2 was operated at two currents (and therefore generated two different HO_2 concentrations). The methodology for measuring H_2O_2 concentrations was described in Section 2.13. The H_2O_2 concentrations exiting the injector were measured as 40 ± 10 ppt ($\sim 9.9 \times 10^8$ molecule cm^{-3}) for the lower lamp current (lower $[\text{HO}_2]$) and 230 ± 20 ppt ($\sim 5.7 \times 10^9$ molecule cm^{-3}) at the higher lamp current (higher $[\text{HO}_2]$). Therefore, it might be expected that at the higher gas phase H_2O_2 concentration, more H_2O_2 would partition to the aerosol phase and a larger proportion of HO_2 would be reformed in the aerosol which could then partition back to the gas phase thereby lowering the uptake coefficient by a larger amount. In order to check the effect of including a Fenton-like reaction, the experimental conditions shown in Table 8.2 were inputted into the KM-SUB model. A Fenton-like reaction was also included into the model as shown below:



	NaCl (lower HO ₂ concentration)	NaCl (higher HO ₂ concentration)	Ammonium nitrate
[Cu ²⁺ _(aq)] ₀ / molecule cm ⁻³	6.0 × 10 ¹²	6.0 × 10 ¹²	3.0 × 10 ¹³
[HO ₂ _(g)] ₀ / molecule cm ⁻³	7.1 × 10 ⁸	2.1 × 10 ⁹	1.0 × 10 ⁹
[H ₂ O ₂ _(g)] ₀ / molecule cm ⁻³	9.9 × 10 ⁸	5.7 × 10 ⁹	1.5 × 10 ⁹

Table 8.2: The initial copper, HO₂ and H₂O₂ concentrations inputted into the KM-SUB model.

Parameter	Literature values at 293 K (as shown in Table 8.1)	Optimised values outputted by the KM-SUB model	Values with lower Cu (II) reaction rates
$k_{BR,1}$	1.3 × 10 ⁻¹⁵ cm ³ s ⁻¹	1.57 × 10 ⁻¹¹ cm ³ s ⁻¹	1.3 × 10 ⁻¹⁴ cm ³ s ⁻¹
$k_{BR,2}$	1.5 × 10 ⁻¹³ cm ³ s ⁻¹	2.18 × 10 ⁻¹³ cm ³ s ⁻¹	1.5 × 10 ⁻¹² cm ³ s ⁻¹
$k_{BR,3}$	1.7 × 10 ⁻¹³ cm ³ s ⁻¹	6.23 × 10 ⁻¹³ cm ³ s ⁻¹	1.7 × 10 ⁻¹⁷ cm ³ s ⁻¹
$k_{BR,4}$	1.3 × 10 ⁻¹¹ cm ³ s ⁻¹	2.58 × 10 ⁻¹¹ cm ³ s ⁻¹	1.3 × 10 ⁻¹⁵ cm ³ s ⁻¹
$k_{BR,5}$	2.5 × 10 ⁻¹² cm ³ s ⁻¹	1.43 × 10 ⁻¹¹ cm ³ s ⁻¹	2.5 × 10 ⁻¹⁶ cm ³ s ⁻¹
$k_{BR,6}$	1.6 × 10 ⁻¹¹ cm ³ s ⁻¹	4.56 × 10 ⁻¹¹ cm ³ s ⁻¹	1.6 × 10 ⁻¹⁵ cm ³ s ⁻¹
$k_{BR,7}$	N/A	2.39 × 10 ⁻¹² cm ³ s ⁻¹	2.39 × 10 ⁻¹² cm ³ s ⁻¹
k_{GP}	3 × 10 ⁻¹² cm ³ s ⁻¹	3 × 10 ⁻¹² cm ³ s ⁻¹	3 × 10 ⁻¹² cm ³ s ⁻¹
K_{eq}	2.1 × 10 ⁻⁵ M	1.7 × 10 ⁻⁵ M	2.1 × 10 ⁻⁵ M
H_{HO2}	5600 M atm ⁻¹	6475 M atm ⁻¹	5600 M atm ⁻¹
H_{H2O2}	1.65 × 10 ⁵ M atm ⁻¹	2.75 × 10 ⁵ M atm ⁻¹	1.65 × 10 ⁵ M atm ⁻¹
$D_{b,all}$	1 × 10 ⁻⁵ cm ² s ⁻¹	1 × 10 ⁻⁵ cm ² s ⁻¹	1 × 10 ⁻⁵ cm ² s ⁻¹
τ_d	3.5 × 10 ⁻¹¹ s	3.5 × 10 ⁻¹¹ s	3.5 × 10 ⁻¹¹ s
$\alpha_{s,0}$	1	1	1
$D_{g,HO2}$	0.25 cm ² s ⁻¹	0.25 cm ² s ⁻¹	0.25 cm ² s ⁻¹
δ_X	4 × 10 ⁻⁸ cm	4 × 10 ⁻⁸ cm	4 × 10 ⁻⁸ cm
T	293 K	293 K	293 K

Table 8.3: The three different sets of parameters used in this work. See text for details of ‘optimised values’ and ‘lower copper rates’.

It should be noted that Reaction 8.9 is a simplified reaction and that there are many different reactions that could occur between hydrogen peroxide, HO_x and trace amounts of copper and iron (De Laat and Gallard, 1999; Pham et al., 2013). The Fenton reactions are also dependent upon pH which has also not been included into the model (Kremer, 2003). However, Reaction 8.9 has been used in the KM-SUB model (rather than a more complex reaction scheme) to show whether the reformation of HO_2 from hydrogen peroxide has the potential to explain the apparent HO_2 concentration dependence shown in the experimental measurements. In the future, a larger number of reactions could be added into the KM-SUB model to in order to better represent reactions that could be occurring.

Due to Reaction 8.9 being a simplified reaction its effective rate constant is unknown. There are also large errors associated with some of the other parameters. Therefore, a genetic algorithm was written by Thomas Berkemeier (MPI für Chemie Mainz) and used by the KM-SUB model to check whether there was a set of rate constants that could fit the measurements in this work when including Reaction 8.9 and using different H_2O_2 concentrations. The results of running the genetic algorithm are shown in the second column of Table 8.3. With these values an extremely good fit to the data experimentally obtained in this work was found as shown in Figure 8.14.

Figure 8.14 shows that the apparent HO_2 concentration dependence of the HO_2 uptake coefficient experimentally observed during experiments could be explained by a Fenton-like reaction. This is the first time that it has been shown that it is possible to observe larger HO_2 uptake coefficients at lower HO_2 concentrations. The observed trend can be explained by the larger amounts of hydrogen peroxide that can partition to the aerosol phase where it is converted back to HO_2 that then partitions to the gas phase. However, in order to fit the model to the data the rate constant $k_{BR,I}$ had to be increased by approximately four orders of magnitude compared to the literature value. Although such a large increase in $k_{BR,I}$ seems unlikely, values of $k_{BR,I}$ as high as $5.6 \times 10^{-14} \text{ cm}^3 \text{ s}^{-1}$ have been reported in the literature (Christensen and Sehested, 1988). Therefore an investigation was performed to see whether another set of reaction rates could equivalently explain the apparent HO_2 concentration trends observed during experiments.

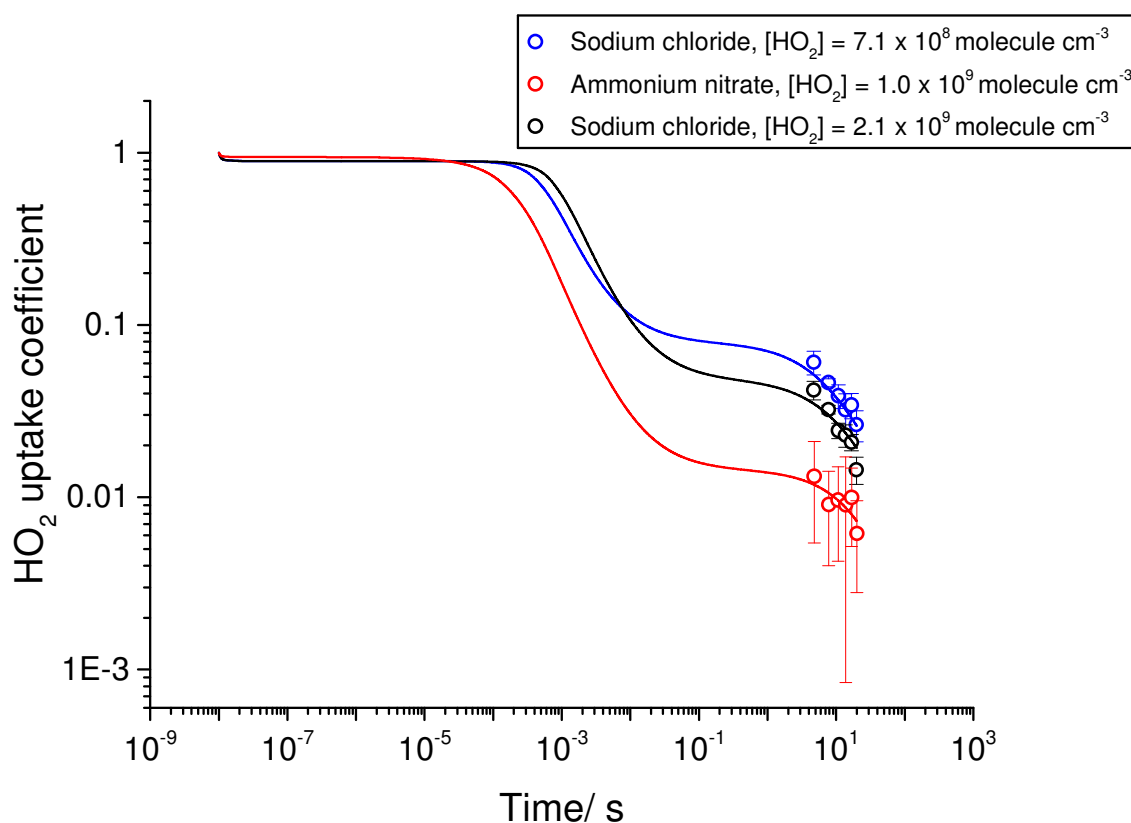


Figure 8.14: The measured HO_2 uptake coefficient onto aqueous sodium chloride aerosols at a maximum aerosol concentration of $1 \times 10^6 \text{ cm}^{-3}$ and with an average radius of 67 nm with an initial HO_2 concentration of $2.1 \times 10^9 \text{ molecule cm}^{-3}$ (black points) and at an initial HO_2 concentration of $7.1 \times 10^8 \text{ molecule cm}^{-3}$ (blue points) as a function of time. The data for ammonium nitrate aerosols at a maximum aerosol concentration of $1 \times 10^6 \text{ cm}^{-3}$ and with an average radius of 44 nm with an initial HO_2 concentration of $1 \times 10^9 \text{ molecule cm}^{-3}$ (red points) is also shown. The HO_2 uptake coefficient outputted by the KM-SUB model under the same conditions as the experiments are shown for the data assuming the rate constants shown in the second column of Table 8.3.

Another set of reaction rates were found that could explain the apparent HO_2 concentration dependence, with the results shown in Figure 8.15. The rate coefficients that were used to create Figure 8.15 are shown in the third column of Table 8.3 and show that by decreasing the rate constants associated with the copper ion reactions ($k_{BR,3} - k_{BR,6}$) by four orders of magnitude the $k_{BR,1}$ rate does not need to be increased by the extent that was required to get the good fitting in Figure 8.14. Although decreasing the rate constants for the reactions involving copper ions by four orders of magnitude may also seem unrealistic, there is evidence that suggests that this may be the case as will be discussed in Section 8.7.

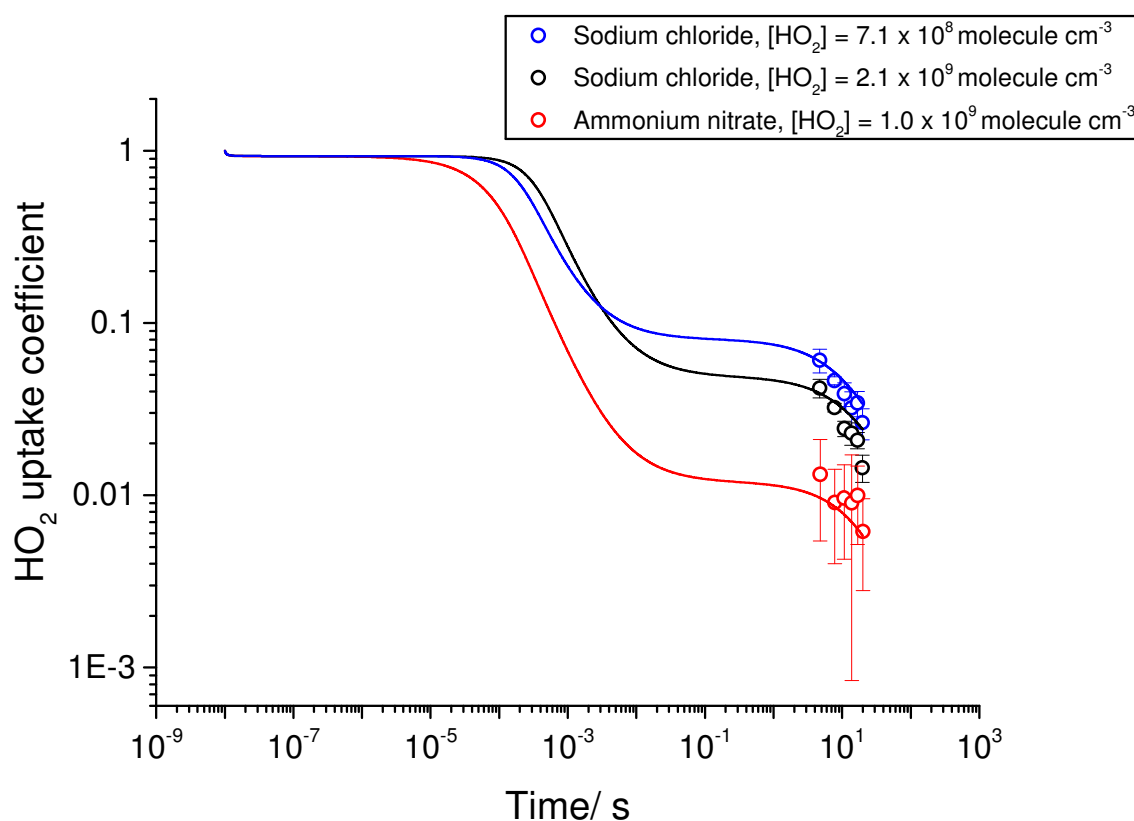


Figure 8.15: The measured HO_2 uptake coefficient onto aqueous sodium chloride aerosols at a maximum aerosol concentration of $1 \times 10^6 \text{ cm}^{-3}$ and with an average radius of 67 nm with an initial HO_2 concentration of $2.1 \times 10^9 \text{ molecule cm}^{-3}$ (black points) and at an initial HO_2 concentration of $7.1 \times 10^8 \text{ molecule cm}^{-3}$ (blue points) as a function of time. The data for ammonium nitrate aerosols at a maximum aerosol concentration of $1 \times 10^6 \text{ cm}^{-3}$ and with an average radius of 44 nm with an initial HO_2 concentration of $1 \times 10^9 \text{ molecule cm}^{-3}$ (red points) are also shown. The HO_2 uptake coefficient outputted by the KM-SUB model under the same conditions as the experiments are shown for the data assuming the rate constants shown in the third column of Table 8.3. The initial pH of the aerosols was set to 7 for the sodium chloride aerosols and 4.9 for the ammonium nitrate aerosols.

8.7 The dependence of the HO_2 uptake coefficient upon the aerosol copper concentration

In Section 3.5 measurements of the HO_2 uptake coefficients as a function of aerosol copper ion concentration were discussed. In this work the HO_2 uptake coefficient was measured as increasing from a copper ion molarity of approximately 10^{-4} M with the HO_2 uptake coefficient being limited only by mass accommodation at a copper ion molarity of 10^{-2} M . These measurements were in agreement with measurements made by Mozurkewich et al.

(1987) However, the measurements were in disagreement with the Thornton et al. (2008) model that predicted that the HO₂ uptake coefficients would start to increase at $\sim 10^{-9}$ M, and would be limited by mass accommodation at 10^{-4} M. Thornton et al. (2008) suggested that the discrepancy between the model and the work by Mozurkewich et al. (1987) may be due to diffusion limitations within the aerosol (as described by Equations 8.21 and 8.22 in Section 8.4). However, this seems unlikely to be the case as the diffusion coefficient of HO₂ would have to be decreased from 10^{-5} cm² s⁻¹ to 10^{-10} cm² s⁻¹ in order to start to obtain HO₂ concentration gradients in the aerosol that could slow the overall uptake coefficient by the required amount. Investigations with the KM-SUB model also showed that changing the diffusion coefficient of HO₂ into the aerosol had the effect of decreasing the uptake coefficient but did not shift the copper concentration at which the uptake coefficient started to increase or reached the maximum value. Due to the discrepancy between the measurements and the Thornton et al. (2008) model, the KM-SUB model was also run over a range of copper ion concentrations. As shown in Figure 8.16, the KM-SUB model predicted that the HO₂ uptake coefficient would start to increase at a copper ion concentration of 10^{-8} M and would be fully limited by mass accommodation by 10^{-6} M when inputting the literature values shown in Table 8.1.

The black points in Figure 8.16 show the measurements of the HO₂ uptake coefficients made in this work whilst the blue line shows the HO₂ uptake coefficients outputted by the KM-SUB model as a function of aerosol copper ion concentration. Although both the experimental measurements and the KM-SUB points show that the HO₂ uptake coefficient increases over a copper ion concentration increase of 3 orders of magnitude, the KM-SUB model predicts that the increase in the HO₂ uptake coefficient occurs at a copper concentration which is four orders of magnitude lower than observed during measurements. Therefore, several parameters were investigated to see whether the predicted increase in the HO₂ uptake coefficient could be made to fit the measurements. The parameters that were investigated were the Henry's law coefficient, the addition of a Fenton-like reaction and the rate constants of the reactions involving copper.

The first parameter that was investigated was the Henry's law constant. The Henry's law constant for HO₂ is estimated to be 5600 M atm⁻¹ at 293 K. However, as discussed in Section 3.5, based on the measurements by Schwartz (1984) and Golden et al. (1990), the Henry's

law coefficient could lie in the range of 1200 M atm^{-1} to 9000 M atm^{-1} . Therefore, the effect of lowering the Henry's law coefficient to 1200 M atm^{-1} was investigated and the results of this are shown by the green line in Figure 8.16. As can be seen in Figure 8.16, there is a small decrease in the HO_2 uptake coefficient (in the range of copper ion concentrations of 10^{-8} to 10^{-6} M) when lowering the Henry's law coefficient from 5600 M atm^{-1} to 1200 M atm^{-1} . The small decrease in the HO_2 uptake coefficient is due to a decrease in the flux of HO_2 from the surface to the bulk of the aerosol. However, the increase in the HO_2 uptake coefficient still occurs between aerosol copper concentrations of 10^{-8} M and 10^{-6} M . Therefore, decreasing the Henry's law coefficient cannot remove the discrepancy between the measurements in this work and the KM-SUB model.

The second parameter that was investigated was the addition of a Fenton-like reaction as discussed in Section 8.6.2. For this investigation, the Henry's law coefficient was reset to 5600 M atm^{-1} . The rate of the Fenton-like reaction that was used in Section 8.6.2 of $2.4 \times 10^{12} \text{ cm}^{-3} \text{ s}^{-1}$ was inputted into the KM-SUB model and initial H_2O_2 concentration of $6 \times 10^9 \text{ molecule cm}^{-3}$ was used. The result of including this Fenton-like reaction is shown by the grey line in Figure 8.16. Similarly to the results when decreasing the Henry's law coefficient a small decrease in the HO_2 uptake coefficient (in the range of copper concentrations of 10^{-8} to 10^{-6} M) was outputted. The decrease was due to the reformation of HO_2 from H_2O_2 . However, the increase in the HO_2 uptake coefficient still occurred between copper concentrations of 10^{-8} and 10^{-6} M and could therefore not explain the discrepancy between the measurements in this work and the KM-SUB model.

Lastly, the effect of lowering the rate constants of the reactions involving copper ions ($k_{BR,3} - k_{BR,6}$) was investigated. Although several studies have investigated the copper ion rate constants with HO_2 and O_2^- in aqueous solutions (Bielski et al., 1985; Cabelli et al., 1987; Rabani et al., 1973; Vonpiechowski et al., 1993) the only parameters that could be changed to obtain agreement between the measurements in this work and the KM-SUB model was by decreasing the copper ion rate constants by four orders of magnitude, as shown by the red line in Figure 8.16. Although, this seems like a large decrease in the copper rate constants this decrease was the only way to gain good agreement between the HO_2 uptake coefficient dependence on copper measured in this work (and also measured by Mozurkewich et al. (1987) as shown in Section 3.5) and the KM-SUB model.

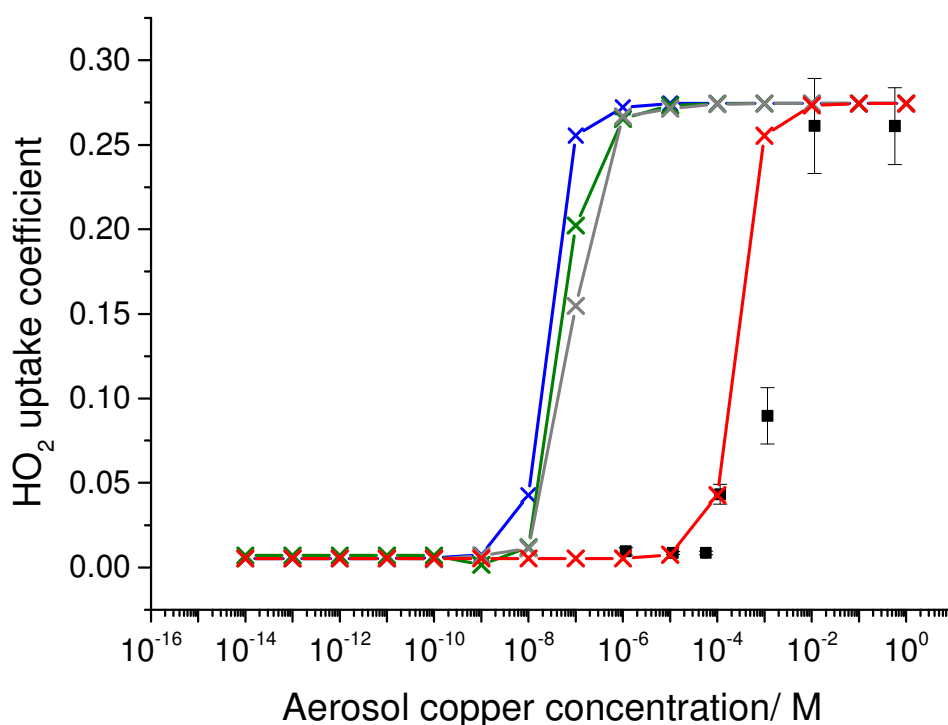


Figure 8.16: The HO_2 uptake coefficient dependence upon the aerosol copper ion concentration measured in this work (black points) and predicted by the KM-SUB model using literature values (blue line), with a lower Henry's law coefficient of 1200 M atm^{-1} (green line), with a Fenton-like reaction with a rate constant of $2.4 \times 10^{-12} \text{ cm}^3 \text{ s}^{-1}$ and an initial H_2O_2 concentration of $6 \times 10^9 \text{ molecule cm}^{-3}$ (grey line) and with the copper rate constants being decreased by four orders of magnitude (red line).

8.8 The dependence of the HO_2 uptake coefficient upon time and initial HO_2 concentration for copper doped aerosols

The time dependence for the non-copper doped aerosols was explained and investigated in Section 8.5. As the HO_2 concentrations dropped along the flow tube the uptake coefficient decreased due to the rate of the second order HO_2 reaction in the aerosol decreasing. However, a time dependence was also experimentally observed for the copper-doped aerosols as discussed in Section 3.10. The time dependence observed for copper-doped aerosols cannot be explained by a decrease in HO_2 along the flow tube as the rate of HO_2 loss becomes first order in the aerosol in terms of HO_2 . By inputting the literature values shown in Table

8.1 into the KM-SUB model and inputting an aerosol copper ion concentration of 2×10^{20} molecule cm^{-3} (~ 0.3 M) (estimated from the concentration in the atomiser solution and the aerosol humidity) the blue line in Figure 8.17 was obtained. It should be noted that by decreasing the copper ion rate constants by four orders of magnitude (as discussed Section 8.7) the green line was obtained showing a decrease in the HO_2 uptake coefficient at longer times. Due to the lower rate constants, the rate of HO_2 destruction increased leading to the slightly lower HO_2 uptake coefficient. However, the HO_2 uptake coefficient only increased very slightly at longer time. This is due to a slight increase in the aerosol pH leading to an increase in the aerosol solubility.

As shown in Figure 8.17, when the Fenton-like reactions were included in the model, a further decrease in the HO_2 uptake coefficient was observed over time (as observed during measurements in Section 3.10). This was due to the conversion of aqueous H_2O_2 back to HO_2 followed by partitioning to the gas phase leading to higher HO_2 gas phase concentrations, compared to when a Fenton-like reaction was not included, as shown in Figure 8.18. As more H_2O_2 was added into the model the HO_2 uptake coefficient decreased further as there was more HO_2 reformation which partitioned to the gas phase. This may explain the apparent dependence of the HO_2 uptake coefficient upon the initial HO_2 concentration for copper-doped aerosols as discussed in Section 3.11. At higher HO_2 concentrations there were also higher H_2O_2 concentrations exiting the injector (confirmed by preliminary experiments performed in Switzerland) which would have led to a higher reformation of HO_2 and therefore a potential decrease in the HO_2 uptake coefficient.

Although it has been shown that the apparent time and HO_2 concentration dependence can potentially be explained by the inclusion of a Fenton-like reaction, a good fitting to the measurements in this work (shown in Section 3.10) has not yet been achieved. In Figure 3.12 in Section 3.10 measurements of the HO_2 uptake coefficient time dependence onto copper doped aerosols at an initial HO_2 concentration of 1×10^9 molecule cm^{-3} were shown. These measurements showed that the HO_2 uptake coefficient decreased from 0.95 ± 0.02 at 5 seconds to 0.37 ± 0.04 at 20 seconds. However, the model output in Figure 8.17 showed that the HO_2 uptake coefficient decreased between 5 and 20 seconds to approximately 0.1. The HO_2 concentration data for moving injector experiments also did not fit particularly well with the decays shown in Figure 8.18.

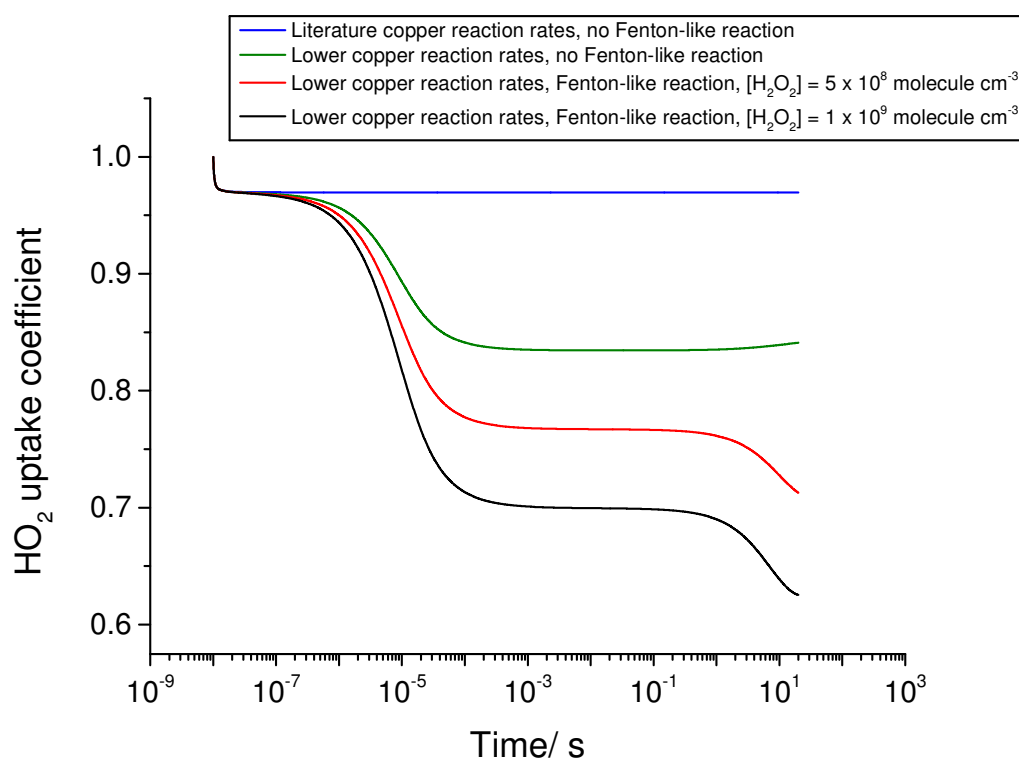


Figure 8.17: The HO_2 uptake coefficient outputted by the KM-SUB model for copper doped aerosols with an average radius of 30 nm at a concentration of $5 \times 10^4 \text{ cm}^{-3}$. The copper ion concentration was set to $2 \times 10^{20} \text{ molecule cm}^{-3}$ and the initial HO_2 concentration was set to $1 \times 10^9 \text{ molecule cm}^{-3}$. Four sets of conditions were run with the KM-SUB model. First the literature values shown in column 1 of Table 8.3 with no Fenton-like reactions (blue line), secondly the conditions shown in column 3 of Table 8.3 and with no Fenton-like reactions (green line), thirdly the conditions shown in column 3 of Table 8.3 with a Fenton-like reaction and an initial H_2O_2 concentration of $5 \times 10^8 \text{ molecule cm}^{-3}$ (red line) and lastly the conditions shown in column 3 of Table 8.3 with a Fenton-like reaction and an initial H_2O_2 concentration of $1 \times 10^9 \text{ molecule cm}^{-3}$ (black line).

In order to match the measurements with the model output several changes could be investigated with the KM-SUB model in the future. Currently, the loss of HO_2 at the walls of the flow tube is set to produce no products. However, if the model was altered so that the HO_2 loss at the walls of the flow tube was fully or partially converted to H_2O_2 , this would increase the H_2O_2 concentrations along the flow tube potentially leading to a greater decrease in the HO_2 uptake coefficient due to a greater reformation of gas phase HO_2 in the flow tube. Measurements of how the H_2O_2 concentrations vary along the flow tube would be essential in

modelling the HO₂ uptake coefficient for copper-doped aerosols. Once more measurements of both H₂O₂ concentrations and the HO₂ uptake coefficient at these H₂O₂ concentrations have been made with aerosols containing different copper (and possibly iron) concentrations, the HO₂ reaction rate constants and other parameters in the model should be able to be better constrained and may lead to a better understanding of the HO₂ uptake mechanism both in the flow tube and in the troposphere.

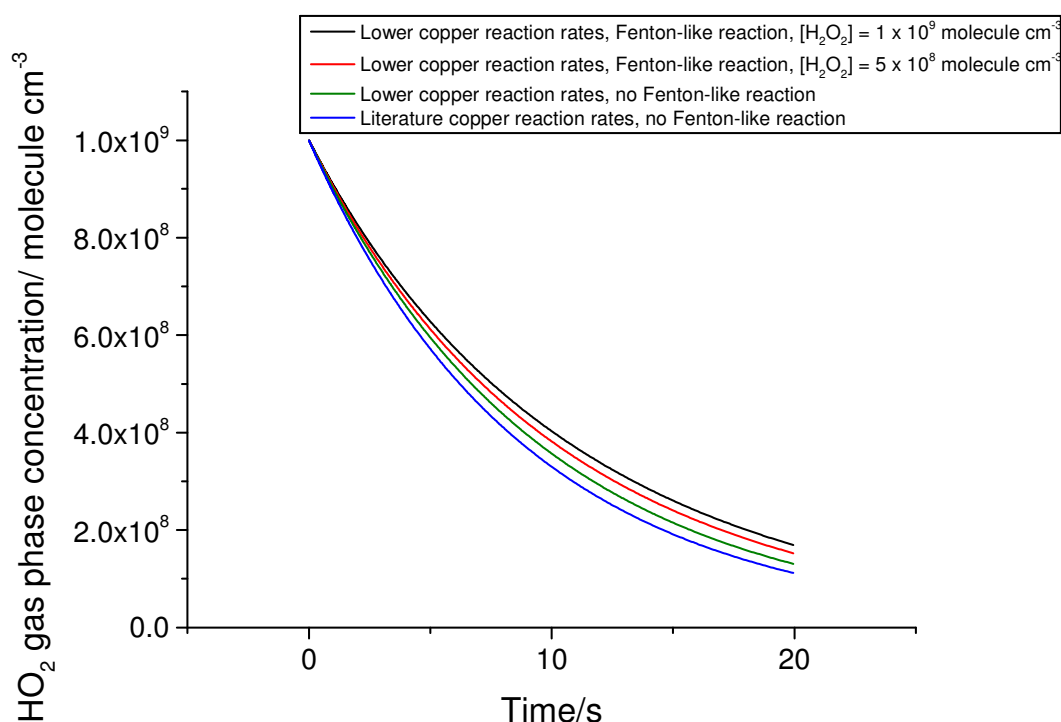


Figure 8.18: The HO₂ gas phase concentrations outputted by the KM-SUB model for copper doped aerosols with an average radius of 30 nm at a concentration of $5 \times 10^4 \text{ cm}^{-3}$. The copper concentration was set to $2 \times 10^{20} \text{ molecule cm}^{-3}$ ($\sim 0.3 \text{ M}$) and the initial HO₂ concentration was set to $1 \times 10^9 \text{ molecule cm}^{-3}$. Four sets of conditions were run with the KM-SUB model, firstly the literature values shown in column 1 of Table 8.3 with no Fenton-like reactions (blue line), secondly the conditions shown in column 3 of Table 8.3 and with no Fenton-like reactions (green line), thirdly the conditions shown in column 3 of Table 8.3 with a Fenton-like reaction and an initial H₂O₂ concentration of $5 \times 10^8 \text{ molecule cm}^{-3}$ (red line) and lastly the conditions shown in column 3 of Table 8.3 with a Fenton-like reaction and an initial H₂O₂ concentration of $1 \times 10^9 \text{ molecule cm}^{-3}$ (black line).

8.9 Modelling of the effect of changing the viscosity of the aerosols upon the HO₂ uptake coefficient

In Section 4.4 measurements of the HO₂ uptake coefficient made in this work onto copper doped sucrose aerosols over a range of humidities were presented. It was observed that at higher humidities (> 65% RH) the HO₂ uptake coefficient appeared to be equal to the mass accommodation coefficient, whereas at lower humidities the uptake coefficient decreased with a HO₂ uptake coefficient of 0.012 ± 0.007 being measured at a relative humidity of 17%. The decrease in the HO₂ uptake coefficient was hypothesised as being due to an increase in the viscosity of the sucrose aerosols as the humidity decreased, and therefore in a reduction of the HO₂ diffusion coefficient in the aerosol bulk.

The KM-SUB model was run in order to test the hypothesis that the lower HO₂ diffusion coefficients into the sucrose aerosols would cause a decrease in the HO₂ uptake coefficient. Although there are currently no measurements of the diffusion coefficients of HO₂ in sucrose solutions, the diffusion coefficient of water into sucrose solutions has been extensively studied as discussed in Section 4.4. Therefore, an assumption was made that the HO₂ diffusion coefficient would be the same as the diffusion coefficient of water. In reality, this will not be the case due to the different sizes of the species and their ability to hydrogen bond. The parameters that were utilised are shown in Table 8.1 with the exception that the surface accommodation coefficient at time zero was set to 0.22 to obtain a better fitting with the data. The Fenton-like reaction was not included during this modelling. Figure 8.19 shows the HO₂ uptake coefficients measured in this work as well as the uptake coefficients predicted by the KM-SUB model if the parameterisations of the water diffusion coefficients into sucrose given by Zobrist et al. (2011) and Price et al. (2013) were assumed. The diffusion coefficient dependence of water into sucrose over the range of humidities for both of these references was shown in Section 4.4. It should be noted that the pH of the aerosols was estimated as 4.1 due to the presence of copper (II) sulphate, which is a weak acid, within the aerosols.

Figure 8.19 shows that as the diffusion coefficients in the aerosol bulk decreased, the HO₂ uptake coefficient also decreased. This is due to the slower diffusion within the aerosol

causing HO_2 concentration gradients (and a lower HO_2 concentration in the aerosol overall) within the aerosol which leads to a slower rate of reaction between the copper and the HO_2 or O_2^- . It should be noted that below $\sim 43\%$ RH the aerosols are likely to be slightly less viscous than predicted due to the slow dehydration of sucrose at low relative humidities and the fact that the aerosols only had ~ 10 seconds in which to equilibrate (as discussed in Section 4.4) (Bones et al., 2012; Power et al., 2013). Therefore, below $\sim 43\%$ RH the predicted uptake coefficients shown in Figure 8.19 can be deemed to be a lower limit.

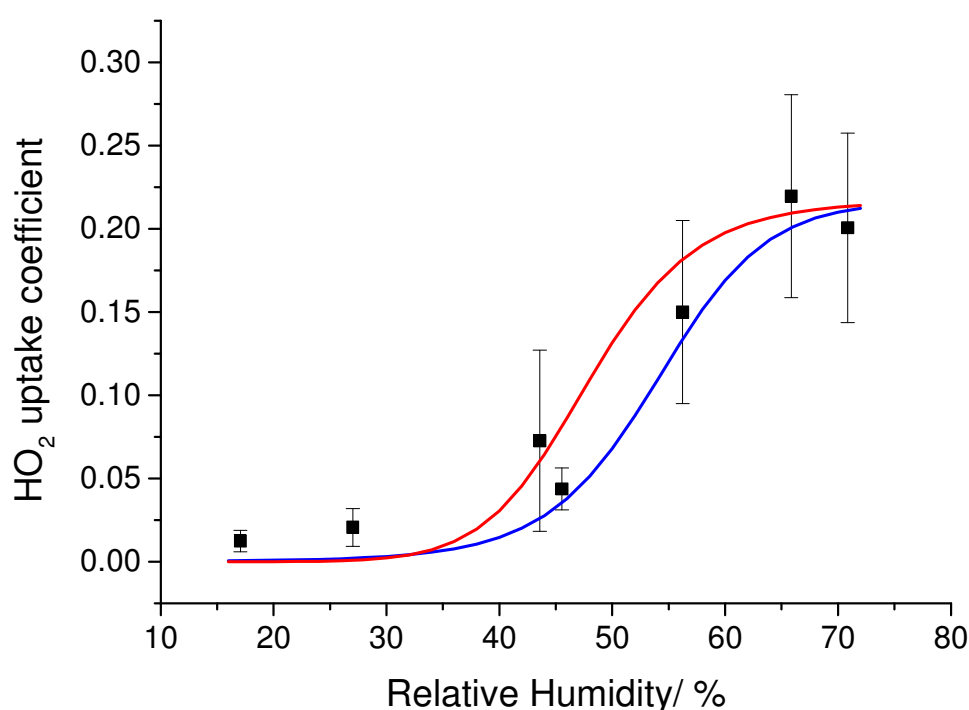


Figure 8.19: The HO_2 uptake coefficients onto copper-doped sucrose aerosols measured in this work as a function of humidity. The surface accommodation at time zero was set to 0.22. The initial pH of the aerosols was set to 4.1 and the number of bulk layers was set to 100 representing a bulk layer thickness of ~ 0.5 nm. The blue and red lines represent the parameterisation of the diffusion coefficient of water into sucrose solutions given by Zobrist et al. (2011) and Price et al. (2013), respectively.

Figure 8.19 shows that the trend predicted by the KM-SUB model and the diffusion parameterisations are in agreement with the measurements in this work. The good agreement suggests that the HO_2 diffusion coefficients are likely to be similar to the diffusion coefficients of water into solutions or aerosols of different viscosities.

8.10 Atmospheric Implications

The modelling in the previous sections in this chapter has attempted to describe how the HO₂ uptake coefficients would change over time and under different conditions in the flow tube. In the flow tube it would be expected that the HO₂ and H₂O₂ concentrations would change over time (or along the flow tube). However, during field campaigns HO₂ concentrations are measured continuously. Therefore, once the mechanism for HO₂ destruction in the aerosol is well understood in the flow tube it could be related to the HO₂ uptake in the troposphere by removing the time dependence from the KM-SUB model. For example, in Figure 8.20 the red line shows the uptake coefficients that would be obtained in the flow tube for an initial HO₂ concentration of 1×10^9 molecule cm⁻³ and with the rate constants given in Table 8.1 for aqueous aerosols containing no copper ions. However, in the flow tube the HO₂ concentration would decrease along the flow tube due to reaction in the aerosol phase and wall losses (assuming gas phase loss processes are negligible). The decrease in HO₂ along the flow tube causes the HO₂ uptake coefficient to decrease. However, if a HO₂ concentration of 1×10^9 molecule cm⁻³ was measured in the troposphere a constant concentration could be inputted into the model that did not decrease over time. In this case, a constant HO₂ uptake coefficient would be outputted as shown by the black lines in Figure 8.20 and the atmospherically relevant value would be the stable uptake coefficient that occurs after 0.1 seconds. It should be noted that at lower HO₂ concentrations (which are more atmospherically relevant) the HO₂ uptake coefficient would decrease due to the second order nature of the HO₂ loss within the aerosol.

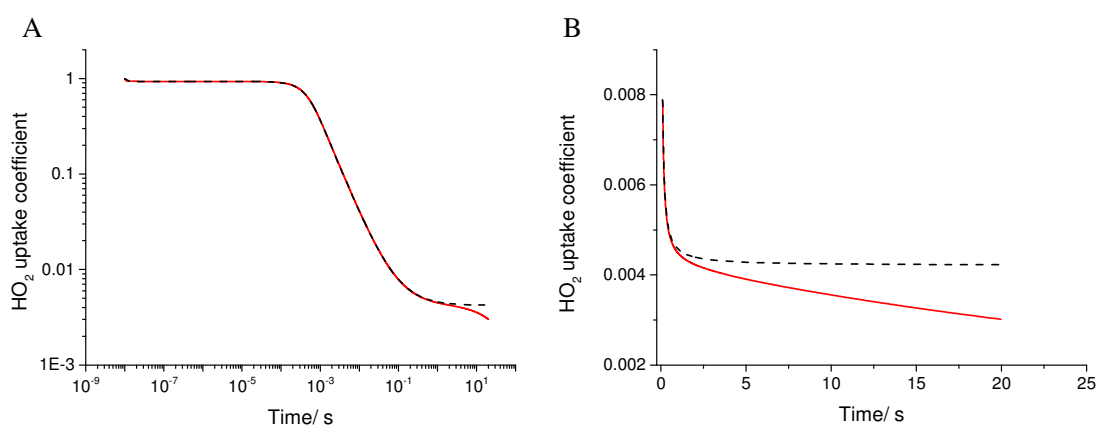


Figure 8.20: An example of the time evolution of the HO₂ uptake coefficient for aqueous non-copper doped aerosols calculated by KM-SUB for the flow tube for an initial HO₂ concentration of 1×10^9 molecule cm⁻³ (red line) and the expected HO₂ uptake coefficient expected under the same conditions at a constant HO₂ concentration of 1×10^9 molecule cm⁻³ (dashed black line). B is an expanded version of A between 0.1 – 20 seconds.

The KM-SUB model can also be used to predict the effect of changing the aerosol radius in both the flow tube (with decreasing HO₂ concentrations along it) and in the troposphere (with constant HO₂ concentrations). This is especially important due as the average radius of the aerosols produced by the atomiser and used in the flow tube are much smaller (~ a factor of 10) than those found in the troposphere which have a peak at several hundred nm. Figure 8.21 shows that the HO₂ uptake coefficient initially drops from a value of 1 (the mass accommodation) to a smaller value for the larger particles due to a greater depletion of HO₂ near the surface of the aerosols. However, for constant HO₂ concentrations when the aerosols are equilibrated after ~ 0.1 seconds the HO₂ uptake coefficient is larger for the larger aerosols as the volume to surface ratio increases as discussed in Section 3.7. Figure 8.21 also shows that the aerosol number concentration does not affect the HO₂ uptake coefficient when the HO₂ concentration is constant. However, in the flow tube a small decrease in the HO₂ uptake coefficient is observed when a larger aerosol volume is present as the HO₂ concentrations decrease at a faster rate along the flow tube leading to slower second order loss of HO₂ within the aerosols. However, when the same aerosol volume is present (red and dashed black line in Figure 8.21) but the aerosols radius is larger the uptake coefficient is also larger.

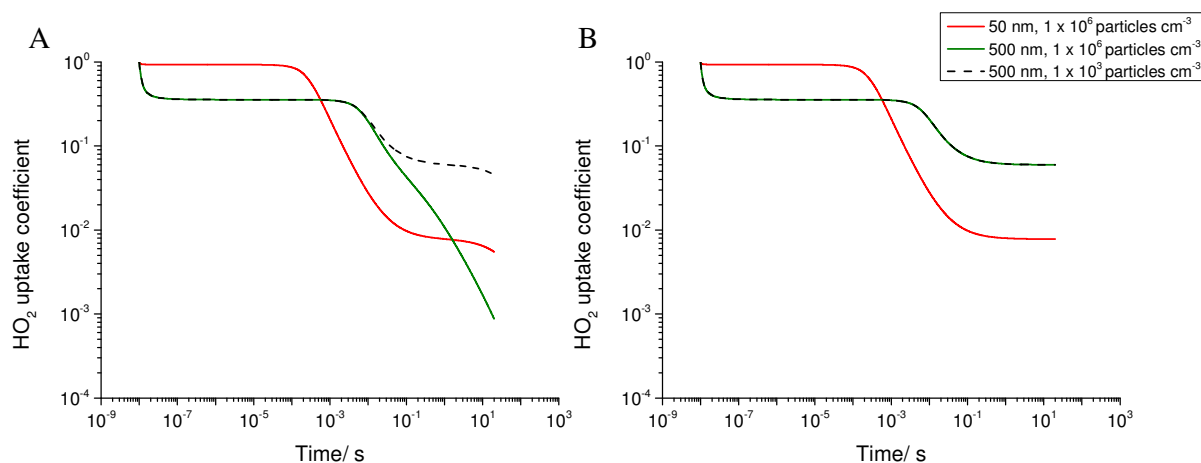


Figure 8.21: The time evolution of the HO₂ uptake coefficient for aqueous non-copper doped aerosols at an initial HO₂ concentration of 1×10^9 molecule cm⁻³ calculated for (A) flow tube conditions and for (B) at a constant HO₂ concentration. The lines represent 50 nm particles at a number concentration of 1×10^6 particles cm⁻³ (red), 500 nm particles at a number concentration of 1×10^6 particles cm⁻³ (green) and 500 nm particles at a number concentration of 1×10^3 particles cm⁻³ (dashed black).

In the troposphere there is also a large range of temperatures as was discussed in Chapter 6. Figure 8.22 shows another example of the difference between the expected HO₂ uptake coefficient under flow tube conditions and the expected uptake coefficient under stable HO₂ concentrations. As expected the HO₂ uptake coefficient was larger at lower temperatures due to the increased Henry's law coefficient. However, until H₂O₂ concentrations in the flow tube are known at different experimental temperatures the data in Chapter 6 cannot be accurately modelled.

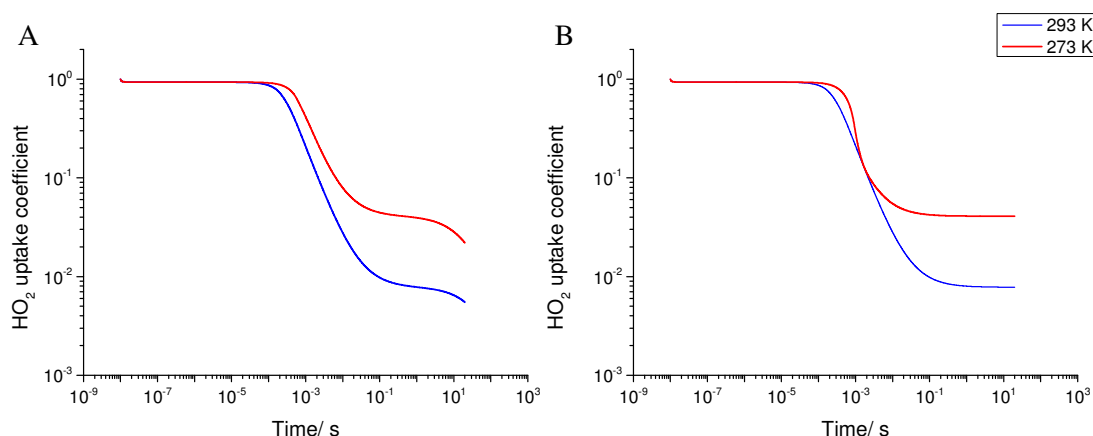


Figure 8.22: The time evolution of the HO₂ uptake coefficient for aqueous non-copper doped aqueous aerosols with a radius of 50 nm, an aerosol number concentration of 1×10^6 particles cm⁻³ and at an initial HO₂ concentration of 1×10^9 molecule cm⁻³ calculated for (A) flow tube conditions and for (B) at a constant HO₂ concentration. The red line represents a temperature of 273 K whereas the blue line represents a temperature of 293 K.

Although as shown by the examples above the model allows the measurements made in the flow tube to be related to uptake coefficients in the troposphere, the mechanism in the flow tube first has to be fully understood. However, there still remains uncertainty in many of the parameters and constants. More measurements would be needed at different HO₂ to H₂O₂ ratios and with different copper and iron ion ratios. There is also uncertainty in the products of the reactions within the aerosol, and also on the walls of the flow tube. It was also hypothesised in this chapter that increasing H₂O₂ concentrations could reduce the observed HO₂ uptake coefficient due to the reformation of HO₂ in the aerosol which partitions to the gas phase. This could also potentially impact on the modelling of tropospheric field measurements where the H₂O₂ concentrations have been measured as being about a factor of 10 to 100 higher than HO₂ concentrations (e.g (Mao et al., 2010)) by reducing the overall loss of HO₂ to aerosols. However, more laboratory measurements are required to optimise the model and to better understand the HO₂ uptake mechanism.

In Section 8.4 it was also shown that the only way of getting agreement between the HO₂ uptake coefficient dependence upon the copper ion concentration in the aerosol predicted by the KM-SUB model and measured in this work and in the work by Mozurkewich et al. (1987) was to decrease the rate constants of the reactions involving copper ions by four orders of magnitude. If this were the case, it would mean that the impact of tropospheric aerosols on

gas phase HO₂ concentrations would be greatly reduced. For example, Mao et al. (2013) stated that a concentration of 3.1 ng of copper in a cubic metre of air could provide a copper concentration of 2.9×10^{-3} M. Therefore, by propagation of this it would mean that with the lower copper rate constants (used to fit the copper dependence in this work) a concentration of ~ 10 ng of copper in a cubic metre of air would be needed to obtain the concentration of 10^{-2} M required for mass accommodation. However, if the literature values of the copper ion rate constants are used, a copper concentration of 10^{-6} M (or ~ 0.001 ng m⁻³) in the aerosols would be required for the HO₂ uptake coefficient to reach a value of the mass accommodation.

Finally, it was shown that the viscosity of the aerosols can have a large impact on the HO₂ uptake coefficient. Glassy aerosols are ubiquitous throughout the troposphere and examples are SOA that can have been shown to have viscosities of $\sim 10^8$ Pa s (Abramson et al., 2013). For viscous aerosols, the HO₂ uptake coefficient would be greatly reduced due to the slow diffusion in the bulk of the aerosol causing a decrease in the HO₂ concentration within the aerosol and therefore a decrease in the rate of reaction within the aerosol. Therefore, viscous aerosols are likely to have very little impact upon gaseous tropospheric HO₂ concentrations and would also have low uptake coefficients for other species.

8.11 Summary and future work

In this chapter the development of the KM-SUB model to attempt to rationalise and explain the HO₂ uptake coefficient measurements made in this work was described. The model consisted of a gas phase, a near surface gas phase layer, a sorption layer and several aerosol bulk layers. The model was shown to be in agreement with the output of the Thornton et al. (2008) expression with the exception that it took into account the depletion of HO₂ in the gas phase near the surface of the aerosol and the fact that it predicted a slightly sharper rise in the HO₂ uptake coefficient when increasing copper ion concentrations in the aerosol.

The KM-SUB model was able to successfully describe the time dependence observed for aqueous aerosols in this work. The time dependence was due to a decrease in HO₂ gas phase concentrations along the flow tube (due to aerosol reactions and wall losses), and therefore to

lower HO₂ concentrations in the aerosols which lead to a decrease in the HO₂ self-reaction in the aerosols. The apparent HO₂ concentration dependence was also able to be modelled by the KM-SUB model by including a Fenton-like reaction into the model. When higher HO₂ concentrations exit the injector there are also higher H₂O₂ concentrations exiting the injector which could potentially partition to the aerosol, undergo reaction and reform HO₂ thereby lowering the observed HO₂ uptake coefficient. However, this mechanism could only explain the measurements made in this work if either the rate of the HO₂ self-reaction was increased significantly or if the rate of the reactions involving copper were reduced significantly. The rate of the Fenton-like reaction also had to be set quite high ($2.39 \times 10^{-12} \text{ cm}^3 \text{ s}^{-1}$). The lower HO₂ uptake coefficients for ammonium nitrate compared to sodium chloride could also be modelled by setting the initial pH of the ammonium nitrate aerosols (pH = 4.9) to be lower than the initial pH of the sodium chloride aerosols (pH = 7). It was also shown that the dissociation of HO₂ within the aerosol could significantly affect the aerosol pH.

The HO₂ uptake coefficient dependence upon aerosol copper ion concentration was also investigated. By using literature values of the rate constants of the reactions involving copper ions it was found that the KM-SUB model predicted that the uptake coefficient would start to increase at a copper concentration of 10^{-8} M , and would be fully limited by mass accommodation by 10^{-6} M . However, measurements showed that the uptake coefficient started to increase at a copper concentration of 10^{-4} M , and would be fully limited by mass accommodation by 10^{-2} M . The discrepancy between the measurements and the model were investigated by changing the HO₂ diffusion coefficient in the bulk of the aerosol, by changing the Henry's law coefficient and by the inclusion of a Fenton-like reaction. However, none of these changes improved the agreement between the model and the measurements, and only a four order of magnitude decrease in the rates of the reactions involving copper ions could produce agreement between the model and measurements. This decrease would mean that the impact of aerosols on tropospheric gas phase HO₂ concentrations would be greatly reduced in box and global models compared to if literature values of the copper rate constants were used.

In this chapter, it was also shown that the time and apparent HO₂ concentration dependence observed in this work for copper-doped aerosols could potentially be explained by a Fenton-like reaction converting H₂O₂ into HO₂. However, the measurements made in this work cannot currently be fitted very well with the model. In order to improve the fitting it would be

important to be able to measure how the hydrogen peroxide concentrations vary along the flow tube. By performing more measurements over a range of initial hydrogen peroxide concentrations, the fitting could also be improved as the rate coefficients and other parameters could also be better constrained.

The effect of aerosol viscosity on the HO₂ uptake coefficient was also investigated using the KM-SUB model. As the aerosol viscosity increased (or the HO₂ bulk phase diffusion coefficient decreased) the model predicted a decrease in the HO₂ uptake coefficient. The trend was in agreement with the HO₂ uptake measurements onto copper-doped sucrose aerosols made in this work. The decrease in the HO₂ uptake coefficient when the bulk phase diffusion coefficients were lower was due to an overall decrease in the HO₂ concentrations in the bulk of the aerosol leading to a reduction in the rate of HO₂ destruction. The diffusion coefficients inputted into the model were estimated as being the diffusion coefficients of water into sucrose which have been fairly well studied. The results suggested that the diffusion of HO₂ into sucrose aerosols was likely to be similar to the diffusion of water into sucrose aerosols. The low uptake coefficients obtained for viscous aerosols suggest that aerosols such as SOA that have a high viscosity would have very little impact on HO₂ gas phase concentrations in the troposphere.

In order to be able to understand the HO₂ mechanism better and therefore be able to relate the HO₂ uptake coefficients measured in the flow tube to tropospheric field measurements, more experiments would be required. By making more measurements of the HO₂ uptake coefficient onto different types of aerosol, with different HO₂ to H₂O₂ ratios and with different copper and iron concentrations, it should be possible to optimise the different parameters. The KM-SUB model could also be used in the future to model the HO₂ uptake onto solid aerosols. This could be done by setting the diffusion into the bulk of the aerosol to zero and adding some reactions on the surface of the aerosol to the model. Once the HO₂ uptake coefficient mechanism at room temperature is fully understood the impact could also be investigated at different temperatures.

Chapter 9: Conclusions and future work

It is important to measure the HO₂ uptake coefficient as several studies have observed much lower HO₂ concentrations during field studies than predicted by box models (e.g. Mao et al. (2010), Whalley et al. (2010)). The discrepancy between box models and measurements was attributed, at least in part, to HO₂ uptake by aerosols. However, very few laboratory studies had measured the HO₂ uptake coefficient, and a large range of values ($\gamma < 0.005$ to $\gamma = 0.94$), as well as both first and second order uptake coefficients in terms of HO₂ concentration, had been reported in the literature. Therefore, it was important to make more measurements of the HO₂ uptake coefficient onto different aerosols and over a range of different conditions to better understand the mechanism and the uptake coefficient values that should be used within models.

In this work, the HO₂ uptake coefficients onto a range of inorganic and organic aerosols were measured. Measurements were made by coupling a flow tube to a sensitive Fluorescence Assay by Gas Expansion (FAGE) cell. The HO₂ radical was formed by the photolysis of water vapour in the presence of oxygen and was injected into the flow tube at a concentration of $(0.3 - 2.5) \times 10^9$ molecule cm⁻³ using a moveable injector. Aerosols were formed by either using an atomiser, a dust disperser or by oxidation of VOCs in a chamber. The aerosol surface area was measured using a Scanning Mobility Particle Sizer (SMPS), a Condensation Particle Counter (CPC) and/or an Aerodynamic Particle Sizer (APS). By changing both the contact time between the HO₂ radicals and the aerosols and the aerosol concentration a HO₂ uptake coefficient was determined.

The HO₂ uptake coefficient measured in this work onto solid salt and organic aerosols was about an order of magnitude lower than onto aqueous salt and organic aerosols. Taketani et al. (2008) also observed the trend of larger HO₂ uptake coefficients for aqueous aerosols than for solid aerosols. The HO₂ uptake coefficients were larger for aqueous aerosols than for solid aerosols as reactions can occur within the bulk of the aerosol and are not limited to the surface of the aerosol. The HO₂ uptake coefficients measured in this work were approximately 1 to 2 orders of magnitude smaller than measured by the majority of other

groups. This may be due to the specific experimental conditions such as time, HO₂ concentration and metal concentrations. No observable increase in the HO₂ uptake coefficient was observed with changing relative humidities or with increasing aerosol pH. The lack of an observable increase for the HO₂ uptake coefficient with increasing pH for unbuffered aerosols may be due to the acidification of the aerosols due to the dissociation of HO₂.

The HO₂ uptake coefficient onto aerosols doped with copper (II) ions were measured in this work as being 0.5 ± 0.3 . This HO₂ uptake coefficient was in agreement with other groups that had made measurements onto copper-doped ammonium sulphate aerosols and was only limited by mass accommodation. The HO₂ uptake coefficient increased with increasing copper (II) ion concentrations due to the catalytic destruction of HO₂ by copper (II) ions within the aerosol. Measurements in this work showed that the HO₂ uptake coefficient started to increase when the aerosol copper (II) ion concentration was about 10^{-4} M and reached a value that was limited by mass accommodation when the copper concentration was 10^{-2} M. The HO₂ uptake coefficient dependence upon the copper concentration was in agreement with the measurements made by Mozurkewich et al. (1987). A shell model containing literature aqueous HO₂ chemistry rate constants as well as transport processes called the kinetic multi-layer model of aerosol surface and bulk chemistry (KM-SUB) was compared to the experimental copper concentration dependences. Agreement between the experimental data and the KM-SUB model output could only be achieved by decreasing the rate of reactions involving copper by four orders of magnitude in the model. A dependence on the concentration of iron in the aerosols was also observed for the first time showing that iron also catalytically destroys HO₂.

The HO₂ uptake coefficient onto several different aerosols containing organics were measured. It was shown that organics can decrease the HO₂ uptake coefficient by acting as surfactants, binding to metals in the aerosol and by changing the viscosity of the aerosol. For example, it was suggested that humic acid might act as a surfactant which could potentially form a diffusion barrier and affect the mass accommodation and Henry's law coefficient. For copper (II) doped ammonium sulphate was studied the uptake coefficient equalled the mass accommodation, however, when oxalic acid was added at 10 times the molarity of the copper the HO₂ uptake coefficient decreased by a factor of fifty. The decrease is likely to have been

due to the oxalic acid forming a copper-oxalate complex that precipitated out of the aerosol or due to a change in the aerosol viscosity. For copper (II) ion doped sucrose aerosols the HO₂ uptake coefficient decreased with decreasing humidity. The decrease in the HO₂ uptake coefficient was likely to be due to a decrease in the diffusion of HO₂ into the bulk of the aerosol thereby lowering the concentration of HO₂ in the aerosol that could be catalytically destroyed by reactions with copper and it was shown that the diffusion coefficient of HO₂ is likely to be similar to the diffusion coefficient of water. The aerosol flow tube – FAGE system was transported to Switzerland where it was interfaced to an aerosol chamber. HO₂ uptake coefficients of $\gamma < 0.001$ and $\gamma = 0.004 \pm 0.002$ for α -pinene and 1,3,5-trimethylbenzene (TMB) derived aerosols, respectively. Low uptake coefficients at high aerosol viscosities could explain the low HO₂ uptake coefficients measured onto secondary organic aerosol (SOA). The higher uptake coefficient for TMB derived aerosols than for α -pinene derived aerosols could either be due to the TMB derived aerosols being less viscous or due to a HO₂ + RO₂ reaction within the aerosol.

Time and apparent HO₂ concentration dependences of the HO₂ uptake coefficient were observed for both copper doped and non-copper doped aerosols with larger HO₂ uptake coefficients being measured at short reaction times and at lower initial HO₂ concentrations. These dependences were modelled using the KM-SUB model, and it was shown that for the non-copper doped aerosols the time dependence could be explained by a decrease in the HO₂ concentrations along the flow tube leading to a lower rate of the HO₂ self-reaction in the aerosol. It was also shown that in principle the apparent HO₂ uptake coefficient dependence upon the initial HO₂ concentration could be explained by the inclusion of a Fenton-like reaction to the model whereby trace transition metal ions in the aerosol convert hydrogen peroxide to HO₂. At higher HO₂ concentrations there was also much more measured H₂O₂ exiting the injector which could potentially reform HO₂, following H₂O₂ partitioning to the aerosol phase, thereby lowering the HO₂ uptake coefficient. The inclusion of the Fenton-like reaction was also shown to have the potential to explain the dependence of the HO₂ uptake coefficient upon both time and initial HO₂ concentration for copper-doped aerosols, although more work would be needed on the mechanism in the KM-SUB model, such as the inclusion of a H₂O₂ product from the HO₂ wall loss in order to better model the measurements. More measurements of H₂O₂ during experiments could also help to elucidate the mechanism.

Experiments were also performed onto solid, aqueous and copper doped salts over a temperature range of 263 - 313 K. For solid salts an increase in the HO₂ uptake coefficient with decreasing temperature was not observed over the temperature range, although this may be due to the higher relative humidities in the flow tube at lower temperatures and water molecules blocking the reactive sites. However, for aqueous ammonium nitrate aerosols an increase in the HO₂ uptake coefficient was observed with decreasing temperature which is likely to be due to an increase in the Henry's law coefficient. A small increase in the HO₂ uptake coefficient was also observed for copper-doped aerosols which may be due to the Gibbs free energy barrier of the transition state between gaseous and solvated species being temperature dependent.

The HO₂ uptake coefficient was measured in this work onto Arizona Test Dust (ATD) aerosols and was found to be much larger than onto aqueous and solid salt aerosols under similar conditions. The larger uptake coefficients could be either due to a very large Brunauer–Emmett–Teller (BET) surface area or due to the composition of the dust with certain components being reactive towards HO₂. Similarly, the larger uptake coefficient measured onto cosmic dust proxy aerosols were much larger than onto ATD aerosols which could either be due to the BET surface area or the composition of the aerosol. A dependence of the uptake coefficient upon the humidity was observed which could be due to the hydroxylation of minerals in the dust leading to a different reactivity, the formation of HO₂-H₂O complexes at the surface of the aerosol leading to faster reactions or decreasing HO₂ concentrations due to larger wall losses. Similar dependences upon time and HO₂ concentrations were observed for the dust aerosols as for the aqueous aerosols, however, the KM-SUB model would need to be modified to remove diffusion into the bulk of the aerosol and reactions at the surface of the aerosol in order to check the cause of these dependencies.

In the future, measurements should focus on (i) better constraining the parameters in the KM-SUB model for aqueous aerosols, (ii) the understanding of the mechanism for solid aerosols and (iii) the investigation of a HO₂ + RO₂ reaction in the aqueous phase. First, by measuring the HO₂ uptake coefficient onto aqueous aerosols containing different copper and iron concentrations, by varying the HO₂ and H₂O₂ concentrations and by measuring over a greater

range of reaction times the different rate coefficients in the KM-SUB model could be better parameterised. Once these have been parameterised at room temperature, experiments could also be performed and modelled over a wider range of temperatures. Secondly, it is important to understand the mechanism onto solid aerosols. In order to better understand the HO₂ uptake coefficients onto solid aerosols measurements should be made onto a variety of dust and soot aerosols with different BET surface areas and compositions. Experiments could also be done with individual minerals that are found within dust aerosols. By comparison of these measurements to each other it should be possible to determine whether the HO₂ uptake coefficient onto solid aerosols is purely determined by the aerosol surface area or whether the composition of the aerosol and the presence of certain metals also affects the HO₂ uptake coefficient. The HO₂ uptake coefficient could then be modelled by altering the KM-SUB model to remove diffusion into the bulk of the aerosol and by including reactions at the aerosol surface. Lastly, measurements of the HO₂ uptake coefficient in the presence of RO₂ showed that the reaction between these two species could potentially be important and should therefore be investigated in greater detail. These measurements could then be extended to measure RO₂ uptake by aerosols.

Bibliography

Abbatt, J. P. D.: Heterogeneous interactions of BrO and ClO: Evidence for BrO surface recombination and reaction with $\text{HSO}_3^-/\text{SO}_3^{2-}$, *Geophysical Research Letters*, 23, 1681-1684, 1996.

Abbatt, J. P. D., Lee, A. K. Y., and Thornton, J. A.: Quantifying trace gas uptake to tropospheric aerosol: recent advances and remaining challenges, *Chemical Society Reviews*, 41, 6555-6581, 2012.

Abramson, E., Imre, D., Beranek, J., Wilson, J., and Zelenyuk, A.: Experimental determination of chemical diffusion within secondary organic aerosol particles, *Physical Chemistry Chemical Physics*, 15, 2983-2991, 2013.

Allan, J. D., Topping, D. O., Good, N., Irwin, M., Flynn, M., Williams, P. I., Coe, H., Baker, A. R., Martino, M., Niedermeier, N., Wiedensohler, A., Lehmann, S., Müller, K., Herrmann, H., and McFiggans, G.: Composition and properties of atmospheric particles in the eastern Atlantic and impacts on gas phase uptake rates, *Atmos. Chem. Phys.*, 9, 9299-9314, 2009.

Allen, A. G., Nemitz, E., Shi, J. P., Harrison, R. M., and Greenwood, J. C.: Size distributions of trace metals in atmospheric aerosols in the United Kingdom, *Atmospheric Environment*, 35, 4581-4591, 2001.

Aloisio, S., Francisco, J. S., and Friedl, R. R.: Experimental evidence for the existence of the $\text{HO}_2\text{-H}_2\text{O}$ complex, *Journal of Physical Chemistry A*, 104, 6597-6601, 2000.

Ammann, M.: Using N-13 as tracer in heterogeneous atmospheric chemistry experiments, *Radiochimica Acta*, 89, 831-838, 2001.

Ammann, M., Kalberer, M., Jost, D. T., Tobler, L., Rössler, E., Piguet, D., Gaggeler, H. W., and Baltensperger, U.: Heterogeneous production of nitrous acid on soot in polluted air masses, *Nature*, 395, 157-160, 1998.

Ammann, M. and Pöschl, U.: Kinetic model framework for aerosol and cloud surface chemistry and gas-particle interactions - Part 2: Exemplary practical applications and numerical simulations, *Atmospheric Chemistry and Physics*, 7, 6025-6045, 2007.

Ammann, M., Pöschl, U., and Rudich, Y.: Effects of reversible adsorption and Langmuir-Hinshelwood surface reactions on gas uptake by atmospheric particles, *Physical Chemistry Chemical Physics*, 5, 351-356, 2003.

Ammann, M., Rössler, E., Baltensperger, U., and M, K.: Heterogeneous reaction of NO_2 on bulk soot samples, *Laboratory of Radio- and Environmental Chemistry Annual Report*, 24, 1997.

Anenberg, S. C., Horowitz, L. W., Tong, D. Q., and West, J. J.: An estimate of the global burden of anthropogenic ozone and fine particulate matter on premature human mortality using atmospheric modeling, *Environmental health perspectives*, 118, 1189-1195, 2010.

Atkins, P. W.: *Physical Chemistry*, Macmillan Higher Education, 1997.

Atkinson, R. and Arey, J.: Atmospheric chemistry of gas phase polycyclic aromatic hydrocarbons - formation of atmospheric mutagens, *Environmental health perspectives*, 102, 117-126, 1994.

Bach, R. D. and Su, M. D.: The Transition-State for the Hydroxylation Of Saturated-Hydrocarbons With Hydroperoxonium Ion, *Journal of the American Chemical Society*, 116, 10103-10109, 1994.

Badger, C. L., George, I., Griffiths, P. T., Braban, C. F., Cox, R. A., and Abbatt, J. P. D.: Phase transitions and hygroscopic growth of aerosol particles containing humic acid and mixtures of humic acid and ammonium sulphate, *Atmospheric Chemistry and Physics*, 6, 755-768, 2006a.

Badger, C. L., Griffiths, P. T., George, I., Abbatt, J. P. D., and Cox, R. A.: Reactive uptake of N_2O_5 by aerosol particles containing mixtures of humic acid and ammonium sulfate, *Journal of Physical Chemistry A*, 110, 6986-6994, 2006b.

Baduel, C., Voisin, D., and Jaffrezo, J. L.: Seasonal variations of concentrations and optical properties of water soluble HULIS collected in urban environments, *Atmos. Chem. Phys.*, 10, 4085-4095, 2010.

Bedjanian, Y., Romanias, M. N., and El Zein, A.: Uptake of HO_2 radicals on Arizona Test Dust, *Atmos. Chem. Phys.*, 2013. 6461-6471, 2013.

Benson, D. R., Erupe, M. E., and Lee, S.-H.: Laboratory-measured H_2SO_4 - H_2O - NH_3 ternary homogeneous nucleation rates: Initial observations, *Geophysical Research Letters*, 36, 2009.

Berkemeier, T., Huisman, A. J., Ammann, M., Shiraiwa, M., Koop, T., and Pöschl, U.: Kinetic regimes and limiting cases of gas uptake and heterogeneous reactions in atmospheric aerosols and clouds: a general classification scheme, *Atmos. Chem. Phys. Discuss.*, 13, 983-1044, 2013.

Berresheim, H., Elste, T., Plass-Dulmer, C., Eisele, F. L., and Tanner, D. J.: Chemical ionization mass spectrometer for long-term measurements of atmospheric OH and H_2SO_4 , *International Journal of Mass Spectrometry*, 202, 91-109, 2000.

Bielski, B. H. J., Cabelli, D. E., Arudi, R. L., and Ross, A. B.: Reactivity of HO_2/O_2^- radicals in aqueous solution, *Journal of Physical and Chemical Reference Data*, 14, 1041-1100, 1985.

Biskos, G., Malinowski, A., Russell, L. M., Buseck, P. R., and Martin, S. T.: Nanosize effect on the deliquescence and the efflorescence of sodium chloride particles, *Aerosol Science and Technology*, 40, 97-106, 2006.

Bloss, W. J., Lee, J. D., Johnson, G. P., Sommariva, R., Heard, D. E., Saiz-Lopez, A., Plane, J. M. C., McFiggans, G., Coe, H., Flynn, M., Williams, P., Rickard, A. R., and Fleming, Z. L.: Impact of halogen monoxide chemistry upon boundary layer OH and HO₂ concentrations at a coastal site, *Geophysical Research Letters*, 32, L06814, 2005.

Bones, D. L., Reid, J. P., Lienhard, D. M., and Krieger, U. K.: Comparing the mechanism of water condensation and evaporation in glassy aerosol, *Proceedings of the National Academy of Sciences of the United States of America*, 109, 11613-11618, 2012.

Braban, C. F., Carroll, M. F., Styler, S. A., and Abbatt, J. P. D.: Phase transitions of malonic and oxalic acid aerosols, *Journal of Physical Chemistry A*, 107, 6594-6602, 2003.

Brown, R. L.: Tubular Flow Reactors With 1st-Order Kinetics, *Journal of Research of the National Bureau of Standards*, 83, 1-8, 1978.

Brune, W. H., Tan, D., Faloon, I. F., Jaegle, L., Jacob, D. J., Heikes, B. G., Snow, J., Kondo, Y., Shetter, R., Sachse, G. W., Anderson, B., Gregory, G. L., Vay, S., Singh, H. B., Davis, D. D., Crawford, J. H., and Blake, D. R.: OH and HO₂ chemistry in the North Atlantic free troposphere, *Geophysical Research Letters*, 26, 3077-3080, 1999.

Bukowiecki, N., Lienemann, P., Hill, M., Figi, R., Richard, A., Furger, M., Rickers, K., Falkenberg, G., Zhao, Y., Cliff, S. S., Prevot, A. S. H., Baltensperger, U., Buchmann, B., and Gehrig, R.: Real-World Emission Factors for Antimony and Other Brake Wear Related Trace Elements: Size-Segregated Values for Light and Heavy Duty Vehicles, *Environmental Science & Technology*, 43, 8072-8078, 2009.

Cabelli, D. E., Bielski, B. H. J., and Holcman, J.: Interaction between copper(II)-arginine complexes and HO₂/O₂⁻ radicals, a pulse radiolysis study, *Journal of the American Chemical Society*, 109, 3665-3669, 1987.

Cantrell, C. A., Shetter, R. E., Gilpin, T. M., and Calvert, J. G.: Peroxy radicals measured during Mauna Loa observatory photochemistry experiment 2: The data and first analysis, *Journal of Geophysical Research-Atmospheres*, 101, 14643-14652, 1996.

Carpenter, L. J., Fleming, Z. L., Read, K. A., Lee, J. D., Moller, S. J., Hopkins, J. R., Purvis, R. M., Lewis, A. C., Müller, K., Heinold, B., Herrmann, H., Fomba, K. W., Pinxteren, D., Müller, C., Tegen, I., Wiedensohler, A., Müller, T., Niedermeier, N., Achterberg, E. P., Patey, M. D., Kozlova, E. A., Heimann, M., Heard, D. E., Plane, J. M. C., Mahajan, A., Oetjen, H., Ingham, T., Stone, D., Whalley, L. K., Evans, M. J., Pilling, M. J., Leigh, R. J., Monks, P. S., Karunaharan, A., Vaughan, S., Arnold, S. R., Tschritter, J., Pöhler, D., Frieß, U., Holla, R., Mendes, L. M., Lopez, H., Faria, B., Manning, A. J., and Wallace, D. W. R.: Seasonal characteristics of tropical marine boundary layer air measured at the Cape Verde Atmospheric Observatory, *Journal of Atmospheric Chemistry*, 67, 87-140, 2010.

Carslaw, N., Creasey, D. J., Heard, D. E., Jacobs, P. J., Lee, J. D., Lewis, A. C., McQuaid, J. B., Pilling, M. J., Bauguitte, S., Penkett, S. A., Monks, P. S., and Salisbury, G.: Eastern Atlantic Spring Experiment 1997 (EASE97) - 2. Comparisons of model concentrations of OH, HO₂, and RO₂ with measurements, *Journal of Geophysical Research-Atmospheres*, 107, ACH 5, 2002.

Carslaw, N., Creasey, D. J., Heard, D. E., Lewis, A. C., McQuaid, J. B., Pilling, M. J., Monks, P. S., Bandy, B. J., and Penkett, S. A.: Modeling OH, HO₂, and RO₂ radicals in the marine boundary layer - 1. Model construction and comparison with field measurements, *Journal of Geophysical Research-Atmospheres*, 104, 30241-30255, 1999.

Cavalli, F., Facchini, M. C., Decesari, S., Mircea, M., Emblico, L., Fuzzi, S., Ceburnis, D., Yoon, Y. J., O'Dowd, C. D., Putaud, J. P., and Dell'Acqua, A.: Advances in characterization of size-resolved organic matter in marine aerosol over the North Atlantic, *Journal of Geophysical Research: Atmospheres*, 109, D24215, 2004.

Chen, H. and Grassian, V. H.: Iron Dissolution of Dust Source Materials during Simulated Acidic Processing: The Effect of Sulfuric, Acetic, and Oxalic Acids, *Environmental Science & Technology*, 47, 10312-10321, 2013.

Christensen, H. and Sehested, K.: HO₂ and O₂⁻ Radicals at Elevated Temperatures, *Journal of Physical Chemistry*, 92, 3007-3011, 1988.

Chung, S. H. and Seinfeld, J. H.: Global distribution and climate forcing of carbonaceous aerosols, *Journal of Geophysical Research-Atmospheres*, 107, 2002.

Ciobanu, V. G., Marcolli, C., Krieger, U. K., Zuend, A., and Peter, T.: Efflorescence of Ammonium Sulfate and Coated Ammonium Sulfate Particles: Evidence for Surface Nucleation, *Journal of Physical Chemistry A*, 114, 9486-9495, 2010.

Clegg, S. L., Brimblecombe, P., and Wexler, A. S.: Thermodynamic Model of the System H⁺-NH₄⁺-Na⁺-SO₄²⁻-NO₃⁻-Cl⁻-H₂O at 298.15 K, *The Journal of Physical Chemistry A*, 102, 2155-2171, 1998.

Clegg, S. L., Pitzer, K. S., and Brimblecombe, P.: Thermodynamics Of Multicomponent, Miscible, Ionic-Solutions. 2. Mixtures Including Unsymmetrical Electrolytes, *Journal of Physical Chemistry*, 96, 9470-9479, 1992.

Cocker, D. R., Clegg, S. L., Flagan, R. C., and Seinfeld, J. H.: The effect of water on gas-particle partitioning of secondary organic aerosol. Part I: alpha-pinene/ozon system, *Atmospheric Environment*, 35, 6049-6072, 2001.

Cooper, P. L. and Abbatt, J. P. D.: Heterogeneous interactions of OH and HO₂ radicals with surfaces characteristic of atmospheric particulate matter, *Journal of Physical Chemistry*, 100, 2249-2254, 1996.

Criegee, R.: Mechanism of ozonolysis, *Angewandte Chemie-International Edition in English*, 14, 745-752, 1975.

Criegee, R. and Wenner, G.: Die ozonisierung des 9,10-oktalin, *Annalen Der Chemie-Justus Liebig*, 564, 9-15, 1949.

Crippa, M., El Haddad, I., Slowik, J. G., DeCarlo, P. F., Mohr, C., Heringa, M. F., Chirico, R., Marchand, N., Sciare, J., Baltensperger, U., and Prevot, A. S. H.: Identification of marine

and continental aerosol sources in Paris using high resolution aerosol mass spectrometry, *Journal of Geophysical Research-Atmospheres*, 118, 1950-1963, 2013.

Crowley, J. N., Ammann, M., Cox, R. A., Hynes, R. G., Jenkin, M. E., Mellouki, A., Rossi, M. J., Troe, J., and Wallington, T. J.: Evaluated kinetic and photochemical data for atmospheric chemistry: Volume V - heterogeneous reactions on solid substrates, *Atmospheric Chemistry and Physics*, 10, 9059-9223, 2010.

Cziczo, D. J. and Abbatt, J. P. D.: Deliquescence, efflorescence, and supercooling of ammonium sulfate aerosols at low temperature: Implications for cirrus cloud formation and aerosol phase in the atmosphere, *Journal of Geophysical Research-Atmospheres*, 104, 13781-13790, 1999.

Cziczo, D. J. and Abbatt, J. P. D.: Infrared observations of the response of NaCl, MgCl₂, NH₄HSO₄, and NH₄NO₃ aerosols to changes in relative humidity from 298 to 238 K, *Journal of Physical Chemistry A*, 104, 2038-2047, 2000.

Cziczo, D. J., Nowak, J. B., Hu, J. H., and Abbatt, J. P. D.: Infrared spectroscopy of model tropospheric aerosols as a function of relative humidity: Observation of deliquescence and crystallization, *Journal of Geophysical Research-Atmospheres*, 102, 18843-18850, 1997.

Danckwerts, P. V.: Absorption by simultaneous diffusion and chemical reaction into particles of various shapes and into falling drops, *Transactions of the Faraday Society*, 47, 1014-1023, 1951.

Danckwerts, P. V.: Gas-liquid reactions, McGraw-Hill Book Co., New York (1970). 276 pages. \$11.50, *AIChE Journal*, 17, 509-510, 1970.

Davidovits, P., Kolb, C. E., Williams, L. R., Jayne, J. T., and Worsnop, D. R.: Mass accommodation and chemical reactions at gas-liquid interfaces, *Chemical Reviews*, 106, 1323-1354, 2006.

Davies, G. and Ghabbour, E. A.: *Understanding Humic Substances: Advanced Methods, Properties and Applications*, Royal Society of Chemistry, 1999.

Davis, E. J.: Interpretation of uptake coefficient data obtained with flow tubes, *Journal of Physical Chemistry A*, 112, 1922-1932, 2008.

De Haan, D. O., Brauers, T., Oum, K., Stutz, J., Nordmeyer, T., and Finlayson-Pitts, B. J.: Heterogeneous chemistry in the troposphere: experimental approaches and applications to the chemistry of sea salt particles, *International Reviews in Physical Chemistry*, 18, 343-385, 1999.

De Laat, J. and Gallard, H.: Catalytic decomposition of hydrogen peroxide by Fe(III) in homogeneous aqueous solution: Mechanism and kinetic modeling, *Environmental Science & Technology*, 33, 2726-2732, 1999.

de Reus, M., Fischer, H., Sander, R., Gros, V., Kormann, R., Salisbury, G., Van Dingenen, R., Williams, J., Zöllner, M., and Lelieveld, J.: Observations and model calculations of trace

gas scavenging in a dense Saharan dust plume during MINATROC, *Atmos. Chem. Phys.*, 5, 1787-1803, 2005.

Debenedetti, P. G. and Stillinger, F. H.: Supercooled liquids and the glass transition, *Nature*, 410, 259-267, 2001.

Decesari, S., Facchini, M. C., Fuzzi, S., and Tagliavini, E.: Characterization of water-soluble organic compounds in atmospheric aerosol: A new approach, *Journal of Geophysical Research: Atmospheres*, 105, 1481-1489, 2000.

Deguillaume, L., Leriche, M., Desboeufs, K., Mailhot, G., George, C., and Chaumerliac, N.: Transition metals in atmospheric liquid phases: Sources, reactivity, and sensitive parameters, *Chemical Reviews*, 105, 3388-3431, 2005.

Dentener, F. J., Carmichael, G. R., Zhang, Y., Lelieveld, J., and Crutzen, P. J.: Role of mineral aerosol as a reactive surface in the global troposphere, *Journal of Geophysical Research-Atmospheres*, 101, 22869-22889, 1996.

Do, S. H., Batchelor, B., Lee, H. K., and Kong, S. H.: Hydrogen peroxide decomposition on manganese oxide (pyrolusite): kinetics, intermediates, and mechanism, *Chemosphere*, 75, 8-12, 2009.

Donahue, N. M., Chuang, W., Epstein, S. A., Kroll, J. H., Worsnop, D. R., Robinson, A. L., Adams, P. J., and Pandis, S. N.: Why do organic aerosols exist? Understanding aerosol lifetimes using the two-dimensional volatility basis set, *Environmental Chemistry*, 10, 151-157, 2013.

Drozd, G., Woo, J., Häkkinen, S. A. K., Nenes, A., and McNeill, V. F.: Inorganic salts interact with organic di-acids in sub-micron particles to form material with low hygroscopicity and volatility, *Atmos. Chem. Phys. Discuss.*, 13, 30653-30685, 2013.

Eisele, F. L. and Tanner, D. J.: Ion-assisted tropospheric OH measurements, *Journal of Geophysical Research: Atmospheres*, 96, 9295-9308, 1991.

Faloon, I. C., Tan, D., Leshner, R. L., Hazen, N. L., Frame, C. L., Simpas, J. B., Harder, H., Martinez, M., Di Carlo, P., Ren, X. R., and Brune, W. H.: A laser-induced fluorescence instrument for detecting tropospheric OH and HO₂: Characteristics and calibration, *Journal of Atmospheric Chemistry*, 47, 139-167, 2004.

Finlayson-Pitts, B. J. and Pitts, J. N. J.: *Chemistry of the upper and lower atmosphere : theory, experiments, and applications* Academic, San Diego, Calif. ; London :, 2000.

Flaschka, H. A.: *EDTA Titrations: An Introduction to Theory and Practice*, Pergamon Press, New York, 1959.

Folkers, M., Mentel, T. F., and Wahner, A.: Influence of an organic coating on the reactivity of aqueous aerosols probed by the heterogeneous hydrolysis of N₂O₅, *Geophysical Research Letters*, 30, 1644, 2003.

Fomba, K. W., Mueller, K., van Pinxteren, D., and Herrmann, H.: Aerosol size-resolved trace metal composition in remote northern tropical Atlantic marine environment: case study Cape Verde islands, *Atmospheric Chemistry and Physics*, 13, 4801-4814, 2013.

Formenti, P., Elbert, W., Maenhaut, W., Haywood, J., Osborne, S., and Andreae, M. O.: Inorganic and carbonaceous aerosols during the Southern African Regional Science Initiative (SAFARI 2000) experiment: Chemical characteristics, physical properties, and emission data for smoke from African biomass burning, *Journal of Geophysical Research: Atmospheres*, 108, 8488, 2003.

Fried, A., Henry, B. E., Calvert, J. G., and Mozurkewich, M.: The Reaction Probability Of N_2O_5 With Sulfuric-Acid Aerosols At Stratospheric Temperatures And Compositions, *Journal of Geophysical Research-Atmospheres*, 99, 3517-3532, 1994.

Fu, P., Kawamura, K., Usukura, K., and Miura, K.: Dicarboxylic acids, ketocarboxylic acids and glyoxal in the marine aerosols collected during a round-the-world cruise, *Marine Chemistry*, 148, 22-32, 2013.

Fuchs, H., Bohn, B., Hofzumahaus, A., Holland, F., Lu, K. D., Nehr, S., Rohrer, F., and Wahner, A.: Detection of HO_2 by laser-induced fluorescence: calibration and interferences from RO_2 radicals, *Atmos. Meas. Tech.*, 4, 1209-1225, 2011.

Fuchs, N. A. and Sutagin, A. G.: *Properties of Highly Dispersed Aerosols*. 1970.

Fuller, E. N., Schettle, P. D., and Giddings, J. C.: A New Method For Prediction Of Binary Gas-Phase Diffusion Coefficients, *Industrial and Engineering Chemistry*, 58, 19-24, 1966.

George, I. J., Matthews, P. S. J., Whalley, L. K., Brooks, B., Goddard, A., Baeza-Romero, M. T., and Heard, D. E.: Measurements of uptake coefficients for heterogeneous loss of HO_2 onto submicron inorganic salt aerosols, *Physical Chemistry Chemical Physics*, 15, 12829-12845, 2013.

Gerecke, A., Thielmann, A., Gutzwiller, L., and Rossi, M. J.: The chemical kinetics of HONO formation resulting from heterogeneous interaction of NO_2 with flame soot, *Geophysical Research Letters*, 25, 2453-2456, 1998.

Gershenson, Y. M., Grigorieva, V. M., Ivanov, A. V., and Remorov, R. G.: O_3 and OH sensitivity to heterogeneous sinks of HO_x and CH_3O_2 on aerosol particles, *Faraday Discussions*, 100, 83-100, 1995.

Golden, D. M., Bierbaum, V. M., and Howard, C. J.: Reevaluation of the bond-dissociation energies (ΔH_{diss}) for H-OH, H-OOH, H-OO \cdot , H-O \cdot , H-OO \cdot , AND H-OO, *Journal of Physical Chemistry*, 94, 5413-5415, 1990.

Griffiths, P. T. and Cox, R. A.: Temperature dependence of heterogeneous uptake of N_2O_5 by ammonium sulfate aerosol, *Atmospheric Science Letters*, 10, 159-163, 2009.

Guenther, A., Hewitt, C. N., Erickson, D., Fall, R., Geron, C., Graedel, T., Harley, P., Klinger, L., Lerdau, M., McKay, W. A., Pierce, T., Scholes, B., Steinbrecher, R., Tallamraju,

R., Taylor, J., and Zimmerman, P.: A Global-model of natural volatile organic-compound emissions, *Journal of Geophysical Research-Atmospheres*, 100, 8873-8892, 1995.

Gysel, M., Weingartner, E., Nyeki, S., Paulsen, D., Baltensperger, U., Galambos, I., and Kiss, G.: Hygroscopic properties of water-soluble matter and humic-like organics in atmospheric fine aerosol, *Atmos. Chem. Phys.*, 4, 35-50, 2004.

Haggerstone, A. L., Carpenter, L. J., Carslaw, N., and McFiggans, G.: Improved model predictions of HO₂ with gas to particle mass transfer rates calculated using aerosol number size distributions, *Journal of Geophysical Research-Atmospheres*, 110, D04304, 2005.

Hamilton, E. J. and Lii, R.-R.: The Dependence on H₂O and on NH₃ of the Kinetics of the self-reaction of HO₂ in the gas-phase formation of HO₂·H₂O and HO₂·NH₃ complexes, *International Journal of Chemical Kinetics*, 9, 875-885, 1977.

Hanel, G.: The Properties of Atmospheric Aerosol Particles as Functions of the Relative Humidity at Thermodynamic Equilibrium with the Surrounding Moist Air, *Advances in Geophysics*, 19, 73-188, 1976.

Hanson, D. R.: Surface-specific reactions on liquids, *Journal of Physical Chemistry B*, 101, 4998-5001, 1997.

Hanson, D. R., Burkholder, J. B., Howard, C. J., and Ravishankara, A. R.: Measurement Of OH And HO₂ Radical Uptake Coefficients On Water And Sulfuric-Acid Surfaces, *Journal of Physical Chemistry*, 96, 4979-4985, 1992.

Hanson, D. R. and Lovejoy, E. R.: The Reaction of ClONO₂ with Submicrometer Sulfuric Acid Aerosol, *Science*, 267, 1326-1328, 1995.

Hanson, D. R. and Ravishankara, A. R.: Uptake of HCl and HOCl onto sulfuric acid - Solubilities, Diffusivities, an reaction, *Journal of Physical Chemistry*, 97, 12309-12319, 1993.

Hanson, D. R., Ravishankara, A. R., and Lovejoy, E. R.: Reaction of BrONO₂ with H₂O on submicron sulfuric acid aerosol and the implications for the lower stratosphere, *Journal of Geophysical Research-Atmospheres*, 101, 9063-9069, 1996.

Hard, T. M., O'Brien, R. J., Cook, T. B., and Tsongas, G. A.: Interference suppression in HO fluorescence detection, *Applied Optics*, 18, 3216-3217, 1979.

Havers, N., Burba, P., Lambert, J., and Klockow, D.: Spectroscopic Characterization of Humic-Like Substances in Airborne Particulate Matter, *Journal of Atmospheric Chemistry*, 29, 45-54, 1998.

He, X., Fowler, A., and Toner, M.: Water activity and mobility in solutions of glycerol and small molecular weight sugars: Implication for cryo- and lyopreservation, *Journal of Applied Physics*, 100, -, 2006.

Heard, D. E.: Atmospheric field measurements of the hydroxylradical using laser-induced fluorescence spectroscopy, *Annual Review of Physical Chemistry*, 57, 191-216, 2006.

Heard, D. E. and Pilling, M. J.: Measurement of OH and HO₂ in the troposphere, *Chemical Reviews*, 103, 5163-5198, 2003.

Hiroki, A. and LaVerne, J. A.: Decomposition of Hydrogen Peroxide at Water–Ceramic Oxide Interfaces, *The Journal of Physical Chemistry B*, 109, 3364-3370, 2005.

Holman, J. P.: Heat transfer, McGraw-Hill, New York ; London, 2002.

Hosny, N. A., Fitzgerald, C., Tong, C., Kalberer, M., Kuimova, M. K., and Pope, F. D.: Fluorescent lifetime imaging of atmospheric aerosols: a direct probe of aerosol viscosity, *Faraday Discussions*, 165, 343-356, 2013.

IPCC: IPCC Fifth Assessment Report, 2013.

Ivanov, A. V., Trakhtenberg, S., Bertram, A. K., Molina, L. T., and Molina, M. J.: HO₂ Uptake by Organic Surfaces, 1999. 1999.

Jacob, D. J.: Heterogeneous chemistry and tropospheric ozone, *Atmospheric Environment*, 34, 2131-2159, 2000.

Jaegle, L., Jacob, D. J., Brune, W. H., Faloon, I., Tan, D., Heikes, B. G., Kondo, Y., Sachse, G. W., Anderson, B., Gregory, G. L., Singh, H. B., Poeschel, R., Ferry, G., Blake, D. R., and Shetter, R. E.: Photochemistry of HO_x in the upper troposphere at northern midlatitudes, *Journal of Geophysical Research-Atmospheres*, 105, 3877-3892, 2000.

Jayne, J. T., Davidovits, P., Worsnop, D. R., Zahniser, M. S., and Kolb, C. E.: Uptake of SO_{2(g)} by aqueous surfaces as a function of pH - the effect of chemical reaction at the interface, *Journal of Physical Chemistry*, 94, 6041-6048, 1990.

Jayne, J. T., Duan, S. X., Davidovits, P., Worsnop, D. R., Zahniser, M. S., and Kolb, C. E.: Uptake of gas-phase alcohol and organic acid molecules by water surfaces, *The Journal of Physical Chemistry*, 95, 6329-6336, 1991.

Kanakidou, M., Seinfeld, J. H., Pandis, S. N., Barnes, I., Dentener, F. J., Facchini, M. C., Van Dingenen, R., Ervens, B., Nenes, A., Nielsen, C. J., Swietlicki, E., Putaud, J. P., Balkanski, Y., Fuzzi, S., Horth, J., Moortgat, G. K., Winterhalter, R., Myhre, C. E. L., Tsigaridis, K., Vignati, E., Stephanou, E. G., and Wilson, J.: Organic aerosol and global climate modelling: a review, *Atmospheric Chemistry and Physics*, 5, 1053-1123, 2005.

Kanaya, Y., Cao, R., Kato, S., Miyakawa, Y., Kajii, Y., Tanimoto, H., Yokouchi, Y., Mochida, M., Kawamura, K., and Akimoto, H.: Chemistry of OH and HO₂ radicals observed at Rishiri Island, Japan, in September 2003: Missing daytime sink of HO₂ and positive nighttime correlations with monoterpenes, *Journal of Geophysical Research-Atmospheres*, 112, D11308, 2007.

Kanaya, Y., Sadanaga, Y., Matsumoto, J., Sharma, U. K., Hirokawa, J., Kajii, Y., and Akimoto, H.: Daytime HO₂ concentrations at Oki Island, Japan, in summer 1998: Comparison between measurement and theory, *Journal of Geophysical Research-Atmospheres*, 105, 24205-24222, 2000.

Kanaya, Y., Yokouchi, Y., Matsumoto, J., Nakamura, K., Kato, S., Tanimoto, H., Furutani, H., Toyota, K., and Akimoto, H.: Implications of iodine chemistry for daytime HO₂ levels at Rishiri Island, *Geophysical Research Letters*, 29, 1212, 2002.

Kang, E., Root, M. J., Toohey, D. W., and Brune, W. H.: Introducing the concept of Potential Aerosol Mass (PAM), *Atmospheric Chemistry and Physics*, 7, 5727-5744, 2007.

Kannosto, J., Yli-Pirila, P., Hao, L.-Q., Leskinen, J., Jokiniemi, J., Makela, J. M., Joutsensaari, J., Laaksonen, A., Worsnop, D. R., Keskinen, J., and Virtanen, A.: Bounce characteristics of alpha-pinene-derived SOA particles with implications to physical phase, *Boreal Environment Research*, 18, 329-340, 2013.

Karagulian, F., Santschi, C., and Rossi, M. J.: The heterogeneous chemical kinetics of N₂O₅ on CaCO₃ and other atmospheric mineral dust surrogates, *Atmospheric Chemistry and Physics*, 6, 1373-1388, 2006.

Kircher, C. C. and Sander, S. P.: Kinetics and mechanism of HO₂ and DO₂ disproportionations, *Journal of Physical Chemistry*, 88, 2082-2091, 1984.

Kolb, C. E., Cox, R. A., Abbatt, J. P. D., Ammann, M., Davis, E. J., Donaldson, D. J., Garrett, B. C., George, C., Griffiths, P. T., Hanson, D. R., Kulmala, M., McFiggans, G., Poeschl, U., Riipinen, I., Rossi, M. J., Rudich, Y., Wagner, P. E., Winkler, P. M., Worsnop, D. R., and O' Dowd, C. D.: An overview of current issues in the uptake of atmospheric trace gases by aerosols and clouds, *Atmospheric Chemistry and Physics*, 10, 10561-10605, 2010.

Kremer, M. L.: The Fenton Reaction. Dependence of the Rate on pH, *The Journal of Physical Chemistry A*, 107, 1734-1741, 2003.

Kuwata, M. and Martin, S. T.: Phase of atmospheric secondary organic material affects its reactivity, *Proceedings of the National Academy of Sciences of the United States of America*, 109, 17354-17359, 2012.

Laing, J. R., Hopke, P. K., Hopke, E. E., Husain, L., Dutkiewicz, V. A., Paatero, J., and Viisanen, Y.: Long-term particle measurements in Finnish Arctic: Part I Chemical composition and trace metal solubility, *Atmospheric Environment*, 88, 275-284, 2014.

Lee, P. and Davidson, J.: Evaluation of activated carbon filters for removal of ozone at the PPB level, *American Industrial Hygiene Association Journal*, 60, 589-600, 1999.

Levy, H.: Normal atmosphere - Large radical and formaldehyde concentrations predicted, *Science*, 173, 141-&, 1971.

Li, X., Rohrer, F., Hofzumahaus, A., Brauers, T., Haeseler, R., Bohn, B., Broch, S., Fuchs, H., Gomm, S., Holland, F., Jaeger, J., Kaiser, J., Keutsch, F. N., Lohse, I., Lu, K., Tillmann, R., Wegener, R., Wolfe, G. M., Mentel, T. F., Kiendler-Scharr, A., and Wahner, A.: Missing Gas-Phase Source of HONO Inferred from Zeppelin Measurements in the Troposphere, *Science*, 344, 292-296, 2014.

Lightstone, J. M., Onasch, T. B., Imre, D., and Oatis, S.: Deliquescence, efflorescence, and water activity in ammonium nitrate and mixed ammonium nitrate/succinic acid microparticles, *Journal of Physical Chemistry A*, 104, 9337-9346, 2000.

Lim, H. J. and Turpin, B. J.: Origins of primary and secondary organic aerosol in Atlanta: Results' of time-resolved measurements during the Atlanta supersite experiment, *Environmental Science & Technology*, 36, 4489-4496, 2002.

Lin, S.-S. and Gurol, M. D.: Catalytic Decomposition of Hydrogen Peroxide on Iron Oxide: Kinetics, Mechanism, and Implications, *Environmental Science & Technology*, 32, 1417-1423, 1998.

Loukhovitskaya, E., Bedjanian, Y., Morozov, I., and Le Bras, G.: Laboratory study of the interaction of HO₂ radicals with the NaCl, NaBr, MgCl₂ · 6H₂O and sea salt surfaces, *Physical Chemistry Chemical Physics*, 11, 7896-7905, 2009.

Macintyre, H. L. and Evans, M. J.: Parameterisation and impact of aerosol uptake of HO₂ on a global tropospheric model, *Atmospheric Chemistry and Physics*, 11, 10965-10974, 2011.

Mao, J., Fan, S., Jacob, D. J., and Travis, K. R.: Radical loss in the atmosphere from Cu-Fe redox coupling in aerosols, *Atmospheric Chemistry and Physics*, 13, 509-519, 2013.

Mao, J., Jacob, D. J., Evans, M. J., Olson, J. R., Ren, X., Brune, W. H., St Clair, J. M., Crounse, J. D., Spencer, K. M., Beaver, M. R., Wennberg, P. O., Cubison, M. J., Jimenez, J. L., Fried, A., Weibring, P., Walega, J. G., Hall, S. R., Weinheimer, A. J., Cohen, R. C., Chen, G., Crawford, J. H., McNaughton, C., Clarke, A. D., Jaegle, L., Fisher, J. A., Yantosca, R. M., Le Sager, P., and Carouge, C.: Chemistry of hydrogen oxide radicals (HO_x) in the Arctic troposphere in spring, *Atmospheric Chemistry and Physics*, 10, 5823-5838, 2010.

Matthews, P. S. J., Baeza-Romero, M. T., Whalley, L. K., and Heard, D. E.: Uptake of HO₂ radicals onto Arizona test dust particles using an aerosol flow tube, *Atmos. Chem. Phys.*, 14, 7397-7408, 2014.

Mayol-Bracero, O. L., Guyon, P., Graham, B., Roberts, G., Andreae, M. O., Decesari, S., Facchini, M. C., Fuzzi, S., and Artaxo, P.: Water-soluble organic compounds in biomass burning aerosols over Amazonia 2. Apportionment of the chemical composition and importance of the polyacidic fraction, *Journal of Geophysical Research: Atmospheres*, 107, 8091, 2002.

McNaughton, C. S., Clarke, A. D., Kapustin, V., Shinozuka, Y., Howell, S. G., Anderson, B. E., Winstead, E., Dibb, J., Scheuer, E., Cohen, R. C., Wooldridge, P., Perring, A., Huey, L. G., Kim, S., Jimenez, J. L., Dunlea, E. J., DeCarlo, P. F., Wennberg, P. O., Crounse, J. D., Weinheimer, A. J., and Flocke, F.: Observations of heterogeneous reactions between Asian pollution and mineral dust over the Eastern North Pacific during INTEX-B, *Atmos. Chem. Phys.*, 9, 8283-8308, 2009.

Mihelcic, D., Müsgen, P., and Ehhalt, D. H.: An improved method of measuring tropospheric NO₂ and RO₂ by matrix isolation and electron spin resonance, *Journal of Atmospheric Chemistry*, 3, 341-361, 1985.

Miller, C. E. and Francisco, J. S.: The formation of a surprisingly stable HO₂-H₂SO₄ complex, *Journal of the American Chemical Society*, 123, 10387-10388, 2001.

Mozurkewich, M., McMurry, P. H., Gupta, A., and Calvert, J. G.: Mass Accommodation Coefficient For HO₂ Radicals On Aqueous Particles, *Journal of Geophysical Research-Atmospheres*, 92, 4163-4170, 1987.

Mueller, K., Lehmann, S., van Pinxteren, D., Gnauk, T., Niedermeier, N., Wiedensohler, A., and Herrmann, H.: Particle characterization at the Cape Verde atmospheric observatory during the 2007 RHaMBLe intensive, *Atmospheric Chemistry and Physics*, 10, 2709-2721, 2010.

Murphy, D. M., Cziczo, D. J., Froyd, K. D., Hudson, P. K., Matthew, B. M., Middlebrook, A. M., Peltier, R. E., Sullivan, A., Thomson, D. S., and Weber, R. J.: Single-particle mass spectrometry of tropospheric aerosol particles, *Journal of Geophysical Research: Atmospheres*, 111, D23S32, 2006.

Myriokefalitakis, S., Tsigaridis, K., Mihalopoulos, N., Sciare, J., Nenes, A., Kawamura, K., Segers, A., and Kanakidou, M.: In-cloud oxalate formation in the global troposphere: a 3-D modeling study, *Atmospheric Chemistry and Physics*, 11, 5761-5782, 2011.

Nathanson, G. M., Davidovits, P., Worsnop, D. R., and Kolb, C. E.: Dynamics and kinetics at the gas-liquid interface, *Journal of Physical Chemistry*, 100, 13007-13020, 1996.

Neusüss, C., Pelzing, M., Plewka, A., and Herrmann, H.: A new analytical approach for size-resolved speciation of organic compounds in atmospheric aerosol particles: Methods and first results, *Journal of Geophysical Research: Atmospheres*, 105, 4513-4527, 2000.

News, B. B. C.: Heatwave in SW America: Temperatures hit 47 degrees (<http://www.bbc.co.uk/news/world-us-canada-23109490>). 2013a.

News, B. B. C.: Severe pollution shrouds Chinese capital (<http://www.bbc.co.uk/news/world-asia-china-21243436>), 2013b. 2013b.

Oiestad, A. M. L., Petersen, A. C., Bakken, V., Vedde, J., and Uggerud, E.: The oxidative power of protonated hydrogen peroxide, *Angewandte Chemie-International Edition*, 40, 1305+, 2001.

Okochi, H. and Brimblecombe, P.: Potential trace metal-organic complexation in the atmosphere, *TheScientificWorldJournal*, 2, 767-786, 2002.

Olson, J. R., Crawford, J. H., Brune, W., Mao, J., Ren, X., Fried, A., Anderson, B., Apel, E., Beaver, M., Blake, D., Chen, G., Crouse, J., Dibb, J., Diskin, G., Hall, S. R., Huey, L. G., Knapp, D., Richter, D., Riemer, D., Clair, J. S., Ullmann, K., Walega, J., Weibring, P., Weinheimer, A., Wennberg, P., and Wisthaler, A.: An analysis of fast photochemistry over high northern latitudes during spring and summer using in-situ observations from ARCTAS and TOPSE, *Atmos. Chem. Phys.*, 12, 6799-6825, 2012.

Pant, A., Fok, A., Parsons, M. T., Mak, J., and Bertram, A. K.: Deliquescence and crystallization of ammonium sulfate-glutaric acid and sodium chloride-glutaric acid particles, *Geophysical Research Letters*, 31, 2004.

Paulsen, D., Dommen, J., Kalberer, M., Prévôt, A. S. H., Richter, R., Sax, M., Steinbacher, M., Weingartner, E., and Baltensperger, U.: Secondary Organic Aerosol Formation by Irradiation of 1,3,5-Trimethylbenzene-NO_x-H₂O in a New Reaction Chamber for Atmospheric Chemistry and Physics, *Environmental Science & Technology*, 39, 2668-2678, 2005.

Pfrang, C., Shiraiwa, M., and Pöschl, U.: Coupling aerosol surface and bulk chemistry with a kinetic double layer model (K2-SUB): oxidation of oleic acid by ozone, *Atmos. Chem. Phys.*, 10, 4537-4557, 2010.

Pham, A. N., Xing, G., Miller, C. J., and Waite, T. D.: Fenton-like copper redox chemistry revisited: Hydrogen peroxide and superoxide mediation of copper-catalyzed oxidant production, *Journal of Catalysis*, 301, 54-64, 2013.

Plane, J. M. C.: Cosmic dust in the earth's atmosphere, *Chemical Society Reviews*, 41, 6507-6518, 2012.

Pope, F. D., Harper, L., Dennis-Smith, B. J., Griffiths, P. T., Clegg, S. L., and Cox, R. A.: Laboratory and modelling study of the hygroscopic properties of two model humic acid aerosol particles, *Journal of Aerosol Science*, 41, 457-467, 2010.

Pöschl, U., Letzel, T., Schauer, C., and Niessner, R.: Interaction of Ozone and Water Vapor with Spark Discharge Soot Aerosol Particles Coated with Benzo[a]pyrene: O₃ and H₂O Adsorption, Benzo[a]pyrene Degradation, and Atmospheric Implications, *The Journal of Physical Chemistry A*, 105, 4029-4041, 2001.

Pöschl, U., Rudich, Y., and Ammann, M.: Kinetic model framework for aerosol and cloud surface chemistry and gas-particle interactions - Part 1: General equations, parameters, and terminology, *Atmospheric Chemistry and Physics*, 7, 5989-6023, 2007.

Power, R. M., Simpson, S. H., Reid, J. P., and Hudson, A. J.: The transition from liquid to solid-like behaviour in ultrahigh viscosity aerosol particles, *Chemical Science*, 4, 2597-2604, 2013.

Pradhan, M., Kalberer, M., Griffiths, P. T., Braban, C. F., Pope, F. D., Cox, R. A., and Lambert, R. M.: Uptake of Gaseous Hydrogen Peroxide by Submicrometer Titanium Dioxide Aerosol as a Function of Relative Humidity, *Environmental Science & Technology*, 44, 1360-1365, 2010.

Price, H. C., Murray, B. J., Mattsson, J., O'Sullivan, D., Wilson, T. W., Baustian, K. J., and Benning, L. G.: Quantifying water diffusion in high-viscosity and glassy aqueous solutions using a Raman isotope tracer method, *Atmos. Chem. Phys. Discuss.*, 13, 29375-29411, 2013.

Rabani, J., Klug-Roth, D., and Lilie, J.: Pulse radiolytic investigations of the catalyzed disproportionation of peroxy radicals. Aqueous cupric ions, *The Journal of Physical Chemistry*, 77, 1169-1175, 1973.

Reid, R. C., Prausnitz, J. M., and Poling, B. E.: *The properties of gases & liquids*, 4th Ed. McGraw-Hill Co., New York, NY, 1987.

Remorov, R. G., Gershenzon, Y. M., Molina, L. T., and Molina, M. J.: Kinetics and mechanism of HO₂ uptake on solid NaCl, *Journal of Physical Chemistry A*, 106, 4558-4565, 2002.

Robinson, E. S., Saleh, R., and Donahue, N. M.: Organic Aerosol Mixing Observed by Single-Particle Mass Spectrometry, *The Journal of Physical Chemistry A*, 117, 13935-13945, 2013.

Rogge, W. F., Mazurek, M. A., Hildemann, L. M., Cass, G. R., and Simoneit, B. R. T.: Quantification of urban organic aerosols at amolecular level: Identification, abundance and seasonal variation, *Atmospheric Environment Part a-General Topics*, 27, 1309-1330, 1993.

Romanias, M. N., El Zein, A., and Bedjanian, Y.: Heterogeneous Interaction of H₂O₂ with TiO₂ Surface under Dark and UV Light Irradiation Conditions, *The Journal of Physical Chemistry A*, 116, 8191-8200, 2012.

Ross, H. B. and Noone, K. J.: A numerical investigation of the destruction of peroxy radical by Cu ion catalyzed-reactions on atmospheric particles, *Journal of Atmospheric Chemistry*, 12, 121-136, 1991.

Saathoff, H., Naumann, K. H., Riemer, N., Kamm, S., Mohler, O., Schurath, U., Vogel, H., and Vogel, B.: The loss of NO₂, HNO₃, NO₃/N₂O₅, and HO₂/HOONO₂ on soot aerosol: A chamber and modeling study, *Geophysical Research Letters*, 28, 1957-1960, 2001.

Salisbury, G., Monks, P. S., Bauguitte, S., Bandy, B. J., and Penkett, S. A.: A Seasonal Comparison of the Ozone Photochemistry in Clean and Polluted Air Masses at Mace Head, Ireland, *Journal of Atmospheric Chemistry*, 41, 163-187, 2002.

Sander, S. P., Abbatt, J., Barker, J. R., Burkholder, J. B., Friedl, R. R., Golden, D. M., Huie, R. E., Kolb, C. E., Kurylo, M. J., Moortgat, G. K., Orkin, V. L., and Wine, P. H.: *Chemical Kinetics and Photochemical Data for Use in Atmospheric Studies*, Evaluation No. 17, Jet Propulsion Laboratory, Pasadena, 2011.

Sander, S. P., Friedl, R. R., Golden, D. M., Kurylo, M. J., Huie, R. E., Orkin, V. L., Moortgat, G. K., Ravishankara, A. R., Kolb, C. E., Molina, M. J., and Finlayson-Pitts, B. J.: *Chemical Kinetics and Photochemical Data for Use in Atmospheric Studies*, JPL Publication, 14, 2003.

Saukko, E., Lambe, A. T., Massoli, P., Koop, T., Wright, J. P., Croasdale, D. R., Pedernera, D. A., Onasch, T. B., Laaksonen, A., Davidovits, P., Worsnop, D. R., and Virtanen, A.: Humidity-dependent phase state of SOA particles from biogenic and anthropogenic precursors, *Atmospheric Chemistry and Physics*, 12, 7517-7529, 2012.

Saunders, R. W. and Plane, J. M. C.: A photo-chemical method for the production of olivine nanoparticles as cosmic dust analogues, *Icarus*, 212, 373-382, 2011.

Saunders, S. M., Jenkin, M. E., Derwent, R. G., and Pilling, M. J.: Protocol for the development of the Master Chemical Mechanism, MCM v3 (Part A): tropospheric degradation of non-aromatic volatile organic compounds, *Atmospheric Chemistry and Physics*, 3, 161-180, 2003.

Saxena, P. and Hildemann, L. M.: Water-soluble organics in atmospheric particles: A critical review of the literature and application of thermodynamics to identify candidate compounds, *Journal of Atmospheric Chemistry*, 24, 57-109, 1996.

Schladitz, A., Mueller, T., Nowak, A., Kandler, K., Lieke, K., Massling, A., and Wiedensohler, A.: In situ aerosol characterization at Cape Verde Part 1: Particle number size distributions, hygroscopic growth and state of mixing of the marine and Saharan dust aerosol, *Tellus Series B-Chemical and Physical Meteorology*, 63, 531-548, 2011.

Schroeder, W. H., Dobson, M., Kane, D. M., and Johnson, N. D.: Toxic trace-elements associated with airborne particulate matter - a review, *Japca-the International Journal of Air Pollution Control and Hazardous Waste Management*, 37, 1267-1285, 1987.

Schroth, A. W., Crusius, J., Sholkovitz, E. R., and Bostick, B. C.: Iron solubility driven by speciation in dust sources to the ocean, *Nature Geoscience*, 2, 337-340, 2009.

Schwartz, S.: Mass-Transport Considerations Pertinent to Aqueous Phase Reactions of Gases in Liquid-Water Clouds. In: *Chemistry of Multiphase Atmospheric Systems*, Jaeschke, W. (Ed.), NATO ASI Series, Springer Berlin Heidelberg, 1986a.

Schwartz, S. E.: Gas-phase and aqueous-phase chemistry of HO₂ in liquid water clouds, *Journal of Geophysical Research-Atmospheres*, 89, 1589-1598, 1984.

Schwartz, S. E.: Mass-transport considerations pertinent to aqueous phase reactions of gases in liquid-water clouds, Jaeschke, W. (Ed.) *Nato Asi (Advanced Science Institute Series Series G Ecological Sciences)*, Vol. 6. *Chemistry of Multiphase Atmospheric Systems; Symposium*, Corfu, Greece, Sept. 26-Oct. 8, 1983. Xvi+773p. Springer-Verlag: Berlin, West Germany; New York, N.Y., USA. Illus, 1986b. 415-472, 1986b.

Seinfeld, J. H. and Pandis, S. N.: *Atmospheric chemistry and physics : from air pollution to climate change*, Wiley, New York ; Chichester, 2006.

Shi, Z., Krom, M. D., Jickells, T. D., Bonneville, S., Carslaw, K. S., Mihalopoulos, N., Baker, A. R., and Benning, L. G.: Impacts on iron solubility in the mineral dust by processes in the source region and the atmosphere: A review, *Aeolian Research*, 5, 21-42, 2012.

Shiraiwa, M., Garland, R. M., and Pöschl, U.: Kinetic double-layer model of aerosol surface chemistry and gas-particle interactions (K2-SURF): Degradation of polycyclic aromatic hydrocarbons exposed to O₃, NO₂, H₂O, OH and NO₃, *Atmos. Chem. Phys.*, 9, 9571-9586, 2009.

Shiraiwa, M., Pfrang, C., Koop, T., and Pöschl, U.: Kinetic multi-layer model of gas-particle interactions in aerosols and clouds (KM-GAP): linking condensation, evaporation and chemical reactions of organics, oxidants and water, *Atmospheric Chemistry and Physics*, 12, 2777-2794, 2012a.

Shiraiwa, M., Pfrang, C., and Pöschl, U.: Kinetic multi-layer model of aerosol surface and bulk chemistry (KM-SUB): the influence of interfacial transport and bulk diffusion on the oxidation of oleic acid by ozone, *Atmospheric Chemistry and Physics*, 10, 3673-3691, 2010.

Shiraiwa, M., Pöschl, U., and Knopf, D. A.: Multiphase Chemical Kinetics of NO₃ Radicals Reacting with Organic Aerosol Components from Biomass Burning, *Environmental Science & Technology*, 46, 6630-6636, 2012b.

Shiraiwa, M., Selzle, K., Yang, H., Sosedova, Y., Ammann, M., and Pöschl, U.: Multiphase Chemical Kinetics of the Nitration of Aerosolized Protein by Ozone and Nitrogen Dioxide, *Environmental Science & Technology*, 46, 6672-6680, 2012c.

Slade, J. H. and Knopf, D. A.: Heterogeneous OH oxidation of biomass burning organic aerosol surrogate compounds: assessment of volatilisation products and the role of OH concentration on the reactive uptake kinetics, *Physical Chemistry Chemical Physics*, 15, 5898-5915, 2013.

Smith, G. P. and Crosley, D. R.: A Photochemical model of ozone interference effects in laser detection of tropospheric OH, *Journal of Geophysical Research-Atmospheres*, 95, 16427-16442, 1990.

Smith, S. C., Lee, J. D., Bloss, W. J., Johnson, G. P., Ingham, T., and Heard, D. E.: Concentrations of OH and HO₂ radicals during NAMBLEX: measurements and steady state analysis, *Atmospheric Chemistry and Physics*, 6, 1435-1453, 2006.

Sommariva, R., Bloss, W. J., Brough, N., Carslaw, N., Flynn, M., Haggerstone, A. L., Heard, D. E., Hopkins, J. R., Lee, J. D., Lewis, A. C., McFiggans, G., Monks, P. S., Penkett, S. A., Pilling, M. J., Plane, J. M. C., Read, K. A., Saiz-Lopez, A., Rickard, A. R., and Williams, P. I.: OH and HO₂ chemistry during NAMBLEX: roles of oxygenates, halogen oxides and heterogeneous uptake, *Atmospheric Chemistry and Physics*, 6, 1135-1153, 2006.

Sommariva, R., Haggerstone, A. L., Carpenter, L. J., Carslaw, N., Creasey, D. J., Heard, D. E., Lee, J. D., Lewis, A. C., Pilling, M. J., and Zador, J.: OH and HO₂ chemistry in clean marine air during SOAPEX-2, *Atmospheric Chemistry and Physics*, 4, 839-856, 2004.

Spokes, L. J., Lucia, M., Campos, A. M., and Jickells, T. D.: The role of organic matter in controlling copper speciation in precipitation, *Atmospheric Environment*, 30, 3959-3966, 1996.

Staffelbach, T. A. and Kok, G. L.: Henry law constants for aqueous solutions of hydrogen peroxide and hydroxymethyl hydroperoxide, *Journal of Geophysical Research-Atmospheres*, 98, 12713-12717, 1993.

Stevens, P. S., Mather, J. H., and Brune, W. H.: Measurement of tropospheric OH and HO₂ by Laser Induced Fluorescence at low pressure, *Journal of Geophysical Research-Atmospheres*, 99, 3543-3557, 1994.

Stone, D. and Rowley, D. M.: Kinetics of the gas phase HO₂ self-reaction: Effects of temperature, pressure, water and methanol vapours, *Physical Chemistry Chemical Physics*, 7, 2156-2163, 2005.

Stone, D., Whalley, L. K., and Heard, D. E.: Tropospheric OH and HO₂ radicals: field measurements and model comparisons, *Chemical Society Reviews*, 41, 6348-6404, 2012.

Sun, Y. L., Zhuang, G. S., Ying, W., Han, L. H., Guo, J. H., Mo, D., Zhang, W. J., Wang, Z. F., and Hao, Z. P.: The air-borne particulate pollution in Beijing - concentration, composition, distribution and sources, *Atmospheric Environment*, 38, 5991-6004, 2004.

Sweetenham, W. P. and Curtis, A. R.: FACSIMILE/CHEKMAT User's Manual, Harwell Laboratory, 1987.

Taketani, F. and Kanaya, Y.: Kinetics of HO₂ Uptake in Levoglucosan and Polystyrene Latex Particles, *Journal of Physical Chemistry Letters*, 1, 1701-1704, 2010.

Taketani, F., Kanaya, Y., and Akimoto, H.: Heterogeneous loss of HO₂ by KCl, synthetic sea salt, and natural seawater aerosol particles, *Atmospheric Environment*, 43, 1660-1665, 2009.

Taketani, F., Kanaya, Y., and Akimoto, H.: Kinetic Studies of Heterogeneous Reaction of HO₂ Radical by Dicarboxylic Acid Particles, *International Journal of Chemical Kinetics*, 45, 560-565, 2013.

Taketani, F., Kanaya, Y., and Akimoto, H.: Kinetics of heterogeneous reactions of HO₂ radical at ambient concentration levels with (NH₄)₂SO₄ and NaCl aerosol particles, *Journal of Physical Chemistry A*, 112, 2370-2377, 2008.

Taketani, F. K., Y. Akimoto, H.: Measurement of Uptake Coefficients of HO₂ Radical by Dicarboxylic Acid Particles, 21st International Symposium Gas Kinetics., Leuven, Belgium, 2010.

Tang, M. J., Schuster, G., and Crowley, J. N.: Heterogeneous reaction of N₂O₅ with illite and Arizona test dust particles, *Atmospheric Chemistry and Physics*, 14, 245-254, 2014.

Tang, M. J., Thieser, J., Schuster, G., and Crowley, J. N.: Kinetics and mechanism of the heterogeneous reaction of N₂O₅ with mineral dust particles, *Physical Chemistry Chemical Physics*, 14, 8551-8561, 2012.

Textor, C., Schulz, M., Guibert, S., Kinne, S., Balkanski, Y., Bauer, S., Berntsen, T., Berglen, T., Boucher, O., Chin, M., Dentener, F., Diehl, T., Easter, R., Feichter, H., Fillmore, D., Ghan, S., Ginoux, P., Gong, S., Kristjansson, J. E., Krol, M., Lauer, A., Lamarque, J. F., Liu, X., Montanaro, V., Myhre, G., Penner, J., Pitari, G., Reddy, S., Seland, O., Stier, P., Takemura, T., and Tie, X.: Analysis and quantification of the diversities of aerosol life cycles within AeroCom, *Atmospheric Chemistry and Physics*, 6, 1777-1813, 2006.

Thornton, J. and Abbatt, J. P. D.: Measurements of HO₂ uptake to aqueous aerosol: Mass accommodation coefficients and net reactive loss, *Journal of Geophysical Research-Atmospheres*, 110, D08309, 2005.

Thornton, J. A., Braban, C. F., and Abbatt, J. P. D.: N₂O₅ hydrolysis on sub-micron organic aerosols: the effect of relative humidity, particle phase, and particle size, *Physical Chemistry Chemical Physics*, 5, 4593-4603, 2003.

Thornton, J. A., Jaegle, L., and McNeill, V. F.: Assessing known pathways for HO₂ loss in aqueous atmospheric aerosols: Regional and global impacts on tropospheric oxidants, *Journal of Geophysical Research-Atmospheres*, 113, D05303, 2008.

TSI: Model 3076 Constant Output Atomizer Instruction Manual. 2005.

TSI: Series 3080 Electrostatic Classifiers Operation and Service Manual, 2009.

Usher, C. R., Michel, A. E., and Grassian, V. H.: Reactions on mineral dust, *Chem Rev*, 103, 4883-4940, 2003.

Vaden, T. D., Imre, D., Beranek, J., Shrivastava, M., and Zelenyuk, A.: Evaporation kinetics and phase of laboratory and ambient secondary organic aerosol, *Proceedings of the National Academy of Sciences of the United States of America*, 108, 2190-2195, 2011.

Valorso, R., Aumont, B., Camredon, M., Raventos-Duran, T., Mouchel-Vallon, C., Ng, N. L., Seinfeld, J. H., Lee-Taylor, J., and Madronich, S.: Explicit modelling of SOA formation from α -pinene photooxidation: sensitivity to vapour pressure estimation, *Atmos. Chem. Phys.*, 11, 6895-6910, 2011.

Virtanen, A., Joutsensaari, J., Koop, T., Kannosto, J., Yli-Pirila, P., Leskinen, J., Makela, J. M., Holopainen, J. K., Poschl, U., Kulmala, M., Worsnop, D. R., and Laaksonen, A.: An amorphous solid state of biogenic secondary organic aerosol particles, *Nature*, 467, 824-827, 2010.

Vonpiechowski, M., Nauser, T., Hoigne, J., and Buhler, R. E.: O₂⁻ decay catalyzed by Cu²⁺ and Cu⁺ ions in aqueous solutions - a pulse radiolysis study for atmospheric chemistry, *Berichte Der Bunsen-Gesellschaft-Physical Chemistry Chemical Physics*, 97, 762-771, 1993.

Weinhold, B.: Ozone nation - EPA standard panned by the people, *Environmental health perspectives*, 116, A302-A305, 2008.

Weinstock, B.: Carbon monoxide - residence time in the atmosphere, *Science*, 166, 224-225, 1969.

Wershaw, R.: Model for Humus in Soils and Sediments, *Environmental Science & Technology*, 27, 814-816, 1993.

Wexler, A. S. and Clegg, S. L.: Atmospheric aerosol models for systems including the ions H⁺, NH₄⁺, Na⁺, SO₄²⁻, NO₃⁻, Cl⁻, Br⁻, and H₂O, *Journal of Geophysical Research-Atmospheres*, 107, 4207, 2002.

Whalley, L. K., Blitz, M. A., Desservettaz, M., Seakins, P. W., and Heard, D. E.: Reporting the sensitivity of laser-induced fluorescence instruments used for HO₂ detection to an interference from RO₂ radicals and introducing a novel approach that enables HO₂ and certain RO₂ types to be selectively measured, *Atmos. Meas. Tech.*, 6, 3425-3440, 2013.

Whalley, L. K., Furneaux, K. L., Goddard, A., Lee, J. D., Mahajan, A., Oetjen, H., Read, K. A., Kaaden, N., Carpenter, L. J., Lewis, A. C., Plane, J. M. C., Saltzman, E. S., Wiedensohler, A., and Heard, D. E.: The chemistry of OH and HO₂ radicals in the boundary layer over the tropical Atlantic Ocean, *Atmospheric Chemistry and Physics*, 10, 1555-1576, 2010.

Whalley, L. K., Stone, D., George, I. J., Mertes, S., van Pinxteren, D., Tilgner, A., Herrmann, H., Evans, M., and Heard, D. E.: Influence of clouds on the oxidising capacity of the troposphere, *Atm. Chem. Phys. Disc.*, submitted, 2014. 2014.

Widmann, J. F. and Davis, E. J.: Mathematical models of the uptake of ClONO₂ and other gases by atmospheric aerosols, *Journal of Aerosol Science*, 28, 87-106, 1997.

Worsnop, D. R., Zahniser, M. S., Kolb, C. E., Gardner, J. A., Watson, L. R., Vandoren, J. M., Jayne, J. T., and Davidovits, P.: Temperature - dependence of the mass accommodation of SO₂ and H₂O₂ on aqueous surfaces, *Journal of Physical Chemistry*, 93, 1159-1172, 1989.

Wyche, K. P., Monks, P. S., Ellis, A. M., Cordell, R. L., Parker, A. E., Whyte, C., Metzger, A., Dommen, J., Duplissy, J., Prevot, A. S. H., Baltensperger, U., Rickard, A. R., and Wulfert, F.: Gas phase precursors to anthropogenic secondary organic aerosol: detailed observations of 1,3,5-trimethylbenzene photooxidation, *Atmos. Chem. Phys.*, 9, 635-665, 2009.

Zeng, G., Heard, D. E., Pilling, M. J., and Robertson, S. H.: A master equation study of laser-generated interference in the detection of hydroxyl radicals using laser-induced fluorescence, *Geophysical Research Letters*, 25, 4497-4500, 1998.

Zhang, J. K., Sun, Y., Liu, Z. R., Ji, D. S., Hu, B., Liu, Q., and Wang, Y. S.: Characterization of submicron aerosols during a month of serious pollution in Beijing, 2013, *Atmos. Chem. Phys.*, 14, 2887-2903, 2014.

Zhang, Q., Jimenez, J. L., Canagaratna, M. R., Allan, J. D., Coe, H., Ulbrich, I., Alfarra, M. R., Takami, A., Middlebrook, A. M., Sun, Y. L., Dzepina, K., Dunlea, E., Docherty, K., DeCarlo, P. F., Salcedo, D., Onasch, T., Jayne, J. T., Miyoshi, T., Shimono, A., Hatakeyama, S., Takegawa, N., Kondo, Y., Schneider, J., Drewnick, F., Borrmann, S., Weimer, S., Demerjian, K., Williams, P., Bower, K., Bahreini, R., Cottrell, L., Griffin, R. J., Rautiainen, J., Sun, J. Y., Zhang, Y. M., and Worsnop, D. R.: Ubiquity and dominance of oxygenated species in organic aerosols in anthropogenically-influenced Northern Hemisphere midlatitudes, *Geophysical Research Letters*, 34, L13801, 2007.

Zhao, Y., Chen, Z., Shen, X., and Zhang, X.: Kinetics and mechanisms of heterogeneous reaction of gaseous hydrogen peroxide on mineral oxide particles, *Environ Sci Technol*, 45, 3317-3324, 2011.

Zhou, S. M., Shiraiwa, M., McWhinney, R. D., Poschl, U., and Abbatt, J. P. D.: Kinetic limitations in gas-particle reactions arising from slow diffusion in secondary organic aerosol, *Faraday Discussions*, 165, 391-406, 2013.

Zobrist, B., Soonsin, V., Luo, B. P., Krieger, U. K., Marcolli, C., Peter, T., and Koop, T.: Ultra-slow water diffusion in aqueous sucrose glasses, *Physical chemistry chemical physics : PCCP*, 13, 3514-3526, 2011.